Institute of Physical Chemistry
Polish Academy of Sciences
Kasprzaka 44/52
01-224 Warsaw, Poland

PhD Thesis

Electrodes modified with carbon nanotubes and enzymes

Adrianna Złoczewska

Supervisor: Prof. dr hab. Marcin Opałło
Auxiliary supervisor: Dr Martin Jönsson-Niedziółka

Institute of Physical Chemistry Polish Academy of Sciences
Warsaw, Poland

This dissertation was prepared within the International PhD in Chemistry Studies at the Institute of Physical Chemistry of the Polish Academy of Sciences in Warsaw.

Project operated within the Foundation for Polish Science International PhD Projects Programme co-financed by the European Regional Development Fund, Operational Program Innovative Economy 2007-2013.

INNOVATIVE ECONOMY
NATIONAL COHESION STRATEGY

FNP
Foundation for Polish Science

EUROPEAN UNION
EUROPEAN REGIONAL
DEVELOPMENT FUND

Warsaw, October 2013

For all scientists who are crazy about nanotubes

Life is like riding a bicycle. To keep balance,
you must keep moving.

A. Einstein

Acknowledgements

There are many people who somehow contributed to finishing this thesis. For no reason I will list them in chronological order. I would like to thank:

- Malgorzata Swierzowicz - for introducing me into an exciting world of chemistry
- my parents - for your support during my studies
- Madzia - for all your hints concerning life and science
- Kamil - for helping me to put the first step toward my PhD studies
- Marcin - for adopting me to your group-family
- **Martin** - for your invaluable help, supervision, understanding and Lilla Gubben
- Foundation for Polish Science - for founding
- Alina Ciach and Malgorzata Kanoza - for the coordination of the MPD project
- Eleanor, Andy and Neil - for the opportunity to work in your labs
- Kama - for being more than a 'daughter'
- Andrew - for cheering me up when nothing worked
- Kirsten - for all your positive energy
- Niklas - for your work done on the chip preparation
- Johan and Oleg N. - for making me a bigger CNT freak than I used to be before working in Edinburgh
- Andrei - for the waffle
- Robert - for teaching me how to grow titania nanotubes
- Arek - for a synthesis of the porphyrin
- Nina and Tracy - for teaching me how to make DSSCs
- Asia U. - for your huge contribution to the study presented in Chapter 4
- Wojtek N. and Ewa - for fruitful discussions
- Doris and Ania - for your CNP electrodes
- Piotrek - for being a very good student
- Amano Enzyme Europe Ltd for the donation of bilirubin oxidase
- all my buddies and colleagues from the group, especially Madzia K., Iza, Wojtek A., Marta S., Marcin D., Marta, Piyush, Chaweewan, Olof, Matt, Maddy, Paul and Oleg - for a nice atmosphere in the office and in the institute.

Abstract

Different ways of electrode modification with non-functionalised and functionalised carbon nanotubes (CNTs) and enzymes are presented in this thesis. The study is mostly focused on the preparation and electrochemical characterisation of the bioelectrodes for O_2 reduction. Bilirubin oxidase without a mediator or laccase with a mediator such as 2, 2'-azinobis (3-ethylbenzothiazoline-6-sulfonate) or syringaldazine were chosen to catalyse O_2 electroreduction. CNTs give a huge increase in the electrode active area as well as enable and/or enhance electron transfer between the electrode substrate and the enzyme. The best biocathode - the one which gives the highest reduction current density - is obtained for a breathing system with functionalised CNTs and BOx. In a breathing system the electrode substrate is a semipermeable membrane and is exposed form one side to gas, and from the other side to an electrolyte. This construction allows to avoid problems with diffusion of O_2 in electrolyte limiting the current and convection of the electrolyte which typically have a large influence on the obtained current of O_2 reduction.

Different attempts to obtain biobatteries, biofuel cells (BFCs) and biosensors with the above mentioned biocathodes are described. The biobatteries are prepared by using a Zn wire as an anode. The anodes modified with vertically aligned CNTs or carbon nanoparticles (CNPs) are used in ascorbic acid (AA) oxidation. This modification enables to apply these electrodes in BFCs with the breathing biocathode acting as self-powered sensors for AA. Moreover it is shown that the CNP-BFC in connection with a Prussian blue display acts as a truly self-powered sensor which can be used for the quantitative analysis of AA in a real sample. A photo-BFCs and a self-powered sensor for glucose with titania nanotubes are also constructed and studied.

A small part of this thesis describes the way of growing CNTs in a defined place on a specially designed chip. The local heating method is used for the growth.

Keywords: Carbon nanotubes, vertically aligned carbon nanotubes, bilirubin oxidase, laccase, oxygen reduction, biocathode, titania nanotubes, air-breathing biobattery, biofuel cell.

Streszczenie

W niniejszej rozprawie prezentuję różne sposoby modyfikacji elektrod niesfunkcjonalizowanymi i sfunkcjonalizowanymi nanorurkami węglowymi oraz enzymami. Zaprezentowane badania są skupione głównie na otrzymaniu i charakterystyce bioelektrod wykorzystywanych do redukcji tlenu. Oksydaza bilirubiny bez mediatora oraz lakaza bez lub z mediatorami takimi jak 2,2'-azino-bis(3-etylobenzotiazolino-6-sulfonian) lub syryngaldazyna zostały wybrane do katalizy elektroredukcji tlenu. Nanorurki węglowe powodują ogromny wzrost powierzchni aktywnej elektrody oraz umożliwiają i/lub zwiększają szybkość przeniesienia elektronów pomiędzy elektrodą a enzymem. Najlepsza biokatoda - która pozwala uzyskać najwyższy prąd redukcji - została skonstruowana jako oddychający układ zawierający sfunkcjonalizowane nanorurki węglowe i oksydazę bilirubiny. W układzie oddychającym elektroda jest umieszczona na półprzepuszczalnej membranie, która z jednej strony pozostaje w kontakcie z powietrzem a z drugiej strony z elektrolitem. Taka konstrukcja pozwala na uniknięcie powolnej z dyfuzji tlenu limitującej wartość prądu oraz z konwekcją elektrolitu, która zazwyczaj ma duży wpływ na uzyskany prąd redukcji O_2.

Ponadto opisuję różne próby otrzymania biobaterii, bioogniw paliwowych i bioczujników zawierających wyżej wymienione biokatody. Biobaterie są przygotowane z wykorzystaniem drutu cynkowego jako anody. Elektrody modyfikowane prostopadle zorientowanymi nanorurkami węglowymi lub nanocząstkami węgla są wykorzystane do utleniania kwasu askorbinowego. Taka modyfikacja umożliwia zastosowanie elektrod z nanorurkami lub nanocząstkami w bioogniwach paliwowych działających jako samozasilające się czujniki kwasu askorbinowego. Pokazuję także, że bioogniwo paliwowe z nanocząstkami węgla po połączeniu z wyświetlaczem zawierającycm błękit pruski działa jak prawdziwie samonapędzający się czujnik. Sensor ten może być wykorzystany do jakościowej analizy kwasu askorbinowego w próbce rzeczywistej. Kolejne skonstruowane i zbadane urządzenia to fotobioogniwo paliwowe i samonapędzający się czujnik na glukozę zawierające nanorurki z dwutlenku tytanu.

Niewielka część tej dysertacji opisuje metodę hodowania nanorurek węglowych w ściśle określonym miejscu, na specjalnie zaprojektowanym czipie. Metoda wykorzystana do ich hodowli to metoda lokalnego grzania.

Słowa kluczowe: Nanorurki węglowe, pionowo zorientowane nanorurki węglowe, oksydaza bilirubiny, lakaza, redukcja tlenu, biokatoda, nanorurki dwutlenku tytanu, oddychająca biobateria, bioogniwo paliwowe.

Abbreviations

AA	ascorbic acid
ABTS	2, 2'-azinobis (3-ethylbenzothiazoline-6-sulfonate)
ACN	acetonitrile
AFM	atomic force microscopy
AirB	air-breathing
BFC	biofuel cell
BOx	bilirubin oxidase
BPPG	basal plane pyrolytic graphite
CA	chronoamperometry
CE	counter electrode
CNPs	carbon nanoparticles
CNTs	carbon nanotubes
CTAB	hexadecyl-trimethyl-ammonium bromide
CV	cyclic voltammetry or cyclic voltammogram
CVD	chemical vapour deposition
DET	direct electron transfer
DSSC	dye-sensitized solar cell
EEM	epoxy embedding medium
EPPG	edge plane pyrolytic graphite
FMCA	ferrocenecarboxylic acid
GDH	glucose dehydrogenase
GOx	glucose oxidase
HOPG	highly ordered pyrolytic graphite
ITO	tin-doped indium oxide coated glass
LV	laser varporisation
LbL	layer-by-layer
Lc	laccase
LQ	liquid crystal
MCOxs	multicopper oxidases
MET	mediated electron transfer
MTMOS	methyltrimethoxysilane
MWCNTs	mutli-walled carbon nanotubes
NAD^+	nicotinamide adenine dinucleotide
NHE	normal hydrogen electrode

NPs	nanoparticles
NTs	nanotubes
OCP	open circuit potential
ORR	oxygen reduction reaction
OTEOS	n-octyltriethoxysilane
Por	5-(4-carboxyphenyl)-10,15,20-tris(4-methylphenyl)-porphyrin
PSA	1-pyrenesulfonic acid sodium salt
PTSA	pyrene-1,3,6,8-tetrasulfonic acid tetrasodium salt hydrate
PB	Prussian blue
PW	Prussian white
RE	reference electrode
Ru-dye	di-tetrabutylammoniumcis-bis(isothiocyanato)bis(2,2'-bipyridyl-4,4'-dicarboxylato)ruthenium(II)
SEM	scanning electron microscopy
SWCNTs	single-walled carbon nanotubes
Syr	3, 5-dimethoxy-4-hydroxybenzaldehydazine (syringaldazine)
*t*BuFc	*tert*-butylferrocene
TMASiCl	N-trimethoxysilylpropyl-N,N,N-trimethylammonium chloride
TMOS	tetramethoxysilane
TNTs	titania nanotubes
Tris	2-amino-2-hydroxymethyl-propane-1,3-diol
WE	working electrode

Introduction

The world's energy needs have been growing for the last decades. So far they have been mostly fulfilled by burning natural fuels such as gas and crude oil which will not last for ever. Thus it is desirable to develop new sources of energy based on renewable sources. One of the device designed to face this challenge is a fuel cell (FC) converting chemical energy into electric energy. The FC utilises renewable fuel and in theory generates electricity as long as the fuel is supplied. A biofuel cell is a type of FCs which contains biocatalysts, e.g. enzymes. One of the benefit from using these biomolecules is the possibility to miniaturise the cell so that it can become an implantable source of energy consuming the fuel directly from the body. The most explored type of a BFC uses glucose and oxygen and typically generate power of about dozens of microwatts. Although at the moment these devices are not able to solve the energy problem, they are expected to help people by powering the implantable medical devices such as cardiac pacemakers, drug-delivering pumps or nerve-simulators [1].

The development of new miniaturised devices would not be possible without the use of nanomaterials. The exceptional properties of these nanometre size materials give huge possibilities to tune the properties of the modified objects. Carbon nanotubes (CNTs) are examples of nanomaterials which have been successfully used e.g. for the preparation of bioelectrodes for BFCs.

The **goal of my thesis** is to prepare and characterize mainly electrochemical properties of electrodes with CNTs and enzymes. These electrodes are used for the construction of new biofuel cells, biosensors and hybrids of a battery and a biofuel cell (biobatteries). The characteristics of these devices is also the aim of my studies. Thus this thesis presents a contribution to the development of new types of bioelectrodes and related biodevices.

I start this dissertation from an overview on the subjects concerning the work described in the next chapters. Thus in Chapter 1 I describe the most important properties and methods of growing carbon and titania nanotubes. I also present selected, in my opinion the most interesting, examples of the use of these tubes as electrode materials. Additionally I describe properties of the chosen enzymes and their application in biofuel cells and biosensors.

The main part of my thesis presents Experiments together with Results and Discussion forming a clear structure of seven chapters. Chapter 2 is about experimental methods, materials and procedures used in more than one of the following chapters. The procedures of the experiments described only in a given chapter are presented at the beginning of it. In Chapter 3 I describe a novel way of obtaining electrodes with vertically aligned carbon nanotubes (VACNTs) based on transferring the tubes to a conductive substrate. I also show detailed characteristics of these VACNT-electrodes and their use as platforms for enzyme immobilisation. A crucial part of Chapter 3 is about preparation of different types of biocathodes containing the enzyme laccase embedded in a silicate matrix on VACNT-electrodes.

I also show characteristics of zinc/oxygen batteries comprising these biocathodes. The work described in this chapter is also presented in the publication [2].

In Chapter 4 I shortly introduce the problem of the convection of the electrolyte in the electrochemical cells and its influence on the performance of biocathodes for O_2 reduction. In cooperation with J. Urban and W. Stryczniewicz the convective flow of the electrolyte inside the cell is modelled. We show that the theoretical value of O_2 reduction current matches the experimental results only when the convective flow of the solution is taken into account [3].

Chapter 5 describes the way of obtaining and characterisation of air-breathing biocathodes with functionalised CNTs and the enzyme bilirubin oxidase. The construction of the breathing electrodes allowed to avoid the problems with O_2 diffusion and electrolyte convection giving a very efficient biocathode. In this chapter, I also present an application of our biocathode in the construction of Zn/O_2 battery and a stack of batteries which were used for powering various devices [4].

A part of Chapter 6 presents the connection of the electrode with the VACNTs (Chapter 3) with the air-breathing biocathode (Chapter 5) which acts a biofuel cell for ascorbic acid (AA). This BFC can be also used as a self-powered sensor for AA. Besides I present the characteristics of another anode - with carbon nanoparticles (CNPs) - and an AA/O_2 BFC with this anode and the air-breathing biocathode. I show the way of constructing the first truly self-powered AA sensor with an electrochromic display connected to the second type of the BFC. Moreover, I demonstrate the use of this sensor in the real sample analysis.

In Chapter 7 I present the idea of obtaining a lab-on-chip device with directly grown CNTs. I also describe the attempts to grow CNTs in localised place on a chip by using a local heating method.

The last chapter describing the experimental work (Chapter 8) is about the construction of photoelectrochemical BFCs with anodes containing titania nanotubes (TNTs). In that chapter I show the method of TNT growth and the characteristics of a few different photo-BFCs. Moreover I present the use of one of the photo-BFCs as a self-powered sensor for glucose.

The thesis in summarised in Chapter 9 where I describe a contribution of my work to the studies on electrodes modified with CNTs and enzymes.

Contents

Background

Chapter 1

Literature review

This chapter presents a background relevant to the research described in Chapters 2 - 8. Here one can find information about carbon nanotubes, their properties, methods of their synthesis as well as their use in electrode preparation. Besides the term bioelectrocatalysis is explained together with a presentation of the use of enzymes in the preparation of electrodes for biofuel cells and self-powered biosensors. At the end a short introduction to the electrodes with titania nanotubes is given.

1.1 Carbon nanotubes

Carbon nanotubes (CNTs) are tubular nanostructures made entirely of carbon atoms. They have a diameter in the range of nanometers (from 0.3 [5] up to 100 nm) but their length might reach several centimeters. So far the record length of more than 18 cm was obtained for the SWCNTs [6]. The diameter of a typical single-walled CNT (SWCNT) is around 1 nm and for multi-walled CNTs (MWCNTs) it is ca. 10 nm [7]. One can imagine CNTs as rolled sheets of graphene (a layer of graphite). If one such a layer is rolled, a SWCNT is formed. In case of rolling more than one layer around the same axis a MWCNT is created. Moreover, in case of SWCNTs, depending on the axis along which the layer is rolled, it is possible to obtain CNTs of different chirality. For a better description of the term chirality, one defines the chiral vector:

$$\mathbf{C}_h = n\mathbf{a}_1 + m\mathbf{a}_2 \tag{1.1}$$

where $\mathbf{a}_1$ and $\mathbf{a}_2$ are the unit vectors of graphene and m and n are indices. In other words $\mathbf{C}_h$ indicates how the axis of the rolled tube is rotated in comparison to the initial unit vector. By further simplification of the notation one can write:

$$\mathbf{C}_h = (n, m) \tag{1.2}$$

to distinguish different types of tubes. Then CNTs with $n = m$ are called armchair tubes, these with $(n, 0)$ are zig-zag and others ($n \neq m \neq 0$) are chiral (see Eq. 1.1). The SWCNT

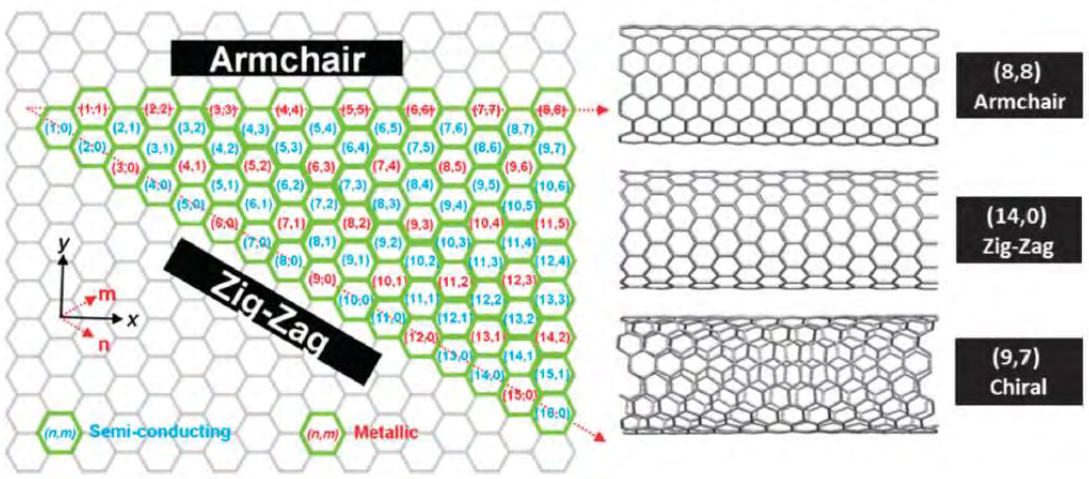

Figure 1.1: SWNT chirality map and examples of (n, m) chiral vectors that give rise to armchair, zig-zag and chiral nanotube structures with metallic or semiconducting electronic character [8].

chirality determines the electric properties of the tubes, so that they can be either metallic or semiconducting. However, MWCNTs are almost always metallic [9]. This phenomenon can be explained by taking into account that the MWCNT is a collection of SWCNTs. It is enough when one of the SWCNTs is metallic and then the whole MWCNT is also metallic. Thus the CNT with more walls is more likely to behave as a metal and MWCNTs are almost always metallic.

Before moving on to the description of CNT properties it is a good moment to mention the interesting history of their discovery. Surprisingly most articles concerning these nanomaterials state that Iijima discovered them. He indeed was the first one who observed, understood and described CNTs [10]. In his paper from 1991 he used the expression microtubules of graphitic carbon to describe the needle-like structures (later called CNTs) observed under HRTEM. But he was not the one who obtained this material. The specimen was given by his friend Yoshinori Ando who was only mentioned in the acknowledgements of that seminal paper. Moreover, the same Ando was aware that tubular carbon nanostructures were described much earlier than Iijima's report by Endo's group [11–13]. What is even more interesting; even Ando never mentioned the truly first discoverers of CNTs - Radushkevich and Lukyanovich [14]. They described the tubes in 1952 after observing them under TEM. Unfortunately that paper did not bring them the fame, which is understandable taking into account that it was written in Russian and not everyone outside the Soviet Union had an access to it at that time. More details about the early history of CNTs were described by Monthioux and Kuznetsov who "in the name of truth and for the benefit of all" answered the question *Who should be given the credit for the discovery of carbon nanotubes?* [15].

1.1.1 Electronic properties and applications

An ongoing interest in research concerning CNTs comes from their exceptional properties. These properties are the result of their nanometre size and electronic structure. As mentioned before, MWCNTs behave like a metal. SWCNTs can be either semiconducting or metallic - depending on their chirality which is related to (n, m) (Eq. 1.2). All armchair CNTs ($n = m$) are metallic, with no band gap even at 0 K. If the indices n and m have different values and fulfil the relation $n - m = 3i$ (i is an integer), the nanotube is metallic. This type of tube has a negligible band gap at room temperature [8]. All other SWCNTs are semiconducting and have a band gap on the order of 500 meV that varies inversely with their diameter [8].

In 1998 White and Todorov used local density-functional calculations to show that armchair SWCNTs can act as ballistic conductors [16]. In the same year Heer's group confirmed experimentally that the MWCNTs indeed show this type of conductance [17]. The authors measured the conductance of single nanotubes which was constant (near $G_0 = 2e^2/h$) along the tube length of ca. 2 μm. However, they showed that the application of a high voltage did not damaged the CNTs by heat dissipation. 6 V applied to the single MWCNT (20 nm in diameter) could have caused its heating up to very high temperature in case of non-ballistic conductance. The nanotubes would definitely be destroyed at that temperature. Thus a non-destructive influence of the high voltage on CNTs is another proof that the MWCNTs examined by Heer's group showed ballistic conductance. Furthermore, the authors found that the conductance of MWCNTs is quantized [17].

Taking into account the above mentioned electronic properties of CNTs and bearing in mind their nanosize dimension as well as a huge aspect ratio, one can imagine a very wide spectrum of their applications. CNTs have been proposed to be used e.g. as/to construct:

- metal-semiconductor, semiconductor-semiconductor or metal-metal junctions [18],
- molecular electronic devices such as: a Fabry-Perot electron resonators [19], ballistic field-effect transistors [20],
- flexible electronics based on CNT thin films [21],
- power sources such as: batteries, fuel cells, capacitors [22] and dye-sensitized solar cells [23],
- optoelectronic devices, e.g. terahertz polarizers and large-area broadband photodetectors [24],
- electron sources in high-brightness luminescent elements and an X-ray tubes [25],
- different types of sensors, including artificial skin sensors [26],
- neural regeneration [27].

More about CNT electronics can be found in the (relatively) recently published review by Wang *et al.* [28]. However, from the point of view of this thesis the most interesting

application of CNTs is the electrode modification to obtain new power sources such as biobatteries and biofuel cells.

Although I am mainly interested in electronic properties of CNTs, it is also worth mentioning that these materials also have other extraordinary properties such as thermal conductivity similar to diamond [29] and mechanical strength 100 times stronger than steel [30].

Although the perspectives of exploiting CNTs are very promising one need to be aware of the safety issues concerning handling them. There is still an ongoing debate about CNT toxicity [31–33]. For example Poland *et al.* suggested toxicological similarity between these materials and asbestos and warned against carcinogenic effects [34]. Moreover, CNTs can induce inflammatory response, granuloma formation and development of pulmonary fibrosis [35].

1.1.2 Methods of growing CNTs

The first CNTs were grown in an arc-discharge chamber. The idea of using this equipment came from a method used for the first time by Krätshmer (in 1990) to obtain another carbon nanomaterial - fullerene (C_{60}) [36]. The scientific world was very excited about C_{60} at that time since its discovery[1]. But only when Krätschmer presented the production of C_{60} in macroscopic amounts everyone started to believe that this material could be used outside the laboratory. That is why his method was very popular at the end of the 1990's.

The CNTs described by Iijima in 1991 were multi-walled. The first SWCNTs were reported two years later independently by Iijima and Ichihashi [38] and Beyers' group from IBM [39]. Although it was possible to produce big amounts of CNTs with the arc-discharge method it had a big drawback - the CNTs were polluted with soot and/or metal nanoparticles. To obtain cleaner CNTs other methods were developed. Laser vaporisation (LV) and chemical vapour deposition (CVD) were used for the synthesis of both SWCNTs and MWCNTs. To obtain only MWCNTs diffusion flame, electrolysis of graphite electrodes in molten ionic salts, ball-milling of graphite, heat treatment of polymer etc. were developed [40]. One of the most intriguing methods was presented by Banhart's group. They showed that it is possible to grow MWCNT inside a bigger MWCNT under an electron beam [41].

In this section I will shortly describe three main methods which are well established to produce a wide variety of CNTs (arc-discharge, LV and CVD). Then I will focus on the so-called local heating method (a type of CVD) which I mainly used.

[1]The fullerenes were discovered by Kroto *et al.* in 1985 [37]

Arc discharge

As I mentioned earlier the first well described CNTs were prepared by Ando [9] in his direct current (DC) arc-discharge chamber. He used an arc discharge (>100 Amp., ca. 300 °C) between two graphite electrodes placed $1-2$ mm apart in helium atmosphere.

In this method the electrons emitted from the cathode hit the anode with so high energy that carbon atoms evaporate from the latter electrode. A kind of carbon plasma is created which is next cooled and forms a deposit inside the chamber. $20-40$ % of this deposit is left on the cathode and here MWCNTs are found. But this type of arc-discharge is not very effective in the production of CNTs because it mostly produces carbon sooth. Only when rare earth metals are added to a graphite anode a high yield of MWCNTs is obtained [42].

SWCNTs were obtained for the first time as an unexpected product of the reaction which supposed to give MWCNTs incorporated with metal nanoparticles [38]. Ijima and Ichihashi filled the graphite anode with iron and surprisingly got a new type of CNTs. These SWCNTs were found not only in the cathode deposit but in the whole arc-discharge chamber. After this discovery a wide range of metals and metal alloys were tested to give the best nanotubes, e.g. Ni, Co, Fe/Ni. Also different gases were introduced inside the chamber (Ar, H_2) to optimise the way of obtaining SWCNTs. So far the highest yield was obtained by Ando *et al.* - 1.24 $\mathrm{g\,min^{-1}}$) [43]. They used Ni as a catalyst in their arc plasma jet method (APJ)[2].

The costs associated with the production of CNTs by the arc-discharge method are high because the substrates need to be of high purity. The main advantage of this method is the very high crystallinity of the obtained tubes. However, the drawbacks such as no control over the CNTs' size and lots of impurities imply that this method is not the best for the production of CNTs.

Laser varporisation

LV was used for the first time for the synthesis of MWCNTs by Smalley's group [44]. In this method a graphite target is vaporised by a laser beam in an inert atmosphere. The quality of obtained the MWCNTs depends on the temperature inside the chamber - the best is around 1200 °C.

Here like in the arc-discharge method the use of a metal catalyst induces the growth of SWCNTs. The reaction yield depends on the catalysts in the following order: Ni > Co > Pt > Cu > Nb for monometals and Co/Ni, Co/Pt > Ni/Pt > Co/Cu for bimetals. The best yield was obtained for Co/Ni catalyst - 50 %. Later this result was beaten and reached 70 %

[2]In APJ method the electrodes are inclined at 30° not at 180° as it is done in a standard arc-discharge method

due to the use of a dual pulsed LV [45]. In this case two successive laser pulses were used to first ablate the anode and then break up the larger carbon particles and feed them into the growing CNTs.

Although LV gives the better control over the CNTs size distribution, it does not give a better quality material than the arc-discharge method. Moreover, it also requires high quality substrates which increase the production costs. Thus LV is not economically advantageous at the moment.

Chemical Vapour Deposition

The CVD method of CNT growth is based on the decomposition of gaseous carbon precursors in the presence of a catalyst. Up to now a huge range of precursors was tested with acetylene and ethylene as the most often used [46]. Also the use of hundreds of different catalysts was reported, where most of them are transition metals (mostly Fe nanoparticles), their alloys or compounds such as ferrocene [47] or ferritin [48]. Depending of the source of energy which induces the decomposition of the precursor one can distinguish a few types of CVD: thermal CVD (T-CVD), plasma-enhanced CVD (PE-CVD) [49–51], hot-filament CVD [52] and others.

In T-CVD the gas precursor is thermally heated ($700-1200\,^{\circ}\mathrm{C}$ [50]) in a furnace together with the catalyst. The catalyst can be either deposited on a substrate or be introduced in the gas phase (the floating catalyst method). The typical apparatus for T-CVD comprises a quartz tube furnace, pumps and a cooling system. The precursor is carried by an inert gas (or gas mixture) and flushed though the heated tube. There the starting carbon material decomposes and reacts with the catalyst. The question *how does the carbon precursor react with the catalyst?* is still not answered explicitly, so I will leave the discussion concerning it for the end of this section.

There are very many factors influencing the formation of CNTs which make their synthesis a very complex field to study. Alan Windle called it a *technology in a multidimensional parameter space* [53]. This space comprises parameters such as [46]:

- chosen materials: catalyst, underlayer, substrates, dual catalyst plates, etc.
- chosen gases: mix, flow rates, reducing agents, oxidizing agents, hydrocarbons, etc.
- temperatures of the substrate and gas phase, thermal profile inside the furnace, etc.
- reactor technology i.e. tube furnace, substrate heater, etc.
- duration of the steps such as annealing, growth, post-growth, etc.

Choosing different parameters one can grow SWCNTs or MWCNTs which are either straight (high quality) or curly (with defects); grow as single tubes or as forests; obtain a shape of bamboo or spaghetti. The variety of shapes comes e.g. from many defects appearing

on their walls which bend the tubes. These defects are not desirable because they reflect a poor quality of the material. Hence a good way of growing means obtaining high quality tubes. One of example of high quality tubes are arrays of SWCNTs "super-grown" in the presence of water [54]. A major advantage of CVD is that the CNTs can be used directly after the growth, without further purification which is indispensable in case of the arc-discharge method. Moreover, CVD gives the possibility to grow CNTs in predefined position which opens the door for bottom-up nanoengineering and building different nanodevices, which is presented e.g. in Figure 1.2

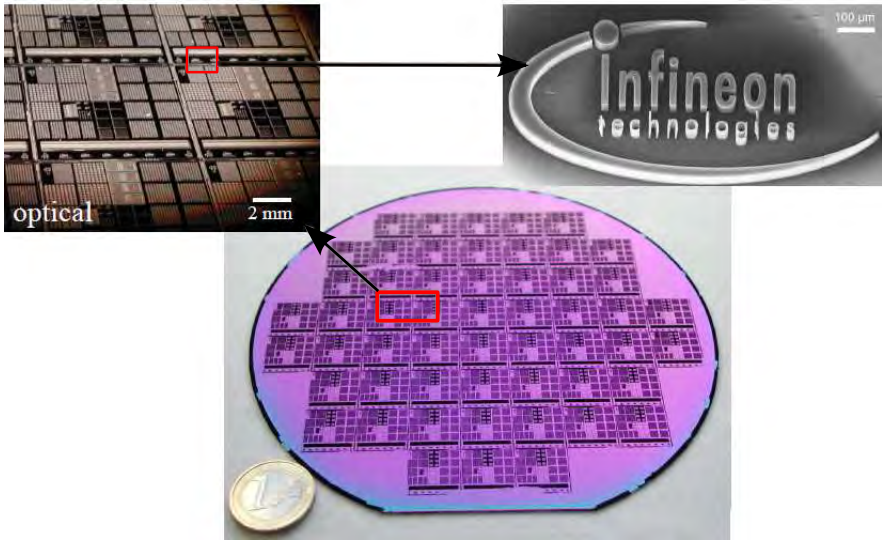

Figure 1.2: CNTs growth on a patterned 6-inch silicon wafer [55].

CNTs are promising parts of electronic devices, but one needs to remember that this application requires compatibility with microelectronic fabrication. This in turn requires keeping the processing temperature below 400 °C for industrial implementation [56]. Typical apparatus for CVD do not allow to grow good CNTs in such a low temperature. Even the sophisticated way of incorporating plasma-enhanced hot filament CVD and ammonia decreases the temperature only to around 660 °C [57]. A turning point appeared when Englander *et al.* reported the growth of CNTs by localised heating in a room-temperature chamber [58]. This process is selective, scalable and compatible with on-chip microelectronics. Here the catalyst is deposited on a suspended polysilicon microbridge which is resistively heated by applying a voltage up to 10 V. The obtained CNTs are believed to be mutli-walled and are up to 5 µm long (Figure 1.3). Later Wierold's group used a very similar approach to also obtain SWCNTs [59].

The local heating method was used e.g. by Slocum's group to investigate the influence of the temperature of the gas mixture introduced into the chamber on the growth rate of CNTs. They found out that the CNTs grow ca. 14 times faster when the gases (acethylene, argon and hydrogen) were preheated, in comparison with gases kept in room temperature [60].

Another interesting way of exploiting this type of CVD was presented by Graham's

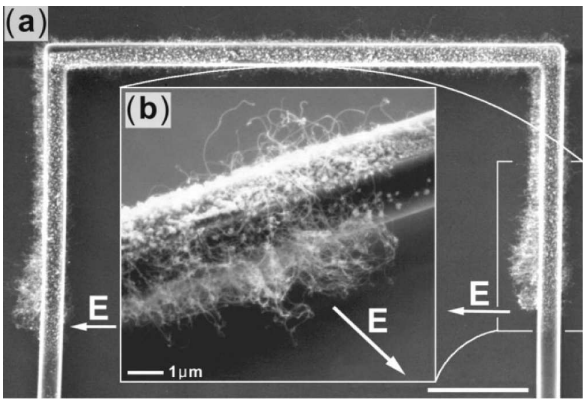

Figure 1.3: a) Synthesis localized to microbridge legs. Growth occurs largely in the direction of the local E field. b) High resolution SEM of the right microbridge section oblique view. Note how the CNT curves and follows the E field. Scale bar 10 μm [58].

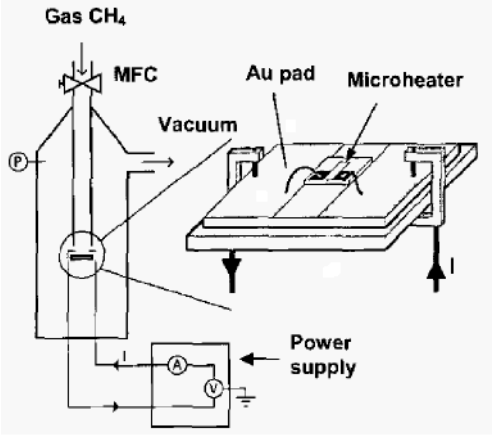

Figure 1.4: Scheme of experimental setup for the fabrication process in the local heating method. Here MFC stands for a mass flow controler [59].

group [61]. They grew CNTs on an AFM cantilever and in this way created new opportunities for interfacing nanomaterials with microstructures. Unfortunately the fabrication process is too complicated and even the authors are aware that their invention will not replace the standard silicon or silicon nitride cantilevers.

More information about the local heating method can be found in the references [7,62,63]. The last two describe the setup which I used to grow CNTs.

Although thousands of papers about CNT growth have been published since Iijima's crucial paper [10] the exact mechanism of this process is still not fully understood. The description of different models can be found e.g. in Lubej and Plazl's review [64]. Up to now the most accepted model derives from the vapour-liquid-solid (VLS) originally used for the first time to explain the mechanism of growth of silicon whiskers [65]. In this model decomposed hydrocarbon gas i) precipitates on the surface of the catalyst, ii) diffuses into the catalyst and iii) nucleates the nanotube growth at the edges of the catalyst. There is still an ongoing debate weather the catalyst is in a liquid or in a solid state. For example some researchers claim that the catalyst is liquid [66]. They proposed that both the temperature

and the carbon concentration are uniformly distributed across the metal particles. While others claim that the catalyst is in its solid state during the CNT formation [46].

When the catalyst is placed on the surface a CNT can grow in one out of two ways:

- tip-growth - where the nanotube nucleates and grows below the catalyst (it lifts the catalyst),
- base-growth - where the nanotube nucleates and grows above the catalyst (the catalyst remains attached to the substrate).

Taking into account all the above information concerning CNTs one can simply conclude that growing these tubes is like cooking. It is necessary to make many attempts and precisely examine the results to find the best recipe. On the other hand obtaining nanotubes of predetermined parameters is an art not yet fully mastered. Thus this section was an introduction to the description of my work as a cook and an artist (see Section 7).

1.2 Bioelectrocatalysis

In 1981 Hill and Higgins defined the term bioelectrocatalysis[3] as "the use of materials derived from biological systems as catalysts for reactions occurring at electrodes" [68]. The authors underlined that biomolecules have characteristic features such as specificity, selectivity, spacial and temporal organization. Moreover, the biomolecules are able to control electron transfer, which all in all make them a desirable material for electrode modification.

In recently published reviews one can read that an interest in bioelectrocatalysis has been growing mainly because it opened the path for obtaining new kinds of power sources (biofuel cells, BFCs) and sensors (biosensors) [69]. Moreover, bioelectrocatalysis started to be used in electrochemical bioprocessing (producing fuels or other valuable products) [70]. But looking into the literature from the early 1980's reveals different expectations from bioelectrocatalysis, e.g. obtaining biological memories to computers and electrically driven biocatalysis for chemical synthesis [71]. At that time the interest in biosensors and biofuel cells was just in its early stage. Probably - as was suggested by Aston and Turner - the later expansion of interest in biosensors and BFCs was caused by whims of political and economic pressure [71]. Nowadays a huge number of publications concerning this topic shows how broadly bioelectrocatalysis has been exploded.

Biological catalysts can be divided into a few classes depending on their origin. Typically the literature distinguishes two types of catalysts: enzymes and microbes (microorganisms) [72–74]. A more rare classification was presented by Freguia *et al.* who listed three classes of

[3]To be more accurate - this term was for the first time used in a report published by Brezin's group in 1976 [67]. But they used it to describe enzymatic electrocatalysis exclusively.

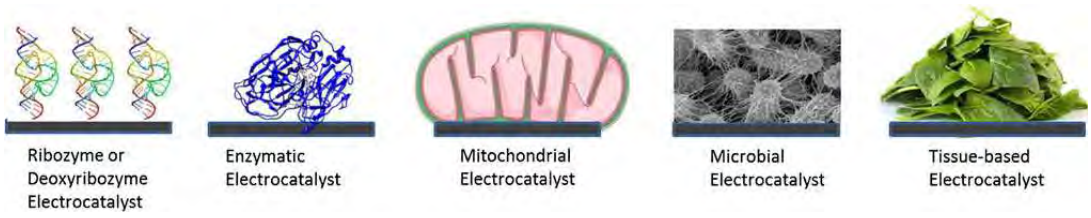

Figure 1.5: Different types of bioelectrocatalysts, according to Minteer [70].

bioelectrocatalysts: i) enzymes, ii) enzyme arrays and organelles, and (iii) microbial cells [75]. An even longer list of biological entities can be found in Minteer's paper [70], i.e. protein biocatalysts (enzymes), nucleic acid biocatalysts (ribozymes and deoxyribozymes), organelle biocatalysts (thylakoid membranes or mitochondria), functioning tissues and complete living cells (bacteria or fungi).

For the purpose of this thesis I will focus only on enzymes.

1.2.1 Mediated and direct bioelectrocatalysis

There are two types of bioelectrocatalysis classified according to the mechanism of electron transfer between the enzyme and the electrode: mediated and direct (mediator free). In the case of the mediated bioelectrocatalysis the electrons are shuttled via a mediator which is a (inorganic or organic) redox compound or some redox protein [76]. Mediators can be either diffusional (such as ferrocene derivatives, ferricyanide, quinones, and bipyridinium salts) or can be attached to the electrode surface together with the enzyme. The immobilization of the mediator can be done by e.g.: covalent tethering, cross-linking or surface reconstitution of apo-enzymes on mediator-cofactor-functionalized electrodes [77].

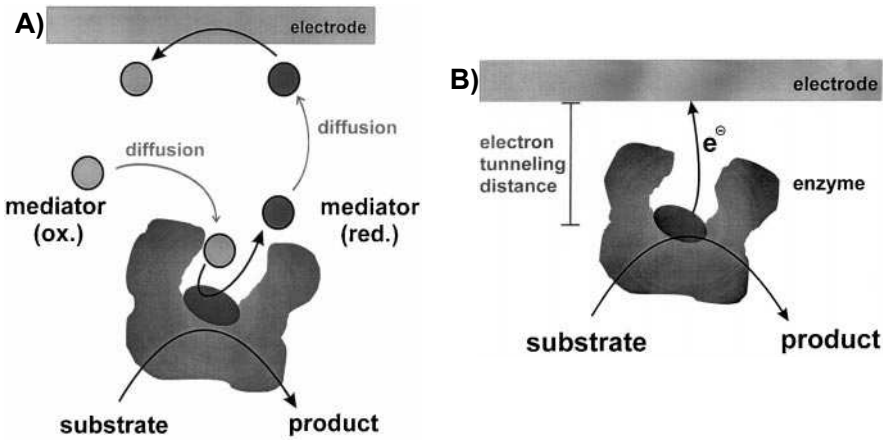

Figure 1.6: Scheme of mediated - via a diffusional mediator - (A) and direct (B) electron transfer between the electrode and the enzyme [78].

The main advantage of mediated electrocatalysis is that there is no need of having the enzyme oriented properly on the electrode surface [79]. As a consequence it is easier to get an electron transfer between the enzyme and the electrode by using the mediator. Such a system

has high initial activity but unfortunately it introduces an additional source of long-term instability in addition to the instability of the enzyme [74]. Moreover, its redox potential is lower than the potential of a non-mediated system, which comes from the differences between the redox potentials of the mediator and the enzyme. In the case of mediated process the final potential of the bioelectrode depends on the mediator and that is why it is lower than the potential of a non-mediated system. More details concerning mainly the kinetics of mediated bioelectrocatalysis can be found in Kano and Ikeda's review [76].

In direct bioelectrocatalysis[4] no electron-shuttling species are needed, which paves the way for obtaining smaller and more stable systems having higher potential than the mediated ones. But not each enzyme can be efficiently used without the mediator. For example only less than about a hundred out of more than 1400 known oxidoreductases can take part in direct electron transfer [80]. In most cases the active centre of the enzyme is deeply buried inside the protein, hence the electron tunnelling between the electrode and this centre is not possible. However, research concerning direct bioelectrocatalysis has exploded in the last decade, mainly due to exploiting nanomaterials which improve transfer rates and therefore increase current densities [70].

1.2.2 Selected enzymes

In my thesis I mainly used the enzymes responsible for O_2 reduction - laccase from *Cerrena Unicolor* and bilirubin oxidase from *Myrothecium sporae*, which belong to the multicopper oxidases (MCOxs) family. Beside these two I also used enzymes responsible for glucose oxidation, i.e. glucose oxidase from *Aspergillus niger* and glucose dehydrogenase from *Pseudomonas sp.*. Therefore in this section I will describe these four selected enzymes.

Multicopper oxidases and the O_2 reduction reaction

MCOxs are the class of redox-active enzymes with four copper ions. These ions are classified into three active centres: T1 (blue copper which is located close to the protein surface [81]), T2 and T3 (coupled binuclear copper centre) [82] (Fig. 1.7a). Although the main role of MCOxs in nature is oxidation of e.g. phenolic compounds[5], more interesting is the ability of some of them to reduce O_2 directly to water [79]. Moreover, this reaction occurs at relatively high potentials in comparison with the potential on Pt electrode under similar conditions. It

[4] Karyakin in his review concerning this topic wrote that the discovery of direct bioelectrocatalysis by the enzymes is "a pride of Russian enzymology and electrochemistry schools" [69]. Unfortunately - as it was in case of the first synthesis of CNTs - the first reports were written in Russian, so not everyone noticed that discovery.

[5] Thus some of them, like laccases, are widely used by the industry e.g. for the detoxification of effluents and cosmetics production (e.g. hair dyes) [83]

means that MCOxs are very good biocatalysts for the construction of biocathodes for biofuel cells [84].

There are more than 200 kinds of MCOxs. Among them only 6 are known to take part in O_2 reduction: laccase (Lc), copper efflux oxidase (CeO), bilirubin oxidase (BOx), cytochrome-c oxidase, L-ascorbate oxidase, ceruloplasmin and phenoxazinone synthase [85]. Each enzyme derived from a different source can have a different redox potential which is related to different onset potential of O_2 reduction. This diversity of potentials is due to different electronic structures of the MCOxs, which in turn comes from small differences in the surroundings of the active centre [86].

As mentioned above the main natural activity of MCOxs is the oxidation of some organic compounds. In that case the biomolecule takes the electrons from the substrate. But in the absence of the oxidizable species the enzyme can transfer the electrons directly from the electrode to the active centre where O_2 reduction takes place. The mechanism of this reaction by MCOxs was described in detail by Solomon and co-workers [87]. This is in overall a 4-electron reaction and it is usually coupled to four 1-electron reactions of substrate oxidation. First the electrons are transferred from the substrate to the T1 (from a distance of ca. 1 nm). Then they are passed trough a tripeptide His-Cys-His chain (ca. 1.3 nm long) to the trinuclear cluster (TNC) comprised of the T2 and the T3 centres and dioxygen is reduced at the TNC. The more precise description of this reaction is depicted in Figure 1.7b. The reaction steps which occur at the TNC are the following: i) generation of peroxy-intermediate (PI) - where O_2 molecule has been reduced by two electrons and an O-O bond remains; ii) generation of a negative-intermediate (NI) - where the last bond between oxygen atoms has been broken and all copper atoms are in the 2+ state; iii) complete regeneration of the TNC, fast 4-electron transfer and release of two water molecules. The step ii) is faster than i) so the generation of PI is the rate determining step. But one also need to take into account that the scheme 1.7b does not include the electron transfer process from the electrode. This step can also be the rate determining.

Laccase

Laccase (Lc) is present in different plants or fungi where it plays a role in e.g.: pigment formation, lignin degradation or detoxification [82]. It is an extracellular metalloprotein, thus it is relatively easy to extract, in comparison with other MCOxs. This ease of extraction is the reason why Lc is the most studied enzyme so far among all MCOx. Laccase was used for the first time in electrocatalysis (in 1978) by Berezin *et al.* [88]. They reported O_2 electroreduction on a carbon electrode with adsorbed enzyme.

When considering the use of Lc for electrode modification one need to bear in mind that the catalytic potential of this enzyme (which is equal to the redox potential of the T1 centre)

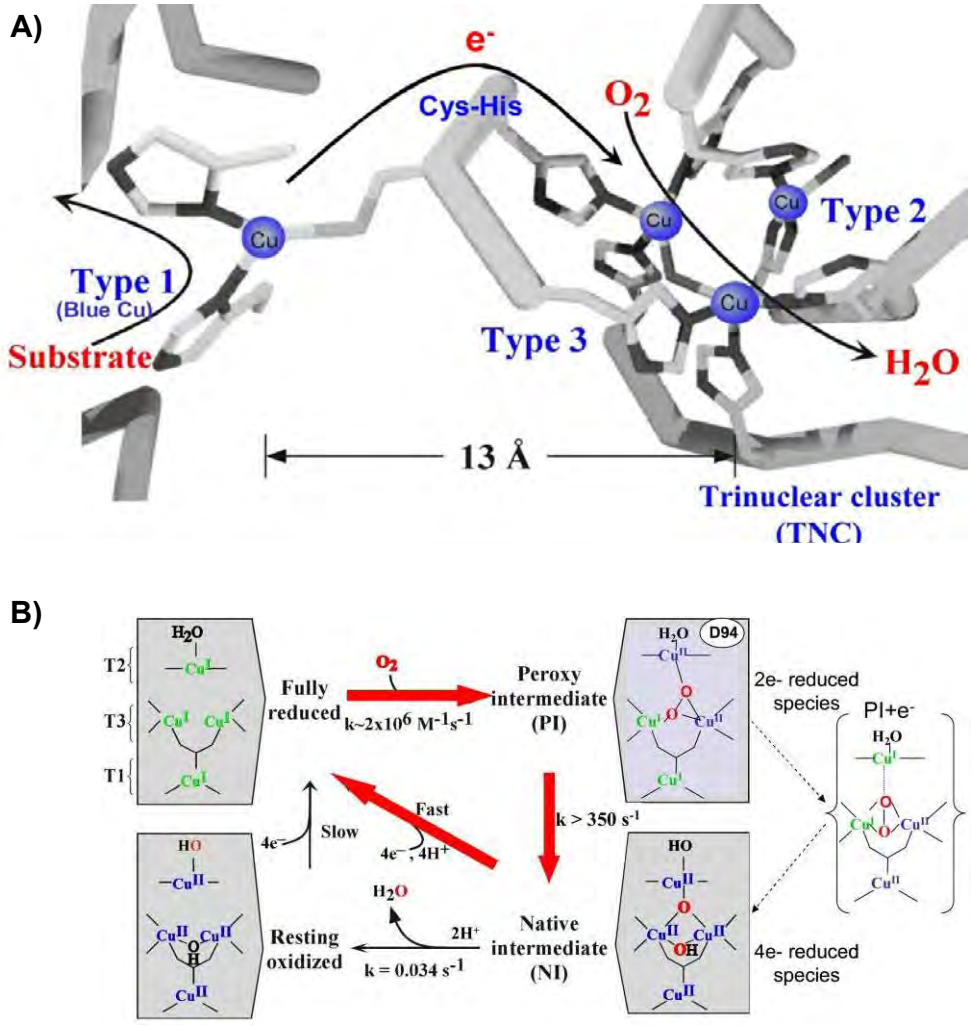

Figure 1.7: a) The structure of the MCOx active site with arrows marking the flow of substrates, electrons. b) Mechanism of O_2 reduction to water by the MCOxs. Red arrows illustrate the steps taking place in the catalytic cycle of the enzyme. The black ones indicates steps out of the catalytic cycle but the ones which can be observed experimentally. The dashed arrows indicate the transfer of an electron from the T1 to the T2. [87].

Figure 1.8: Ribbon diagram of Lc from *Trametes versicolor* showing the two channels leading to the TNC. Red and blue spheres represent water molecules and copper ions respectively [89].

is dependent on its origin. Thus this type of MCOx can be divided into three groups [90,91]:

- high redox potential Lc - with the potential ca. 0.78 V vs. NHE, obtained mainly form fungi (e.g. 0.785 V for Lc from *Polyporus versicolor* [92], 0.750 V for Lc from *Cerrena Unicolor* [93]),
- medium potential Lc - with the redox potential $0.47 - 0.71$ V vs. NHE, isolated from fungi, e.g. *Coprinus cinereus* - 0.55 V vs. NHE [94],
- low potential Lc - with the redox potential below 0.47 V vs. NHE, obtained mainly from trees, such as *Rhus vernicifera* - 0.434 V vs. NHE [92].

Other factors which can influence the redox potentials of Lc are: electrostatic interactions between the metal site and the protein, water environment, and hydrogen bonding interactions of the active site ligands [82]. That is why this enzyme behaves differently in different pH, with the optimum pH in the range of 3 - 5. Unfortunately this pH is not suitable for *in vivo* applications where pH is around 7.4. Thus this enzyme is not a proper biocatalyst for the preparation of electrodes for implantable biofuel cells. So although high-potential Lc are desirable in bioelectrocatalysis form the point of view of high catalytic activity [95] they would poorly work *in vivo*.

Bilirubin oxidase

Bilirubin oxidase (BOx) is another example of an enzyme from MCOx family. It can be found in different organisms such as fungi, bacteria and animals, where it acts as a catalyst in oxidation reactions (of e.g. bilirubin, diphenols and aryl amines) [96]. Similarly to Lc this enzyme can also catalyse O_2 reduction reaction at a potential similar to the one for high-potential Lc. The redox potentials of the T1 site for BOx from *Myrothecium verrucaria* and from *Trachyderma tsunodae* are 0.67 V vs. NHE and >0.65 V vs. NHE respectively [97]. Interesting is the electron transfer (ET) from the electrode surface to the inside of BOx might be dependent on the electrode material. In case of carbon electrodes BOx might be oriented in a way that the T1 site is at the tunneling distance form the electrode surface (up to 1.4 nm [98]). The orientation of this enzyme might be reversed on functionalized gold electrodes where the TNC is responsible for the ET (see ure 1.9) [99].

The crystal structure of BOx (from *Myrothecium verrucaria*) was recently resolved (Fig. 1.9) [81]. Untypically, in comparison to other MCO, this enzyme has two non-coordinating hydrophilic amino acids - asparagine and threonine - located close to the T1 site. Thus a long, narrow and hydrophilic pocket is formed near this active site. Cracknell *et al.* used the interaction between this hydrophilic binding pocket and bilirubin to stabilise the enzyme on a pyrolytic graphite electrode [81]. As a result they obtained more than twice higher electrocatalytic activity of BOx in comparison to the one obtained by simple adsorption of the protein to the carbon surface.

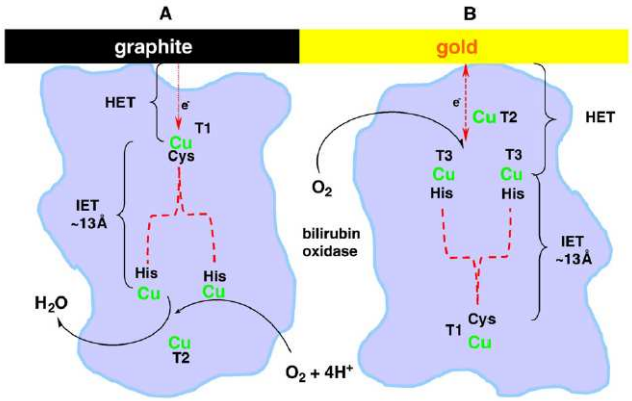

Figure 1.9: Proposed mechanisms of DET from electrodes to BOx (*Trachyderma tsunodae*) connected via (A) the T1 site and (B) the TNC [99].

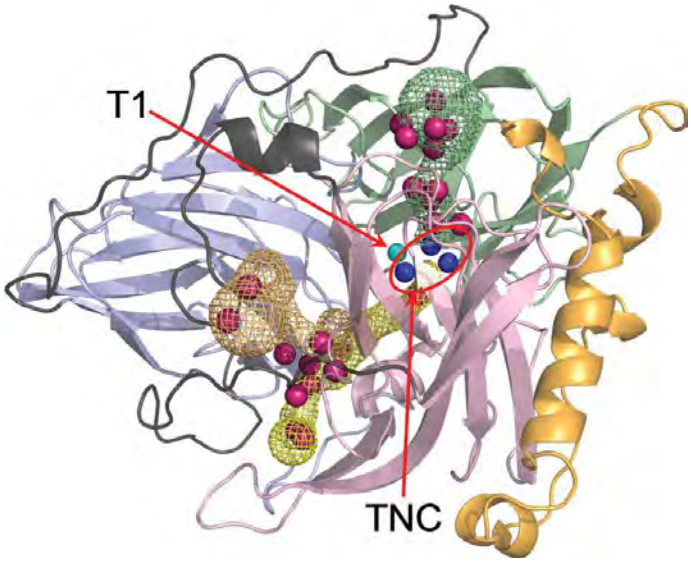

Figure 1.10: A cartoon representation of the X-ray determined crystal structure of BOx from *Myrothecium verrucaria* [81].

From the point of view of future application in biofuel cells BOx is more interesting than Lc because it retains its activity and catalyses O_2 reduction in pH close to neutral. Moreover, it is more resistant to chloride ions. Both of these features make BOx more suitable to be utilized in implantable devices.

Glucose oxidase

Glucose oxidase (GOx) is of a fungal origin, with *Aspergillus Niger* being the most utilised source of this enzyme. It catalyses β-D-glucose oxidation to D-glucono-δ-lactone. Later D-glucono-δ-lactone is further non-enzymatically hydrolyzed to gluconic acid [100]. GOx utilizes O_2 as an electron acceptor, with the simultaneous production of hydrogen peroxide [101]. Glucose oxidation with GOx would not be possible without a cofactor which is in this case flavin adenine dinucleotide (FAD). This cofactor is first reduced by glucose and then oxidised

by O_2, as described in the following reactions [102]:

$$\beta - D - glucose + \mathrm{FAD} \rightleftarrows D - glucono - \delta - lactone + \mathrm{FADH_2} \quad (1.3a)$$

$$\mathrm{FADH_2} + \mathrm{O_2} \rightleftarrows \mathrm{FAD} + \mathrm{H_2O_2} \quad (1.3b)$$

The pH optima of GOx vary from 5.0 to 8.6 [100], so it is appropriate for *in vivo* applications

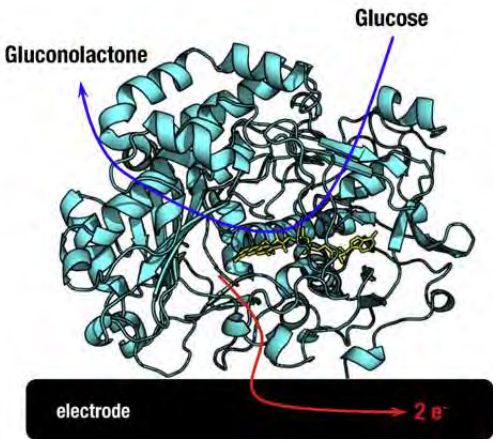

Figure 1.11: Structure of glucose oxidase from *Asperigillus niger* indicated as cyan ribbons, the flavin cofactor is indicated with yellow sticks [75].

such as electrochemical glucose sensors and biofuel cells [103]. Moreover, at least till 2011, all the commercial optical sensors relied on the use of this enzyme [102]. Apart from that GOx has a considerable industrial importance e.g. as food preservative and the production of gluconic acid or oral hygiene products [100, 101].

Glucose dehydrogenase

Glucose dehydrogenase (GDH) belongs to the family of oxidoreductases, as MCOx do. It can be found in a liver and different bacteria and where it is involved in glucose metabolism. GDH needs the presence of a cofactor to be able to catalyse the glucose oxidation. Thus, depending on the coenzyme, glucose dehydrogenase is classified into three types: i) NAD^+- and $NADP^+$-dependent (e.g. from *Gluconobacter suboxydans* and *Pseudomonas sporae*), ii) flavin adenine dinucleotide (FAD)-dependent (e.g. from *Aspergillus niger*) and iii) pyrolloquinoline quinone (PQQ)-dependent (e.g. from *Pseudomonas fluorescens*) [104].

GDH from *Pseudomonas sp.*, which was used in this thesis, is responsible for the catalysis of the following, oxygen-insensitive, reaction:

$$\beta{-}D - glucose + \mathrm{NAD(P)^+} \rightleftarrows D - glucono - \delta - lactone + \mathrm{NAD(P)H} + \mathrm{H^+}. \quad (1.4)$$

NAD and NADP stand for nicotinamide adenine dinucleotide and nicotinamide adenine dinucleotide phosphate, respectively. Both of them are cofactors for this type of GDH, so

one can say that this enzyme has a dual-cofactor specificity. It preferentially utilises NADP, whereas it binds NAD with lower affinity [105].

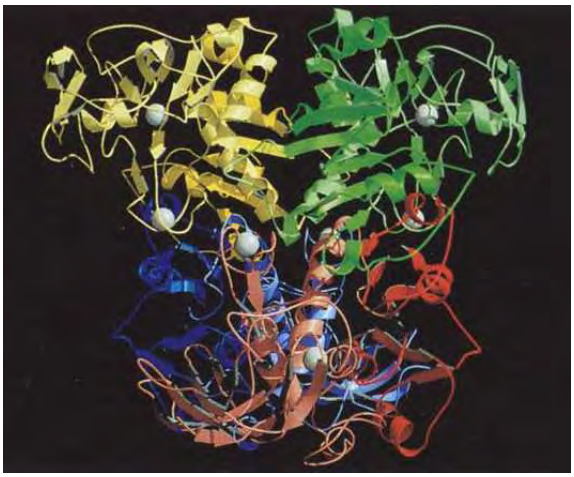

Figure 1.12: Schematic representations of the tetramer of GDH from *Thermoplasma acidophilum*, with each monomer shown in a different colour. Zinc atoms are depicted as spheres [105].

The optimum pH for GDH depends on its source, the kind of buffer and the kind of an electron acceptor [106], but generally it is in the range of 5 - 9. For example for GDH from *Bacillus megaterium* the optimum pH is 8.0 in Tris[6]/HCl buffer and 9.0 in acetate/borate buffer [107].

An example of the GDH crystal structure is presented in Figure 1.12. It is worth noticing four monomeric parts which build this enzyme, as well as the presence of Zn atoms.

At the end of this section I would like to mention two important issues concerning all enzymes. The first one is the use of a properly matched pH to the certain enzyme. Since the ionization state of the amino acids in the enzyme active site is dependent on pH, one can easily change the enzyme activity by changing pH. Thus pH plays an important role in maintaining the proper conformation of the biomolecules and most of them are only active within a narrow pH range [100].

The second issue concerns enhancing enzymes properties by genetic engineering by binding functionalities to surfaces [74]. Such a treatment is expected to tune the redox potentials of enzymes active sites and to facilitate electric communication at the interface between the enzyme and electrode [108]. It is also expected to obtain more stable enzymes. Thus it is understandable why Brito and Turner [74] underline the necessity of joining the knowledge of biologists, chemists, chemical engineers and materials scientists to improve the performance of bioelectrodes. The joined efforts of all of the listed scientists will lead to a development of better biodevices for electrical energy production.

[6]Tris stands for tris(hydroxymethyl)aminomethane.

1.3 Biofuel cells and biobatteries

Biofuel cells (BFCs) are devices comprising two electrodes (an anode and a cathode) which convert chemical energy into an electrical energy, where at least one of the electrodes [70] utilises bioelectrocatalysis. The reactants in these power devices are fed from external reservoirs [1]. Batteries contain the reactants and there is no possibility to feed them externally [1]. In this thesis I use the term biobatteries to describe the hybrids of BFCs and batteries. In non-scientific literature the BFCs are often called biobatteries [109,110] which is misleading. Here I use these two terms for different devices.

There are two main groups of BFCs - depending on the exploited biocatalyst - microbial and enzymatic. The microbial BFCs use whole organisms to catalyse the reactions occurring on the electrodes, while the enzymatic BFCs use specific enzymes. The first BFC was a microbial one, constructed by Potter in 1912 [111]. He generated electricity with the help of microbial cells placed on platinum electrode. The first example of an enzymatic-BFC was reported almost half a century ago by Yahiro *et al.* [112]. They used GOx on the anode which was connected to the platinum cathode. Apart from the above mentioned two types of BFC another hybrid design - a combination of microbial- and enzymatic-BFC - was also examined. An example of this type of a hybrid was reported by Schaetzle *et al.* who showed that a BFC with a microbial-bioanode can be improved by using an enzymatic cathode [113]. Since my thesis is about electrodes modified with enzymes, I will now focus only on the enzymatic-BFCs and enzymatic biobatteries.

The main advantages of enzymatic-BFCs in comparison with microbial-BFCs are: they do not require nutrients or biomass; the processes occurring on the electrodes can be more easily controlled; they generally produce higher current densities than microbial-BFCs; it is easier to miniaturise them [74,114]. These advantages are possible due to high catalytic activity of the enzymes and their smaller size in comparison with the micoorganisms. For example many oxidoreductases are able to increase the reaction rate by as much as 10^{14} times the rate. Moreover, oxidoreductases often have turnover rates on the order of 10^3 s^{-1} [72]. A comparison of electrodes with enzymes and electrodes comprising metal catalysts (such as Pt) clearly shows that the former can give lower overpotential at pH close to neutral. That in turn gives better power output of the BFC at pH similar to the pH of blood. Besides enzymes are less expensive than precious metals, which is another plus for enzymatic-BFCs.

On the other hand enzymatic-BFCs have several disadvantages. Among the most important are: the short lifetime of the enzymes and their low power density. Both of these issues are related to enzyme instability, electron transfer rate and enzyme loading [115]. Therefore for practical application of BFCs two main difficulties need to be overcome: i) finding the way to maximise power densities by understanding which important parameters affect the

BFC performance and ii) stabilizing[7] the enzyme so that it is active for a reasonably long operating time [74, 114]. A very good way to manage these tasks is to immobilize the enzyme on the electrode in an appropriate way. The proper immobilisation means providing the enzyme an orientation which makes it active and enabling the substrates to get to the active site. That is why the immobilization of enzymes is extensively studied since the late 1960s [116] and a vast majority of reports concerning enzymatic-BFCs in fact describe new ways of enzyme immobilisation.

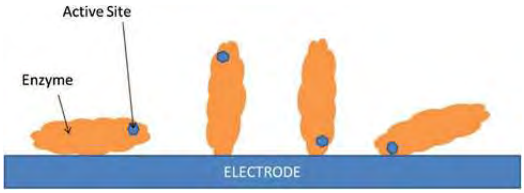

Figure 1.13: Schematic showing the importance of orientation on the electron tunneling distance from the active site to the electrode [70].

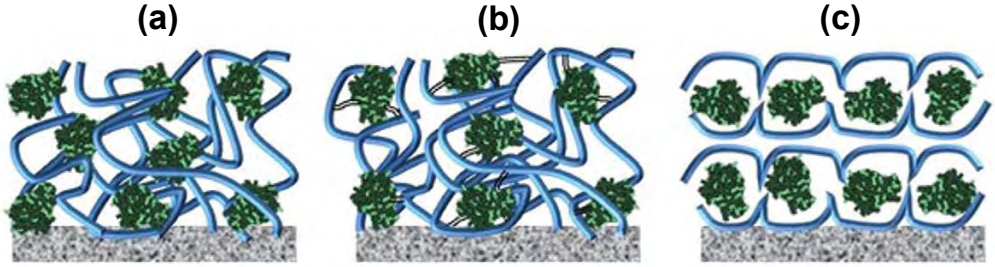

Figure 1.14: Enzymes immobilized on an electrode surface via (a) physical adsorption to a polymer, (b) covalent attachment to a polymer (as shown by the black and white tethers) or (c) encapsulation in polymer micelles. [117].

There are a few ways to immobilize the enzyme on electrode surface: i) adsorption, ii) covalent attachment, iii) encapsulation iv) and combinations of i), ii) and iii) [114, 118] (see Fig. 1.14). Physical adsorption is the easiest approach to stabilise the enzyme on the electrode surface. It utilises interactions such as: hydrophobic, ionic, van der Waals or the formation of hydrogen bonds between the enzyme and the electrode. The main drawback of this immobilisation technique is leaching out of the protein. It does not concern the covalent attachment approach, where the enzyme is covalently bound to the electrode material or to other enzyme molecules. Therefore covalent immobilisation often results in obtaining a better stabilised enzyme, in comparison with the adsorption approach. On the other hand the encapsulation retaining the proper orientation of the enzyme is more desirable method of enzyme stabilization than the adsorption and covalent attachment. The encapsulation prevents from leaching out the protein and it might improve its selectivity.

The use of nanomaterials for enzyme immobilisation can lead to obtaining improved stability and activity of the protein [115]. The most interesting properties of nanomaterials

[7]The enzyme stabilisation means preserving its unchanged native structure, which is equal to preventing enzyme denaturation [116].

from the point of view of this application are: large surface area, pores sizes tailored to the enzyme dimensions, multiple sites for interaction or attachment of proteins [118]. All of these properties make the use of nano-structured materials to be an expected milestone in overcoming the major obstacles in the development of powerful biofuel cells.

The literature concerning the enzymatic BFC preparation is so broad that it is not possible to briefly summarise it in this thesis. In Section 1.5.2 I will present a more detailed description of different ways of the enzyme and CNT entrapment on the electrode surfaces. The same or very similar immobilisation methods are used in the case of all biomolecules and nanomaterials. Thus most of the bioelectrodes to the BFCs can be obtained in the ways which will be mentioned in Section 1.5.2. Here I will restrict myself to presenting the most interesting examples of BFCs and biobatteries.

From my point of view the most interesting BFCs are the ones which were truly implanted in some living beings. These examples are the proofs that the field of interest of my thesis has already left the lab bench and was used *in vivo*.

The first example of an implanted BFC was developed in Cosnier's group and presented in 2010 [119]. The authors used a simple mechanical compression of graphite particles, selected enzymes and mediators to obtain the bioelectrodes in the shape of graphite discs. The bioanode comprised GOx, catalase and ubiquinone. The biocathode comprised polyphenol oxidase (PPO) and quinhydrone, and it was wrapped in a dialysis bag (to prevent quinhydrone diffusion). Both electrodes were packed in another dialysis bag which was permeable for oxygen and glucose. The constructed BFC was implanted in a retroperitoneal space of a rat and was operating for 3 months. The principle of the operation of this BFC was based on the oxidation of ubiquinol generated by GOx and a coupled reduction of quinone, which was in turn generated by PPO. The generated power had a peak of 6.5 μW at 0.13 V, which was equal to a maximum specific power of 24.4 $\mu W\,ml^{-1}$. Such a result is better than the requirements of pacemakers [120]. On the other hand the cell produced 2 μW for several hours, which was still not enough to power any implanted medical device. However, this BFC was a promising first small step to the further developments.

Miyake *et al.* constructed a needle-like BFC and inserted it in a rabbit's ear (see Fig. 1.15) [121]. The bioanode design was far more complicated than in the case of the cell obtained by Cosnier's group. It contained glucose dehydrogenase (GDH) and diaphorase as well as poly-L-lysine modified with the enzyme cofactor NAD^+ and with the mediator - vitamin K_3. Moreover, the bioanode comprised ketjenblack (KB)[8] and a material which immobilised all the compounds on the surface of a gold wire - poly(ethylene glycol) diglycidyl ether. The modified wire was inserted into a plastic needle filled with agarose mixed with buffer. To get a biocompatibile anode, the needle was coated with 2-methacryloyloxyethyl phosphorylcholine

[8]KB is a kind of amorphous carbon which is electroconductive and has a very high surface-are-to-volume ratio.

(MPC)-polymer. The gas-diffusion (air-breathing) biocathode was located on the top of the needle and had an ionic contact with the anode via the gelled agarose mix. The biocathode was made of a Toray carbon paper coated with KB, poly(tetrafluoroethylene) (PTFE) and bilirubin oxidase. As prepared biocathode was in a direct contact with the air and due to that it was able to utilise more oxygen than it would be possible inside the rabbit's vain. The power output of this needle-like BFC reached 115 $\mu W\,cm^{-2}$ (26.5 μW) at 0.34 V [121]

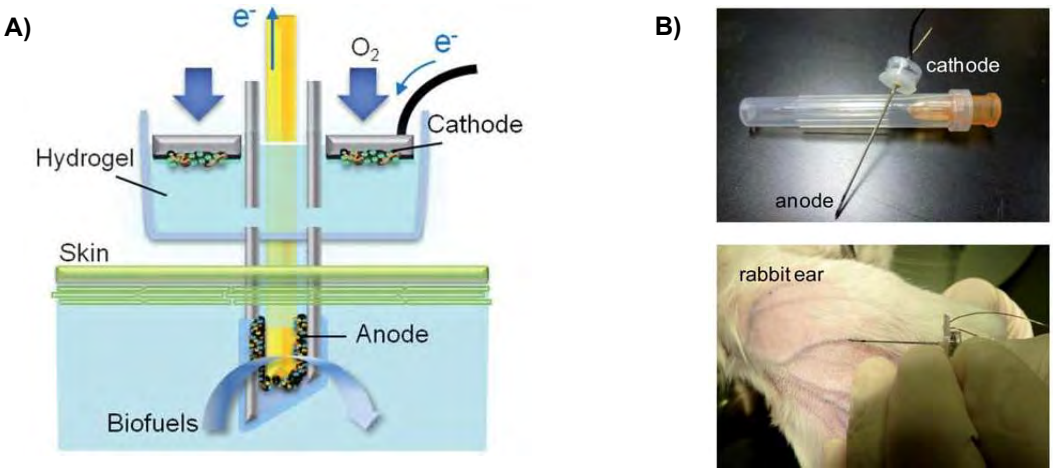

Figure 1.15: A) Schematic structure of a biofuel cell designed to utilize biochemical energy in living organisms. B) Photographs of the assembled biofuel cell for power generation from a rabbit vein [121].

which was a ca. 4 times better result than in case of the BFC implanted in the rat [119].

Next a few examples of BFCs implanted in living beings were constructed by Katz's group. Each of these BFC was prepared in the same way, but they were implanted in different animals: a snail [122], clams [123] and lobsters [124]. As a substrate for both bioelectrodes a buckypaper[9] was used. The compressed CNTs were modified with a cross-linker (1-pyrenebutanoic acid succinimidyl ester, PBSE) so that they were bound via π-π stacking with the polyaromatic part of PBSE. The PBSE was also bonded to the selected enzyme. The Katz group chose the pyrroloquinoline quinone-dependent glucose dehydrogenase (PQQ-GDH) as an enzyme responsible for glucose oxidation. PQQ-GDH was immobilised on the buckypaper/PBSE to form a bioanode. To get a biocathode laccase was immobilised on the same substrate. The first BFC obtained in this way was implanted in a snail which contains glucose in its hemolymph. The cell was working as long as the mollusc was treated properly. A proper treatment of the snail made it to produce glucose which was the BFC fuel. The maximum power output obtained from this BFC reached ca. 30 $\mu W\,cm^{-2}$ (7.45 μW) [122], so very similar to the one reported for the BFC implanted in the rat [119]. It was also similar to the maximum power output of the BFC implanted in the clam - 40 $\mu W\,cm^{-2}$ (10 μW) [123]. But in case of the clams used as a source of glucose the Katz group went a bit further with their work. They showed that a stack of BFCs powered an electronic device. They connected three BFCs in parallel and charged a capacitor. Then the capacitor was discharged on a

[9]Buckypaper is a conductive material made of densely packed CNTs, see the section 1.5.2.

DC-rotary motor resulting in its rotation.

The most recent example of the BFC reported by the Katz group was implanted in lobsters. One such a cell gave a maximum power output of 640 $\mu W\,cm^{-2}$ (160 μW) [124]. After connecting two BFCs in series the authors used them for powering a digital watch for over an hour. Moreover, when five of those BFCs were connected in series and were used in a system mimicking human physiological conditions, they could power a pacemaker. That was the first reported example of the pacemaker activation by the BFC working in the conditions closely similar to the conditions found *in vivo*.

The final example of an implanted BFC was presented by Scherson's group [125]. This power device was inserted in a cockroach (*Blaberus discoidalis*). Due to the presence of trehalase oxidase and glucose oxidase at the bioanode the BFC utilised the disaccharide trehalose (present in the hemolymph of a living cockroach) as a fuel. Bilirubin oxidase was immobilised on the biocathode to perform the oxygen reduction. Both electrodes needed the presence of osmium complexes as mediators of the oxidation and the reduction reactions. The maximum specific power density of this BFC reached ca. 55 $\mu W\,cm^{-2}$ at 0.2 V and decreased ca. 5 % after operating for 1.5 h.

Very recently Wang's group reported a non-invasive way of energy harvesting from the human perspiration [126]. They constructed a BFC which utilised lactate as a fuel. Because lactate is produced by humans and it is present in a sweat, this BFC does not need to be implanted in a person to generate electrical energy. Lactate oxidase and CNTs functionalized with tetratiafulvalene (TTF) were immobilised on the bioanode. Platinum black was used as a cathode responsible for O_2 reduction. Both electrodes were prepared by the screen-printing method and were supported on a Gore-Tex textile. The assembled BFC looked like a tattoo and was easily transferable on the human skin. The power output was dependent on the person who was testing the BFC performance. The highest maximum power output was obtained with less fit individuals - 70 $\mu W\,cm^{-2}$.

Due to the low power outputs BFCs are still not used commercially for powering useful devices. However, so far at least the Sony Corporation made an attempt and co-financed research which resulted in obtaining a very well performing BFC (P_{max} = 1.45 $mW\,cm^{-2}$ at 0.3 V) [127]. The bioanode comprised GDH, vitamin K_3, diaphorase and NADH deposited on carbon fibre sheets. BOx and ferricyanide were immobilised on the biocathode. A stack of four of these BFCs were successfully used for operating a toy car or portable music player for at least 2 h. However, due to the two-compartment design and the size of this power source it would not be possible to implant it in some small animals. But glucose-powered iPad with this BFC seems to be an interesting solution for an external use of this power device.

The presented examples of BFCs generate little powers when one considers powering big electronic devices. However, the obtained powers have been increasing and hopefully it will

be possible in future to use BFCs for powering implanted medical devices such as nerve-simulators, pacemakers and drug-delivering pumps. More about BFCs can be found e.g. in the following reviews: [1, 70, 75, 78, 114, 128–130].

1.4 Electrochemical biosensors

According to recommendations given by the International Union of Pure and Applied Chemistry (IUPAC) an electrochemical biosensor is "a self-contained device, which is capable of providing specific quantitative or semi-quantitative analytical information using a biological recognition element (biochemical receptor) which is retained in direct spatial contact with an electrochemical transduction element" [131]. Being self-contained in this case means that all parts of the biosensor are integrated and form the same unit. Examples of biological recognition elements are: enzymes, whole cells, membrane receptors and plant or animal tissues. Thus the process occurring on the sensor is the previously described bioelectrocatalysis (see Section 1.2). The electrochemical biosensor is one among several types of chemical biosensors such as optical, piezoelectric and thermal biosensors.

1.4.1 Self-powered biosensors

Self-powered biosensors are these biosensors which do not need an external power source to convert an input form the analyte into a signal [132]. The first example of such a device was described by Katz and Willner in 2001 [133][10]. They presented a new concept of a self-powered biosensor comprising a BFC generating different open circuit voltage (OCV) dependent on the concentration of the fuel. Depending on the enzyme immobilized on the surface of a bioanode (GOx or lactate dehydrogenase, LDH) either glucose or lactate was used as an analyte/fuel. In both cases the same biocathode was used - containing immobilised cytochrome c/cytochrome oxidase (Cyt c/COx) responsible for O_2 reduction (Fig. 1.16). In the absence of the fuel the BFCs did not generate any voltage. The OCV increased logarithmically with the increase of the fuel concentration showing expected Nernstian dependence. Both BFCs produced very little power to drive a device to show the change of OCV. Thus the term "self-powered" was rather assigned to the fact that the cell was able to give any different output related to the change of the fuel concentration.

Following the Katz and Willner's definition a few different types of self-powered biosensors were presented, mainly by Dong's, Minteer's and Nishizawa's groups. An example of mitochondrial bioelectrocatalysis harnessed for detecting the presence of explosives was presented by Minteer's group [136]. In the absence of nitroaromatic compounds the bioanode

[10] At the same time patent applications concerning self-powered biosensors started to be submitted to patent offices [134, 135].

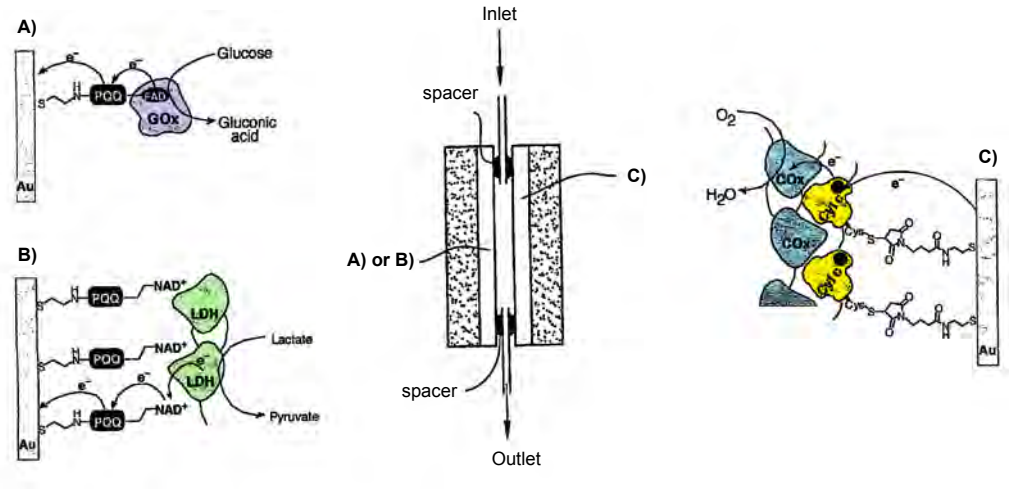

Figure 1.16: Configuration of the self-powered BFC-based biosensors composed of: A) PQQ-FAD/GOx-functionalized anode utilizing glucose-analyte as a fuel or B) PQQ-NAD^+/LDH-functionalized anode utilizing lactate-analyte as a fuel, and C) Cyt c/COx-functionalized cathode utilizing O_2 as an oxidizer in combination with either the anodes A) or the anode B) [133,134]. PQQ stands for pyrolloquinoline quinone

containing mitochondria was inhibited by oligomycin and was not able to oxidize pyruvate present in the solution. The addition of explosives caused the decoupling of the inhibitor which resulted in power generation by the BFC. The power output was not related to the concentration of explosives. The sensor acted rather like a binary device and detected the presence of nitrobenzene in a solution with a concentration as small as 1 fM.

The first device which in my opinion is an example of a truly self-powered biosensor was presented by Hanashi *et al.* in 2009 [137]. They used a capacitor as a transducer coupled to a light-emitting diode and connected it to a glucose/O_2 BFC. The BFC charged the capacitor with a rate proportional to the fuel concentration. Then the capacitor was discharged through a LED. As a consequence the LED blinked with a frequency indicating glucose concentration. The so called BioCapacitor did not need any external devices such as a potentiostat or a multimeter to convert an analytical signal into a signal visible by naked eye. Thus I would suggest to call it the first "truly self-powered biosensor". The same idea of charging a capacitor by a BFC (glucose/O_2 or fructose/O_2) was further used by Nishizawa's group [121,138], but surprisingly without referring to Hanashi's paper.

In 2010 Deng *et al.* [139] introduced another interesting approach to self-powered biosensing - utilising inhibition of the biocatalyst. The authors presented a way of cyanide sensing by using a glucose/O_2 BFC. In this case the decrease of the power output of the BFC was caused by the inhibition of laccase by CN^- ions. As a result a linear dependence of the power output on the CN^- concentration was registered. In this case the signal from this biosensor could be analysed with the use of a potentiostat.

So far the self-powered biosensors were used for sensing glucose [133,137,140], acetylthiocholine [141], lactate [133], nitroaromatics [136], cyanide [139], Hg^{2+} [142], ethylenediaminetetraacetic acid (EDTA) [143], fructose [121], acetaldehyde [144] and herbicides [145]. My

thesis added to this list a self-powered sensor for ascorbic acid (see Chapter 6).

1.5 Electrochemistry at electrodes modified with CNTs

Carbon materials have been extensively used for electrode modification since around 1960s [146, 147]. The main advantages of using these materials in electroanalytical chemistry are ready availability, chemical stability, wide electrochemical potential window in aqueous solutions, biocompatibility and the possibility of forming strong covalent bonds to a variety of surface modifiers [148, 149]. CNTs have also been considered as an excellent material for electrode modification. This is mainly due to electronic properties of CNTs (see Section 1.1.1) and their high aspect ratio. Interestingly, together with the growing interest in using CNTs in electrochemistry, some controversies concerning their wonderful properties have appeared.

In this section I will describe different attempts of CNT electrode preparation and the most interesting applications of these electrodes in electroanalysis and bioelectrocatalysis. Moreover, I will point out the most important uncertainties about CNT electrochemistry.

1.5.1 CNT electrodes in electroanalysis

The preparation of the first electrode modified with CNTs was reported in 1996 by Ajayan's group [150]. It was made by packing a paste made of unpurified CNTs mixed with bromoform into a glass tube. The electrode was not characterised in a very detailed way and it was used for dopamine sensing. Moreover, it was suggested for *in vivo* for neurotransmitters sensing. During the few years after that paper CNTs were not used very often for electrode preparation. The explosion of interest in electrochemistry with CNTs appeared around 2002 when Lin's group observed stable NADH detection at low potential at a CNT-modified glassy carbon electrode [151].

Electrodes modified with CNTs can have randomly distributed tubes or tubes which are organised in a defined way. The random distribution of CNTs is easier to obtain and can be achieved by a number of ways, such as [152, 153]:

- deposition of CNTs without any binders [154–156],
- dispersing CNTs with a binder, e.g. Nafion [157], dihexadecyl hydrogen phosphate [158] or Teflon [159],
- making a "nanotube paper" (a buckypaper) by vacuum filtration of the suspension of purified CNTs [160],
- embedding CNTs with a polymer [161] or a sol-gel silicate matrix [162].

Different CNT pastes, composites or mixes can be deposited on the electrode surface in several ways, such as drop coating, screen printing, inkjet-printing, layer-by-layer assembly method or by spraying. Moreover, CNT thin film modified electrodes can be obtained by electrodeposition [163, 164] or electrophoretic deposition [165]. All the deposition methods listed so far give electrodes with randomly distributed CNTs. To achieve a better control over the CNT orientation a self-assembly phenomenon [166] or a direct growth of the tubes on the electrode surface was used [167–169]. The directly grown tubes can cover the whole area of the electrode or can form an array of microelectrodes made of vertically aligned CNT. The main advantage of the electrodes with a controlled distribution of CNTs is an improved electron transfer, in comparison with the electrodes with randomly oriented tubes.

The number of analytes which were studied using CNT-electrodes is huge and includes compounds such as: hydrogen sulfide [170], morphine [171], carbohydrates [172], nitric oxide [173], insuline [174], uric acid [175] and capsaicin [176]. Networks of SWCNTs appeared to be very effective for trace level CV measurements because they are relatively simple to prepare and they allow to detect analyte concentration at levels inaccessible to other electrode materials [177].

One of the most elegant ways of using CNTs in electroanalysis, in my opinion, is the detection of dopamine (DA) recently reported by Sansuk *et al.* [178]. In this example a network of SWCNTs was first grown on silicon substrate using catalyzed CVD method and then used as a microfluidic electrode. A specially designed microfluidic cell (Fig. 1.17) with this CNT-electrode was used in a flow injection analysis (FIA) to detect DA with a limit of detection of ca. 5 pM in 50 µl.

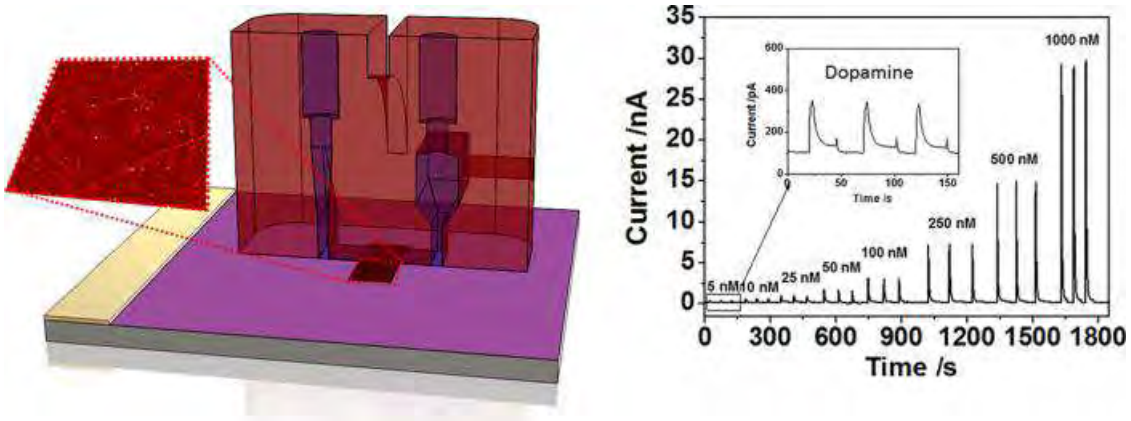

Figure 1.17: Left: A microfluidic cell with a CNT-electrode and (inset) a 3D AFM profile (3 µm × 3 µm) of a typical SWCNT network. Right: Typical FIA amperometric signal for the detection of 50 µl injection volumes of DA in 10 mM PBS pH 7.4 at concentrations in the range of 5 – 1000 nM. The inset shows the triplicate current response of 5 nM DA [178].

Usually the use of CNTs in electroanalysis is explained by favourable low detection limits, increased sensitivity, decreased overpotentials and a resistance to surface fouling [179, 180]. However, not all the authors praising their CNT-electrodes are aware of the influence of impurities or CNT defects on the electrode performance. The impurities such as amorphous

carbon or metal nanoparticles (NPs) used for CNT growth can be responsible for changing the electrochemical response of particular redox systems [148]. The NPs can greatly enhance the response of the electrode [181–183] and moreover their influence is still noticeable after a purification of CNTs [184, 185].

Some of the favourable electrode features can be a result of CNT acid purification process. Usually this process not only removes impurities from the nanotubes but also cuts them and leaves open ends and damaged sidewalls [148]. The CNT damages introduced during the acid-treatment lead to the formation of oxygen-containing groups, e.g. ketones and carboxylic acids, which in turn can facilitate certain electrochemical reactions [186]. Moreover, what is probably even more important, the acid-treatment introduce also so called edge-plane-like sites on CNTs which act as edge plane pyrolytic graphite (EPPG). Pumera *et al.* showed that EPPG-like sites present on MWCNTs increased the rate constant of electron transfer for the ferrocyanide/ferricyanide by over two orders of magnitude [187]. On the other hand the presence of the sidewall defects causes changes in electronic states of CNTs which usually results in the increase of CNT resistivity [148]. Thus one should bear in mind above mentioned findings during the fabrication of CNT-electrodes to be able to properly explain their performance.

The main uncertainty about the CNT electrochemistry concerns the question "*What is more active: nanotube tips or its sidewall?*". The answer is still under a debate. Initially it was assumed that only the CNT tips are active, whereas the sidewalls are inactive. This assumption came from the experiments conducted on MWCNT-electrodes (presented below) and were unreasonably transferred on SWCNT-electrodes.

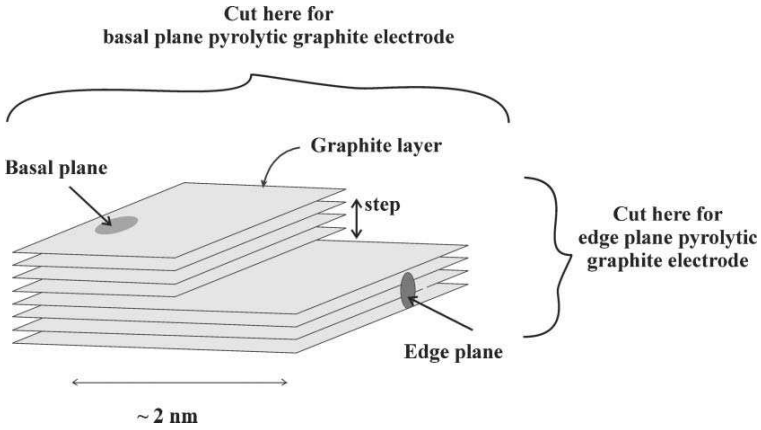

Figure 1.18: A schematic representation of the edge plane and the basal plane pyrolytic graphite electrodes derived from highly ordered pyrolytic graphite (HOPG) [180].

A significant contribution to the studies on MWCNT-electrodes was made by Compton's group. First they demonstrated that the use of CNTs gives similar effects on an oxidation of NADH, epinephrine, and norepinephrine as a graphite powder modified basal plane pyrolytic graphite (BPPG) electrodes [188]. Then they showed that the CNT sidewalls are similar to the BPPG and the tips behave like the EPPG (Fig. 1.18). Compton's group suggested that

only the MWCNT sidewalls are responsible for the observed ET activity [189,190]. They also proved that the electrode kinetics at EPPG are at least three times faster than at BPPG [190]. Moreover, they indicate that it is possible to easily introduce the EPPG-like defects on the BPPG and (in this way) make it more electroactive [191]. By analogy it is possible to make the sidewalls of MWCNTs more active, but still their electroactivity is assigned to the presence of the EPPG-like sites [180]. Furthermore Compton's group also showed that the CNT defects such as terraces are voltammetrically inert [180]. So the main conclusion drawn from the work done in Compton's group is that there is nothing extraordinary in MWCNTs from the point of view of electrochemistry. The electroactivity of MWCNTs has its origin in the presence of EPPG-like sites and these sites have been known for a long time.

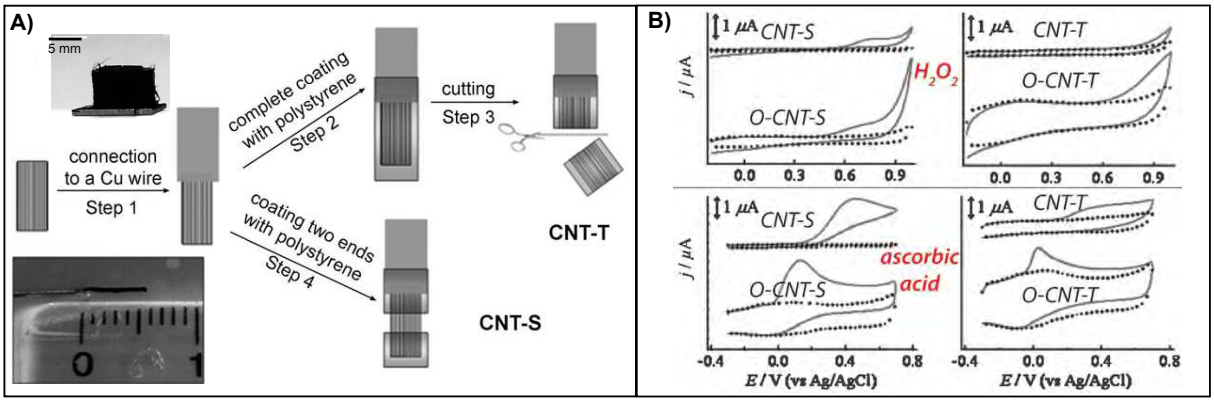

Figure 1.19: A) A schematic representation of the procedure for preparing the CNT electrodes with only the nanotube tip (CNT-T) or sidewall (CNT-S) accessible to electrolyte. The insets show a digital photographs of as grown CNTs and a nanotube electrode prepared with an aligned superlong CNT bundle connected to a copper wire [192]. B) CVs for H_2O_2 and ascorbic acid oxidation at CNT-S and CNT-T electrodes with or without oxygen surface functionalities [148].

An interesting study was presented by Dai's group who used super long VACNTs (5 mm long, Fig. 1.19 A) to check electrochemical response of different redox species on the nanotube sidewalls (CNT-S) or nanotube tips (CNT-T) [192] before and after introducing oxygen-functionalities (O-CNT). It was shown that the electrochemistry of investigated probes is facilitated only in certain examples (Fig. 1.19 B)). E.g. ascorbic acid oxidation was promoted by O-CNT on both CNT-S and CNT-T [148]. On the other hand CNT-T were not active towards H_2O_2 oxidation.

Another studies lead to contradictory conclusions concerning SWCNTs. On the one hand Dekker's group showed that SWCNTs have electroactive sidewalls and that no impurities were needed for an electron transfer to the used redox specie [193]. On the other hand Compton's and Gooding's groups showed that the electrochemical properties of SWCNTs arise from their tips which have EPPG-like defects [194,195].

In contrast to what had been reported previously, a very surprising result was recently presented by Unwin's group. They developed a new technique called scanning electrochemical cell microscopy (SECCM) [196,197] and used it for spatially resolved electrochemical imag-

ing of the isolated BPPG [198]. The performed electrochemical measurements showed unambiguously that ET is fast (close to reversible) for the two most studied redox couples ($[Ru(NH_3)_6]^{3+}$ and $[Fe(CN)_6]^{4-/3-}$). The authors' comment on the BPPG performance was: "After all, it's active". Their finding made a big impact on our understanding of not only the highly oriented pyrolytic graphite (HOPG) but also on other related sp^2 materials, such as CNTs and graphene.

Another example of studies done by Unwin's group, which again was an turning point in understanding the performance of CNTs, was published recently [199]. This time the authors investigated forests of SWCNTs using the SECCM. The results showed that both closed ends of CNTs and CNT sidewalls promote fast electron transfer. The ET was observed without any activation or processing of CNTs, what was contrary to the former models present in the literature [200].

After all above mentioned contradictory observations the question arises why some groups claim that CNT sidewalls are active only when they have the exposed EPPG-like sites, while other groups are able to show that even BPPG-like sites are electroactive? Is this divergence a result of using different experimental techniques which give the data interpreted in a slightly different way? Or it is a result of using CNTs prepared not in exactly the same way? One can say that the problem with the different results might be underlain by an inappropriate interpretation of the obtained data.

Compton's group has drawn the electrochemists' attention to the following issue - the models describing diffusion on a naked and modified electrode can be different [201]. The semi-infinite planar diffusion model is a proper model for interpreting the kinetics of the electron transfer at the naked (flat) electrode. However, the CNT modified electrode is typically porous and it is possible that pockets of solution are trapped between the layers of CNTs. Then oxidation of electroactive species on such a CNT-electrode should be described by the model of a thin layer cell of high electrode area. The main difference between these two models is that the thin layer model predicts a smaller peak-to-peak separation than the semi-infinite diffusion model. Thus some electrochemists who do not take the thin film model into account can make a conclusion that their CNT-electrode shows faster kinetics[11] than the naked electrode so it shows electroactivity. All in all Compton's group showed how important is a correct interpretation of the obtained voltammetric data.

Currently the biggest interest in CNT modified electrodes is in the properly matched way of CNT functionalization which would lead to obtaining the electrodes of desirable properties. This nanoengineering of electrodes can be done by the use of various CNT modifiers, such as: organic compounds and functional groups (polymers, DNA, proteins, oxygen

[11] "The diagnostic criterion for the faster electrode kinetics is often simply based on the peak-to-peak potential separation of the forward and reverse waves in the cyclic voltammetric experiment" [201].

functional groups, etc.), inorganic materials (metal NPs, metal oxides, etc.) and organic-inorganic hybrids [202]. An interesting example of an electrochemical sensor with a SWCNT-DNA hybrid was presented by Guo *et al.* [203]. In the absence of Hg^{2+} ions the nanotubes wrapped by single stranded DNA (ssDNA) were not adsorbed on the Au electrode modified with self-assembled monolayer (SAM) of alkanethiol. At that state no redox current was generated at the electrode immersed in ferrocenecarboxylic acid (FcCOOH) solution. The addition of Hg^{2+} ions caused the removal of the ssDNA from the SWCNT sidewalls and the formation of double stranded DNA (dsDNA)[12]. Then SWCNTs assembled on the SAM and mediated the ET between electroactive indicators and the electrode (Fig. 1.20). The obtained sensor was ultrasensitive, with limit of detection of 16.3 fM.

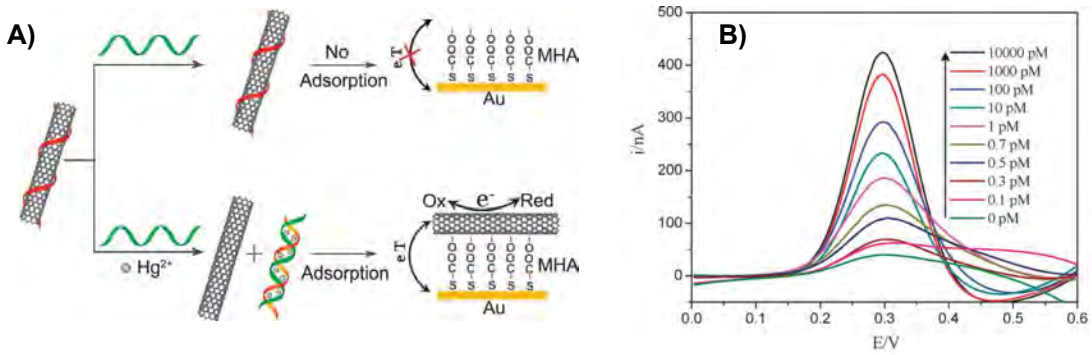

Figure 1.20: A) A scheme of an electrochemical sensing strategy for the detection of Hg^{2+} ions. B) Typical differential pulse voltammetry responses for different Hg^{2+} concentrations [203].

More about the functionalized CNTs used in the electroanalytical chemistry can be found in the following reviews: [205–214]. The most interesting reports from the point of view of this thesis treating of the sol-gel composites with CNTs [153, 215, 216] and the bioelectrodes with CNTs and enzymes will be wider discussed in the next subsection.

1.5.2 Bioelectrodes with CNTs

The interest in immobilisation of e.g. proteins and enzymes on the electrode surface comes from the possibility of obtaining high selectivity (unique recognition) and sensitivity to specific molecules [202]. The selective bioelectrocatalysis achieved by this modification is desired to construct e.g. effective sensors and bioelectrodes to biofuel cells.

Because of the unfeasibility of direct stable immobilisation of the proteins and enzymes on the electrode surface there is a need of using materials which form a conductive support holding the biomolecules. Nanomaterials are very good examples of such modifiers because they are able to increase the electrode surface area, conductivity and electrode ability for the ET. Moreover, they can decrease an overpotential for coenzyme/cofactor electrochemical

[12] Ono's group demonstrated that Hg^{2+} ions possess an unique property to bind specifically to two DNA thymine bases (T) and form stable base pairs (T-Hg^{2+}-T) [204].

regeneration [70]. Carbon nanotubes are one of the most commonly used nanomaterials for the bioelectrode preparation. They act as electrical bridges between the electrode surface and the biomolecule [202]. It was showed that direct ET reactions of redox-active biomacromolecules can be much improved by the use of CNTs [210, 217–219]. Besides the enhanced electrochemical activity of the electrodes they can also be helpful in accumulation of some biomolecules [220] and decreasing surface fouling [151, 221].

So far CNTs have been used together with biomolecules such as enzymes, mitochondria, deoxyribozymes and living cells to modify electrodes further applied as biocathodes, bioanodes, sensors, batteries and electrodes in solar cells [70]. Here, I will focus on CNT electrodes with enzymes and thus I will extend the topic started in Section 1.3.

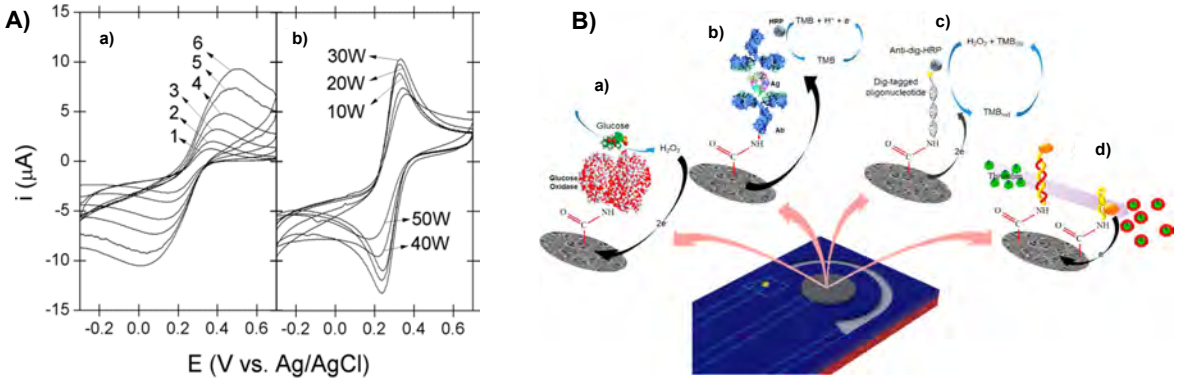

Figure 1.21: A) a) CV characteristics of the SWCNT before the O_2 plasma treatment at $\nu = 10$ (1), 20 (2), 50 (3), 100 (4), 200 (5), and 300 (6) mVs^{-1}, b), and after the O_2 plasma treatment at various plasma power ($\nu = 100$ mVs^{-1}), ferrocyanide/ferricyanide redox couple. B) a) A schematic illustration of glucose sensing mechanism occurring on the pfSWCNT/GOx electrode. b)-d) Schematic drawings of sensors prepared with different biomolecules attached to the pfSWCNT-electrode in the same way as GOx in an example a) [222].

The most reliable method of permanent biomolecule immobilisation on CNTs is covalent cross-linking [222]. This way of immobilisation requires CNT functionalization - most often with carboxylic groups. There are two main ways of introducing -COOH groups on the CNTs: oxidative acid treatment and exposure to a plasma atmosphere. Min's group used the second approach to obtain CNT-based devices for electrochemical biosensing [222]. They constructed a miniaturised three-electrode system where the working electrode (WE) was covered with O_2 plasma treated SWCNTs. Due to the plasma treatment the WE had ca. six times larger effective area than the untreated electrode. Moreover, the plasma functionalized tubes (pfSWCNTs) could easily be exploited for covalent binding of biomolecules. In this example [222] the pfSWCNT WE was first immersed to a solution containing 1-ethyl-3-(3-dimethylaminopropyl) carbodiimide (EDC) and N-hydroxysulfosuccinimide (sulfo-NHS). Due to such treatment several biomolecules (GOx, *Legionella*-specific antibody, *Legionella pneumophila* (*L. pneumophila*)-originated probe DNA and a peptide aptamer) could be covalently immobilised on the CNTs via EDC/sulfo-NHS chemistry. The obtained electrodes acted as sensors for: glucose, *Legionella*, *Legionella pneumophila* and thrombin (Fig. 1.21B a, b, c and d respectively).

Another example of the covalent immobilisation of biomolecules to CNTs was shown by Rusling's group [218]. They utilised amide linkers to bind horseradish peroxidase and myoglobin to oxidised ends of SWCNTs forest standing on the electrode surface. The modified electrode acted as a hydrogen peroxide sensor with a detection limit of ca. 100 nM.

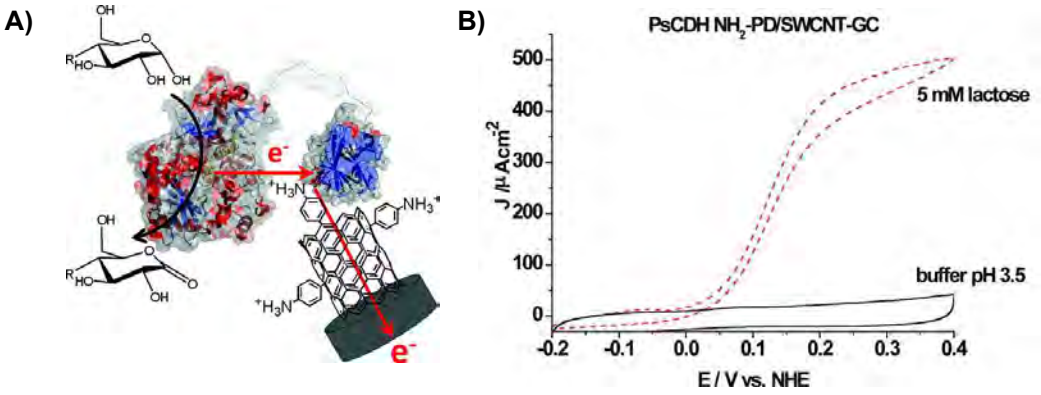

Figure 1.22: A) A scheme of lactose oxidation on the GC electrode modified with SWCNTs with covalently bounded cellobiose dehydrogenase (PsCDH). B) CV of a PsCDH NH_2-PD/SWCNTs-GC electrode in the presence of 5 mM lactose (red) and in the absence of substrate (black). 0.1 M acetate buffer, pH 3.5, scan rate 1 mV s^{-1} [223].

Tasca. *et al.* used a way of SWCNT modification by *in situ* generated functionalized aryl diazonium species[13] to steadily immobilize cellobiose dehydrogenase (CDH) from *Phanerochaete sordida* (PsCDH) [223]. The SWCNTs were first adsorbed on a glassy carbon electrode (GC) and then functionalized by the use of p-aminobenzoic acid (COOH-PD) and p-phenylenediamine (NH_2-PD), see Fig. 1.22. The obtained covalent functionalization gave a very efficient DET between the enzyme and CNTs. The oxidation current density was the highest among all which were reported before for an oxidizing enzyme working without the mediator. Moreover, the presented way of PsCDH immobilization enhanced the enzyme stability - there was only 15 % decrease of the current after 50 hours of continuous cycling (scan range: from -0.2 to 0.4 V, $\nu = 0.1$ mV s^{-1}).

Another way of enzyme immobilization is the use of a sol-gel method. Thank to this approach one can obtain a hybrid of an inorganic/organic material which is usually composed of a porous silicate matrix encapsulating the biomolecules. The main advantages of using the sol-gel process are: (i) the biocompatibility of the inorganic material with the enzyme, (ii) retaining or enhancing the enzyme activity, (iii) the possibility of obtaining the desired pore size distribution of the matrix, (iv) thermal stability of the matrix, (v) prevention of enzyme leakage, (vi) the ease of obtaining these hybrid materials [225] and (vii) an extreme pH-protectability of enzymes [226].

The first attempts to immobilize biomolecules in a silica. matrix were described almost 60 years ago [227, 228]. Then colloidal silicic acids were used as the precursors for the formation of the porous silica. Currently the term sol-gel process is rather restricted to the use

[13]This method of SWCNT functionalization was developed by Bahr and Tour [224].

of silicon alkoxide precursors. These precursors undergo hydrolysis and condensation [229], and form polymeric silicates with a structure controlled e.g. by the catalyst used in the process, temperature and humidity. The first example of enzymes encapsulated by the sol-gel process was reported by Mosbach's group [230]. They imprinted horseradish peroxidase and GOx in silica. coated with sol-gel made from a mix containing alkoxides such as bis(2-hydroxyethyl)aminopropyltriethoxysilane and tetraethoxysilane. The obtained hybrid materials were stable and allowed the enzymes to retain from 10 to 40 % of their activity. The authors correctly predicted already in 1985 that in the future organic silanes would find an increased use in solid state biochemistry.

A new class of composite sol-gel materials with CNTs or CNTs and enzymes was introduced by Bachas' group [162, 231]. They used the sol-gel process for the enzyme (L-amino acid oxidase) encapsulation on the electrode surface. The conductive CNTs were added to this composite to facilitate the ET. The enzyme retained ca. 40 % of its activity over 1 month and the obtained modified electrode was used as a biosensor (Galavas *et al.* [231]).

After Galavas' work a big number of enzymes were immobilised in sol-gel/CNT composites, e.g.: GOx [232], laccase [233], BOx [234], GDH [235,236], D-sorbitol dehydrogenase [237], diaphorase [236], acetylcholinesterase and choline oxidase [238]. This way of electrode modification is still developing and most likely the sol-gel method will long remain as one of the most important ones for the bioelectrode preparation.

One of the laccase mediators is 2,2'-azinobis(3-ethylbenzothiazoline-6-sulfonate) (ABTS) [239]. Usually it is present in the electrolyte in which the biocathode is immersed. So far a few examples of ABTS immobilisation on the CNT-modified biocathodes has been presented, e.g. with Nafion [240] or polypyrrole [241]. The first example of such encapsulation in a sol-gel silicate matrix was presented by Opallo's group [233]. They immobilised MWCNTs in the silicate matrix, adsorbed ABTS on the tubes and then coated the electrode with thin film of the same type of sol-gel with Lc. Although the obtained system was not very stable, this method of electrode modification was relatively simple and showed a new direction toward obtaining biocathodes with a mediator.

An interesting example of a method used for obtaining a silica/CNTs/enzyme hybrid material via a biomimetic process was presented by Johnson's group [242]. They immobilised GOx by a one-step silicification reaction (a rapid ambient precipitation of silica) catalysed by lysozyme. Lysozyme is one of the biomolecules responsible for silica. formation. In this example it was coimmoblized with a chosen enzyme and formed a mechanically stable material which allows to retain a high level of the enzyme catalytic activity. Due to the biosilicification the authors got a system revealing direct bioelectrocatalysis of glucose oxidation (see Fig. 1.23).

The idea of the utilisation of liquid crystals (LQs) for enzyme immobilization was developed by Bilewicz and co-workers [243–245]. Inter alia they described a few approaches to the

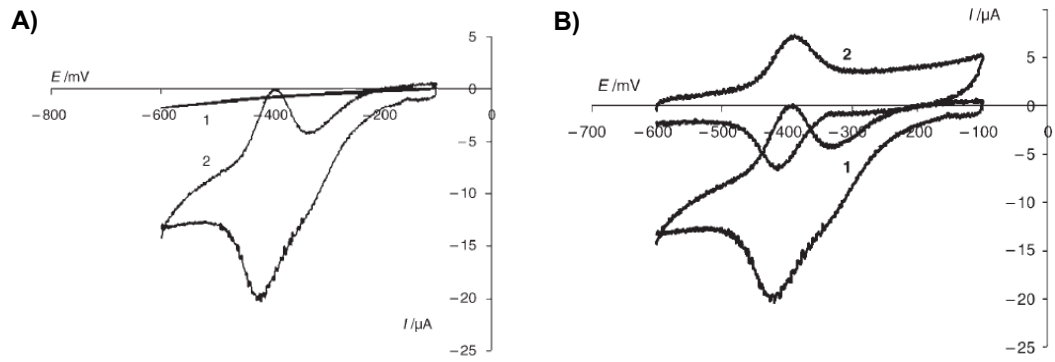

Figure 1.23: A) CVs of GOx modified electrodes: GOx in silica. (line 1); GOx and CNT in silica. (line 2). (KCl in phosphate buffer, $\nu = 20$ mV s^{-1}.), B) CVs of GOx and CNT in silica. in the absence (line 1) and presence (line 2) of 40 mM glucose, $\nu = 20$ mV s^{-1}) [242].

utilisation of CNTs in this type of hybrid material. The nanotubes were mainly used to enhance the electron transfer between the electrode and the enzyme active centre. Stolarczyk *et al.* immobilized Lc (from *C. Unicolor*) in the lipid liquid-crystalline cubic phase [246]. The obtained modified electrode demonstrated oxygen reduction but it was very unstable. A better stability of the modified electrode was obtained for the biocathode with the CNTs covalently functionalized with 2,2'-azinobis (3-ethylbenzothiazoline-6-sulfonate) diammonium salt (ABTS) and Lc [247].

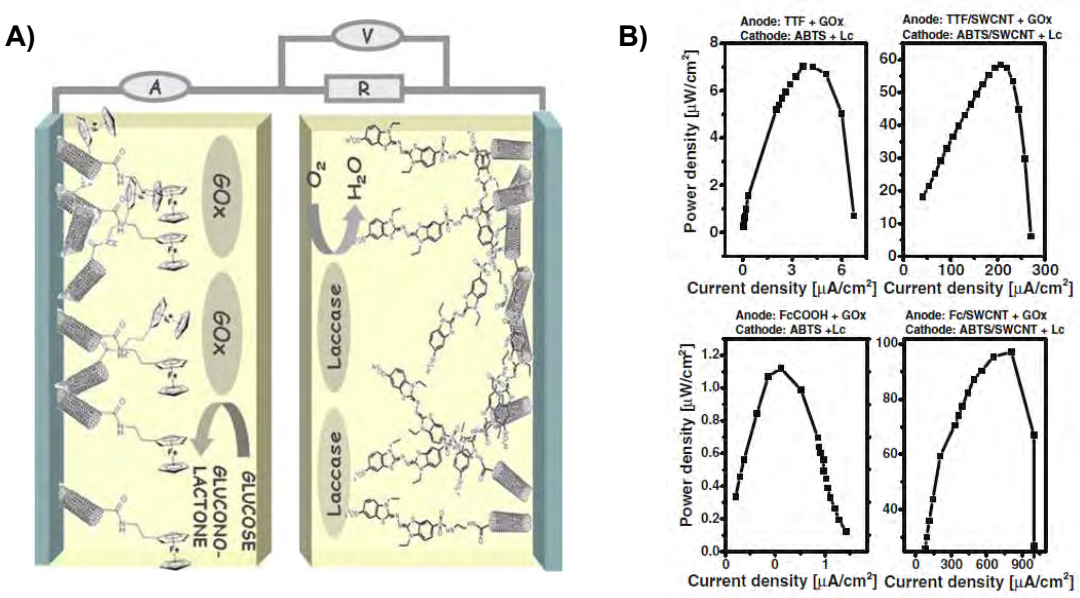

Figure 1.24: A) Schematic representation of the biofuel cell circuit. B) Comparison of power densities of biofuel cells with and without CNTs [248].

A nice example of CNT utilisation for enzyme immobilisation in LQ was presented by Nazaruk *et al.* (see the Fig. 1.24) [248]. They synthesised SWCNTs and MWCNTs with covalently bound mediators for GOx and Lc. Usually, in case of MET, mediator leaching is a big problem with maintaining the bioelectrode active. Here the authors overcame this problem by the covalent immobilisation of ferrocene (Fc) and ABTS. Moreover, Nazaruk *et al.* used the LQ for the immobilization of tetratiafulvalene (TTF) - a molecule which acts

as a mediator for GOx. Due to its hydrophobicity TTF was permanently immobilised in the lipid phase of the liquid crystal. The comparison of the power outputs from the BFCs with and without the CNTs is shown in the Figure 1.24 B.

Another method of CNT modification - based on the adsorption of oppositely charged molecules - was developed by Lin's group. They used a layer-by-layer (LBL) technique to immobilise three different enzymes (intrinsically negatively charged) alternately with a positively charged polymer. In all cases they first put a layer of poly(diallyldimethylammonium) chloride polymer (PDDA) on MWCNT modified glassy carbon electrodes. Then they put a second layer made of enzyme molecules - one of the following: acetylcholinesterase (AChE) [249], GOx [250] (Fig. 1.25), choline oxidase (ChO) and a bienzyme of ChO and horseradish peroxidase (HRP) [251]. The obtained biosensors were used to detect organophosphate pesticides and nerve agents [249], glucose [250] and choline respectively [251].

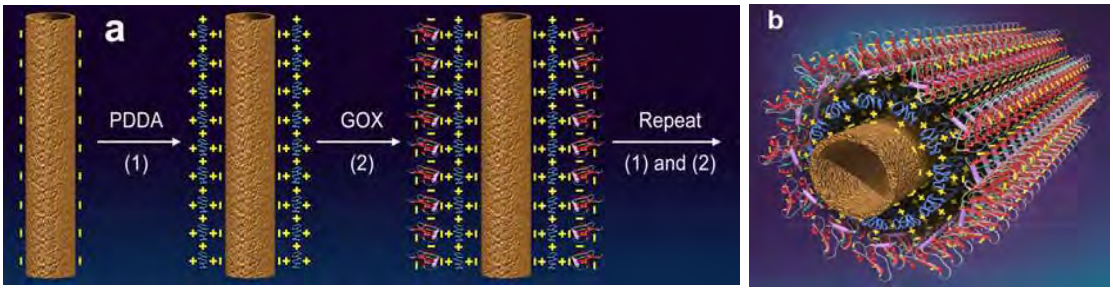

Figure 1.25: a) Procedure of assembling enzymes on a CNT by LBL technique. b) 3D image of PDDA/enzyme/PDDA/CNT nanocomposite [249].

A different approach to obtain the bioelectrodes with CNTs was presented by Mano's group [252]. They used a previously developed method of a CNT fibre preparation called a coagulation spinning process. First the acid treated CNTs were dispersed in sodium dodecyl sulphate (SDS) water solution. The CNT fibre was obtained by injecting the CNT dispersion into a spinning bath made of polyvinyl alcohol (PVA) solution. The coagulated fibre contained ca. 80 wt.% of PVA, so it was further thermally treated (Ar, 600 °C) to get rid of the unwanted material and leave very porous fibres made solely of CNTs. Next the CNT fibres were modified with an appropriate osmium polymer and the enzymes BOx or GOx to obtain a biocathode and a bioanode respectively. These two bioelectrodes were used to make a glucose/O_2 BFC (see Fig. 1.26), which is still the most powerful among all BFCs demonstrating MET. The obtained BFC gave the power density of 740 $\mu W\,cm^{-2}$ at +0.57 V in 15 mM glucose solution (physiological conditions).

All the ways of CNT-bioelectrodes preparation described so far represent a small part of the work done in this field of electrode modification. Besides the above mentioned methods it is worth to add that the enzymes can also be immobilised together with CNTs with the use of e.g. Nafion [157], clay composite (hydroxyapatite with glutaraldehyde) [253] and chitosan [254]. In these cases the obtained biocomposites with CNTs form porous thin films on the modified electrodes.

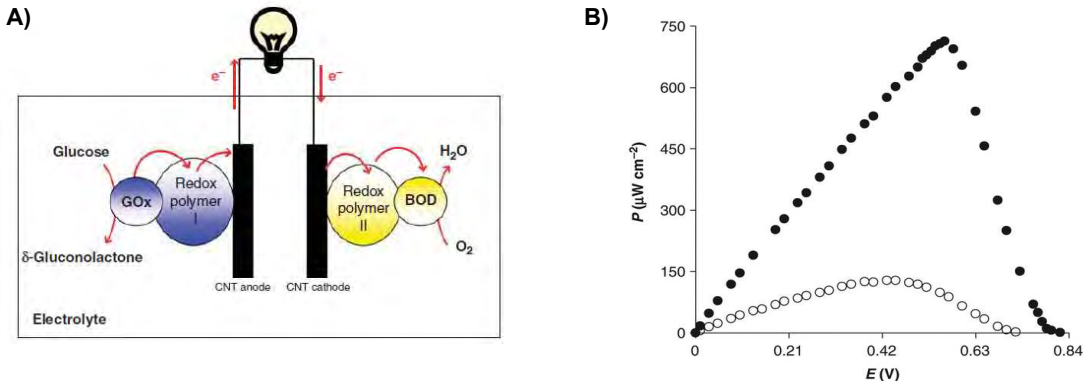

Figure 1.26: A) A scheme of an efficient glucose/O_2 BFC. B) Power density curves for a BFC made with carbon fibre (open circles) and CNT fibre (solid circles). Conditions: a quiescent phosphate-buffered saline buffer, air, 15 mM glucose, 37 °C [252].

Among other methods which use CNTs as an electrode substrate one can distinguish fabrication of buckypaper-based bioelectrodes [255], compression of the nanotubes together with the enzyme [256] and induced shrinkage of CNTs entrapping the biomolecules [138]. The buckypaper electrode is prepared by a filtration of the CNT suspension on the nylon membrane, drying the obtained CNT-film and then a mechanical removal of the membrane. This type of CNT-electrode is very fragile but when treated carefully it can be further modified with the enzymes immobilised by some binders, e.g. Nafion [255] to obtain the bioelectrode.

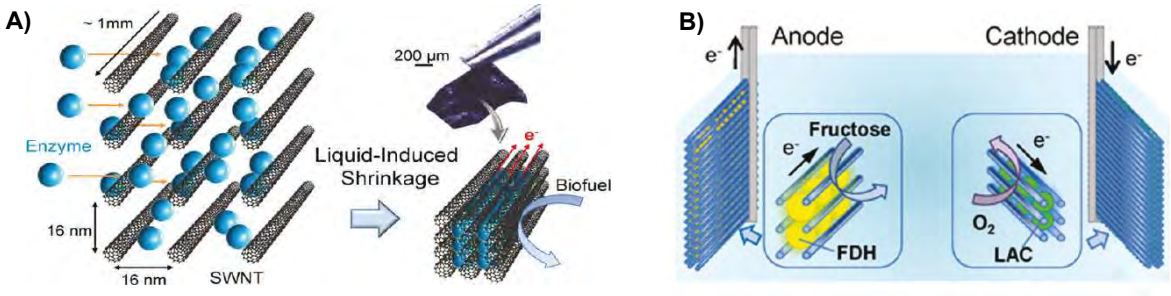

Figure 1.27: A) A schematic diagram of enzyme entrapment inside a CNTF by liquid-induced shrinkage. The photograph shows a free-standing enzyme-CNTF ensemble film that can be manipulated with tweezers. B) A scheme of the BFC with enzyme-entrapped CNTF [138].

Completely binder-free CNT bioelectrodes were obtained by Nishizawa's group by the use of a liquid-induced shrinkage method [138]. A forest of very long CNTs (ca. 1 mm) was first grown by CVD. Then the CNT-film was removed from the substrate and treated by a surfactant (Triton X-100) solution. Next the CNT-electrode was immersed in the enzyme solution (D-fructose dehydrogenase or Lc) which induced shrinkage of the forest and the entrapment of the biomolecules in between the nanotubes (see Fig. 1.27). As prepared bioelectrodes were used to construct a fructose/O_2 BFC which gave a maximum power output of 1.8 mW cm^{-2} (at 0.45 V) in stirred oxygenated 200 mM fructose solution.

As mentioned before, one of the main challenges of bioelectrode preparation is to obtain efficient electron transfer between the electrode and the enzyme active centre. CNTs are in-

teresting materials to fulfil these challenges not only because they are conductive and have a high aspect ratio, but also because they can be easily functionalized. CNT functionalization can lead to obtaining the MET - as was presented by Bilewicz's group who attached the mediators to the nanotubes [248]. On the other hand some ways of CNT functionalization can lead to DET. An example was presented by Jönsson-Niedziolka *et al.* who functionalized SWCNTs with different types of pyrene-derivatives which were non-electroactive [257, 258]. The authors used a non-covalent bonding by π-electron stacking to modify CNTs with: 1,3,6,8-pyrenetetrasulfonate (PTSA), 1-pyrenesulfonate (PSA), 1-pyrenecarboxylate (PCA), 1-pyrenebutyrate (PBA) or 1-pyrenemethylamine (PMA). Then they co-immobilized the functionalized CNTs with Lc or BOx in a silicate matrix prepared by the sol-gel method or they adsorbed the enzyme (BOx) on the CNT/sol-gel modified electrode. The obtained biocathodes showed DET and gave the best (and similar) reduction current in case of electrodes with PTSA and PSA/SWCNTs. The poorest oxygen reduction was obtained for the biocathode with PMA/SWCNTs, which indicated that the sign of the ion bonded to SWCNTs was more important than the specific functional group [258].

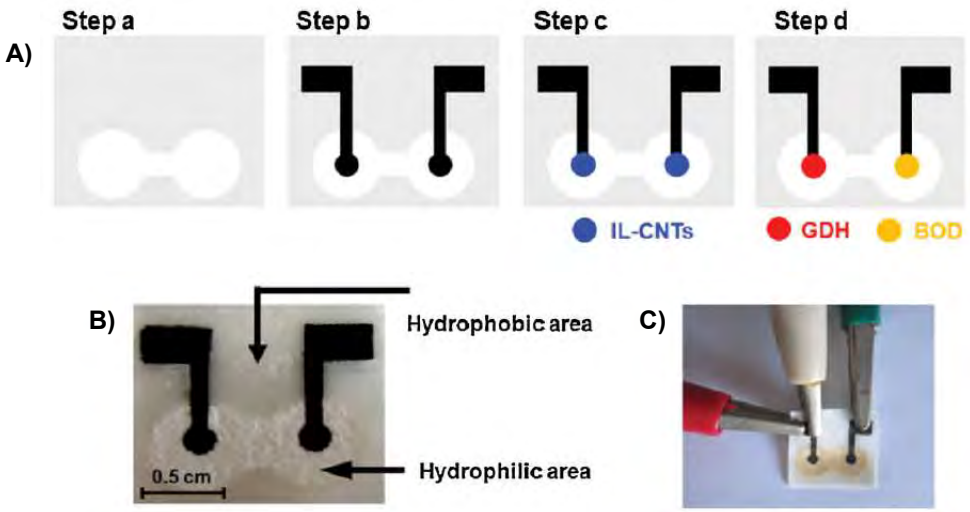

Figure 1.28: A) Fabrication process for the BFC based on a paper chip. Steps: a) patterned paper chip; b) paper chip-based carbon electrodes (C-PE); c) CNTs-IL modified C-PE (CNTs-IL/C-PE); d) bioanode (GDH/CNTs-IL/C-PE) and biocathode (BOx/CNTs-IL/C-PE) of paper chip-based BFC. B) Digital photo of the BFC. C) Digital photo of the BFC operating by utilizing commercial Nescafe instant coffee-based solution as the biofuel [144].

Another way of promoting the ET between the CNT-electrode and the enzyme is the use of ionic liquid (IL). Dong's group used 1-butyl-3-methylimidazolium hexafluorophosphate ([bmim]PF_6) to functionalize MWCNTs by simple mixing in a mortar [249]. As prepared paste was immobilised on carbon fibre microelectrodes and formed a system which displayed a good promotion of electron transfer to GOx. The following work of Dong's group was crowned by obtaining a small paper membraneless glucose/air BFC (see Fig. 1.28) [144]. The bioelectrodes substrate was made of the CNTs modified with [bmim]PF_6 screen-printed on the paper chip with patterned carbon electrodes. The enzymes (GDH and BOx) were immobilized on the electrode surfaces with chitosan. The BFC performance was checked

in a glucose solution as well as in Nescafe instant coffee, Maidong vitamin water, fresh watermelon juice and Minute Maid grape juice. The highest power output (ca. 18 $\mu W\,cm^{-2}$) was registered for the BFC operating in the coffee. The described device was small (1.5 cm $\times$ 1.5 cm), easy to prepare and relatively inexpensive. Thus it might be a model for future portable bioenergy devices.

For those who are interested in comparisons between different BFCs prepared with CNT-bioelectrodes, I recommend to read a relatively new review published by Cosnier's group [259].

1.6 Titanium dioxide nanotubes

Titanium dioxide (titania) is the most extensively studied material among all transition metal-oxides [260]. It is also one of the most interesting compounds for material scientists due to the wide range of current and future applications, e.g. in photocatalysis, medicine, solar cells, production of white paints or sun-blockers.

The interest in this material has boomed in 1972, when Fujishima and Honda reported the first successful water photoelectrolysis [261]. They used a cell comprising platinum and n-dopped rutile modified electrodes and "visible light"[14]. As a result they decomposed water into O_2 and H_2 without applying any external voltage. Although that work provoked a debate about the mismatch between a theory and the results concerning water splitting, it also induced an interest in H_2 generation. The world needs new energy carriers and hydrogen is regarded to be one of them. Thus photoelectrochemistry of TiO_2 might lead to solving one of problems with the world energy crisis [262].

In the following subsections I will mainly focus on the description of TiO_2 nanotubes which I used in my thesis as photoanodes in photo-biofuel cells.

1.6.1 Properties and applications

All the intrinsic properties of TiO_2 nanotubes derive from the electronic structure of titania and the organised tubular geometry. TiO_2 is a non-toxic, wide-bandgap semiconductor which naturally occurs in three forms: anatase (band gap $E_g \approx 3.2$ eV [260]), rutile ($E_g = 3$ eV [263]) and brookite ($E_g = 3.1$ eV [264]). The bandgap (E_g) - which is defined by the gap between the edges of the conduction and the valance bands - in TiO_2 is equal to the gap between the Ti3d states and the O2p levels, respectively (for anatase and rutile) [265, 266]. However, the band

[14] In fact they used 500 W Xe lamp in their experiment, but in the conclussions they suggested that water can be decopmosed by the visible light.

edges can be shifted by the presence of defects in the TiO_2 crystalline structure. The defects such as oxygen vacancies and Ti^{3+} states provide additional states and result in a change of E_g. That is why the presence of defects is crucial for the most important properties of TiO_2 and why the Ti^{3+} content seems to entirely dominate its conductivity [260]. The defect-dependent properties include: electrical properties, mass transport and charge transport kinetics, reactivity, catalytic properties and light-induced properties [267]. In his recently published book Janusz Nowotny focuses on the detailed description of studies concerning different types of defects influencing the properties of binary metal oxides, especially titania [267]. He shows that TiO_2 is not a formula which correctly reflects titania composition because of a non-stoichiometric behaviour of this compound. He also points out that even a trace amount of impurities can substantially affect the properties of this material. The most important message taken from this book is that the defect chemistry can be used for engineering of TiO_2 properties. Thus the control of titania structure at the atomic scale can lead to obtaining enhanced materials needed for solar energy conversion.

Undoped anatase and rutile have similar resistivity - 10^4 — 10^7 Ω cm. This value is significantly decreased by thermal reduction of TiO_2 (10^{-1} Ω cm for anatase and 10^2 Ω cm for rutile) and then stays temperature-independent [260, 268, 269]. Titania is very stable against corrosion and photocorrosion. Usually it has the form of a white powder which has a high refractive index, thus it is mainly used as a white pigment in e.g. paints, plastics, papers and cosmetics. Moreover, TiO_2 has a strong UV light absorbance and that is why it is also applied as a sunscreen blocker [267]. Other properties are: photoinduced superhydrophilicity [270] and voltage-induced wettability control used in obtaining anti-fogging and self-cleaning coatings, respectively. But the most interesting are the photoelectrochemical properties of TiO_2 which can be used in photocatalysis (e.g. for water purification), harvesting of solar energy and obtaining new types of sensors (e.g. gas sensors).

The photocatalytic properties of TiO_2 result from the formation of electron-hole pairs [271] (see Fig. 1.29). These charge carriers are formed when titania is illuminated with the light of the energy higher than the bang gap. Thus the undoped TiO_2 is photoactive under the ultraviolet (UV) radiation[15]. The photogenerated electrons and holes (h^+) exist as long as they are separated. The simplified model of the activity of these charge-carriers can be described as follows. The electrons are promoted from the valence band to the conduction band (see Fig. 1.29a). The holes reach an interface between TiO_2 and environment, where they can react with appropriate redox species [260]. When TiO_2 is in contact with water several highly reactive species are generated, e.g. $OH^{\cdot}$. That radical generation is possible due to the high energy of the holes [272] and can be further used for an oxidation of organic compounds. Moreover, the decomposition of species adsorbed on the TiO_2 surface may be initiated by direct transfer of h^+ from the valance band to those species.

[15] E_g higher than 3 eV is equal to the light wavelength lower than 400 nm.

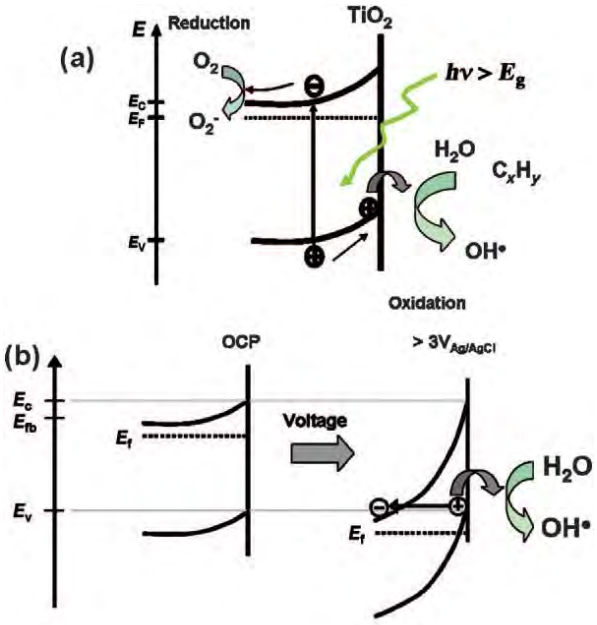

Figure 1.29: Photocatalytic activity of TiO_2 nanotubes: a) the mechanism of photoinduced formation of electron-hole pairs and reaction with surroundings. b) Dark photocatalysis: sufficient voltage-induced band-bending creates valence band holes (h^+) that can react with the environment, in analogy to photon-induced hole (h^+) generation [260].

Interestingly, reactions similar to the photocatalytic ones can be triggered by the voltage applied to sufficiently doped TiO_2 [272]. For example annealed TiO_2 nanotubes have a doping concentration of ca. $10^{18} - 10^{19}$ cm^{-3} and by applying voltage larger than 3 V (vs. Ag|AgCl) it is possible to ionise their valance band and generate the holes (see Fig. 1.29b). This effect is called a dark photocatalysis and might can be used for self-cleaning in the dark as well as for performing photocatalytic reactions without the use of UV light [260].

Nanosized titania is far better than the bulk TiO_2 from the point of view of most of its applications. That is mainly due to different electronic properties and a higher specific area of nanoparticles which in turn lead to improved overall efficiency of the reactions catalysed by this material. Physical and chemical properties of TiO_2 supposed to be even better controlled in the case of nanotubular and nanorod-like geometries [260]. The most important advantages of the TiO_2 nanotube structure is a defined geometry and a large surface area. Moreover, the nanotubes show very good biocompatibility [273, 274]. The tubular geometry results in a narrow distribution of diffusion paths of species such as electrons, holes and ions (transported through the tube wall) and reactants which should be transported to the tube bottom [275, 276]. For example Schmuki's group showed that the electron diffusion length in aligned tubes can be 30 times greater than in the nanoparticulate TiO_2 [277]. Thus the nanotubes, in comparison to other titania structures, showed enhanced properties when applied in photocatalysis [278, 279], sensing [280–282], photoelectrolysis [283, 284] and photovoltaics [285–287]. One of the most interesting applications of TiO_2 nanotubes presented so far was a controllable drug delivery system presented by Schmuki's group [288]. They

prepared amphiphilic[16] TiO_2 nanotubes by a two-step anodization process. The obtained tubes had hydrophobic caps which prevented uncontrolled leakage of the hydrophilic drug from the inside of the tubes into an aqueous environment. The drug was released by applying UV irradiation which caused scission of organic monolayers on the tube caps. Thus the drug release was highly controlled by the photo-scission.

1.6.2 Methods of growing TiO_2 nanotubes

TiO_2 nanotubes (TNTs) can be fabricated in many ways, such as template-assisted methods, hydro/solvothermal processes, an atomic layer deposition, anodic oxidation, freeze-drying, an electrodeposition and a seeded growth [260,289,290]. The first report about the formation of titanium dioxide nanotubes was published by Hoyer in 1996 [291]. He introduced a rather complicated template-assisted method coupled with an electrochemical deposition of titania. The obtained material was amorphous and gained the anatase structure after the heat treatment. Many of the methods introduced later involved sol-gel processes where hydrolysis of titanium alkoxide precursors was followed by hydrolysis and condensation reactions. The control of the nanotube structure was usually obtained by the use of different types of template [292, 293].

In contrast to other methods of TiO_2 growth, anodic oxidation (at proper conditions) gives self-organised vertically aligned nanotubes which are usually attached to the substrate. Moreover, the anodization technique is one of the simplest, cheapest and most straightforward approaches leading to ordered porous structures [275]. Thus this method is very interesting from the point of view of electrode preparation. The first description of TiO_2 nanotube formation using the anodization technique was presented in 1999 by Zwilling *et al.* [294]. They described the formation of "columnar pores of nanometre size" by the anodization of Ti in an electrolyte containing HF. Their method gave rather disorganized layer on the top of the Ti plate.

Dense, uniform and aligned TiO_2 nanotubes were for the first time described by Dickey's group [295] in 2001. By changing the anodization voltage and the concentration of HF in the aqueous solution they were able to control the pore diameters of the nanotubes. The pore sizes were in the range from 25 to 65 nm, where the higher voltage the bigger diameter. All the obtained tubes had the same length, so no dependence on the anodization time was found. The authors also presented a possible mechanism of the tube formation which was similar to the mechanism of a field-enhanced oxidation of aluminum.

After that crucial report different approaches to the anodization technique were tested to achieve better control over the nanotube size and understand the growth mechanism. Many

[16] Amphiphilic means having both hydrophilic and hydrophobic properties.

variations of electrolytes were tested, also organic ones such as ethylene glycol, DMSO, glycerol and ionic liquids, which generally gave smoother and better oriented nanotubes [296]. It was also showed that the pH of the electrolyte influences the thickness of a TiO_2 nanotube layer. For the pH close to neutral it was possible to control the tube length, which could not be done at low pH [297, 298]. Moreover, it was found that a porous oxide layer or nanotubes are formed when the fluoride concentration is in the range $0.05 - 1$ wt.% [299]. In most of the presented variations of anodic oxidation the obtained nanotubes were amorphous until the anodization was followed by annealing. In general amorphous TiO_2 is converted by thermal treatment (in air) into an anatase phase at the temperature $300 - 500\,^{\circ}C$ and into a rutile phase above $550\,^{\circ}C$ [260]. Before this annealing step the amorphous tubes contain such a high density of recombination centers that there is virtually no photoconductivity in the tube walls [260].

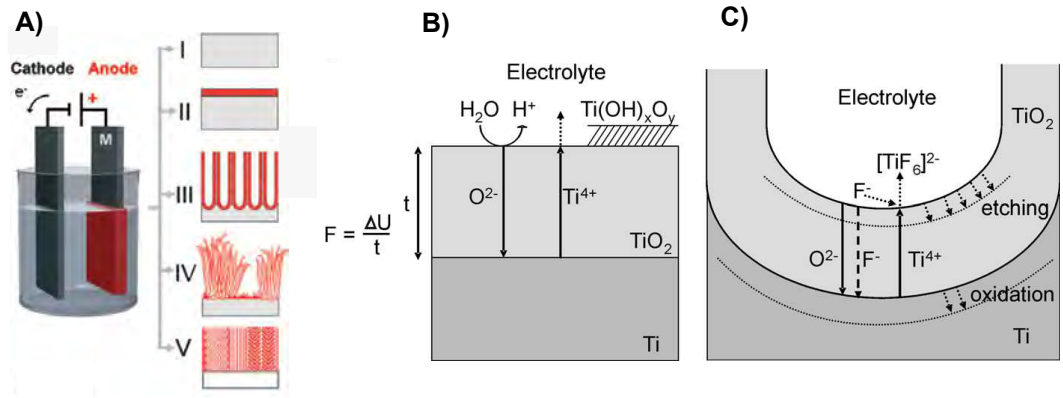

Figure 1.30: A) The electrochemical anodization process and possible anodic morphologies: I) metal electropolishing, II) formation of compact anodic oxides, III) self-ordered oxides (nanotubes or nanopores), IV) rapid (disorganized) oxide nanotube formation, V) ordered nanoporous layers [260]. Schematic representation of the Ti anodization B) in absence of fluorides (results in flat layers), and C) in presence of fluorides (results in the tube growth) [275].

The mechanism of TiO_2 nanotube growth during the anodization is very similar to the mechanism of self-organization of porous alumina [260, 287, 300]. Generally it describes the competition between the oxidation of the metal and dissolution of the oxide layer. The key processes of the mechanism of TiO_2 nanotube growth are:

- growth of an oxide layer on titanium (Ti is used as an anode - see Fig. 1.30) as a result of an interaction between Ti and O^{2-} or OH^- ions, where OH^- ions are created by field-aided deprotonation of H_2O,
- migration of Ti^{4+} from Ti to the TiO_2/electrolyte interface under the applied electric field,
- field-assisted dissolution of the oxide at the oxide/electrolyte interface which results in the migration of the O^{2-} ions towards the metal/oxide interface,
- chemical dissolution of the Ti or TiO_2 by the electrolyte.

The most important process which leads to the formation of the nanotubes rather than a

nanoporous structure of TiO_2 is the chemical dissolution in the HF electrolyte. The chemical dissolution keeps an electrochemical etching process (field-assisted oxidation and dissolution) active by reducing the thickness of the oxide layer (barrier layer) [287]. Only a proper balance between the Ti oxidation and the etching processes gives self-organized aligned TiO_2 nanotubes. This balance is achieved only by the utilisation of optimised parameters of anodization such as: applied voltage, HF concentration, pH, electrolyte type, anodization type. Thus TiO_2 growth is also a multi-parameter process, like the CNTs growth. Those who are interested in a more detailed description of TiO_2 nanotube growth, please refer to an excellent review from Schmuki's group [260]. Here it is only worth mentioning that it is also possible to grow titania nanotubes in electrolytes containing e.g. HCl and H_2O_2 [301, 302], but they are shorter than the tubes grown in fluorine electrolytes.

1.6.3 Electrodes with titania

Fujishima and Honda can be called the fathers of titania electrochemistry. Their seminal paper which appeared in Nature in 1972 [261] was mentioned at the beginning of this section. Besides they were the first who made electrodes with n-type rutile crystals and then performed the electrochemical studies in aqueous solution. They determined the flat band potential of TiO_2 electrode [303–305]. Fujishima and Honda also showed the use of oxide films formed on Ti as anodes in an "electrochemical photocell" [306]. The stack of their photocells generated 1.1 litre of hydrogen per day under the illumination of a sunlight. Moreover, they were involved in the first studies concerning a dye-photosensitization of TiO_2 [305]. Nowadays this effect is exploited mostly in dye-sensitizes solar cells (DSSCs) [307] which will be mentioned in Chapter 8.

The way of TiO_2 synthesis and then the way of electrode preparation have a very big influence on the final photoelectrochemical properties of titania electrode. The preparation of the electrodes with the structure optimised for a particular application is still a challenge [308–311]. The electrode preparation methods can be divided into two groups [311]:

- involving the use of presynthesized TiO_2: "doctor blading" [310], screen printing [312,313], dip coating [314], spin coating [310, 315] and electrophoretic deposition [316–318],
- based on the direct growth on the conducting substrate: electrodeposition [319], electrochemical anodization (section 1.6.2), chemical bath deposition (CBD), spray pyrolysis deposition [315] and chemical vapour deposition (CVD) [320, 321].

A comparison of the methods based on direct growth of TiO_2 on the electrode surface indicates that the chemical bath deposition can be the simplest and the least expensive [311]. The CBD leads to obtaining films of a large area and quality comparable with the ones obtained e.g. by CVD, which is a much more expensive method. The CBD is based on the hydrolysis

of TiO_2 precursor followed by the precipitation and deposition of nanostructures. The obtained material can have a well defined morphology controlled by the synthesis parameters, e.g. needle-like crystals [322] or nanowires [323].

Those who are interested in more details concerning photoelectrochemical investigations of titania electrodes, please refer to the following papers [311, 324].

1.7 Photoelectrochemical biofuel cells

Merging the ideas of a current photogeneration on the anode with an enzymatic fuel oxidation results in obtaining a photoelectrochemical BFC (photo-BFC). The main advantages of making this hybrid cell are that it can operate at higher voltage than a standard type of a BFC with the same cathode and than a standard dye-sensitized solar cell with the same anode. First examples of photo-BFCs were presented by the Gust group. They used a photoanode comprising either nanoparticulate SnO_2 [325] or TiO_2 [326] sensitized with a porphyrin. The anode was kept in the solution containing reduced form of β-nicotinamide adenine dinucleotide (NADH - reduced form of NAD^+), GDH and glucose. As a cathode Pt

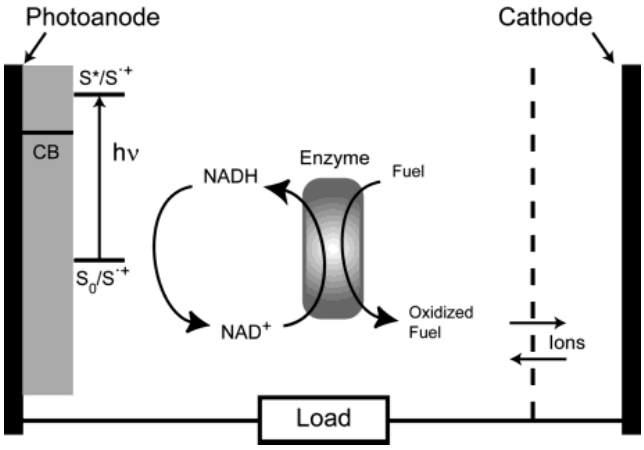

Figure 1.31: Schematic diagram of the hybrid photoelectrochemical biofuel cell [326].

gauze or $Hg|Hg_2SO_4\ _{K_2SO_4}$ separated from the anode by an anion-permeable membrane was used (see Fig. 1.31). When the photoanode is illuminated with light (520 nm, 1 mW cm^{-2} [325]) the porphyrin molecules absorb photons and go into their excited single state. Then they inject electrons to the conduction band of the semiconductor and turn into radical cations. The electrons generated in this way are transferred via an external circuit to the cathode. The porphyrin radical cations are further regenerated by NADH, so that they come back to their ground state and NAD^+ ions are generated. NAD^+ ions act as a GDH cofactor for glucose oxidation. Thus the NADH/GDH/glucose system is exploited for the regeneration of the dye on the anode and glucose is used as a fuel for the photo-BFC. The first photo-BFC with titania nanoparticulate electrode gave the OCV of 1.10 V and the maximum power density of 37 μW cm^{-2}.

Next examples of photo-BFC were very similar to the first one, the only difference was in the use of different dye, such as copper chlorophyll trisodium salt [327], chlorophyll [328], triarylamine dye [329], H_2-mesoporphyrin IX or Zn-mesoporphyrin IX [330] and only a slightly different porphyrin than used by Moore's group [235]. Almost no work concerning the use of a different cathode was presented. As far as I am concerned Moore's group presented the only BFC with a photoanode based on porphyrin/NADH/GDH/glucose system and a biocathode with immobilised enzyme. They used [FeFe]-hydrogenase for the production of H_2 [331]. So far no one used a biocathode for oxygen reduction working together with a photoanode developed by Moore's group. However, biocathodes with bilirubin oxidase were used in photo-BFCs together with the anodes comprising e.g. photosystem II [332] or cyanobacteria [333].

Very simple approach to the construction of a photo-BFC was presented by Dong's group [334]. They connected a biocathode with BOx to an anode with titania nanotubes in one-compartment cell filled with glucose solution. Under the illumination of UV light and a presence of 20 mM of the fuel the photo-BFC generated maximum power of 47 $\mu W\,cm^{-2}$. The authors expect their photo-BFC would generate electricity also under the solar irradiation, but that has not been checked yet.

In the last chapter of my thesis I will present the attempts of obtaining two types of photo-BFCs. Both of them comprise the biocathode with BOx and the anode based on titania nanotubes.

Experiments, Results and Discussion

Chapter 2

Materials, Instrumentation and Procedures

2.1 Materials

- Inorganic compounds

Disodium hydrogen phosphate (POCH), FMCA (⩾ 97%, Fluka), Hydrochloric acid (35%, POCH), Hydrogen peroxide (30%, Chempur), Hydrofluoric acid (40%, POCH), Iron(III) chloride (Chempur), Monosodium phosphate hydrate (POCH), Phosphoric acid (85%, Chempur), Potassium chloride (Sigma-Aldrich), Potassium hexacyanoferrate (II) trihydrate (POCH), Potassium hexacyanoferrate (III) (Sigma-Aldrich), N719 Ru-dye (Solaronix), Sodium chloride (Chempur), Sodium hydroxide (POCH), Sulfiric acid (95%, Chempur), Titanium (IV) chloride (⩾ 99.0%, Sigma-Aldrich)

- Organic compounds

$ABTS^{2-}$ (98%, Sigma-Aldrich), ACN (99.5%+, Sigma-Aldrich), L(+)-ascorbic acid from Riedel-de Haël, CTAB (95%, Aldrich), Citric acid monohydrate (Merck), EEM Kit (contains: 1,2-epoxypropane (EEM), hardeners: dodecenylsuccinic anhydride (DDSA) and methyl nadic anhydride (MNA), and an accelerator - 2,4,6-tris(dimethylaminomethyl)phenol (PDM-30), Fluka), Ethanol (96%, Chempur), Ethylene glycol (Merck), Glucose (99.5%, Sigma-Aldrich), Latex beads (polystyrene, 3 µm mean particle size, Sigma-Aldrich), Methanol (99.8%, Chempur or Sigma-Aldrich), Nafion ® (5% solution in 2-propanol, Sigma-Aldrich), 2-Propanol (⩾ 99.8%, Merck), PSA (Sigma-Aldrich), tBuFc (98%, ABCR), Tris (⩾ 99.9%, Sigma)

- Silicate precursors

MTMOS (98%, Sigma-Aldrich), OTEOS (97%, ABCR), TMASiCl (50% in methanol, ABCR), TMOS (99%, Sigma-Aldrich)

- Enzymes

BOx from Myrothecium sp. fungus (EC 1.3.3.5, Amano Enzyme Inc.), GDH from Pseudomonas sp. (Sigmna-Aldrich), GOx from Aspergillus niger fungus (EC 1.1.3.4, Amano En-

zyme Inc.), Lacc from *Cerrena unicolor* fungus (EC 1.10.3.2, isolated and purified by Prof. Rogalski group according to procedure described in literature [335])

- Nanomaterials

CNPs with phenylsulfonic acid surface functionalities (ca. 7.8 nm mean diameter, Emperor 2000, Cabot Corporation), CNPs with sulfonamide group (obtained from Prof. Marken, synthesized according to procedure described in literature [336]), MWCNTs (outer diameter $20-30$ nm, inner diameter $5-10$ nm, length $0.5-200$ µm, Sigma-Aldrich), Platisol T - Transparent Platinum Catalyst Paint (Solaronix), SWCNTs (Shenzhen Nano-tech Port Co. Ltd.), Titania paste (Dyesol, DSL 18NR-T, 10 - 30 % TiO_2 NPs, 20 nm in diameter)

- Others

Argon and Oxygen (N5. 0, Multax), Bynel foil (35 µm thick, Bynel 4164, DuPont), Copper tape (adhesive conducting tape, 3M), cover glass (9 Rmm in diameter and 0.13 Rmm thick, VW International), FTO glass (TCO 30-8, Solaronix), ITO (resistivity $15-30\,\Omega$ cm and $8-12\,\Omega$ cm, Image Optics Components Ltd., and Delta Technologies, respectively), Nafion ® Membrane (N115, 127 µm thick, Du Pont), Platinum wire (Goodfellow), Toray Teflon Treated Carbon Paper (TGP-H-090, Fuel Cell Store, Colorado), Titanium foil (0.25 nm thick, 99.7%, Sigma-Aldrich), Water (resistivity >15 Ωcm, demineralized with ELIX system, Milipore), zinc foil (0.25 mm, purity 99.98%, Alfa Aesar), Zinc wire (250 µm diameter, 99.95%, Goodfellow)

All reagents were used as received.

2.2 Instrumentation

Most of the instrumentation was used in Warsaw, unless otherwise stated.

- Electrochemical measurements

Autolab PGSTAT 30 (Eco Chemie), μAutolab III (Metrohm Autolab) and Solartron electrochemical workstations

- Microscopes

Zeiss Supra Field Emission microscope, FEI Nova NanoSEM system or Hitachi 4700 II cold Field-emission Scanning Electron Microscope (BIOSEM, Edinburgh)- SEM microscopes, Nikon Eclipse LV150 metallurgical microscope (Nikon) - optical microscope, AFM Veeco Nanoman VS with Dimension 3100 controller - AFM measurements

- Ultrasonic instrumentation

Sonorex RK 31 (Bandelin electronic GmbH & Co.) and Sonic05 (Polsonic) ultrasonic baths, Ultrasonic finger Sonopuls HD2070 (Bandelin electronics)

- Balances

Discovery (OHAUS) and CP124S (Sartorius AG) analytical balances

- Ovens and hot plate

Tube furnace (Barnstead Inc.), drying oven (BINDER), RET basic magnetic stirrer with hot plate (IKA)

- Power supply and power meter

Power supply, 150V/2A (UNITRA UNIMA); Power meter 815 (Newport Research)

- Raman spectromter

InVia Raman spectrometer (Renishaw)

- Solar simulator

150W Xe lamp (Instytut Fotonowy Sp. z o.o.) and AM 1.5 G filter (Sciencetech)

- Others

Mass flow controllers (Sierra Instruments, The Netherlands), Reference cell for the solar cell calibration (0.13 mm thick, RC/5024, NIELSEN)

2.3 Experimental methods

In this section I will shortly describe experimental methods used during my research. For the characterisation of electrodes' surface. I mainly used electrochemical methods such as cyclic voltammetry, chronoamperometry and chronopotentiometry. All all them require the use of a specialized equipment called a potentiostat. This apparatus is responsible for forcing enough current through the tested electrode (here working electrode) to achieve the intended potential.

Apart from the above mentioned methods I also used scanning electron microscopy, Raman spectroscopy and atomic force microscopy for looking at the sample topography, checking the quality of CNTs and checking the electric contact between the grown CNTs and the substrate, respectively.

2.3.1 Cyclic voltammetry

In cyclic voltammetry (CV) the potential of WE is swept forward and backward between two desired potentials with the speed called the scan rate, ν $[Vs^{-1}]$. As a result a cyclic voltammogram is obtained - a curve showing current-voltage dependency. It shape depends on e.g. the type of WE, the electrolyte, the type of the reaction occurring on the electrode and diffusion of the electroactive species to the electrode's surface. This is why this technique is very powerful for studying electrochemical processes and the properties of the modified electrode's surfaces. Information about the examined system which one can obtain using CV include: qualitative and quantitative composition, thermodynamics and kinetics of the processes such as heterogenous reactions, catalysis and adsorption [337, 338].

The current recorded during CV has capacitive or capacitive and faradaic origin. The first one appears because the interface between the electrode and an electrolyte behaves like a capacitor which is charged and discharged during the electrochemical experiment. The faradaic current comes from charge-transfer processes occurring on the electrode. Its shape looks like waves or peaks. For example for a reversible process of dissolved electroactive compound the i-E curve has two peaks - anodic and cathodic (for the situation when the diffusion to the electrode surface is planar and the temperature is 25 °C). The value of the peak current [in amperes] is described by the Randles-Sevcik equation [337]:

$$i_p = 0.4463nFAC^* \left(\frac{nF\nu D}{RT}\right)^{\frac{1}{2}} \tag{2.1}$$

where: n - number of transferred electrons; F - the Faraday constant, A - electrode projected area [cm^2]; C^* - concentration of electroactive species in the solution [$\mathrm{mol\,cm}^{-3}$];
D - diffusion coefficient [$\mathrm{cm}^2\,\mathrm{s}^{-1}$];, ν is given [Vs^{-1}]; R - gas constant;, T - temperature [°C].
Thus for a reversible process i_p depends linearly on the square root of ν. On the other hand, in case when the electroactive compound adsorbs on the electrode surface, the peak current shows the linear dependence on ν.

The shape of the voltammogram can indicate the reversibility of the electrode process. One can say that the redox reaction is chemically, thermodynamically and/or electrochemically reversible [339]. The latter type of reversibility means that the surface concentrations of reduced and oxidized species obey Nernst equation (Eq. 2.2):

$$E = E^{\ominus} - \frac{RT}{nF} \ln \frac{a_{red}}{a_{ox}} \tag{2.2}$$

where: E - equilibrium electrode potential at temperature T; $E^{\ominus}$ - potential of a redox couple at standard state; a_{red} - chemical activity of a reductant; a_{ox} - chemical activity of an oxidant. Thus the reaction is reversible electrochemically when the difference between the potentials of the anodic and cathodic peaks recorded on a CV is approximately equal to $\frac{59}{n}$ mV at 25°C. A chemical reversibility means that the reaction can proceed in two directions. The thermodynamic reversibility indicates that the reaction is in equilibrium at any moment.

In my research I used CV mainly for the characterisation of modified electrodes, e.g. to find out the electrodes capacitance and to compare the bioelectrocatalytic currents obtained after different modification processes. However, I used this technique to control the adsorption of electroactive species and to obtain the transient $i-V$ curves for photoelectrochemical biofuel cells.

2.3.2 Chronoamperometry

During chronoamperometry (CA) experiment a constant potential is applied to the working electrode - versus the reference electrode. The resulting current is recorded as a function of time. The obtained curve is usually proportional to $t^{-\frac{1}{2}}$ which nicely visualises the effect of depleting the electroactive species near the surface. This behaviour is described by the Cottrell equation [337]:

$$i_d(t) = \frac{nFAD_O^{\frac{1}{2}}C_O^*}{\pi^{\frac{1}{2}}t^{\frac{1}{2}}} \tag{2.3}$$

where: n - charge number of electrochemical reaction, C_O^* - bulk concentration of species O, D_O - diffusion coefficient of electroactive species.

E.q. 4 was derived from the linear diffusion equation and one needs to remember that it is valid only for the diffusion-limited current. For example the long term measurements might cause the disruption of the diffusion layer by the convection and end up with i_d higher than predicted by the Cottrell equation.

CA was used in this thesis mainly for checking the stability of the bioelectrodes.

2.3.3 Chronopotentiometry

In chronopotentiometry (CP) the potential is measured as a function of the applied current. There are different types of this technique, depending on the way how the current is applied, eg: CP with current reversal, cyclic CP, programmed current CP and constant-current CP (the one used in this thesis). They are used for obtaining information about the kinetics of the reaction, eg: heterogenous electron transfer rate constants or dimerization rate constants.

I used CP for testing the stability of the biobatteries and photo-biofuel cells, for obtaining the galvanostatic $V - i$ characteristics of these cells as well as for the electrodeposition of thin layers on the electrodes.

2.3.4 Scanning Electron Microscopy

In this technique the sample is kept inside the microscope (Fig. 2.1) where it is scanned by an electron beam. The beam is generated by an electron gun and focused by magnetic lenses. Its position is controlled by deflection coils so that it can scan the chosen part of the sample surface.

The interaction of the electron beam of the energy $0.2 - 40$ keV with the sample induces a variety of different signals, such as: secondary-electrons (SE), back-scaterred electrons (BSE),

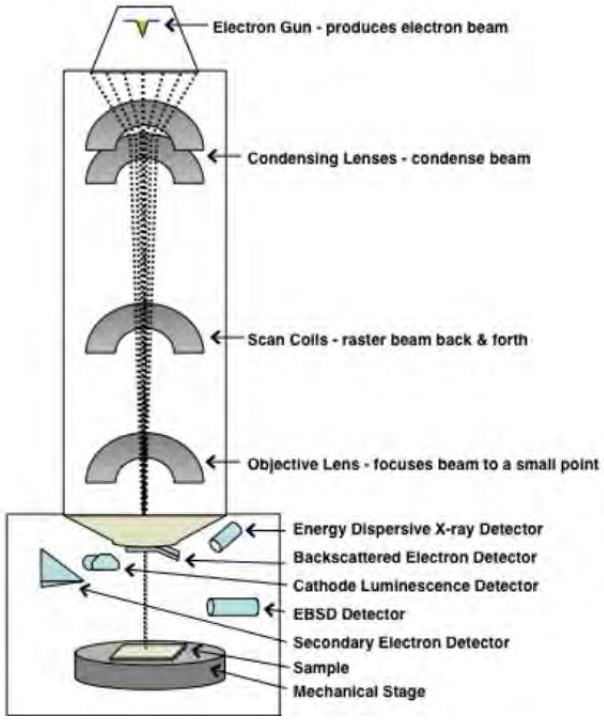

Figure 2.1: A scheme of scanning electron microscope [340].

characteristic X-rays, cathodoluminescence (CL) and transmitted electrons. To detect each of these signals the microscope needs to be equipped with suitable detectors. Standard SEM detectors collect mainly low-energy SE which are generated very close to the sample surface. Therefore the obtained image represents the topography of the examined sample. It is also possible to get the information about the composition of the sample surface by measuring the difference of electron scattering efficiency which depends on the material.

Using SEM one can obtain images with a very high resolution - about 250 times higher than for the optical microscopes (down to 1 nm). That is why this technique is a very powerful tool for surface characterisation. Moreover, this is the reason why SEM was used in my thesis for taking images of CNTs and TiO_2 nanotubes.

2.3.5 Atomic Force Microscopy

The basis of the AFM is scanning a sample surface with a microscope probe (a sharp tip). Here the sample is placed on a piezoelectric table which is able to change its position in x, y and z directions (Fig. 2.2). The tip is mounted to the cantilever and - depending on the AFM mode - it can be static (contact mode) or can oscillate (dynamic mode).

In the contact mode the atomic force between the sample and the tip is kept constant while the deflection of the cantilever is measured. In the dynamic mode the cantilever is subjected to the oscillations with the given frequency. This frequency should vary together

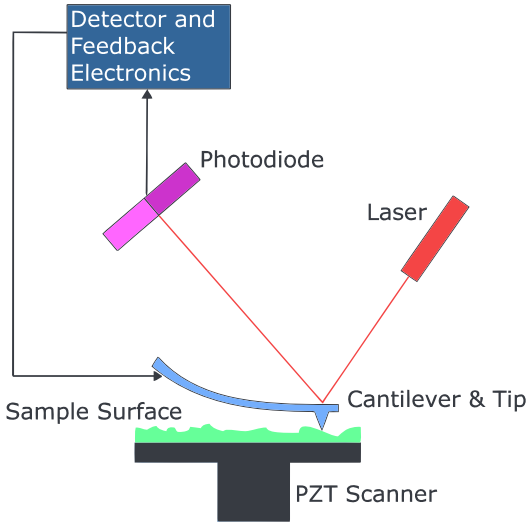

Figure 2.2: A scheme of atomic force microscope [341]. PZT stands for piezoelectric.

with the change of the distance between the tip and the sample surface. But the use of a so called feedback mode allows to keep a constant frequency by moving the table and in consequence keeping the distance constant. To do that the deflection of the cantilever needs to be controlled. Usually it is done by the detection of the laser beam reflected by a mirror placed on the back of the cantilever.

Multitude of types of AFM derives from a big number of forces which can be indirectly measured, e.g. mechanical contact, van der Waals, magnetic and electrostatic forces. The information obtained with this technique depend on the type of AFM. In this thesis it was important to check the topography of the sample with a hight resolution and to perform conductance measurements. Thus the mechanical contact type and conductive AFM (C-AFM) was used. In C-AFM the tip is scanned in contact mode with the sample and the voltage is applied between them. As a result a current image and topography image are obtained.

2.4 Experimental setups

2.4.1 Electrochemical measurements on the non-photoactive electrodes

Al the measurements were done in room temperature, i.e. $20 - 24\,^{\circ}\mathrm{C}$. Cyclic voltammetry (CV) and chronoamperometry (CA) were performed in a conventional three-electrode cell (see Fig. 2.3), unless otherwise stated. A typical cell had a cylindrical shape and had a volume of 7 ml. $\mathrm{Ag|AgCl|KCl}_{3M}$ and a platinum wire were used as reference (RE) and counter electrode (CE), respectively. An electrode modified with CNTs or CNPs was used a working electrode.

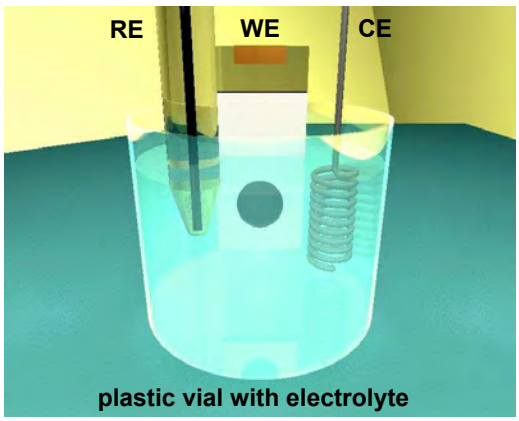

Figure 2.3: A scheme of the three-electrode cell. RE, WE and CE stand for reference electrode, working electrode and counter electrode, respectively.

Chronopotentiometry (CP) was used in a two-electrode cell with (i) a (bio)cathode and (ii) a (bio)anode of the tested biofuel cells or biobatteries. Various currents were applied between the electrodes until the measured potential differences become stable. This method was used mainly for obtaining polarisation curves and power outputs of tested biobatteries and biofuel cells.

2.4.2 Electrochemical measurements on the photoactive electrodes

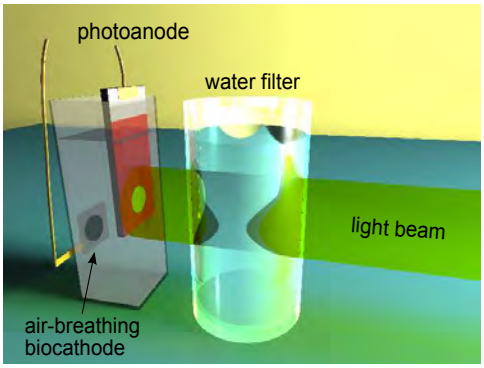

Figure 2.4: Scheme of the photo-biofuel cell illuminated by the beam of light passing through a water filter.

The measurements done with titania electrodes (Fig. 2.4) and solar cells were done in the darkness or under the illumination of a 150 W Xe lamp and a filter. The sample was placed in a way that the photoactive electrode was exposed to the light beam going through the filter. Two types of filters were used (depending on the availability): a quartz beaker filled with deionised water (water filter) or an AM 1.5 G filter (Sciencetech). The electrode surface was parallel to the plane of a lamp quartz window. Moreover, in some cases a special mask was used to cover the area around the illuminated part of the anode. The mask was made od a piece of a thin black metal plate with a hole of 0.7 cm in diameter.

2.5 Experimental procedures

2.5.1 Cleaning ITO

All ITO electrodes (ca. 1 cm x 1.5 cm) used in this thesis were cleaned in the same way before their modification. They were sonicated in ethanol for 15 min., rinsed in water and sonicated in water for 3 min. Then they were annealed in a tube furnace at 500 °C for 15 min. to burn out the remained organic pollution. They were left to cool down in air.

2.5.2 Pretreatment of Nafion membrane

Nafion membrane was pretreated according to a standard procedure [342] by heating it at the temperature of 80 °C in the following solutions:

1. 5 wt% H_2O_2 for 1 h,
2. H_2O for 1 h,
3. 0.5 M H_2SO_4 for 1 h,
4. H_2O for 1 h.

Then it was stored in water before being used.

2.5.3 Buffer preparation

Phosphate buffer 0.1 M H_3PO_4 solution was mixed with concentrated NaOH solution until the desired pH was obtained (usually pH 4.8).

McIlvaine's buffer Solutions of 0.2 M Na_2HPO_4 and 0.1 M citric acid were mixed in a proportion which gave the desired pH.

Tris buffer Solution containing 0.1 M KCl and 0.25 M Tris was mixed with concentrated HCl until the desired pH was obtained (usually pH 8.0).

2.5.4 Laccase purification

Laccase from *Cerrena unicolor* was purified by J. Rogalski using a procedure described in literature [335, 343]. This protein was purified by ion exchange chromatography on DEAE Sepharose (fast flow) and concentrated on a Pellicon 2 ultrafiltration semiprep cell (10 kDa cut off). The laccase was then distributed into lyophilisation vials and lyophilised in Labconco FreeZone 12. Each vial contained 1 mg of protein and 1.5×10^7 nkat of laccase.

2.5.5 Sol-gel matrix preparation

Silicate sol-gel matrices were obtained from precursors such as MTMOS [344], OTEOS (modified recipe from [345]) and TMOS [258]. Due to the similarities in the preparation of all matrices one can divide it into the same several steps:

1. mixing the precursor with a catalyst (HCl or NaOH) solution,
2. sonication of the mix in a sonication bath for a determined time,
3. one or several dilutions of the obtained mix followed by sonication or vortexing,
4. drop-coating of the final sol on the electrode surface and drying.

The details concerning first three steps of the matrix preparation are listed in Table 2.1.

Table 2.1: Details concerning the following steps of different sol-gel matrix preparations.

Precursor	Mix composition	Sonication	Dilution
MTMOS	375 µl of MeOH + 250 µl of MTMOS and 14 µl of 11 M HCl	15 min	1 µl mix : 99 µl buffered solution which can contain enzyme and/or CNTs, vortex for 3 min
OTEOS	100 µl of OTEOS + 5 µl of EtOH + 20 µl H_2O + 7.5 µl of 0.04 M NaOH	10 min	1 µl mix : 99 µl buffered solution which can contain enzyme and/or CNTs, vortex for 3 min
TMOS	500 µl of TMOS + 125 µl H_2O + 27.5 µl of 0.04 M HCl	20 min	250 µl of the mix + 250 µl of buffer (pH 5.0), you get mix **(i)**
		3 min	25 µl of diluted mix **(i)** + 225 µl of buffer (pH 5.0)
		3 min	12.5 µl of diluted mix **(ii)** + 12.5 µl of buffer (pH 5.0) + 100 µl buffered solution which can contain enzyme and/or CNTs, vortex for 3 min

MTMOS - methyltrimethoxysilane; OTEOS - n-octyltriethoxysilane; TMOS - tetramethoxysilane

The goal of using the sol-gel matrix for electrode modification was to immobilise the enzyme, thus typically the final diluter contained the chosen biocatalyst. Depending on the electrode surface which was modified, the final sol either contained or did not comprise CNTs. Further details of the dilution step will be described in next chapters. Usually the last step was the same for all modified electrodes - 20 µl of the final mix was drop-coated on the substrate of the area 0.2 cm^2. Then it was left in ambient conditions (typically ca. 50 % humidity and 22 °C) for ca. 17 h.

2.5.6 SWCNT functionalisation

SWCNTs were functionalised by the sonication of nanotubes and pyrene-1,3,6,8-tetrasulfonic acid tetrasodium salt hydrate (PTSA) in water. The suspension of 2 mg ml^{-1} SWCNT pellets and 10 mM PTSA was sonicated with an ultrasonic finger for 2 h at the amplitude of 40 %. Then the suspension was left over night and sonicated in a bath just before the filtration. It was further filtered with at least 1 l of water on a nylon filter. The obtained PTSA-SWCNTs were dried together with the filter in a tube furnace and then scraped off it. Then they were redispersed in water to obtain the concentration of 2 mg ml^{-1} [257].

Chapter 3

Electrodes with vertically aligned CNTs

CNTs have been used in electrochemistry almost since they were first produced in large quantities [150, 346, 347]. Their exceptional properties described in Section 1.1.1 make them popular as material for electrode modification (see Section 1.5.1). One of the ways of such modification is the attachment of aligned CNTs perpendicularly to the electrode surface. The vertical orientation allows for good utilisation of the electrode surface extended by CNTs. Furthermore, this arrangement takes advantage of the very fast electron transfer along the CNTs [348]. Vertically aligned CNT (VACNT) electrodes can be prepared either by (i) functionalisation of the CNT ends and covalently binding them to the surface [217,219] or, more commonly, (ii) using the aligned forests of CNTs grown on a substrate by chemical vapour deposition (CVD) [349].

A few cases of the as grown CNTs used in electrochemistry can be found in the literature, e.g. [350–353]. However, the most common way of the preparation of this type of electrodes involves attaching the VACNT arrays in a binder and often transferring them to a new substrate which serves as an electrode base. The transferred VACNTs should be attached in a way which both ensures an electric contact to the electrode surface and increases the mechanical stability of the tubes. A creation of the electric contact is often necessary, as the growth of VACNTs by CVD on a Si-wafer, which is the most common support, creates a thin amorphous silicate layer between the CNTs and the silicon [354]. Moreover, the mechanical contact between the tubes and the growth surface is generally very weak and it is easy to accidentally scrape off the VACNT film from the support.

Electrodes modified with VACNTs have been shown to support very fast electrochemistry of redox-probes or enzymes [217, 355]. They have been used previously for electroanalysis [152, 175, 351, 356], but to the best of my knowledge, the work presented in this chapter describes the first example of the VACNT utilisation as a platform for enzyme immobilisation and used for oxygen reduction.

Here I will present a simple method of transferring the as grown tubes on the electrode

substrate. I will focus on the description of the electrodes with laccase (see Section 1.2.2) immobilised on the VACNTs. Additionally I will show that other enzymes have also been successfully immobilised on the VACNT electrodes. I will also present the use of the obtained bioelectrodes for the construction of biobatteries and biofuel cells.

3.1 Electrode preparation

VACNT growth

Vertically aligned carbon nanotubes were grown by thermal CVD as described in detail earlier [357]. This part of work was done by Martin Jönsson-Niedziolka in the cooperation with Eleanor Campbell's Group at Göteborg University in Sweden. A silicon wafer was used as a growth substrate. As a catalyst 1 nm layer of Fe was deposited by electron beam evaporation. Between the substrate and a catalyst 10 nm of Al_2O_3 was deposited - to act as a buffer layer preventing the catalyst diffusing into the Si wafer. Moreover, the alumina layer enabled a better dispersion of Fe particles formed during heating of the wafer [358].

The as prepared substrate was loaded into a tube furnace which was first pumped out by a vacuum pump and then was flushed with a mix of inert gases: Ar/H_2 in the proportion 900/100 sccm[1]. The furnace was heated up to 700 °C and it was left at this temperature for 5 min. Acetylene was used as a carbon feedstock for CNT growth. It was introduced to the furnace by flushing the furnace with the gas mix of: $C_2H_2/H_2/Ar$, 5/500/500 sccm for 30 min. The CNTs were grown on the substrate as long as C_2H_2 was introduced into the furnace. Thus flushing the furnace with a mix of Ar/H_2 (900/100 sccm) amounts to stopping the tube growth. During all the above described steps the chamber was kept at a constant temperature of 700 °C.

The electrodes with the aligned nanotubes were prepared by glueing the as-grown VACNTs to tin-doped indium oxide coated glass electrode (ITO electrode) with a home-made conductive adhesive. Just before spreading the adhesive, the ITO electrode surface was wiped with a tissue moistened with acetone.

Preparation of the adhesive

The conductive adhesive was prepared by mixing a non-conductive epoxy adhesive with conductive MWCNTs. The obtained paste was conductive the most likely due to the percolation paths formed by the nanotubes. The epoxy adhesive was prepared from the commercially

[1] Sccm stands for standard cubic centimetres per minute

available Epoxy Embedding Media Kit (EEM, Fluka) as follows. First two mixes, denoted as A and B were made by mixing:

Mix A 1.25 ml EEM with 2 ml dodecenylsuccinic anhydride
Mix B 2 ml EEM with 1.75 ml methyl nadic anhydride.

Both A and B were stirred on a magnetic stirrer. 500 µl mix B was stirred with 1 drop of an accelerator - 2,4,6-tris(dimethylaminomethyl)phenol for 6 min. Then 250 µl mix A was added and stirred for further 10 min. 100 µl as prepared epoxy was mixed by hand with 10 mg MWCNTs (ca 8 wt.%) and 20 µl methanol. MeOH was used here to facilitate mixing. The obtained conductive adhesive was not viscous enough for glueing the VACNTs in a desired way. Thus it was left for a week in room temperature to gain proper viscoelastic properties. After that time it was possible to make a very thin and sticky layer of the epoxy-MWCNT paste.

VACNT transfer on ITO electrode

An approximately 50 µm thin layer of the epoxy-MWCNTs adhesive was spread on the conductive side of cleaned ITO electrode. The VACNT transfer was done by placing the wafer with the tubes upside down on the sticky paste and pressed gently with a finger. Thus only one side of the tubes was covered with the adhesive. Stronger pressure applied to the wafer could result in glueing the whole VACNT length.

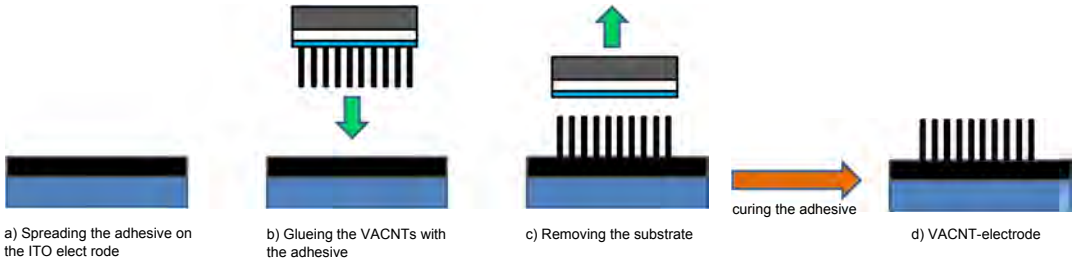

Figure 3.1: A scheme of the VACNT-electrode preparation.

Then the wafer was removed with the tweezers and all nanotubes were left on the electrode surface, still in vertical position. The ITO electrode modified in this way was then put into the tube furnace or a laboratory dryer and heated at 60 °C for ca. 18 h. The heating resulted in curing the epoxy paste.

The electrode was stored in dry place in room temperature when not in use. Not the whole area of ITO-electrode was covered with VACNTs. Thus an unmodified part of the electrode was covered with Scotch tape, nail varnish or an insulating tape. The electrodes were further characterised as VACNT films or they were used as platforms for the immobilisation of the mediators and/or the enzymes.

Electrodes with randomly aligned MWCNTs

The epoxy-MWCNTs paste was thinly spread on clean ITO electrode. Then powder of MWCNTs (the same ones which were used for making the paste) was pressed into the conductive adhesive. All the glued CNTs were left on the electrode surface and the excess was removed before curing the paste. The last step of the preparation was the same as in case of VACNT electrode. The electrode was heated for 18 h in at 60 °C.

Mediator immobilisation

Two different mediators were used to further facilitate the mediated electron transfer between the enzyme and the CNTs: ABTS or Syr. They were immobilised on the VACNTs in different ways. ABTS was adsorbed from a 0.1 mM solution in McIlvaine's buffer as described earlier [233]. The electrodes were immersed in the ABTS solution for at least 2 h and then they were rinsed in pure buffer. Syr was drop coated on VACNTs from 1 mM solution in EtOH due to its insolubility in water.

Laccase immobilisation

Laccase (Lc) was immobilised on the VACNT electrodes in the following ways: (i) adsorption from solution, (ii) encapsulation in drop-coated hydrophobic sol-gel silicate film and (iii) encapsulation in drop-coated silicate film preceded by non-covalent functionalisation of the CNTs with 1-pyrenesulfonic acid sodium salt (PSA).

(i) The VACNT-electrode (with or without the mediator) was immersed into 16 μg ml^{-1} Lc solution (in phosphate buffer, pH 4.8) for 1 V.
(ii) First the final MTMOS sol was prepared according to the recipe written in the Experimental procedures (Section 2.5.5). The mix was diluted in Lc solution (1.6 μg ml^{-1} in water). The obtained sol was drop-coated onto the VACNTs so that 10 μl was used for the electrode area of 0.2 cm^2. The electrode was left to dry for ca. 20 h under ambient conditions.
(iii) The VACNT-electrode was first immersed in 2 mM PSA solution (in water) for 24 h. It was dried for a few hours in air, rinsed with water and then used as a platform for Lac immobilisation in the same way as described in **(ii)**.

In total six different types of electrodes were obtained by the modification of the VACNT-electrodes. The ways of their preparation, as well as their symbols which will be further used, are listed in Table 3.1. Each electrode prepared by drop-coating the sol with Lc contained the same amount of enzyme - 80 μg cm^{-2}. The amount of Lc adsorbed on the electrodes from the solution is unknown.

Table 3.1: A list of abbreviations used for the description of different types of electrodes obtained by the modification of the VACNT platforms.

Name	Mediator	Laccase
VACNT/ABTS/Lc	ABTS	adsorbed from solution
VACNT/ABTS/MTMOS/Lc	ABTS	immobilised in a silicate film
VACNT/Syr/MTMOS/Lc	Syr	immobilised in a silicate film
VACNT/Lc	-	adsorbed from solution
VACNT/MTMOS/Lc	-	immobilised in a silicate film
VACNT/PSA/MTMOS/Lc	-	immobilised in a silicate film (VACNTs were functionalised with PSA)

Immobilisation of other enzymes

Glucose oxidase (GOx) and glucose dehydrogenase (GDH) were immobilised on various VACNT-electrodes in the MTMOS silicate matrices. The same way of electrode preparation as in case of VACNT/MTMOS/Lc was used, the only difference was the composition of the buffered solution used for the dilution of the MTMOS mix. The solution of 1 mg GOx ml^{-1} of McIlvaine's buffer (pH 4.8) was used for the preparation of the electrode VACNT/MTMOS/GOx. GDH solution of the same concentration and in the same buffer was used as a diluter for MTMOS mix for obtaining VACNT/MTMOS/GDH electrode. In both cases the dilution was done in the proportion 99:1. 3 µl of the final sol with the enzyme was drop-coated on 0.03 cm^2 of the projected area of the VACNT-electrode and left to dry in ambient conditions.

Zn anode

The anode was made of a piece of a Zn wire rolled to a spiral. The active surface area was around 1 cm^2. The Zn wire was coated with Nafion by dipping it into 0.5 % solution of Nafion in isopropanol and drying in air.

3.2 Results and discussion

3.2.1 Film electrodes with as-grown VACNTs

Before the characterisation of the electrodes modified with VACNTs, initial experiments were performed on the tubes grown in the same way, but not transferred on ITO electrode. The as-grown tubes were used with Si-wafer as a substrate. In this case an electric contact with the tubes was made by attaching an adhesive copper conductive tape to the edge of the wafer. The non-transferred CNTs showed a very good electrochemical behaviour in the

case of adsorption of $ABTS^{2-}$ (more details below). Furthermore, an efficient electrocatalytic O_2 reduction was observed on the electrode with adsorbed $ABTS^{2-}$ in the electrolyte containing laccase. However, the as-grown VACNT electrodes have two major drawbacks. The more important problem concerns the poor adhesion of the tubes to the substrate. E.g. taking the electrode out of an aqueous solution and drying in air results in collapsing the CNT forest by the surface tension of the evaporating water. That makes this electrode essentially one-time-use.

The second drawback of using non-transferred VACNTs as the electrode material is the unreliable electric contact with the silicon wafer. This effect the most likely comes from the use of a buffer layer placed between wafer and Fe. On the other hand the use of a conductive adhesive for the VACNTs transfer results in improved adhesion to the electrode surface, as well as in more reliable electric contact.

3.2.2 Transferred VACNT electrodes

SEM images

At SEM images of the VACNT electrodes prepared by the transfer method one can clearly see that the CNTs remain vertically aligned, as they were before in the as-grown state (Fig. 3.2A). The transferred CNTS were approximately 500 µm long and had an outer diameter of $10 - 20$ nm. In Figure 3.2B one can see that the tips of the tubes are not covered by the epoxy paste. The VACNTs covered with silicate film (Fig. 3.2C) form a wavy structure of vertical sheets of silicate coated CNTs. Close inspection into this structure (Fig. 3.2D) shows that the VACNT-silicate forms a porous composite. Such a porous matrix allows the diffusion of electrolyte through the film - as noted in previous experiments [233].

Electroreduction of H_2O_2

Valuable information about the active surface area of the electrodes can be obtained by the slow, heterogeneous and highly irreversible electroreduction of hydrogen peroxide in an acidic solution [359, 360]. This is because the control of the electrode reaction kinetics by electrochemical step allows for penetration of the reactant through the nanotube forest. It is clearly seen in Fig. 3.3 that the Faradaic current is about 2 orders of magnitude times higher on the VACNT electrode compared to the bare ITO electrode. Moreover, the enhanced current observed for the electrode with only the CNT-epoxy paste indicates that the adhesive does not form a fully compact surface but that it is somewhat porous. The presence of the CNTs does not seem to affect the onset of the current. It means that the current enhancement comes from the increased surface area and not from catalysis [157]. Striking in Fig. 3.3 is

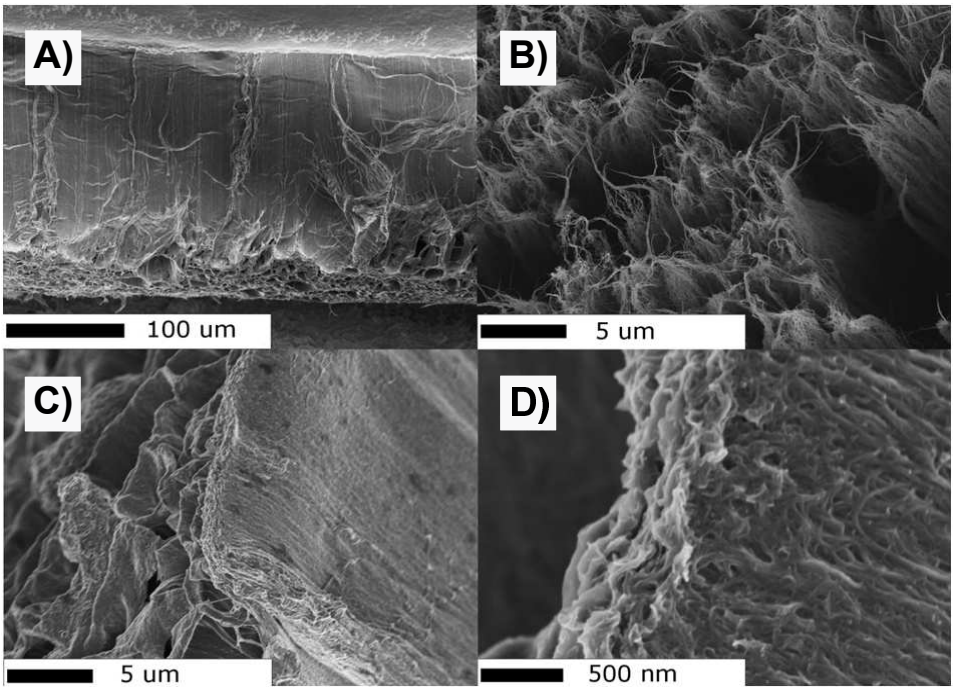

Figure 3.2: SEM images of the transferred VACNTs. (A) Side view of the edge of the electrode. Note that at this magnification the individual CNTs are not visible. The lower part of the image shows the epoxy covered side of the VACNT film peeled from the electrode surface. (B) Close-up of the tips of the VACNTs, (C) silicate-covered VACNT electrode, (D) close-up of the silicate covered VACNT tips, all taken at an oblique angle of 45°.

also the comparatively large capacitive current at the VACNT electrode resulting from their large surface area.

Characterisation with the use of simple redox systems

Simple redox systems were employed to further characterise the electrochemical performance of the VANCT electrodes. The one electron electrooxidation and reduction of the $Fe(CN)_6^{3-}$ complex ion is a fast outer sphere reaction. Thus $K_3Fe(CN)_6$ solution (5 mM in 0.1 M KCl) was used to compare the electroactivity of a few different electrodes: (i) bare ITO, (ii) electrode with randomly aligned MWCNTs, (iii) VACNT electrode and (iv) electrode covered with CNT-epoxy paste without any VACNTs. As shown in Fig. 3.4A the peak current is much higher for the VACNT electrode than for the bare ITO. Interestingly the peak separation (ΔE = 141 mV) is close to that at the bare ITO electrode despite a much higher current. That is in contrast to the electrode (iv) where the peak separation is very large (ΔE = 465 mV). This behaviour comes from the partially blocked electrode surface by the epoxy glue. The electrode (ii) - with randomly aligned MWCNTs - shows even higher current than the VACNT electrode, which is probably caused by the slow diffusion into the VACNT forest. The reaction therefore takes place mainly on tips of these tubes. This conclusion is supported by the scan rate dependence of the redox current which shows a typical planar electrode mass transfer limited behaviour (Fig. 3.4B). For this kind of a behaviour I is proportional to $v^{1/2}$

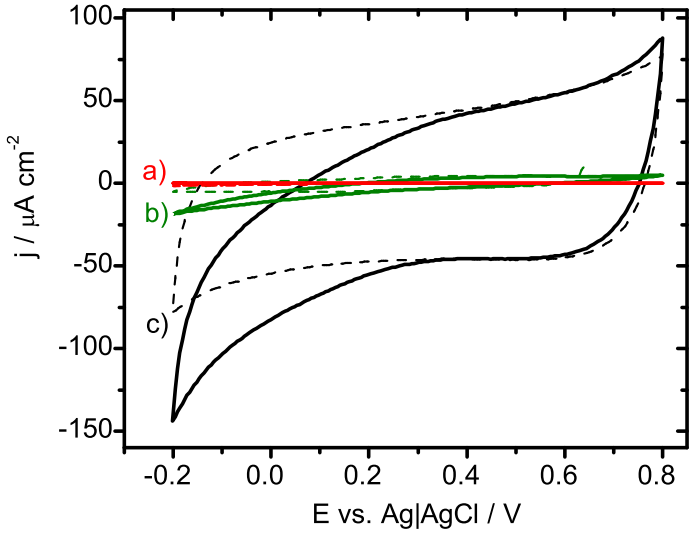

Figure 3.3: Cyclic voltammograms obtained in deaerated 0.1 M H_2SO_4 $_{aq.}$ at a bare ITO electrode a), an electrode covered with CNT-epoxy paste b) or with VACNTs c). The voltammograms shows measurements with (solid lines) and without (dashed lines) the presence of 50 mM H_2O_2. Scan rate 2 mV s^{-1}.

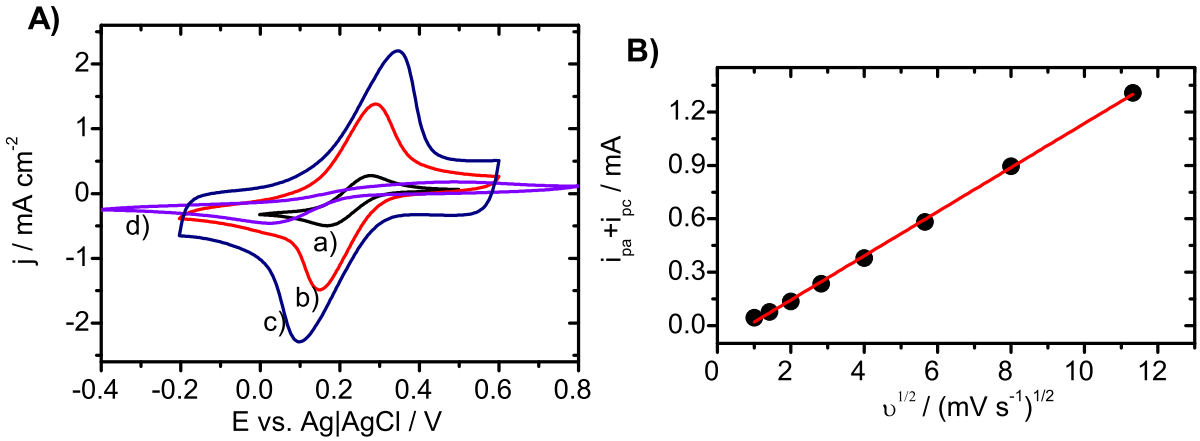

Figure 3.4: A) CVs obtained in 5 mM $K_3Fe(CN)_6$ in 0.1 MKCl at a) a bare ITO electrode, b) an electrode with randomly aligned MWCNTs, c) a VACNT electrode, and d) an electrode covered with CNT-epoxy paste without any VACNTs. ν = 16 mV s^{-1}. B) Dependence of the peak current against the square root of the scan rate for the VACNT electrode. The red line is a linear fit to the data from 4 to 128 mV s^{-1}.

and not to v as would be expected in the restricted geometry inside the CNT array [201]. A slight deviation from the peak current vs. $v^{1/2}$ linear dependence can possibly be spotted at the lowest scan rates (lower than 4 mV s^{-1}). That might be caused by VACNTs forming a thin cell with trapped electrolyte [201]. However, this behaviour is noticeable only for very small scan rates.

The resistance of the VACNT electrodes measured both by the impedance spectroscopy and by a two-probe multimeter gave a value of between $100 - 150\,\Omega$.

Tert-butylferrocene (*t*BuFc) was chosen as another redox probe indicating the degree of the enhancement of the active surface of the ITO-electrode after the modification with the VACNTs. 50 nmol of *t*BuFc was deposited on the VACNT-electrode by drop-coating with

*t*BuFc diluted with hexane. Cyclic voltammetry on such modified electrode was performed in aqueous solution of 0.1 M $NaClO_4$ - see Fig. 3.5. The obtained voltammograms (black

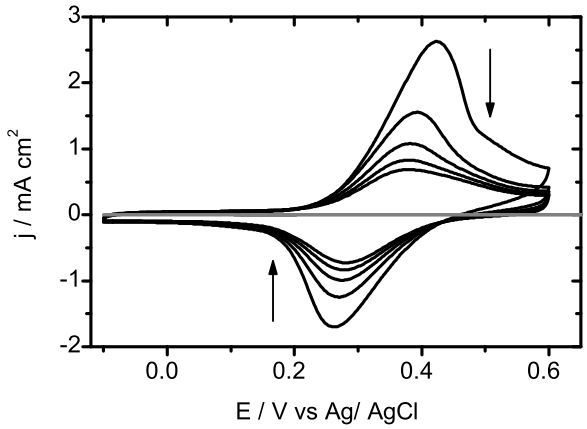

Figure 3.5: CV on the VACNT-electrode coated with 50 nmol *t*BuFc in 0.1 M $NaClO_4$ performed under air, $\nu = 10$ mV s^{-1}. Gray line shows the result for the ITO-electrode with the same amount of *t*BuFc.

lines) show a peak-shaped response related to *t*BuFc oxidation to *t*BuFc$^+$ [345, 361, 362]. The following scans give a decrease in anodic and cathodic peaks, what is a result of *t*BuFc$^+$ cations transfer from the organic to aqueous phase of the system (Eq. 3.1).

$$t\mathrm{BuFc}_{\mathrm{org}} - \mathrm{e}^- \rightarrow t\mathrm{BuFc}^+_{\mathrm{aq}} \tag{3.1}$$

The reaction of *t*BuFc oxidation is expected to occur at the three-phase-junction between the electroactive material, the organic phase with the redox probe and the aqueous electrolyte. Thus an increase in the voltammetric signal for the modified electrode, in comparison with bare electrode, indicate an increase of the length. Such increase is caused by the enlargement of the electroactive surface of the electrode. A comparison of CVs from the bare ITO-electrode and the VACNT-electrode (Fig. 3.5, grey and black lines, respectively) indicates a tremendous enlargement of the electroactive surface due to the electrode modification. That in turn means that the sidewalls of VACNTs are active. Thus our simple experiment with *t*BuFc gave another argument for stating the electroactivity of CNT sidewalls, which is the subject of undergoing debate described in Section 1.5.1.

The next compound which was used as a relevant redox probe for the characterisation of the VACNT electrodes was ABTS. It was chosen first of all because it is a popular mediator shuttling the electrons between the electrode surface and the active centre of laccase [82]. It contains benzothiazoline group which has an extended π electron system in a benzene ring. This system is easily adsorbed by π-orbit overlapping onto graphite-like surfaces, like CNTs [233, 240]. Figure 3.6 presents cyclic voltammetry performed after the VACNT electrode was immersed into the ABTS solution. From these measurements it is clearly seen that this mediator is adsorbed on the electrode. Moreover, the adsorption took place for approximately from 2 to 3 hours. After that time the voltammograms showed a stabilised current.

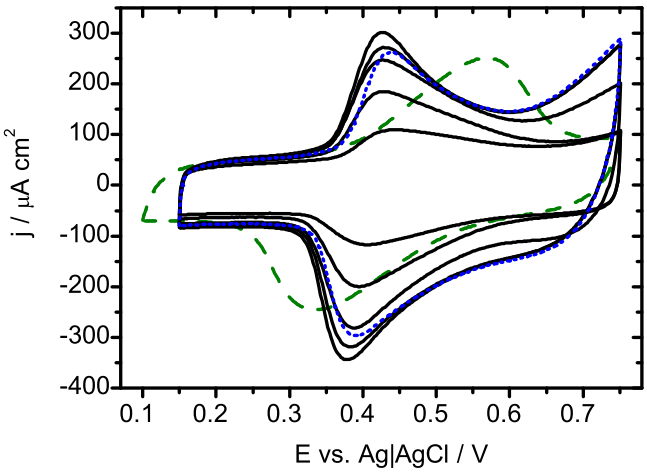

Figure 3.6: CVs of the $ABTS^{2-}$ adsorption. Solid lines (in direction of arrow): VACNT/epoxy paste electrodes after 10, 30, 80, 160 and 180 min immersion in 0.1 mM ABTS in McIlvaine's buffer. Dotted blue line: in clean buffer after adsorption. Dashed green line: As-grown VACNTs after adsorption saturated. Scan rate 10 mV s^{-1}.

As a comparison the electrode with as-grown VACNTs was used (with Si wafer acted as a substrate). The current density measured for the situation when the $ABTS^{2-}$ adsorption was saturated was very similar for the two electrodes: with the transferred and the as-grown VACNTs. It shows that the transfer method results in only a small blockage of the tubes by the epoxy (Fig. 3.6). Moreover, the peak separation obtained for the non-transferred tube forest is much bigger than for the transferred one, which is a result of a worse electric contact made with the former ones.

The VACNT electrodes were removed form the ABTS solution after 3 h and immersed in the clean buffer. Again the CV was performed - dashed line in Fig. 3.6. The charge indicated that a small fraction of the mediator was desorbed from the tubes. This amount was a bit different from sample to sample (here ca. 24 % was desorbed) but in general most of $ABTS^{2-}$ stayed at the VACNTs.

The oxidation peak obtained for the VACNTs with adsorbed $ABTS^{2-}$ was used for estimation of the electroactive electrode area. A reasonable estimation was made that the tubes are almost completely covered with the mediator ions. Thus, having the charge passed during the oxidation and knowing the size of ABTS, the electrode active area was calculated to be 0.11 cm^{-2}. This rough estimation indicates that the area of the VACNT electrode was almost 200 times higher than bare ITO. However, this is a low estimate because the electrode active area could have been calculated larger if a big area of VACNTs was not covered with probe molecules.

Oxidation of dopamine, ascorbic and uric acid

Dopamine (DA) is a very important neurotransmitter responsible e.g. for coordination and higher mental activities. The abnormal concentrations of DA found in the human body can lead to serious diseases such as Parkinson's disease or schizophrenia [363]. Thus a good method of reliable and fast DA detection in the body fluids containing different interfering species such as ascorbic acid (AA) or uric acid (UA) is sought [364].

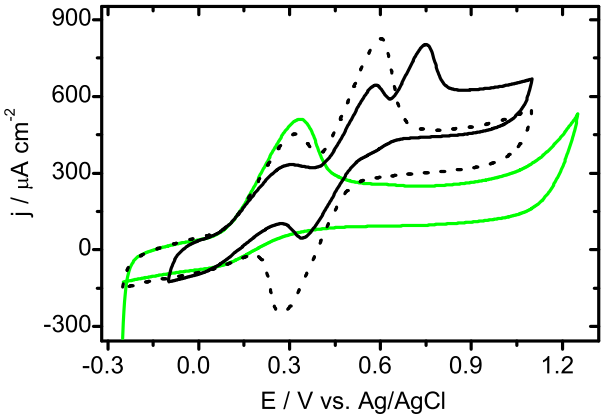

Figure 3.7: CVs on the VACNT-electrode performed in deoxygenated solutions containing (green line) 0.2 mM ascorbic acid (AA); (dotted line) 0.2 mM AA and 0.2 mM dopamine (DA); (black line) 0.2 mM AA, 0.2 mM DA and 0.1 mM uric acid. Phosphate buffer (pH 4.7) was used as an electrolyte. $\nu = 5$ mV s^{-1}.

We performed simple cycle voltammetric experiment to check the response of the VACNT-electrode in the presence of DA, AA and UA (Fig. 3.7). Each of the organic specie gives the a pronounced oxidation peak, but the peaks are not separated as it was obtained e.g. on the carbon nanoparticulate electrodes [364]. Moreover, the capacitive current related to a huge surface area of the electrode is very disadvantageous from the point of view of using the VACNT-electrode as a sensor. The signal from the tiny concentrations of the analyte might be hidden in the signal related to the CNT capacitance. Thus although we obtained a relatively nice signal from DA, AA and UA oxidised on our electrode we did not use it as a platform for DA sensing. However, the VACNT-electrode will be further exploited for the construction of a self-powered sensor for ascorbic acid described in detail in Chapter 6.

3.2.3 Platform for enzyme immobilization

So far we checked that the VACNT-electrodes have a very large electroactive surface. Moreover, it is possible to permanently immobilise ABTS on these electrodes which results in obtaining a stable extended system being able to mediate electron transfer to the Lc active centre (VACNT/ABTS). Thus our electrodes are expected to be very good platforms for Lc immobilisation and thus biocathode preparation.

The method of biocathode preparation was based on our previous experience concerning Lc immobilisation [233,257,365,366]. First we prepared electrodes with or without the mediator such as ABTS or Syr. Taking into account the hydrophobicity of our VACNT-electrodes we have chosen a hydrophobic type of sol-gel matrix for a stable enzyme immobilisation which is $MTMOS_{gel}$. All in all six types of electrodes were obtained and checked towards O_2 reduction with slow scan cyclic voltammetry and chronoamperometry. The obtained results are divided into two groups depending on the given mediated or non-mediated bioelectroreduction oxygen.

3.2.4 Biocathodes for mediated electrocatalysis

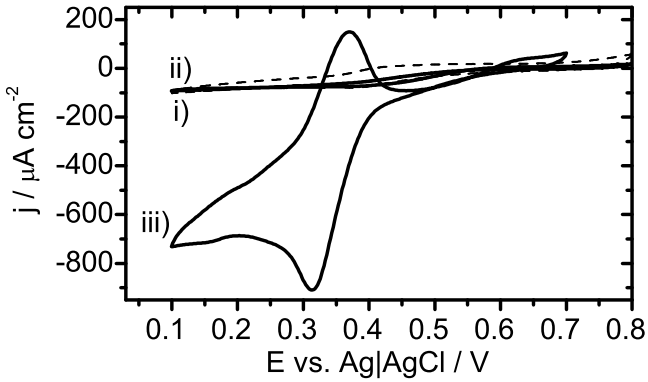

Figure 3.8: CVs of mediated oxygen reduction in oxygenated McIlvaine's buffer (pH 4.8) with the electrodes i) VACNT/ABTS/Lc ii) (dashed line) VACNT/ABTS/MTMOS/Lc and iii) VACNT/Syr/MTMOS/Lc, scan rate 1 mV s^{-1}.

Both electrodes with ABTS and Lc, VACNT/ABTS/- Lc and VACNT/ABTS/MTMOS/-Lc give O_2 reduction currents density of around 100 µA cm^{-2} - see Fig. 3.8A i-ii. Thus the current level is the same either Lc was adsorbed from the solution or it was embedded in a sol-gel matrix. Moreover, the obtained current is ca. two times higher that the current obtained form the biocathodes with the same amount of Lc but 50 times less CNTs which were randomly oriented [233]. The bioelectrodes without the mediator did not show any oxygen reduction (data not shown).

A remarkably high anodic current of ca. 700 µA cm^{-2} (at 0.10 V vs. RE) was observed for the electrode with another Lc mediator - syringaldazine, (Fig. 3.8Aiii). The shape of the curve for VACNT/Syr/MTMOS/Lc indicates a large non-catalytic contribution, which was also observed earlier [367]. The onset potential of mediated O_2 reduction on our bioelectrodes is at ca. 0.60 V vs. RE . This value is close to the redox potential of T1 site in Lc which is around 0.58 V vs. RE. Besides the value 0.60 V is similar to the onset potential obtained for the same mediated system immobilized on carbon nanoparticles [368].

3.2.5 Biocathodes for non-mediated electrocatalysis

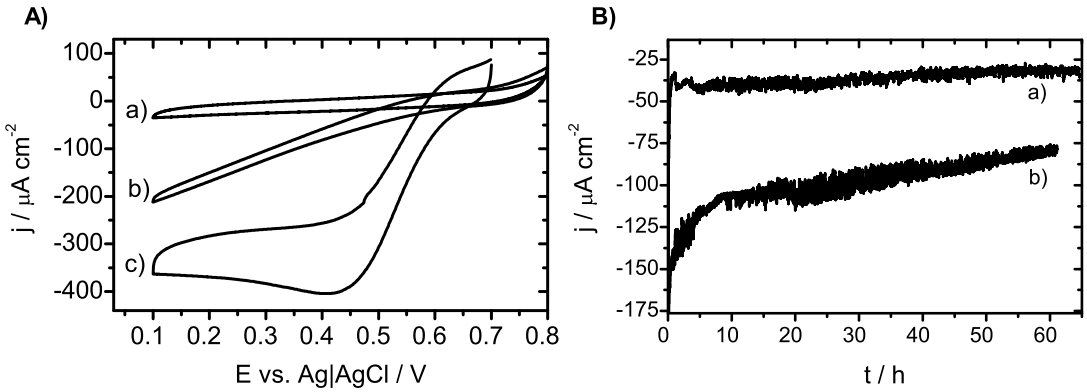

Figure 3.9: A) CVs of Non-mediated electron transfer with the electrodes a) VACNT/Lc, b) VACNT/MTMOS/Lc and c) VACNT/PSA/MTMOS/Lc, scan rate 1 mV s^{-1}. B) Chronoamperometry at 0.20 V in Mc Ilvaine's buffer kept under air, pH 4.8, a) VACNT/PSA/MTMOS/Lc, b) VACNT/Syr/MTMOS/Lc. Measurements done in McIlvaine's buffer kept under air.

In case of the non-mediated systems we observed a difference between the performances of VACNT/Lc and VACNT/MTMOS/Lc electrodes. No oxygen reduction was found for the electrode with Lc adsorbed on bare nanotubes (graph a). However, when Lc was immobilised in $MTMOS_{gel}$ on the VACNTs the electrode showed a large catalytic current. The current density at 0.10 V is ca. 200 µA cm^{-2}, which is a two times bigger value than in case of the mediated bioelectrocatalysis with ABTS (Fig. 3.8 A i-ii). This result indicates a favourable enzyme orientation in a silicate matrix. Interestingly, the shape of the CVs shows that the saturation current of O_2 reduction was not reached. That was caused by the limited rate of diffusion of oxygen to the electrode surface.

Taking into account our success in obtaining efficient biocathodes with the functionalised CNTs [257, 258] we used one of the pyrene derivatives for the modification of our VACNTs. PSA was non-covalently bound to the VACNTs for the solution. The obtained electrode was coated with $Lc/MTMOS_{gel}$ and named VACNT/PSA/MTMOS/Lc. It gave a very high reduction current of ca. 400 µA cm^{-2}.

Chronoamperometry was performed on VACNT/PSA/MTMOS/Lc and VACNT/Syr/-MTMOS/Lc - see Figure 3.8B a and b, respectively. In both cases a very fast initial decline of current is followed by a slower decrease. For the electrode without the mediator the current is almost stable in comparison with the electrode with Syr. The latter one loses ca. 48 % of its activity after 60 h which might be caused by the leakage of the mediator. Thus Lc immobilised on the VACNT-electrodes in sol-gel processed silicate films retain its activity, which is in agreement with [233, 366, 369].

3.2.6 Bioanodes for mediated electrocatalysis

Electrodes with GOx and GDH in $MTMOS_{gel}$ were prepared to show the ease of obtaining bioanodes with the use of our platform for enzyme immobilisation. Both enzymes are responsible for glucose oxidation and they are often used in the construction of glucose biosensors or biofuel cells. Our goal here is just to show that the immobilisation method which we used for Lc is also successful for obtaining other bioelectrodes.

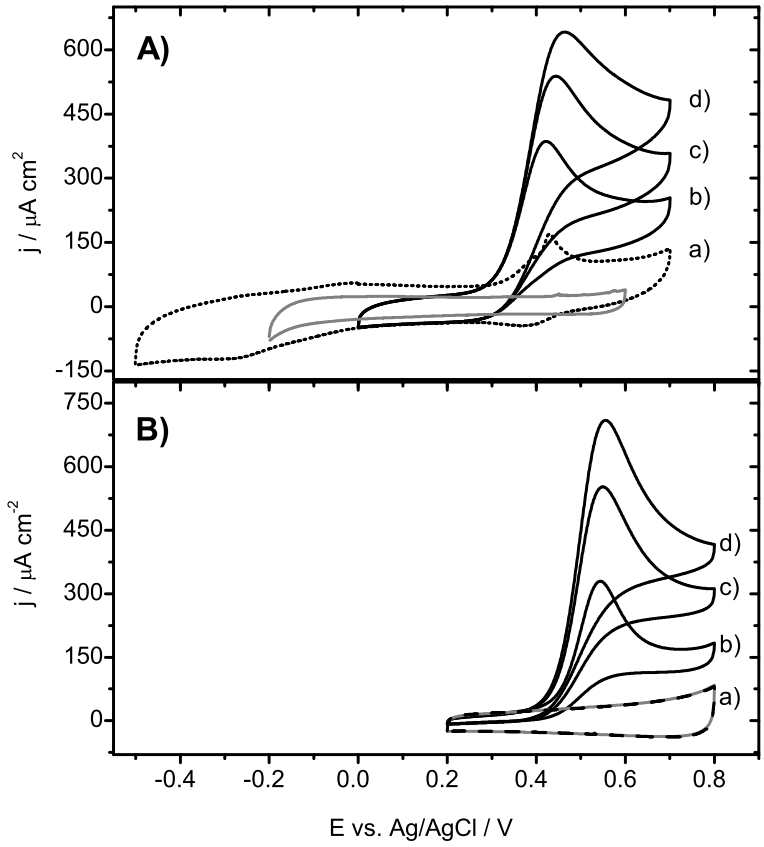

Figure 3.10: A) CV of VACNT/MTMOS/GOx in 0.5 mM FMCA in McIlvaine's buffer (pH 4.8) (a) without glucose and with (b) 1, (c) 2 and (d) 3 portions of glucose. B) CV of VACNT/MTMOS/GDH in Tris buffer (pH 8.0) (a, dashed black line) with 1 portion of glucose; with 2 mM NADH and (b) 1, (c) 2 and (d) 3 portions of glucose. 1 portion is equal glucose concentration of 6.3 mM. Gray graph is a CV obtained in pure Tris buffer. All solutions were kept under air.

Cyclic voltammograms presented in Figure 3.10A as solid lines show the increase in anodic current at the potential around 0.45 V vs. RE with the increase of glucose concentration. That increase is due to glucose oxidation by GOx immobilised on VACNT/MTMOS/GOx in the presence of ferrocenecarboxylic acid (FMCA). FMCA acts as a mediator for GOx and without it no glucose oxidation is observed as an anodic peak (data not shown). Reactions occurring in the presented system with GOx are described in Section 1.2.2.

Figure 3.10B presents glucose oxidation on VACNT/MTMOS/GDH in the presence of its coenzyme nicotinamide adenine dinucleotide, NAD^+. The increase of glucose concentration results in the increase of anodic current. However, no anodic peak is observed for the situation

when NAD^+ is not present in the glucose solution (Fig. 3.10Ba). This kind of bioanode behaviour is expected and the reaction describing it is presented in Section 1.2.2.

3.2.7 Biobatteries

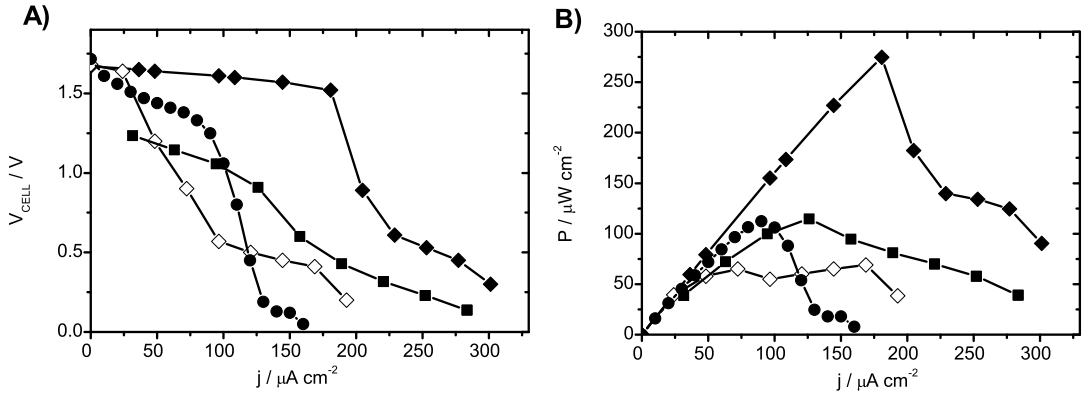

Figure 3.11: A) Polarisation curve and B) the dependence of the power output on the current density of the zinc-dioxygen battery in O_2-bubbled McIlvain's buffer with (squares) VACNT/Syr/MTMOS/Lc, (circles) VACNT/MTMOS/Lc and (diamonds) VACNT/PSA/MTMOS/Lc as a cathode. The open diamonds are measured in air.

To show the potential application of our biocathodes based on VACNT-electrodes we used the best of them for making biobatteries with zinc anodes. Zn was chosen as an anode material due to the low potential of the Zn/Zn^{+2} redox couple [370]. Thus the obtained hybrid biobattery should give higher operating voltages than typical biofuel cells such as glucose/O_2 BFC.

VACNT/Syr/MTMOS/Lc, VACNT/MTMOS/Lc and VACNT/PSA/MTMOS/Lc were connected with properly pretreated Zn wire. The zinc pretreatment was done by coating the wire with thin film of Nafion which promoted the growth of Zn^{+2} conductive hopeite $[Zn_3(PO_4)_2] \cdot 4\,H_2O$ [370]. The performances of obtained biobatteries were checked in oxygenated McIlvaine's buffer with the use of chronopotentiometry. The results are plotted in Fig. 3.11 as V-j curves (A) and power outputs (B). The best outputs are from the non-mediated system with PSA-functionalised VACNTs. Open circuit potential for the battery with VACNT/PSA/MTMOS/Lc has a value of 1.67 V, almost the same as for the battery with VACNT/MTMOS/Lc. The maximum power, P_{max}, of 275 $\mu W\,cm^{-2}$ was obtained at the cell potential of 1.50 V (Fig. 3.11, black diamonds). The same system checked without introducing oxygen into the buffer gave P_{max} of 70 $\mu W\,cm^{-2}$, which is almost four times less than for the oxygenated buffer. A comparison of the biobattery with VACNT/PSA/-MTMOS/Lc with a similar battery comprising PSA-functionalised SWCNTs [258] shows that the one with VACNTs gives higher power. It also give higher power output than other Zn/O_2 batteries with Lc reported previously despite our biobattery comprises cheaper and less efficient enzyme.

Systems comprising VACNT/Syr/MTMOS/Lc and VACNT/MTMOS/Lc had the same maximum power density - 115 $\mu W\,cm^{-2}$. However, the potential related to P_{max} was different in each example: 0.90 V for the system mediated with Syr and 1.25 V when Lc was embeded in $MTMOS_{gel}$ without any mediator. This difference comes from a higher overpotential in the first example which in turn comes from the mismatch between the redox potential of the mediator and the catalytic potential of the enzyme[2]. The redox potentials of Syr and the enzyme T1 centre are 0.34 V and 0.58 V vs. RE, respectively.

3.3 Conclusions

We developed a new method of obtaining mechanically stable and electroactive platforms with vertically aligned carbon nanotubes. As grown VACNTs were transferred on ITO-electrodes and glued with home-made conductive adhesive. The transferred CNTs greatly increased the active surface of the electrode and acted as a substrate for enzyme immobilisation. We showed a successful immobilisation of three different enzymes - laccase, glucose oxidase and glucose dehydrogenase. All of them were embedded in a sol-gel silicate matrix known as a very good host which keeps biomolecules active. Thus we showed that the VACNT-electrodes act as very good platforms for obtaining biocathodes for oxygen reduction and bioanodes for glucose oxidation.

We paid special attention to the detailed study on the electrodes modified with Lc. We immobilised the enzyme either with or without the mediator such as ABTS or syringaldazine. Besides we prepared a biocathode without the mediator but with PSA-functionalised VACNTs. Performed electrochemical experiments showed that the most efficient electrode toward oxygen reduction was the biocathode with PSA-VACNTs. It gave a very high non-mediated cathodic current density of 400 $\mu A\,cm^{-2}$ at 0.10 V vs. RE in oxygenated solution. The best result for mediated system was obtained for the biocathode with Syr - ca. 700 $\mu A\,cm^{-2}$ at 0.10 V vs. RE. Thus the obtained current density was higher for MET than for DET. This result can be explained by the easier electron transfer from the electrode surface to the active centre of Lc in case of a mediated system (see Section 1.2.1). The presence of Syr make an ET possible even when the enzyme molecules are not properly oriented on VACNTs. DET is not possible in that case so that the current density for VACNT/PSA/-MTMOS/Lc is lower than for VACNT/Syr/MTMOS/Lc.

The most efficient bioelectrodes were further connected with the Zn anodes and formed biobatteries. The maximum power density was obtained for the non-mediated system with PSA-VACNTs - 275 $\mu W\,cm^{-2}$ was obtained at the cell potential of 1.50 V.

[2]Catalytic potential is an informal name for the potential of an inflection point of the sigmoidal transition toward the plateau [371]

The results which I presented in this chapter clearly show that the VACNT-electrodes are attractive platforms for enzyme immobilisation. Thus these electrodes are useful in obtaining efficient bioelectrocatalytic systems which can be further used for biobattery and biofuel cell preparation.

Chapter 4

Influence of convection on the oxygen bioelectroreduction

Experimental data concerning oxygen bioelectroreduction presented in the literature over the last decade shows the increase in the obtained reduction current density on new types of biocathodes [372–374]. On the one hand this is caused by the use of new nanostructured materials which give bigger active surface of the electrode and enhance the electron transfer rate to the active centre of the enzyme. On the other hand many of the reported results simply do not match the theory. The reduction currents under quiescent conditions are higher then the currents calculated from the Cotrell equation by taking into account the mass transport limitation. The deviations from this equation can be caused by the convection in the long term measurements. This phenomenon and the fact that the natural convection can strongly influence cyclic voltammetry are well known [337, 375]. However it is hard to find a proper model for convection in an electrochemical cell due to many additional sources of a liquid movement such as an air motion or vibrations of the cell [376].

Here we present a combination of the simulations of the bioelectrocatalytic oxygen reduction with experimental data obtained from tracking the electrolyte convection in the electrochemical cell. The convection occurring in a steady electrolyte and in an electrolyte kept under a gas flow is measured and simulated in the program COMSOL. Then this simulation is coupled with a simple model of O_2 reduction occurring on the biocathode. The results are presented in form of cyclic voltammograms which match the experimental data obtained for the non-breathing biocathodes with bilirubin oxidase. Thus we prove that the exceeded currents of O_2 reduction are in fact the results of the convective flows present in the electrochemical cells.

4.1 Experimental

4.1.1 Biocathode for O_2 electroreduction as a non-breathing system

PTSA functionalised SWCNTs were immobilised together with the enzyme in a MTMOS sol-gel matrix (see recipe in Section 2.5.5). 99 µl of PTSA-SWCNT suspension was vortexed together with 99 µl BOx solution (2 mg ml^{-1} in McIlvaine's buffer, pH 4.8) for ca. 2 min. 2 µl of the final MTMOS mix sol from Sec. 2.5.5 was added to the PTSA-SWCNT/BOx suspension and vortexed for 3 min. 20 µl of the final suspension was drop-coated on the ITO electrode of the area 0.2 cm^2 and dried overnight.

4.1.2 Setup for measuring the convective flow in the cell

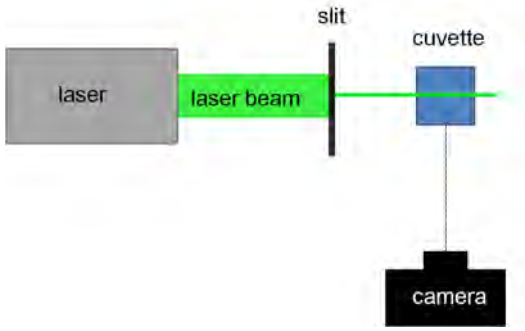

Figure 4.1: Top view on the setup for measuring the convective flow in the cell.

We used a dispersion of latex beads suspended in water in a spectroscopy cuvette. The cuvette was illuminated by a green laser beam from the side. Due to the way of illumination it was possible to observe the light scattering from the beads moving in plane of a longitudinal section of a cuvette. The bead movement was filmed at the right angle to the illumination. The obtained pictures were further analysed by Witold Stryczniewicz with the use of particle image velocimetry (PIV).

4.1.3 2D model of the non-breathing systems

The computer models of two systems containing the non-breathing biocathodes were made in COMSOL. Both of them contained 2D rectangular shaped cell (10 mm × 15 mm) with a linear electrode. The electrode width was the same as the radius of the electrode which we used in our experiments (2.5 mm). Moreover, the electrode was located on one of the walls of the cell, 10 mm in depth. A very simple model of O_2 reduction by BOx was used. It was assumed that the reaction was of the first order [377]:

$$S + 4e^- \rightarrow P, \tag{4.1}$$

where S is a substrate and P is a product (here O_2 and H_2O respectively). Thus the following equation describes the consumption of dioxygen by the enzyme:

$$D_{O_2}\left(\frac{\delta[O_2]}{\delta\overrightarrow{n}}\right)_{on\ electrode} = \frac{1}{\frac{[O_2]+K_M}{\Gamma_E k_{cat}[O_2]} + \frac{1}{\Gamma_E k_f[O_2]}} \tag{4.2}$$

where: K_M - Michaelis constant for BOx; D_{O_2} - diffusion constant of O_2; Γ_E - surface density of BOx on the electrode; k_{cat} - turnover number; k_f - forward reaction rate in Eq. 4.1. k_f is in turn described by a Butler-Volmer type expression:

$$k_f = k_0\ exp[-\alpha f(E - E_0)], \tag{4.3}$$

where k_0 - pre-exponential constant; α - symmetry constant; $f = \frac{nF}{RT}$; E_0 - catalytic potential.

One of the systems defined in COMSOL represented the quiescent conditions. The other one took into account the convection. The hydrodynamic effect was introduced as a volume force in the cell pushing the liquid around and a sliding wall representing the moving gas at the electrolyte surface. The liquid was treated as a water solution in room temperature. Two situations were simulated for each model: (i) the system staying under the nominally quiescent conditions and (ii) the system subjected to the convective flow. In each case O_2 concentration at the liquid surface was fixed to 0.25 mM (under air). COMSOL was used for numerical solving of the convective diffusive equations starting from Eq. 4.2.

4.2 Results and discussion

As a model system of O_2 bioelectroreduction we use an efficient non-breathing electrode with bilirubin oxidase. In quiescent conditions[1] this biocathode gives the current density of O_2 reduction around 40 $\mu A\,cm^{-2}$ (Fig. 4.2, dashed black line). This result is almost three times higher than the current density calculated for the 2D model without the convection. The values of the parameters used for calculating the theoretical shape of the CV (Fig. 4.2, blue dotted line) are listed in Table 4.1. The comparison between the experimental and the modelled CV clearly shows a big deviation for the potentials much lower than the onset potential. However, for the low potentials, the modelled CV follows the mass transfer limited current described by the Cottrell equation (Fig. 4.2, red solid line).

The discrepancy between the shapes of CVs for the modelled and experimental systems comes from the presence of convective flows in the real electrochemical cell under the nominally

[1]Here quiescent condition mean that the cell with the electrode was left undisturbed for ca. 1h before performing the measurement.

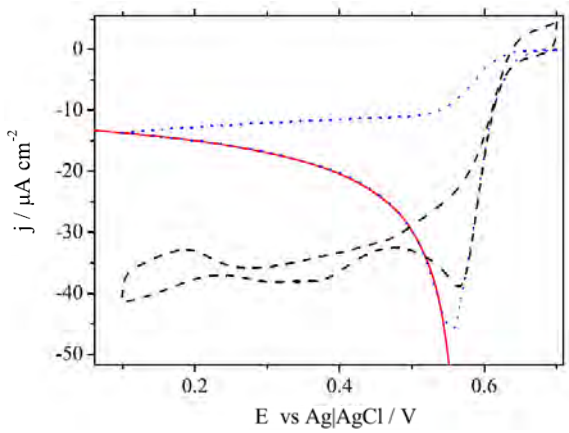

Figure 4.2: CV of oxygen reduction at BOx-modified electrode (dashed line) in McIlvain's buffer under air. Simulated curve without any convection (dotted line) and current calculated using the Cottrell equation (red full line). $\nu = 1$ mV s^{-1}.

Table 4.1: Parameters used for the simulated CVs.

Parameter	Value	How the value was obtained
α	0.375	by fitting an exponential function to the experimental CVs just left of the onset potential of the reaction
E_0	0.602 V	the same way as for α, moreover E_0 was kept close to the onset value reported in the literature [378]
K_M	51 μM	from [333]
k_{cat}	200 s^{-1}	from [333]
Γ_E	2.5×10^{-12} mol cm^{-2}	kept close to values measured on similar electrodes in rotating disc experiments [258]
k_0	100 m^3 s^{-1} mol^{-1}	free fitting parameter

quiescent conditions. To describe the convection we tracked it by with the use of a camera and analysed with the PIV. One of the examples of a convection profile obtained by PIV is shown in Fig. 4.3A. It represents the case when a gas flow of 50 sccm was maintained from a gas nozzle placed several mm above the surface of the liquid. Very similar images were obtained for slightly different ways of setting the experiment (where the conditions such as the gas movement around the cell, position of the gas nozzle, fluctuations in the gas pressure, could vary between the experiments). Due to the use of the PIV we obtained the values of the flow velocities inside the cell, at the depth of the electrode. The velocities measured in case of the induced convective flow were at the level of a few hundred micrometers per second. In case of the cell kept under quiescent conditions the same physical quantity had the value of around $100 - 200$ μm s^{-1}, which is not far from the situation with the forced convection.

The velocity values obtained by the PIV were further used in the simulations of the convection flow done again in COMSOL. Figures 4.3B and C show the result of these simulations for the cell with and without the gas flow above the liquid, respectively. Next the obtained profiles of hydrodynamic movement and the parameters from Tab. 4.1 were used for the simulations of CVs. The obtained voltammograms (Fig. 4.4B) are very similar to the CVs

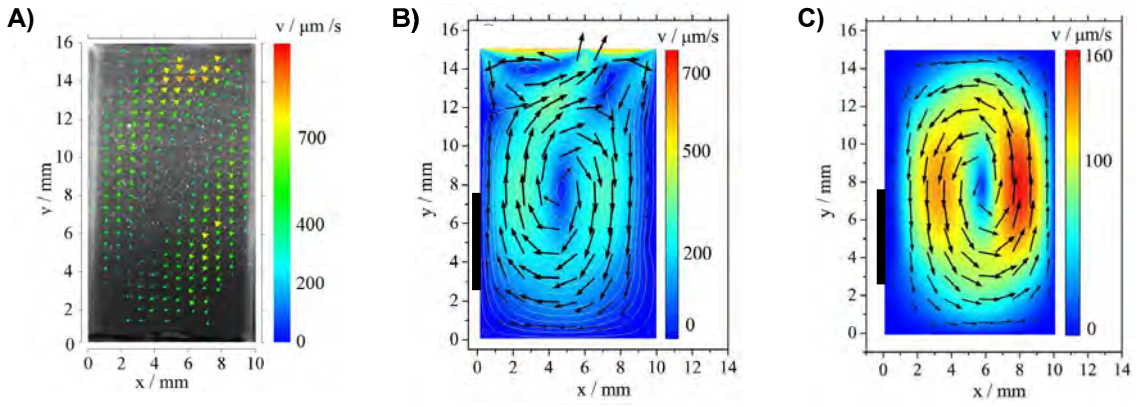

Figure 4.3: A) Example of convection profile analysed using PIV - for the cell subjected to the gas flow. B) and C) Simulated convection to fit the measured liquid velocities with B) and without C) gas flow over the surface. B) corresponds to the conditions measured in A). The position of the electrode is marked in black.

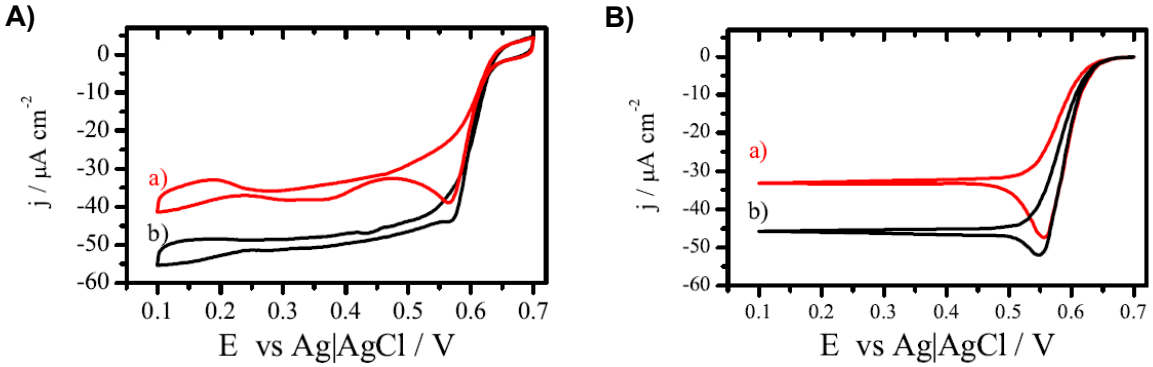

Figure 4.4: A) CVs of oxygen reduction at BOx-modified electrodes in McIlvain's buffer under air. Curve a) is under nominally quiescent conditions and b) with a gas flow of 50 sccm over the cell surface, $\nu = 1\ \mathrm{mV\,s^{-1}}$. B) Simulated CVs in COMSOL with the liquid flow from Fig. 4.3 C (curve a) and B (curve b).

measured in the real cells (Fig. 4.4A). Even such a simple model of O_2 bioelectroreduction which was used in our simulations gave the results matching quite well the experiment. This finding underline the importance of convection present in the electrochemical cell even under the nominally quiescent conditions.

4.3 Conclusions

We looked more carefully at the biocathodes subjected to the limitation of O_2 diffusion. We measured the native convection of electrolyte in an electrochemical cell. Then we included the electrolyte movement in the computer simulations of the bioelectrocatalytic O_2 reduction on the electrode kept under quiescent conditions. The obtained model was used to reproduce the experimental data obtained with the non-breathing biocathode comprising BOx. Thus we showed that the exceeded currents of O_2 reduction come from the convective flows present in the electrochemical cells. We hope that our results described here will make some electrochemists aware of the presented issue and that more of them will take into account the hydrodynamic effects occurring in the studied bioelectrochemical systems. Moreover, the

study presented here is an introduction to the next chapter about air-breathing biocathodes. Here we stressed the importance of convection under quiescent conditions showing an improvement of O_2 transport to the electrode surface. In the next chapter we will describe the way of avoiding the problem of mass transport by changing the design of the biocathode and giving it the possibility to breathe, i.e. use O_2 directly from the air.

Chapter 5

Air-breathing biocathodes with functionalised SWCNTs

So far the most efficient biocathodes for dioxygen reduction have been obtained with the enzymes from the MCOx family, such as bilirubin oxidase and laccase (Section 1.2.2). Although the catalytic potential of Lc is slightly higher than the potential of BOx, the latter one has a higher activity in neutral pH. Thus BOx is considered as a very good enzyme for the preparation of biocathodes for implantable biofuel cells which would operate at a pH of ca. 7.4. The BFCs would exploit the O_2 which is available in the subcutaneous liquids.

The ubiquitous nature of dioxygen indicates its easy accessibility for the biocathodes kept in ambient conditions or implanted into a body. On the other hand one need to take into account problems with diffusion of O_2 to the electrode surface. The values of diffusion coefficients of this gas in water solutions and in air are 2×10^{-5} cm^2 s^{-1} and 2×10^{-1} cm^2 s^{-1}, respectively [121]. Moreover, only a small amount of dioxygen can be dissolved in water (ca. 0.27 mM under air [379]). Thus O_2 is transported much faster to the electrode exposed to air than to the electrode which is immersed in solution. As a logical consequence of this phenomena the biocathode staying in contact with the electrolyte should give much lower reduction current than the electrode exposed to air. Even a very well designed biocathode will not work efficiently without being in direct contact with the air because of the limited O_2 diffusion [380].

So far a few different approaches of overcoming the problem of dioxygen diffusion to the biocathode surface were reported. The use of microfluidic cells [234,381] or rotating disc electrodes [382] are ways to introduce a forced convection enhancing the O_2 transport. Another way is to prepare an air-diffusion electrode which can "breathe" the air exposed directly to one side of the electrode. The first reported example of the air-breathing biocathode was floating on the electrolyte surface [383]. It was prepared by drop-coating the mix of Lc and carbon material on a compressed carbon black pellet. Next examples of air-breathing bio-

cathodes described in the literature contain different enzymes form the MCOx family, such as BOx and copper efflux oxidase [121, 384–390]. These biocathodes usually comprise: (i) a catalytic layer exposed to the electrolyte and (ii) a diffusion layer. The layer (ii) is permeable for gases and not-permeable for the electrolyte.

Non-covalent functionalisation of CNTs with pyrene derivatives comprising sulfonic groups was used for the preparation of different types of biocathodes. For example the SWCNTs functionalised with pyrenesulfonic acid or pyrene-1,3,6,8-tetrasulfonic acid (PTSA) were shown to enable the direct electron transfer to the active centre of BOx and Lc [257, 258]. Moreover, the functionalised nanotubes enhanced the stability of the sol-gel layer which was used for the enzyme immobilisation.

In this chapter I will describe a simple way of obtaining biocathodes for a non-mediated bioelectrocatalytic O_2 reduction. I will present a detailed study of the air-breathing biocathodes. The obtained two-layered biocathodes are easy to prepare and are very efficient. The catalytic layer of these biocathodes is made of the functionalised SWCNTs and BOx immobilised in a sol-gel matrix. A semi-permeable membrane is used as a diffusion layer. The biocathodes were tested in biobatteries but they can also be used in biofuel cells.

5.1 Preparation

Non-breathing electrodes

PTSA functionalised SWCNTs were immobilised together with the enzyme in a MTMOS sol-gel matrix (see recipe in Section 2.5.5). 99 µl of PTSA-SWCNT suspension was vortexed together with 99 µl BOx solution (2 mg ml^{-1} in McIlvaine's buffer, pH 4.8) for ca. 2 min. 2 µl of the final MTMOS sol was added to the PTSA-SWCNT/BOx suspension and vortexed for the next 3 min. 20 µl of the final suspension was drop-coated on the substrate which here was the ITO electrode. The surface coated with the prepared material was defined by an adhesive tape. Thus a circle modified electrode with diameter 0.5 cm was obtained (projected area of ca. 0.2 cm^2). Then the electrode was left to gel under ambient conditions for 17 h (typically ca. 50 % humidity and 22 °C). The electrodes were stored in the fridge when not in use.

For the preparation of the electrodes with BOx embedded in $OTEOS_{gel}$ and $TMOS_{gel}$ the recipes from Section 2.5.5 were used. Each time the final mixture contained the same amount of PTSA-SWCNTs and BOx and was drop-coated on ITO. The drying step was the same as in the case of $MTMOS_{gel}$.

Air-breathing electrodes

The air-breathing electrode (AirB) with both PTSA-SWCNTs and BOx was prepared almost in the same way as the non-breathing one (hereafter called PTSA-CNT/BOx/MTMOS$_{gel}$). The only difference is the used substrate. In case of the breathing electrode Teflon-treated Toray paper was used instead of ITO. The dried electrode was kept in the freezer till it was used. The electrode side covered with the matrix with BOx and SWCNTs will be further called the active side of the air-breathing electrode.

For the preparation of the electrode without the functionalised CNTs 99 µl of water was used instead of the PTSA-SWCNT suspension. The obtained electrode was further called BOx/MTMOS$_{gel}$. For the preparation of the electrode without the enzyme 99 µl of the buffer was used instead of the BOx solution. It was further called PTSA-SWCNT/MTMOS$_{gel}$.

Zinc anodes

The first type of the anode (further used in a single biobattery) was prepared by rolling 30 cm of Zn wire into a spiral. The active surface area was ca. 1.5 cm^2. The Zn wire was coated with Nafion by dipping it into 0.5 % solution of Nafion in isopropanol and drying in air. Then it was coated with hopeite by performing a chronopotentiometry in 0.15 M NaCl in 0.1 M phosphate buffer (pH 7.0). The Nafion-coated Zn wire was used as a working electrode in a three-electrode cell and the current density of 13 µA cm^{-2} was applied for 16 h.

The second type of the Zn anode (further used in a compact stack of four biobatteries) was made from a Zn foil. The anode had a shape of a square (1 cm × 1 cm) connected with a stripe (ca. 1.5 cm long, anode in Fig. 5.1B. It was covered with Nafion in the same way as the first type of Zn anode.

3-electrode cell with air-breathing biocathode

Two plastic spectrometer cuvettes were used for making a cell with the air-breathing biocathode. A hole (area of ca. 0.2 cm^2) was drilled in each cuvette with an electric drill so that both holes overlapped after putting the cuvettes next to each other. The biocathode was placed in between the cuvettes. Copper conductive tape was used for making an electric contact to the AirB. A silicon spacer was put from the active side of the biocathode and then squeezed with the electrode between the cuvettes. All parts of the cell were held by a metal clamp.

The scheme of the obtained cell is presented in Fig. 5.1A. The air-breathing biocathode was used as a working electrode (WE) in 3-electrode cell together with Ag|AgCl|KCl$_{3M}$ and

a platinum wire - as RE and CE respectively. The active side of the WE was exposed to the electrolyte which filled one of the cuvettes - 0.1 M McIlvaine's buffer (pH 4.8, unless otherwise stated).

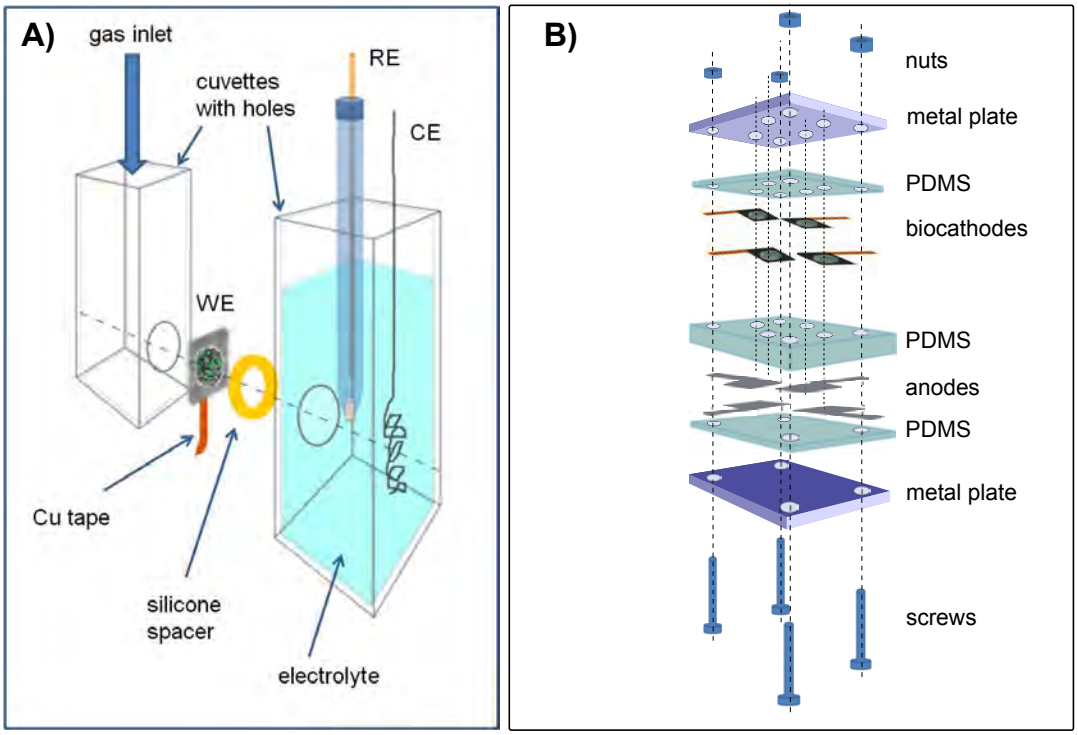

Figure 5.1: Schematic visualisation of: A) the cell with the air-breathing battery used as a working electrode; B) the stack of four biobatteries.

A stack of biobatteries

Four air-breathing biocathodes and four Zn anodes of the second type were used for making a stack of biobatteries. All the electrodes were squeezed in the mould made of PDMS - as shown in Figure 5.1 B. The as formed assembly was held by two parallel metal plates and screws. Four holes in the mould were filled with the buffer (McIlvaine's buffer, pH 4.8) so that each of them formed a small cell for a single biobattery comprising one biocathode and one Zn anode. The obtained four biobatteries were connected in series by the strips of Cu conductive tape.

5.2 Characterisation

5.2.1 Different silicate matrices for BOx/PTSA-CNT immobilisation

We checked current densities of dioxygen reduction generated at the biocathodes with BOx/PTSA-SWCNT embedded on ITO-electrodes in (i) $TMOS_{gel}$, (ii) $MTMOS_{gel}$ or (iii)

$OTEOS_{gel}$. As long as the sol-gel matrices were dried in the same conditions they gave comparable results - see Fig. 5.2. The current densities measured at the potential of 0.10 V vs. Ag|AgCl had values in the range $180 - 200\ \mu A\,cm^{-2}$ in oxygenated buffer. However for further experiments and the preparation of a breathing biocathode we used $MTMOS_{gel}$. Our choice was justified by the following facts: the way of obtaining $MTMOS_{gel}$ is fast and easy, and it requires smaller number of steps than $TMOS_{gel}$; $MTMOS_{gel}$ is hydrophobic so it should interact better with the CNTs; obtaining a good reproducible electrodes with $OTEOS_{gel}$ is very difficult due to obtaining inhomogeneous sol.

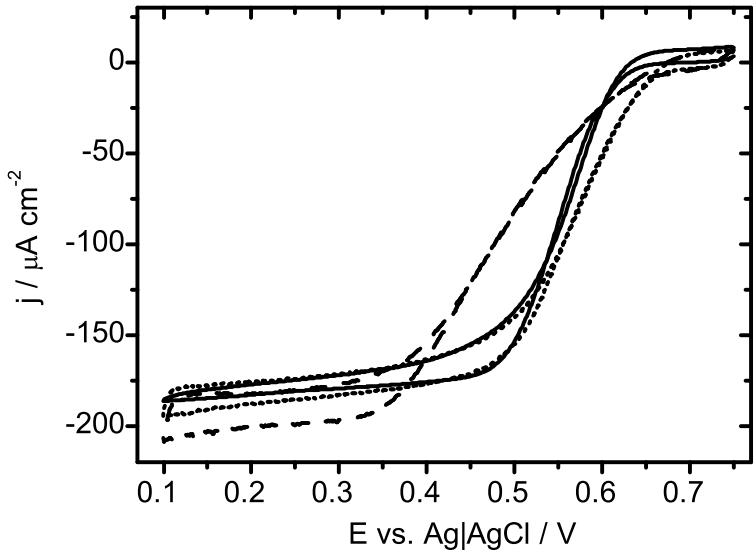

Figure 5.2: CVs of O_2 electroreduction on the biocathodes with BOx and PTSA-SWCNTs immobilised in different sol-gel matrixes: (dashed line) TMOS, (dotted line) MTMOS and (solid line) OTEOS. Measurements were taken in the oxygenated McIlvaine's buffer, pH 4.8, $\nu = 1\ mV\,s^{-1}$

5.2.2 Air-breathing electrodes

SEM images

The active side of the air-breathing biocathode was investigated by the scanning electron microscopy - Fig. 5.3. In the image A the unmodified surface of the Toray paper is shown. It is made of compressed straight randomly oriented carbon microfibres. These microfibres area also visible in the figure C (top right corner) where the zoom-out view on the electrode is presented. On the left part of the image C the silicate matrix with BOx/PTSA-SWCNTs are visible. A closer inspection to the latter part is shown in the images B, D and E. The visible structure is porous which results in the enlarged area of the electrode surface, in comparison with the bare carbon paper. This structure is similar to the one obtained for the electrodes obtained on ITO with SWCNTs in silicate matrix made from tetramethoxysilane (TMOS) precursor [257].

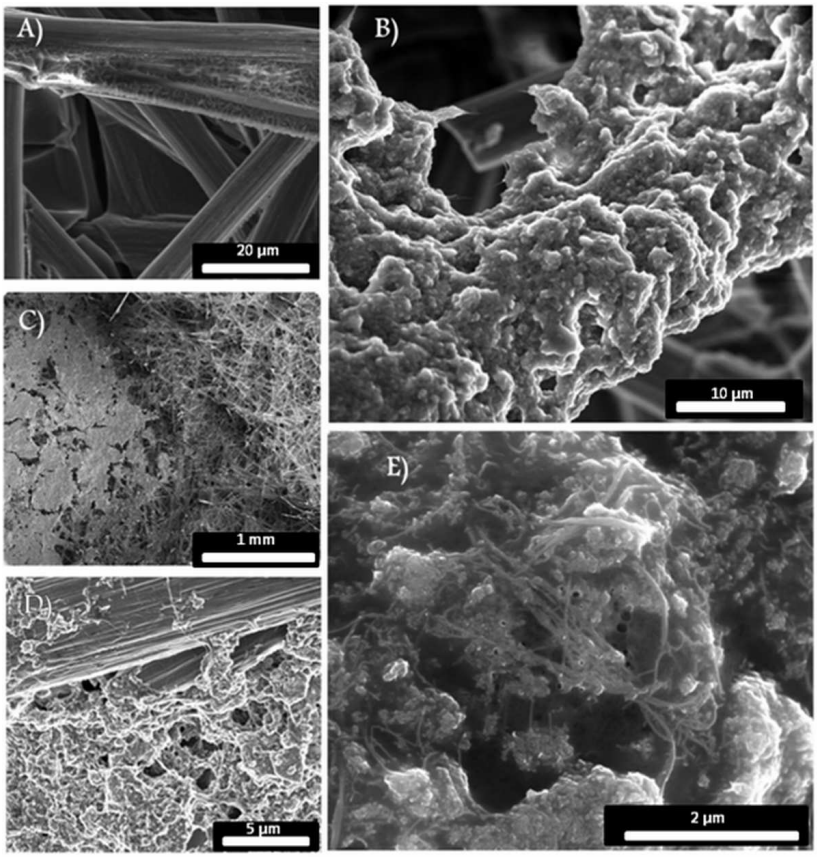

Figure 5.3: SEM images of: Teflon treated Toray paper A) and the same paper modified with a porous silicate matrix in which enzyme and CNTs are encapsulated B), C), D) and E).

Mechanical stability

As long as the sol-gel composite is dried in the proper conditions (ca. 55 % humidity and 22 °C) it forms a mechanically stable thin film on the Toray surface. The composite stays on the substrate after being wetted and dried for a several times. It also does not undergo disintegration during performing long (a few days long) electrochemical measurements. The biocathodes subjected to the gel process in too high or too low humidity were easily damaged in contact with the electrolyte, thus they were not used for the measurements.

Efficient bioelectrocatalytic reduction of O_2

The 3-electrode cell was used for performing cyclic voltammetry on the air-breathing biocathode and checking the efficiency of the O_2 reduction (Fig. 5.1A). The scan range and the scan rate were $0.75 - 0.1$ V and $\nu = 1$ mV s^{-1} respectively. The slow scan sate was chosen because it was suitable for a slow bioelectrocatalytic reaction occurring in the presence of BOx. The suitable design of the cell allowed to easily introduce any type of the gas (argon, air and oxygen) from the non-active side of the AirB.

The results presented in figure 5.4A show first off all that the O_2 reduction has its onset

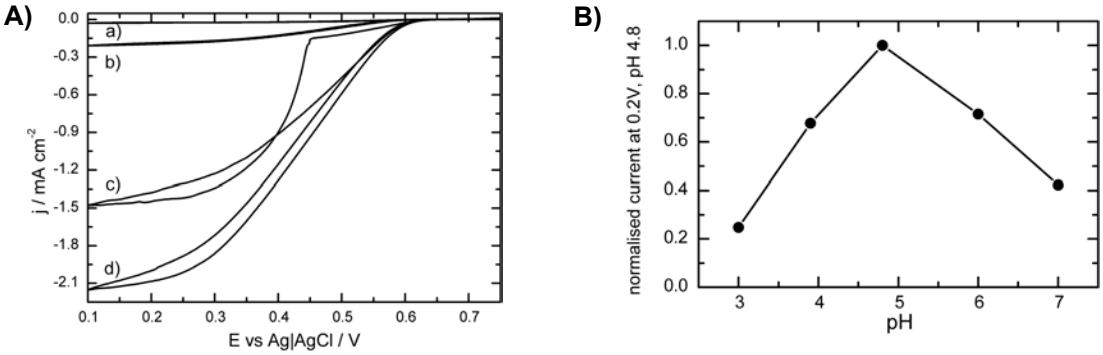

Figure 5.4: A) CV (McIlvaine's buffer under air, pH 4.8, $\nu = 1$ mV s^{-1}: oxygen reduction current with the followiwng gases introduced to the gas-side: argon b), air c) and O_2 d). CV curve a) correspond to the situation where argon is introduced from the gas-side, while the electrolyte is also deaerated. B) pH dependence of O_2 reduction current normalised to the current obtained for the air-breathing electrode in McIlvaine's buffer pH 4.8. All data points were obtained from the current measured at potential 0.2 V vs. the RE ($\nu = 1$ mV s^{-1}).

potential at ca. 0.6 V (vs. Ag|AgCl|KCl$_{3M}$). This potential is not very far from the formal potential of the T1 centre of the enzyme, which is 0.9 V (vs. Ag|AgCl|KCl$_{3M}$) [99].

Figure 5.4A clearly shows that the breathing biocathode gives different current densities of O_2 reduction, depending on the type of the gas introduced to the cell. The more oxygen is carried by the introduced gas, the bigger is the reduction current. Thus the current was the lowest when both the electrolyte was deareated as well as the gas-side was filled with argon - ca. 30 μA cm^{-2} at 0.1 V (Fig. 5.4A, curve a. Curve b in Fig. 5.4A represents the situation where the gas-side is exposed to argon but the electrolyte-side is kept under air. So in these conditions the biocathode should behave as a standard non-breathing electrode. For a comparison the biocathode prepared in the same way but on ITO instead of on Toray paper gave ca. 40 μA cm^{-2} at 0.1 V (Chapter 4). However in case of the AirB the current density of O_2 reduction is ca. 210 μA cm^{-2} at 0.1 V, which is higher than expected. This is probably due to a presence of some oxygen in the gas-side of the cell, which was not deareated ideally.

A highly-responsive behaviour of the air-breathing biocathode on the change of the introduced gas is presented on the scan c in Fig. 5.4A. This scan was started when argon was present in the gas-side of the cell. At the potential of ca. 0.45 V (forward cycle) the Ar flow was stopped and air started to enter the cell and provide the biocathode with dioxygen. As a result the O_2 reduction current increased more than 7 times (up to ca. 1.5 mA cm^{-2}) after 3 min. That indicates how sensitive is the biocathode to the type of the introduced gas, thus to the concentration of O_2. Moreover, it shows that the diffusion of the gas through the Toray paper is very fast because the change of the current was immediate.

The highest current density of O_2 reduction was obtained when pure oxygen was introduced to the gas-side of the cell - ca. 2.15 mA cm^{-2} at 0.1 V. This high value is consistent with the maximum limiting current determined for a similar bioelectrocatalytic composite

on rotating disc electrode (glassy carbon) [258]. Moreover, the value of 2.15 mA cm^{-2} is, to the best of my knowledge, the highest current density of O_2 reduction for non-mediated systems with BOx which were published so far.

The dependence of the reduction current on the pH of the buffer used in the tested cell is presented in Figure 5.4B. The biocathode was exposed to air (air-breathing biocathode) form the gas side and to McIlvaine's buffer of different pH from the electrolyte-side. The current of O_2 reduction was measured at the potential 0.2 V vs. the RE for pH of: 3, 4, 4.8, 6 and 7. Then the current was normalised to the highest obtained value (pH 4.8) and plotted in Figure 5.4B. The obtained results indicate that the most efficient O_2 reduction is obtained for pH close to 5, what is consistent with what was published previously [258,391].

Influence of the film composition on the performance of the biocathode

A few electrodes with different composite material were used to show their influence on the electrocatalytic O_2 reduction. They were examined by the CV. The electrode PTSA-SWCNT/MTMOS$_{gel}$ was air-breathing but did not contain the enzyme. As is shown in Fig. 5.5a, no oxygen reduction was observed in the potential range $0.75 - 0.1$ V. This behaviour was expected due to the lack of BOx. A very low current density of O_2 reduction

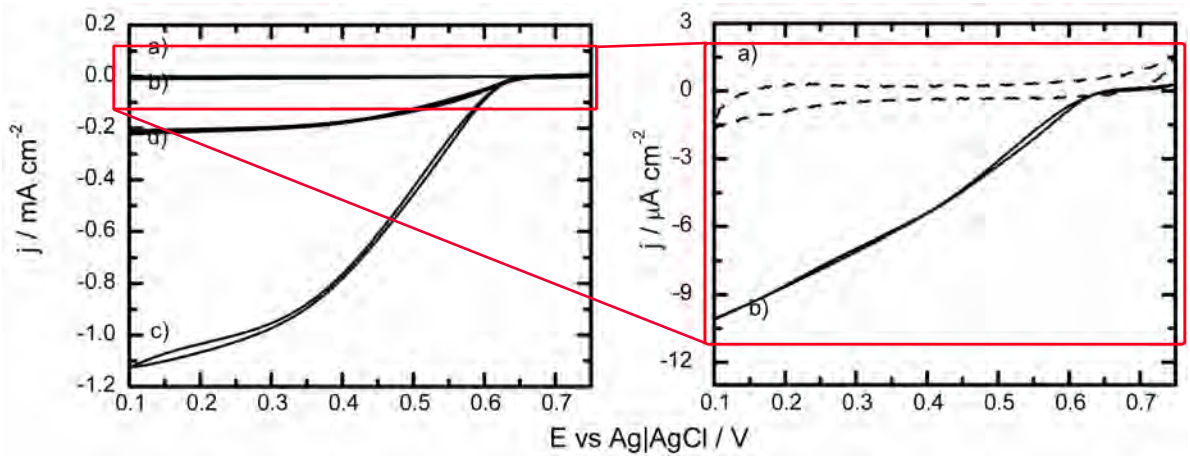

Figure 5.5: CV of dioxygen reduction on the electrodes modified with silicate and: a) PTSA-SWCNT, b) BOx, c) and d) PTSA-SWCNT and BOx. In the case of d) CNTs with the enzyme formed a very compact layer on the Toray paper. McIlvaine's buffer, pH 4.8, $\nu = 1$ mV s^{-1}, air.

was observed for the electrode with the enzyme but without the functionalised SWCNTs (BOx/MTMOS$_{gel}$) - ca. 10 µA cm^{-2} at 0.1 V (Fig. 5.5b). It clearly indicates that even though the Toray paper can provide some electric contact with the enzyme, the PTSA-SWCNTs are indispensable for obtaining a very efficient O_2 reduction. But not only a composition of a thin layer with the enzyme but also a proper dispersion of a composite material has a big influence on the efficiency of the obtained bioelectrode. In case of PTSA-CNT/BOx/MTMOS$_{gel}$ the electrode with too compact layer of the composite material (Fig. 5.5c) is less efficient

than the electrode with nicely distributed material (Fig. 5.5d). A compact layer was formed when a drop of the sol mixture was left to dry undisturbed on the hydrophobic carbon fibre. In the case of a nicely distributed material, the same sol mixture was mechanically spread on the Toray paper before drying. The observation depicted in Figure 5.5c and d is in agreement with the results published by Tarasevich*et al.* They showed that more dispersed carbon nanomaterial improved direct electron transfer between the electrode and the active centre of laccase [383].

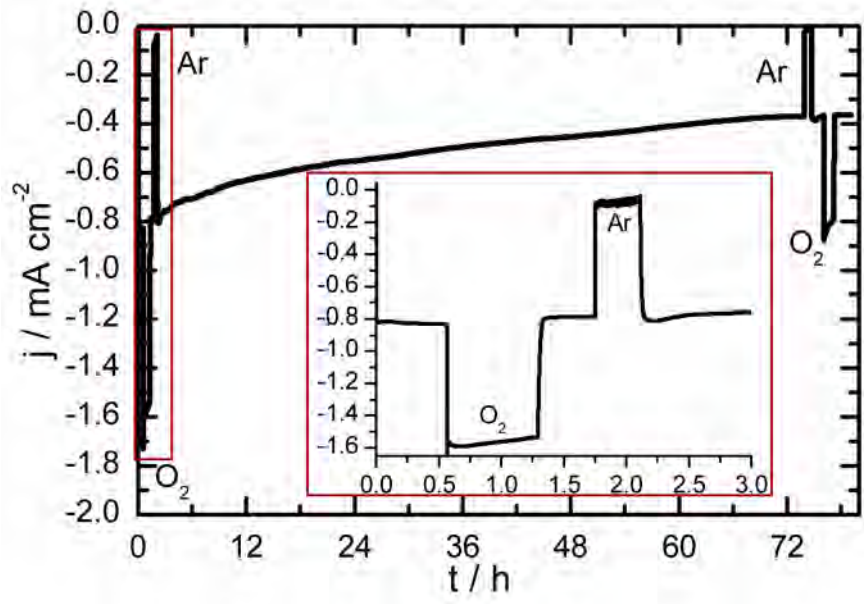

Figure 5.6: Chronoamperometry of the air-breathing biocathode done in McIlvaine's buffer, pH 4.8. The inset graph shows the first 3 h of the presented chronoamperogram.

Chronoamperometry was used to check the stability of the air-breathing biocathode (Fig. 5.6). The potential of 0.2 V vs. RE was applied for almost 80 h. During that time the electrode was kept mostly in air. The change of the gas caused a very fast and pronounced change in the reduction current. The value of the current was almost twice higher under O_2 but negligible under the flow of argon. This result once more show the very fast response of the breathing electrode on the introduced gas. Moreover, CA measurements showed that the electrode retains approximately half of its initial activity after 80 h of constant work.

5.2.3 Biobatteries

A single zinc/oxygen biobattery was constructed in almost the same way as the 3-electrode cell presented in the Figure 5.1A. For obtaining a biobattery the CE and the RE were replaced by the zinc anode pretreated in the described way. The polarisation curves for the biobattery were obtained from the chronopotentiometric measurements done by the potentiostat. Different current loadings were applied to the battery (in a 2-electrode cell) and as a response a stable value of the voltage was measured. The obtained open circuit

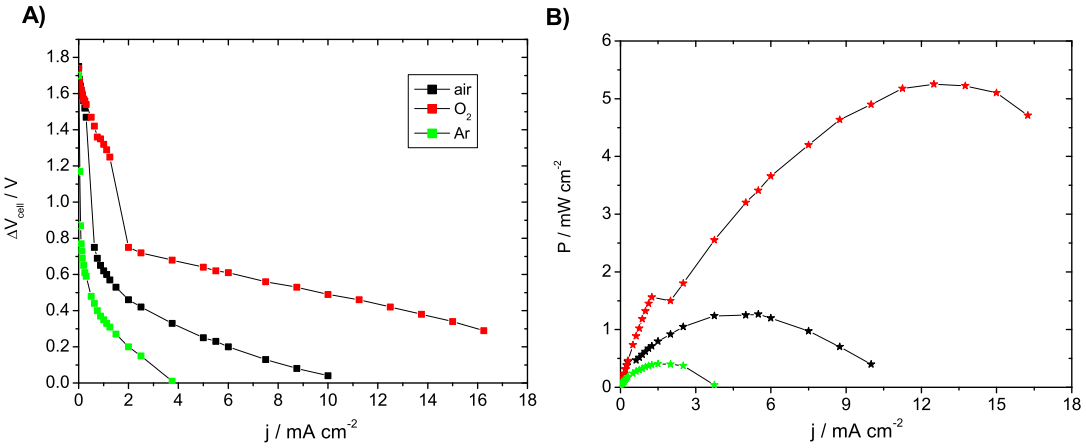

Figure 5.7: A) Galvanostatic polarisation curves and B) the dependences of the power output for the Zn/O_2 biobattery with the electrolyte-side filled with McIlvaine's buffer, pH 4.8 and the gas-side filled with: a) oxygen, b) air or c) argon.

voltage (OCV)[1] was 1.75 V (Fig. 5.7A). This value is very close to the theoretical value of 1.99 V . Moreover, this result is almost the same as the best OCV for biobatteries with CNTs reported so far [259, 392].

The shape of the j-V curves in Fig. 5.7A is typical for this type of biobatteries and biofuel cells [73]. The power outputs of the biobattery were calculated from the j-V curves and plotted in Figure 5.7B. It is clearly visible that the power of Zn/O_2 battery is highly dependent on the type of the gas introduced to the gas-side. The highest value was obtained for the battery working under O_2 - the maximum power density (P_{max}) output was ca. 5 times higher than the output from the oxygenated battery. This dependence between the O_2 concentration of oxygen and P_{max} indicates that the dioxygen reduction reaction in the breathing biocathodes is very efficient.

The stability of the biobattery was checked by performing the chronopotentiometry. Under a very high load of $-1250\ \mu A\ cm^{-2}$ (Fig. 5.8Aa) the biobattery can operate for 4 h in McIlvaine's buffer, pH 4.8. Lower current loadings result in a longer battery lifetime. 5 times lower loading imposed on the battery filled with McIlvaine's buffer (pH 4.8) increased a lifetime up to almost 9 h (Fig. 5.8Ab). Further extension of the stability was achieved by changing the buffer (pH 4.8) into the phosphate buffer at pH 7.0 (Fig. 5.8Ac and Bc). In these conditions the biobattery was working for ca. 45 h, which is fivefold longer than in case of McIlvaine's buffer (pH 4.8). Moreover, this long term stability can be again improved by the immobilization of two times more BOx on the biocathode (Fig. 5.8Bd). This change gives further doubling of the lifetime in comparison with the biocathode with the standard amount of the enzyme.

In all the plots related to the current density loading of -1250 and $-250\ \mu A\ cm^{-2}$ a gradual decrease of the voltage is observed. This is caused by the loss of the catalytic activity

[1]The OCV is the voltage measured at the zero loading.

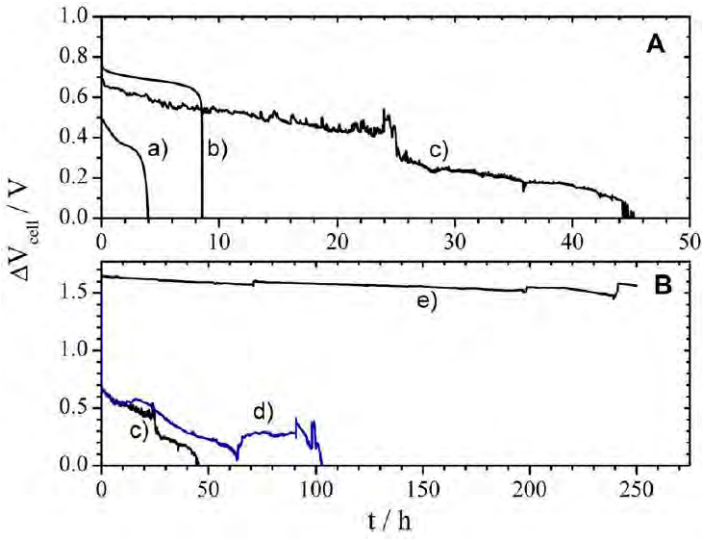

Figure 5.8: A) Long term stability of the batteries checked with CP: A) curve a) $-1250\,\mu A\,cm^{-2}$; b), c) $-250\,\mu A\,cm^{-2}$, B) curve d) $-250\,\mu A\,cm^{-2}$, e) $-50\,\mu A\,cm^{-2}$, curve c) is the same as in A) The gas-side was filled with air and the electrolyte-side with: a), b) and e) McIlvaine's buffer, pH 4.8, c) and d) phosphate buffer, pH 7.0. The amount of enzyme on biocathode d) was twice that of biocathodes a), b), c) and e). Due to evaporation additional electrolyte was added after 71, 197 and 240 h (curve e).

of the biocathode. It was also observed when the CA of the biocathode was performed (Fig. 5.6). However the sudden drop of the voltage at the end of CP measurements is the most likely related to the anode breakdown. This statement is supported by the observations described by Shin *et al.* [370]. Moreover, the slope of the initial gradual voltage decrease in all of the mentioned examples is not dependent on the type of the buffer. Thus this is another evidence for the conclusion that the sudden voltage drop at the end of the CP measurement is related to the anode failure. A dramatical increase of the battery lifetime was observed for a much lower load of$-50\,\mu A\,cm^{-2}$, in McIlvaine's buffer (Fig. 5.8Bd). In this case the cell potential has decreased only 10 % after 250 h of a constant work. This observation is in agreement with what was reported by Shleev *et al.* [393]. They also observed that the high loadings dramatically decrease the biocathode lifetime. Thus the theory that a too high turnover rate for an individual enzyme leads to a loss of catalytic activity is supported by the following observations: an increase of the enzyme loading on the electrode or a decrease of the total current load prolongs the lifetime of the biocathode. However the mechanism of this phenomenon is not known.

Powering electronic devices

The single biobattery was used for powering a small digital clock. The clock was operating for at least 6 h. Thus our biobattery can be used for powering useful devices which do not consume to much power. To use our source of energy for powering more demanding devices which need higher voltages it is necessary to connect a few biobatteries in series. Four air-breathing biobatteries connected in this way acted as a source of power for a bike lamp

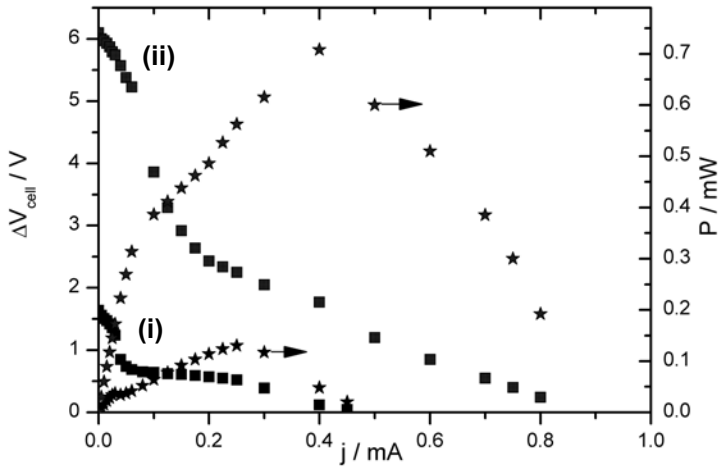

Figure 5.9: Galvanostatic polarisation curves (squares) and the dependences of the power output (stars) for one (i) and a stack of four (ii) zinc/oxygen biobatteries.

comprising two red LEDs. The same type of characteristics as for the single biobattery (see Fig. 5.7) was done for the obtained stack (Fig. 5.9). Galvanostatic polarisation curves and the dependences of the power output were plotted for one and four biobatteries. The results for one of the battery from the stack are different than for the single battery because of the different type of the anode. Here the anode is made of a zinc plate which has much smaller surface area than a zinc wire used in a single cell. The biocathodes used in both cases are the same and they are so efficient that the obtained power output depends on the anode. Thus the obtained maximum power is ca. 10 times smaller for one battery from the stack than for a single biobattery. Moreover, the results presented in the Fig. 5.9 show that the connection of the biobatteries in series gives a relatively small footprint stack. The OCV increases by 1.5 V for each additional cell. That leads to obtaining relatively high cell voltages of the assembly and in consequence it results in a drastic increase of the power output.

5.3 Conclusions

We have presented a simple procedure for the preparation of the efficient air-breathing non-mediated biocathodes with bilirubin oxidase. These biocathodes can be used in Zn/O_2 batteries by connecting them with the zinc anode. The way of the biocathode construction allowed to avoid the problem with O_2 diffusion to the electrode surface. Usually slow mass transport causes the O_2 depletion in the vicinity of the electrode. Thus the slow diffusion is a limiting step of O_2 reduction on the non-breathing bioelectrodes. Our breathing electrodes are constantly supplied with the gas and that is why they give very high reduction current densities. The values of 1.5 mA cm^{-2} under air and over 2 mA cm^{-2} under O_2 were obtained. Our zinc/oxygen battery gave the maximum power density of 5.25 mW cm^{-2} at ca. 0.4 V in O_2. This result is the best among other published so far for such a device. Moreover, we constructed a stack of four biobatteries which was successfully used as an energy source

capable of powering a bike lamp with two red LEDs. However there is still some work left to improve the stability of our bioelectrodes.

Chapter 6

Self-powered sensor for ascorbic acid

Recently biofuel cells started to be interesting as sensors which can power themselves (see Section1.4.1). Although many examples of the analytes were reported in the literature so far, here I will present the first two examples of the self-powered sensors for ascorbic acid. In both examples the air-breathing biocathode is used. As an anode two electrodes modified with carbon nanostructures were used: (i) the VACNT-electrode (Chapter 3) or (ii) electrode with carbon nanoparticles and silicate beads (CNP/beads electrode). Each of the examples of the sensor can be called self-powered because it gives the power output dependent on the concentration of the fuel. However, the easiest way to measure this dependence is to use a dedicated electronic device. Here we present a novel way of showing AA concentration dependency. We use a Prussian blue electrochromic display connected to the AA/O_2 BFC (with CNP/beads on the anode) and analyse the change of its colour with time. The higher the fuel concentration the faster the change of the colour. This change can be noticed with the naked eye, what makes our device a truly self-powered sensor. Moreover, the calibration of the sensor makes it usable for the determination of AA concentration in the orange juice.

6.1 Preparation

VACNT electrodes

The preparation of this type of the electrode was described in Chapter 3.

CNP/beads electrodes

First the silicate beads were prepared via a modified Stöber method [394,395]. 105.5 µl of N-trimethoxysilylpropyl-N,N,N-trimethylammonium chloride and 537 µl of tetramethoxysilane

were mixed with 1 ml MeOH. Then 10 ml of aqueous solution of hexadecyl-trimethyl-ammonium bromide (CTAB), 3 ml NH_{3aq} and 9 ml MeOH were added and constantly stirred for next 2 h. The obtained white precipitate was filtered, washed with EtOH and left to dry in room temperature. White powder was further refluxed for 24 h with 1 mM HCl in EtOH to remove the remains of CTAB. Then it was again filtered, washed with EtOH and water and left to dry. The obtained material is from that time on called TMA-beads.

Two suspensions 5 mg/ml of TMA-beads and carbon nanoparticles (CNPs with phenyl-sulfonic acid surface functionalities from Cabot Corporation) were obtained by the dispersion in MeOH and ACN respectively. The ITO electrode was modified by alternate immersions (5 s) into the TMA-bead and CNP suspensions. Each immersion step was followed by drying in air and immersion in clean solvent to remove loosely bonded material. The active area of the electrode was limited by the Scotch tape and the electric contact was assured by a piece of a copper tape. These electrodes were prepared by Anna Celebanska.

Air-breathing biocathode

The preparation of this biocathode is described in Section 5.1 of this thesis.

Prussian blue display

A thin layer of Prussian blue (PB) was electrodeposited on ITO electrode according to the following procedure [396]. The ITO was masked with the adhesive tape (area of 0.2 cm^2). Aqueous solutions of 50 mM HCl, $K_3[Fe(CN)_6]$ and $FeCl_3 \cdot 6H_2O$ were mixed in the proportions 1:2:2 and stirred with the magnetic stirrer. The ITO electrode was immersed in the mix of solutions and a current of 8 μA was passed through the electrode for 240 s. After the electrodeposition the electrode was rinsed with water and dried. Then it was post-treated in 0.1 M KCl solution (in phosphate buffer, pH 4.8), in a 3-electrode cell, in two steps: (i) by keeping at −0.05 V vs. RE for 600 s [397] and (ii) Cycling three times the potential from 0.6 to −0.2 V with the scan rate of 20 mV s^{-1}. Then the electrode was washed with water, dried and masked with the insulating tape and white nail polish on the area not covered with the PB.

AA/O_2 BFC and a truly self-powered AA sensor

Two types of BFCs for ascorbic acid were used: with VACNT-electrode or CNP/beads-electrode as an anode. In both cases the anode was connected to the air-breathing electrode. Both electrodes were kept in the same cell filled with AA solution in phosphate buffer (pH 4.8, air).

A cell for the truly self-powered AA sensor comprised two compartments. It was made of two cuvettes with the drilled holes connected together with the Nafion membrane placed between them. In one of the compartments the BFC with the CNP/beads-electrode was placed (phosphate buffer, pH 4.8). The PB display was placed in the second compartment which was filled with 0.1 M KCl (in phosphate buffer, pH 4.8). The cell was kept under air in room temperature.

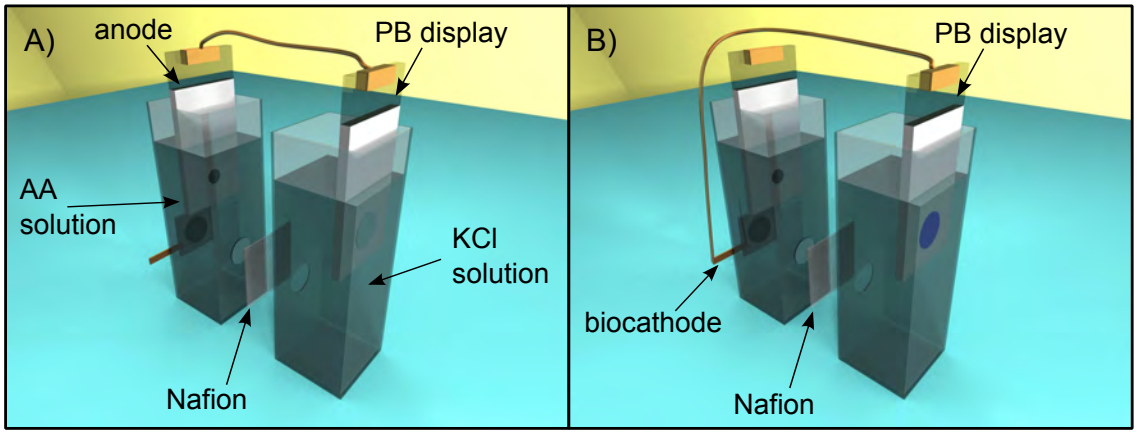

Figure 6.1: A) schematic illustration of the self-powered sensor. In A the configuration used for AA detection and in B the configuration for regeneration of the PB-display.

The display changed the colour from blue to transparent when it was connected to the CNP/beads-anode (Figure 6.1A). The reversed colour change (PB regeneration) was obtained by connecting the display with the biocathode (Figure 6.1B. The differences between the speed of PB decoloration for different AA concentrations were easily observed with the naked eye. However, for a better data presentation we used a camera and precisely monitor the decoloration process. A Canon EOS 5D was placed on a tripod, connected to a laptop and was taking pictures each 5 s. In the pictures the PB display was visible together with another electrode with electrodeposited PB layer kept in air (PB-electrode). This PB-electrode gave a reference colour which was stable in time, while the display was changing the colour.

6.2 Results and discussion

6.2.1 AA oxidation

As mentioned in Section 3.2.2 (Fig. 3.7) the VACNT-electrode can be used for AA oxidation. Here this electrode was examined more accurately by cyclic voltammetry. The VACNT-electrode was immersed in not-stirred solutions of increasing AA concentration (in McIlvaine's buffer, pH 4.8). Each time the electrode was left for at least 10 min in the solution - to enable the solution diffusion into the CNT forest. Then the CV was recorded in the scan range from $0.0 - 0.7$ V and a scan range $\nu = 10$ mV s^{-1}. A well defined peak corresponding

to AA oxidation was observed at the onset potential of 0.1 V, with a peak potential of ca. 0.3 V (Fig. 6.2). The dependence of the peak height on the AA concentration is shown in the inset of Figure 6.2 - a linear relationship is observed up to 3 mM. Linear fitting has the slope of 0.386 A cm^{-2} M^{-1}.

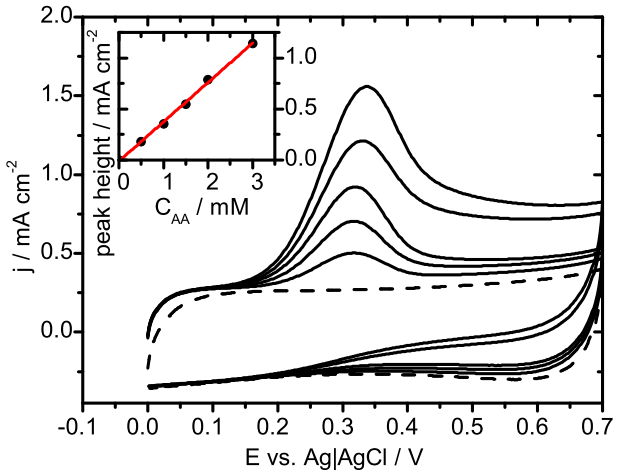

Figure 6.2: CV on VACNT-anode in McIlvaine's buffer, pH = 4.8 (dashed line) and in AA solutions of different concentrations: 0.5, 1.0, 1.5, 2.0 and 3.0 mM; v = 10 mV s^{-1}. Inset: Peak height as a function of on AA concentration. The line shows a least squares linear fit to the data (R^2 = 0.998).

The same method was used to check the performance of the CNP/beads-electrode with 9 double layers. In this example the onset potential of AA oxidation is more negative than in the case of the VACNT-electrode. The oxidation starts at ca. 0.025 V (Fig. 6.3). The dependence of the oxidation peak height on the AA concentration in shown in the inset of Figure 6.3. The linear fit to this data has a slope of 0.157 A cm^{-2} M^{-1} which indicates that the sensitivity of the CNP/beads anode is ca. twice lower than the sensitivity of the VACNT-electrode. Presumably this effect is a result of a formation of a thin layer cell made of a relatively high amount of AA trapped between the aligned CNTs.

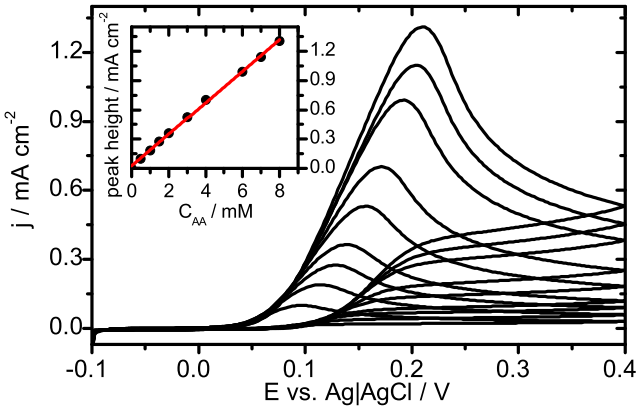

Figure 6.3: CV on the CNP/beads film electrode in phosphate buffer, pH 4.8 (dashed line) and in AA solutions of different concentrations: 0.5, 1.0, 1.5, 2.0, 3.0, 4.0, 6.0 7.0, and 8.0 mM; ν = 10 mV s^{-1}. Inset: Peak height as a function of on AA concentration. The line shows a least squares linear fit to the data (R^2 = 0.999).

The anode with the VACNTs was examined by CA to check the limit of detection of

AA. The electrode was immersed in McIlvaine's buffer and the potential of 0.2 V vs. RE was applied. After obtaining a stable current without the analyte subsequent portions of the concentrated AA solution (30 mM) were added to the buffer. Together with the addition of AA the magnetic stirrer was used to thoroughly stir the solution for ca. 3 minutes. Then the stirrer was turned off and the current was measured after the stabilisation. The measured values are mean values for at least 100 points and error bars are standard deviations from these values. The obtained results are presented in Figure 6.4. The limit of detection was

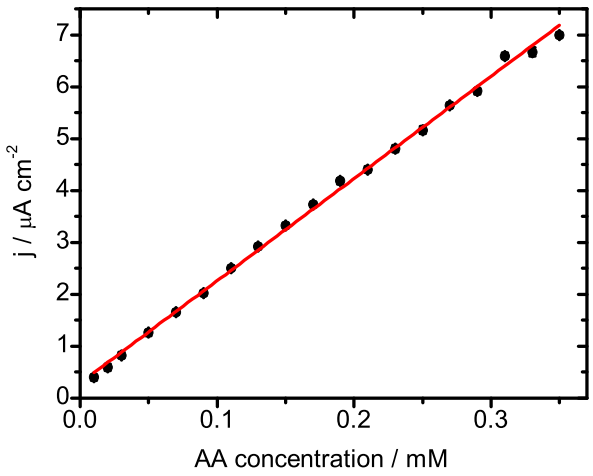

Figure 6.4: Current as a function of AA concentration in chronoamperometric measurement using the VACNT anode. Applied potential: 0.2 V vs. Ag|AgCl. The line shows a least squares linear fit to the data ($R^2 = 0.998$).

calculated for the concentrations from the range $10 - 350\,\mu M$. By taking into account 3 times signal to noise ratio the LOD of $4\,\mu M$ was found. Thus the results obtained for the VACNT-electrode and the CNP/beads electrode indicate that these electrodes act as sensors for ascorbic acid. Moreover, the detection range for these sensors covers the levels found in (i) human serum ($0.5 - 1.51$ mg/l) [398], (ii) urine ($12.5 - 26.8$ mg/l) [398] and vitamin C rich fruits (up to ca. 4 mg/l) [399]. That makes the sensors potentially interesting in the determination of AA level in real samples.

6.2.2 AA/O_2 BFC

Before assembling of the BFC the behaviour of the air-breathing biocathode in the presence of ascorbic acid was checked. Figure 6.5 presents cyclic voltammograms recorded in (a) clear buffer, (b) 1 mM AA and (c) 6 mM AA solutions. It is clearly visible that relatively low AA concentration does not have a big negative effect on the biocathode. The electrode retains ca. 60 % of its activity (at 0.2 V vs. RE) in 1 mM AA in comparison with the clear buffer (Fig. 6.5b). Moreover, AA oxidation on the electrode is negligible. However, the biocathode working in 6 mM AA solution shows lower activity toward O_2 reduction. The oxygen reduction current is ca. 70 % smaller (at 0.2 V vs. Ag|AgCl) than in the clean buffer (Fig. 6.5c). At

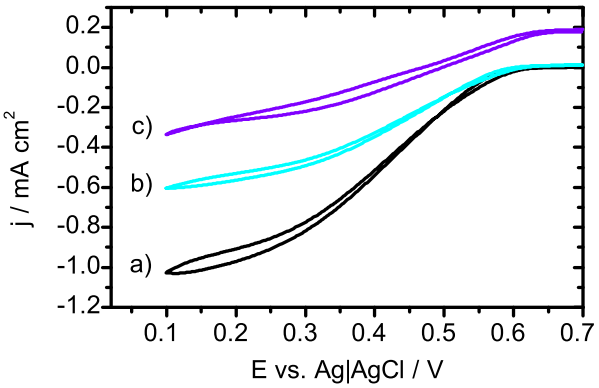

Figure 6.5: CV of O_2 reduction on the air-breathing electrode in: a) clean buffer, b) 1 mM AA and c) 6 mM AA solutions (phosphate buffer under air, pH 4.8, $\nu = 1$ mV s^{-1}).

AA concentrations as high as 6 mM the AA oxidation takes place at the bioelectrode. The current density of AA oxidation at 0.7 V vs. RE is ca. 200 µA cm^{-2}, almost as high as the reduction current. Although the oxidation is very pronounced, the presence of a big amount of AA does not deactivate the enzyme on the biocathode. Moreover, only a very small shift of O_2 reduction potential was noticed between the reaction in a clear buffer and in 6 mM AA. Thus the silicate matrix probably acts as a barrier for AA and is preventing its access to the electrode surface.

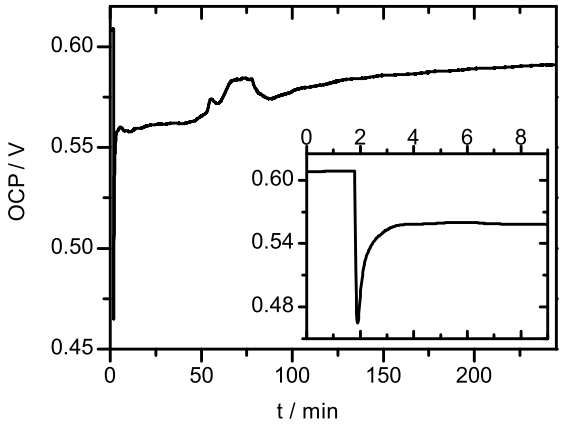

Figure 6.6: Open circuit potential versus time registered for the BFC with the VACNT-anode. At the beginning it was measured in the phosphate buffer (pH 4.8). After 100 s a concentrated AA solution was added to obtain 0.5 mM solution. The inset is a zoom of the first several minutes.

It is known that enzymes such as BOD are very easily deactivated by AA [400]. For example the enzyme in a BFC prepared by Qian *et al.* [401] was deactivated in less than 10 min after the exposure to 0.5 mM AA solution. However, the enzyme stayed active when the biocathode surface was coated with a protective ionic liquid layer. In case of our AA/O_2 BFC we did not use any additional layer. We performed almost the same measurement as the one done by Qian *et al.* [401] to check the BFC stability (see Fig. 6.6). The OCP between the air-breathing biocathode and the VACNT-anode was measured in phosphate buffer (pH 4.8). A the beginning the obtained value of the OCP was 0.61 V. After 100 s AA was added so that its concentration in the cell reached 0.5 mM. An immediate decrease of the OCP was

observed - it dropped up to 0.47 V. Then the OCP increased very fast and after less than 2 min it reached 0.56 V. This very short-lasting OCP drop might have been an effect of an injection of a concentrated AA solution in a very close vicinity of the biocathode surface. The sudden change of the pH of the solution could have been a reason of the change of the biocathode potential. Further measurement showed that the OCP was stable for at least 4 h and had a value of 0.58 V. Thus our air-breathing biocathode is extremely resistant to AA in comparison with the biocathode presented by Qian *et al.* [401]. The silicate acted not only as the matrix which immobilized the enzyme but also as a protection from AA. The most likely the protective effect of the sol-gel matrix is a result of AA repulsion by the negatively charged silanol groups present in the matrix.

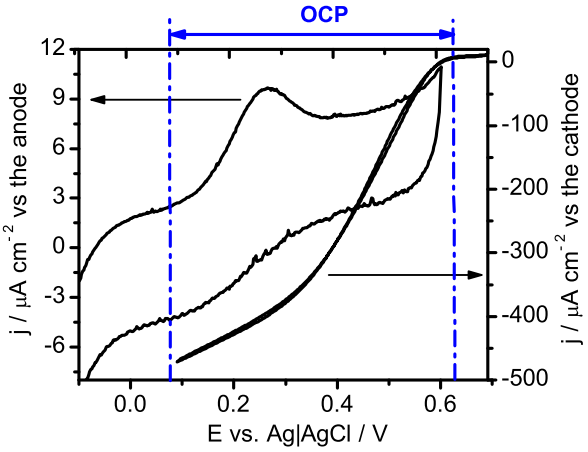

Figure 6.7: CV of the VACNT-anode and the biocathode working in 1 mM AA, v = 1 mV s^{-1}. The dashed blue lines indicate the onset potentials for the AA oxidation and the oxygen reduction.

The performance of the separately working VACNT-anode and the biocathode was checked in 1 mM AA solution. CV at a scan rate of 1 mV s^{-1} showed that the current of O_2 reduction on the biocathode is at least one order of magnitude higher than the current of AA oxidation on the anode (Fig. 6.7). Moreover, taking into account also the previous observation that the potential of O_2 reduction does not shift significantly with the change of AA concentration, it is expected that the power of the AA/O_2 BFC is mostly dependent on the VACNT-anode. The current generated by the BFC should increase together with the increase of AA concentration. Thus with the unchanged cell voltage the power output of the BFC should increase with the addition of the fuel.

The difference between the onset potentials for the VACNT-anode and the air-breathing biocathode is depicted in Figure 6.7 by a blue arrow and it has a value of around 0.55 V. The arrow indicate an open circuit potential (OCP) which can be reached by the AA/O_2 BFC and in fact it is very similar to the OCP measured on the assembled BFC (Fig. 6.8A).

Chronopotentiometry was used to obtain polarisation curves and power outputs for the BFC with the VACNT-anode. The results obtained for four different concentrations (1, 2, 4 and 6 mM) are presented in Figure 6.8. The OCP is almost the same in all cases

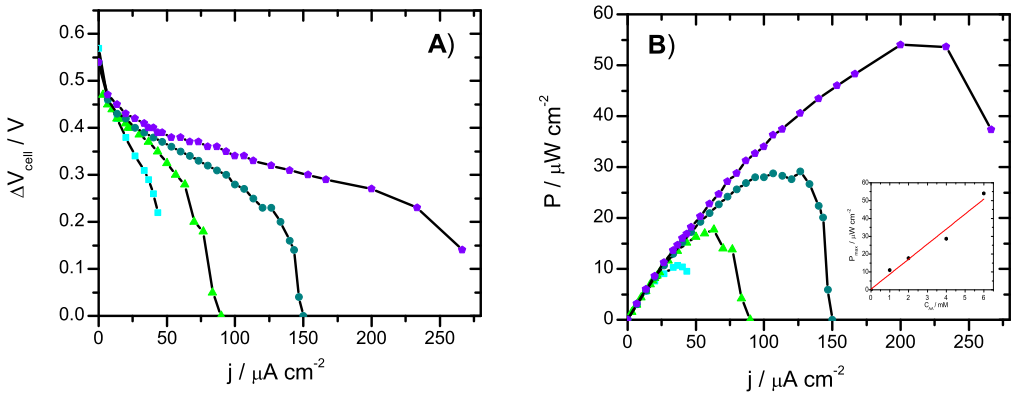

Figure 6.8: A) Polarization curves and B) the cell power as a function of current the BFC with VACNT-anode. The measurements are done for four different AA concentrations: 1 (cyan squares), 2 (green triangles), 4 (dark cyan circles) and 6 mM (violet pentagon). The inset in B) presents the dependence of the maximum power on the AA concentration.

(0.57 – 0.54 V, Fig. 6.8A). As expected the power output of the BFC increased with the increase of AA concentration. Thus our BFC acted as a self-powered sensor for ascorbic acid according to Katz's and Willner's definition [77]. The inset in Figure 6.8 B shows the relationship between the maximum power of the BFC and the AA concentration. This relationship is almost linear in the measured concentration range, with the $R^2 = 0.965$. The slope of the linear fit is $8.42 \pm 0.80\ \mu W\ cm^{-2}\ M^{-1}$. Thus the AA concentration which fulfil the linear dependence is very broad. However, utilizing our BFC as a sensor and determination of the AA concentration from the known power output of the BFC might give an error of ca. 9.5 %.

The presented way of constructing the self-powered sensor for ascorbic acid gave a very nice result in a form of a biofuel cell which generates the power dependent on the concentration of the fuel. However, the sensor characteristics as well as its application requires the use of the externally powered potentiostat. We wanted to obtain a truly self-powered sensor which does not need any power input into sensing. Thus we found out a novel way of the construction of a sensor by the connection of our BFC with an electrochromic display. As a display a thin layer of electrodeposited Prussian blue was used.

6.2.3 Prussian Blue electrochromic display

The use of the electrochromic display is a simple way of showing an electron flow coming in or out of our BFC, without application of any external power. In this case the current flow between the electrodes can be seen as a change in colour of the display. For our purpose we needed to use an electrochromic material which changes its colour at the potential higher than the potential of AA oxidation on the anode (ca. 0.05 V) and lower than the potential of O_2 reduction on the biocathode (ca. 0.6 V, Chapter 5). Prussian blue was chosen because it has a redox potential around 0.2 V [402] and it starts to change its colour at the potential

around 0.4 V vs. RE. Thus the PB display will change its blue form into a transparent form (known as Everitt's salt or Prussian white, PW) after connecting it to the anode kept in AA solution. On the other hand the display will return to its blue form when connected to the biocathode. This reversible process of the colour change is a result of the change in the PB layer composition and is described Equation 6.1 [396, 402]:

$$KFe_4^{III}[Fe^{II}(CN)_6]_3 + K^+ + e^- \rightleftharpoons K_2Fe_4^{III}[Fe^{II}(CN)_6]_3 \tag{6.1}$$

This reversible process of PB decoloration requires the presence of potassium ions, thus the display was kept in the compartment with 0.1 M KCl solution (Fig. 6.1). The display-compartment was separated from the BFC-compartment via a Nafion membrane not only to avoid a negative influence of chlorine ions on BOD but also to eliminate the change of PB into PW caused directly by AA. It is known that AA is responsible for a chemical reduction of PB [403].

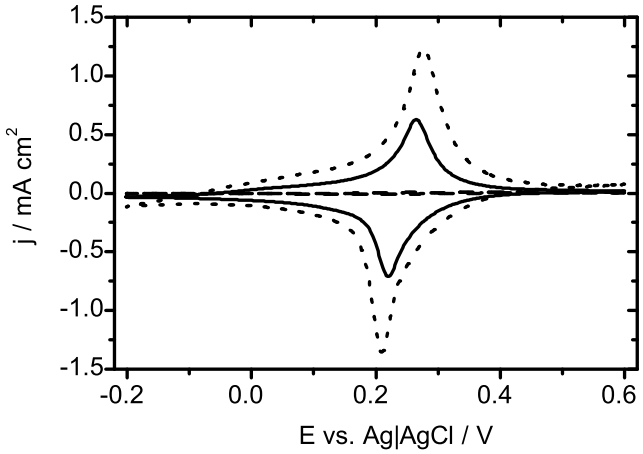

Figure 6.9: CVs of PB layers post treated by performing chronoamperometry at −0.05 V vs. Ag|AgCl for 600 s in different electrolytes: (dashed line) 0.1 M KCl in McIlvaine's buffer; (solid line) 1 M KCl; (dotted line) 0.1 M KCl in phosphate buffer. The buffers had the same pH 4.8. All CVs were recorded in 1 M KCl (in water, under air), $\nu = 20$ mV s^{-1}.

In the research concerning the air-breathing biocathode (5) McIlvaine's buffer was used as an electrolyte. In case of the self-powered sensor phosphate buffer was used because we wanted to avoid the presence of citrate ions in the display-compartment of the device. Citrates are known as chelating agents which form complexes e.g. with Fe(II) [404]. Thus these ions might remove the reduced form of iron from the PB layer by transferring it into the solution in form of complexes. The phenomenon of loosing iron from the PB layer was observed during the post-treatment of the PB display in McIlvaine's buffer solution. Post treatment was done to turn the PB into its more stable form. The potential of −0.05 V vs. RE for 600 s was applied to the display in a chosen electrolyte. Then cyclic voltammetry in 1 M KCl was done and the results are presented in Figure 6.9. It is clearly visible that the post-treatment in 0.1 M KCl in phosphate buffer (dotted line) give the highest PB oxidation and reduction peaks. It means than the smallest portion of PB layer turned into a soluble

form, in comparison with post-treatment in 0.1 M KCl in McIlvaine's buffer (Fig. 6.9, dashed line) and 1 M KCl (solid line). The PB oxidation and reduction peaks were almost invisible (Fig. 6.9, dashed line). This result indicates that a very big amount of the layer was dissolved in the solution by McIlvaine's buffer after PB reduction.

6.2.4 Truly self-powered AA sensor

Taking into account the potentials of AA oxidation and O_2 reduction in the VACNT-BFC as well as the redox potential of the PB display we expected to get a truly self-powered AA sensor by a proper connection of the VACNT-electrode and the electrode modified with PB. The idea was to obtain decoloration of the PB display after connecting it to the VACNT-electrode. The reverse colour change should be obtained by connecting the display to the biocathode. A similar concept was presented by NTERA Limited (Ireland) [405], but that company used different electrodes and did not use them for sensing. The similarity was in exploiting three electrodes. One of them acted as an electrochromic display which changed the colour in the reversible way after being alternately connected to two other electrodes.

Surprisingly the connection to the VACNT-anode did not result in an expected change in the colour of the display linked to the AA concentration. Apparently the potential of AA oxidation on the VACNT-electrode was not low enough to induce a sufficient electron flow to the PB-display and cause its decoloration. Thus another way of electrode modification with carbon nanomaterial was used to obtain the anode which has a suitable potential of AA oxidation.

The first type of anode which worked successfully in our truly self-powered AA sensor was made by modification of ITO-electrode with carbon nanoparticles (data not shown). Oppositely charged CNPs were alternately deposited by layer-by-layer method until three double layers (3L) were obtained [406]. The obtained CNP-electrode (area of 0.03 cm^2) was connected to the PB-display (area of 0.2 cm^2). The colour of the display was changed from blue to transparent with the rate dependent on the AA concentration. The higher the AA concentration in the BFC-compartment of the sensor, the faster the decoloration of the PB layer. Unfortunately the CNP-anodes were not mechanically stable. After several immersions in the aqueous electrolytes at least half of the CNPs were peeled off from the electrode surface. The disintegration of the CNP-layer is unwanted because our sensor is expected to be reusable. It is not possible to use it several times the anode has changeable amount of the material. Thus an improved way of the anode preparation was used to obtain mechanically more stable electrodes. The ITO-electrode was alternately coated with silicate beads and CNP nanoparticles (CNP/beads-electrodes). The electrodes with 6, 9 and 12 double layers were prepared and checked toward AA oxidation (Fig. 6.10Aa, b and c, respectively). The onset potential of AA oxidation is almost the same for all three electrodes, 0.02 V vs. RE.

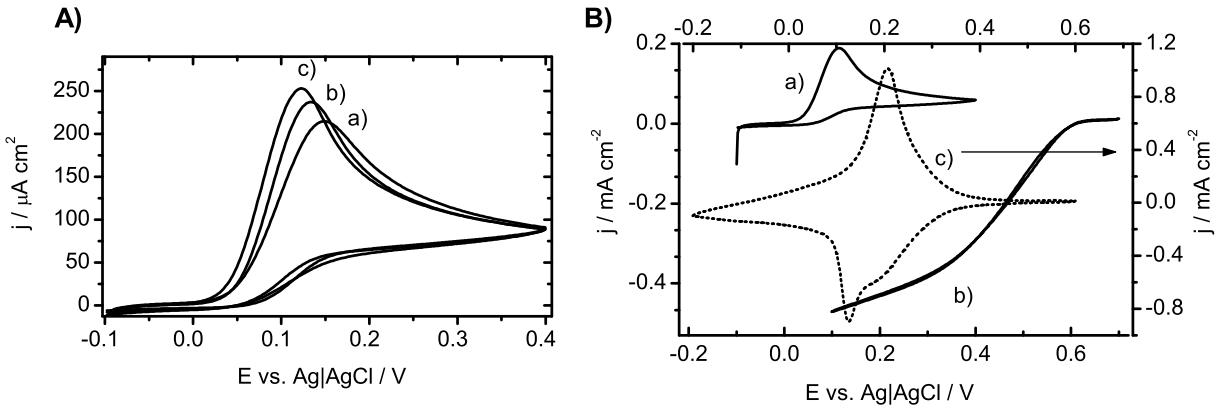

Figure 6.10: A) CV on the CNP/beads film electrodes with different number of double layers: a) 6L, b) 9L and c) 12L. The measurements were performed in 1.5 mM AA in phosphate buffer, pH 4.8 with the scan rate $\nu = 10$ mV s^{-1}. B) CVs of the electrodes used in the self-powered AA sensor: a) CNP/beads-electrode in 1 mM AA, $\nu = 10$ mV s^{-1}; b) air-breathing biocathode in 1 mM AA, $\nu = 1$ mV s^{-1}; c) PB-display, $\nu = 20$ mV s^{-1}, in 0.1 M KCl in phosphate buffer, pH 4.8. The scale on the left axis is related to the graphs a) and b) and the right to the graph c).

The peak potential shifts to negative direction with the increased number of CNP layers. The lowest value of 122 mV was obtained for 12L CNP/beads-electrode. The electrodes with 9L and 6L gave the anodic peak potential of 135 and 148 mV, respectively. Although the electrode with 12L had the same peak position as the CNP-electrode with 3L it was still not mechanically stable enough. CNP/beads electrodes with 9L (9L/CNP/beads) and 6L (6L/CNP/beads) could be immersed in the solution more than ten times without disintegration of CNP layer. Moreover, the peak potential for 9L/CNP/beads was better than for 6L/CNP/beads and the tests done with 6L/CNP/beads did not give satisfactory results. Thus the electrode with 9L CNP/beads was chosen for our truly self-powered AA sensor.

Cyclic voltammetry was performed on all electrodes used in the self-powered sensor in suitable electrolytes which were used during the sensor operation. The air-breathing biocathode and 9L CNP/beads anode were checked in AA buffered solution (in phosphate buffer) and the PB-display was checked in 0.1 M KCl (in phosphate buffer). The results are presented in Figure 6.10B. It is clearly visible that the half wave potential for the PB display is between the onset potentials of AA oxidation and O_2 reduction on the anode and the biocathode respectively. Thus alternate connection of the display to the anode and the biocathode of the BFC should cause a reversible change of the colour of PB, similarly to the work presented by NTERA Limited (Ireland) [405].

As expected the PB-display changed its colour from blue to transparent after connecting with the CNP/beads electrode. The speed of the discolouration was checked for the AA concentrations of 0.5, 1, 1.5, 2, 3 and 4 mM. It was easily visible with a naked eye that the display became transparent much faster for higher AA concentrations. This dependency is due to the fact that the more AA is oxidised on the electrode, the more electrons flow to the electrochromic display and thus cause faster PB electroreduction and consequently faster decoloration.

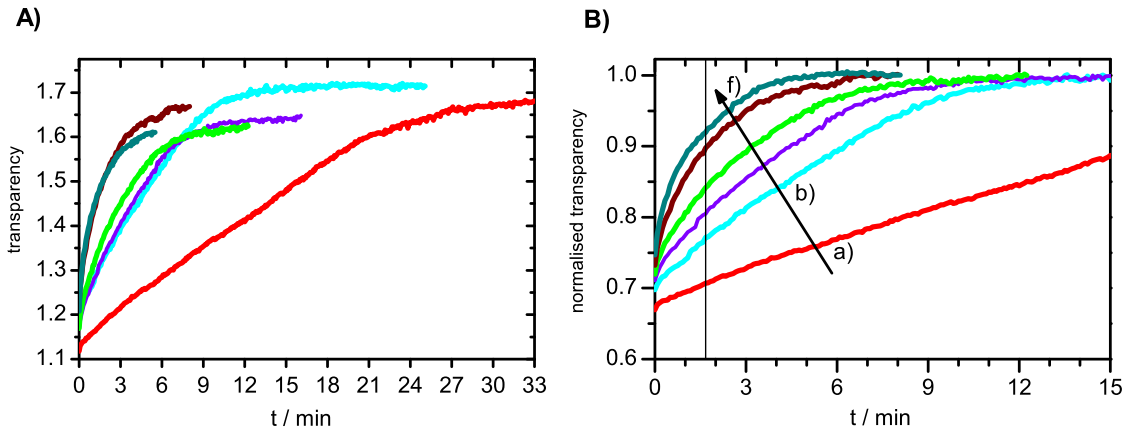

Figure 6.11: A) Relative value of the change of the colour of the PB-display plotted versus time. B) Plots from A after the normalisation with the value of the fully reduced display. For a-d) the display was connected to the anode immersed in 0.5, 1, 1.5, 2, 3 and 4 mM AA respectively. A straight vertical line represents the moment chosen for the calibration of the sensor (100 s).

The pictures taken during the reversible change in PB colour were analysed in the following way. By using ImageJ the greyscale values were measured for the display and the PB-electrode. These values were between 0 which is black and 255, which is assigned to white. Then the values related to the display were normalised with the values of a reference PB-electrode and plotted in Figure 6.11A. Next the graphs from Figure 6.11A were normalised to the transparency of the fully reduced (transparent) display. The latter step of data analysis was done by fitting an exponential function 6.2 to each graph and finding the value of parameter a.

$$y = a - b \times c^x \tag{6.2}$$

Thus the graphs in Fig. 6.11B were obtained by the normalisation of the graphs from Figure 6.11A to the fitted parameters a. Each graph represents the time dependent change of the transparency of the PB-display at a given concentration. For AA concentrations of $1.5 - 4$ mM the time dependency of the discolouration was very reproducible. Figure 6.12A presents results for the concentrations of 2 and 4 mM AA, which were obtained for two and three repeated reductions of PB-display, respectively. It is clearly visible that the graphs plotted for a certain concentration are overlapping. It means that the PB-display changes its colour in the same way each time after being connected to the CNP/beads-anode.

Each time after the complete discolouration of the display it was regenerated by connecting it to the biocathode (Fig. 6.1). Such electrode configuration results in an oxidation of the electrochromic material and thus in a very fast change of its colour. The display regains its initial blue colour in a few seconds (Fig. 6.12B, blue graphs). Moreover, this regeneration is reproducible which is shown in Figure 6.12B. The colour regeneration can be obtained several dozen times which indicates that our self-powered sensor is reusable.

A viable way of the determination of AA concentration in real samples with the use of our self-powered sensor is as follows. The CNP/beads anode is kept in the solution for a

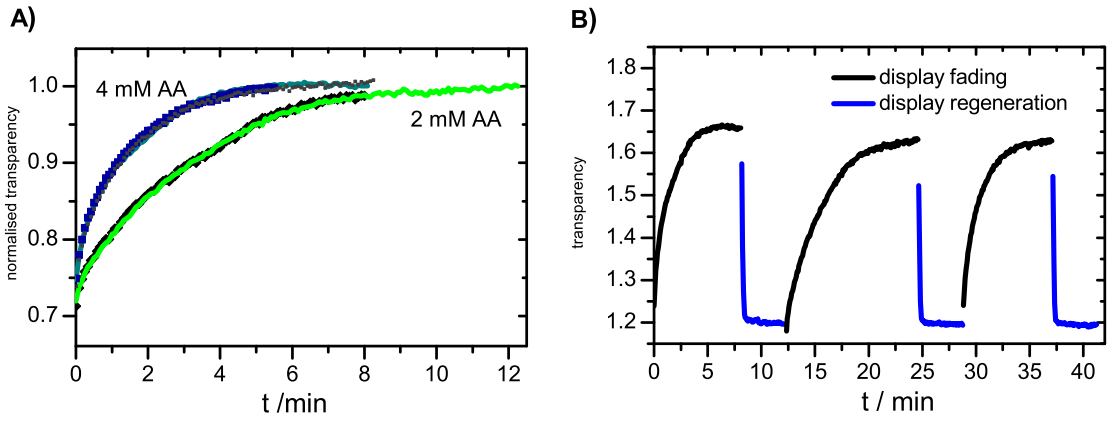

Figure 6.12: A) Reproducibility of the time dependency of the PB-display discolouration for the sensor working in 2 mM (2 graphs) and 4 mM AA (3 graphs) solution. B) Reversible changes of the PB-display transparency for the sensor working in 4 mM AA solution.

determined time. During that time the anode is connected with the display and changes the colour. The final colour of the display is then compared with the calibrated palette of colours and the AA concentration is found. Although our idea is similar to using a litmus paper for pH determination, in case of the self-powered sensor with the electrochromic display the time of sampling matters. Moreover, in case of the PB-display the palette can have only various shades of blue, not several different colours like the litmus paper. Besides after the regeneration of our sensor it can be used many times.

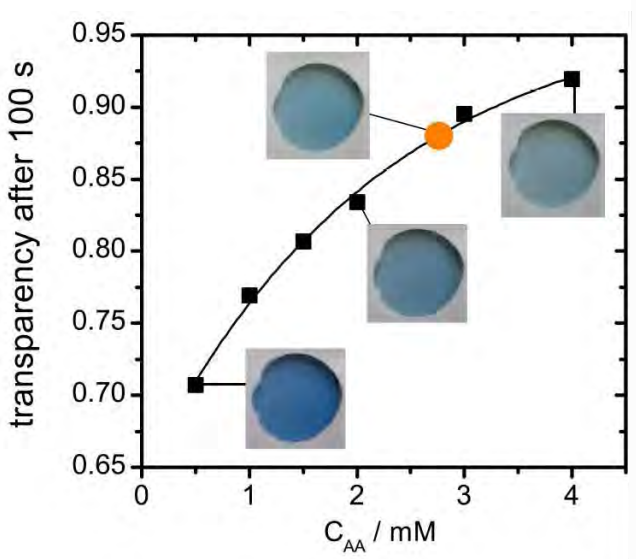

Figure 6.13: Normalised relative value of the change of the colour of the PB-display obtained after 100 s plotted versus AA concentration. Orange circle represents the normalised value for the orange juice from the bottle (2.72 mM AA according to the label).

For the sensor calibration we used the pictures taken 100 s after the start of the display discolouration (Fig. 6.13). This specific time was chosen because then the highest contrast between the sample colour was observed. The values of normalised transparency were found for the chosen pictures and they were plotted versus the AA concentration - Figure 6.13, black squares. The obtained data points were fitted with the exponential function ($y =$

$0.974 - 0.332 \times 0.632^x$, R^2=0.993), so that the calibration curve for the self-powered sensor was obtained (Fig. 6.13, black line).

To show the application of our device in a real sample analysis the BFC-compartment of the cell was filled with the commercially available orange juice (Tymbark orange juice, AA concentration from the label is 48 mg per 100 ml). The value of normalised transparency obtained after 100 s (0.88) was plotted on the calibration curve as an orange circle. Thus the AA concentration of AA found from the calibration curve of our self-powered sensor was 2.7 ± 0.2 mM. This value is almost the same with the value indicated on the label of the bottle with the juice - 2.73 mM.

6.3 Conclusions

In this chapter two examples of AA/O_2 BFC were presented. Both of them comprised a very efficient air-breathing biocathode described in Chapter 5. The first BFC comprised the anode with VACNTs which was described in Chapter 3. This electrode can act as a sensitive AA sensor used in a 3-electrode cell in voltammetric and chronoamperometric measurements. The AA concentration range which can be determined with the use of this electrode covers the values corresponding to the range from serum and urine up to vitamin C citrus fruit. Moreover, it was shown that the BFC with the VACNT-anode gave maximum power output (P_{max}) dependent on the AA concentration (C_{AA}). A linear dependency of $P_{max}(C_{AA})$ was found for the concentration up to 6 mM. Thus this BFC can be called a self-powered sensor, according to the definition suggested by Katz and Willner [77]. However, this definition allows to use an externally powered read-out which indicates the dependency between the power (or the OCP) of the BFC on the fuel concentration. Since we wanted to obtain a sensor which takes all the needed power from the BFC (a truly self-powered sensor), we decided to use an electrochromic material which give a colour change visible with the naked eye. The speed of the decoloration is dependent on the concentration of the fuel. Since the chosen material - Prussian blue - did not give expected dependency, the second type of an anode was prepared for obtaining the self-powered sensor.

The second type of AA/O_2 BFC comprised the anode with alternately deposited 9 layers of CNPs and silicate beads. The CNP/beads anode gave lower current density of AA oxidation than the VACNT-anode at a given AA concentration. Thus it was less efficient toward the oxidation than the VACNT-anode. However, the onset potential of AA oxidation was more negative for the electrode with CNPs than for the VACNT-electrode, which was a desirable effect from the point of view of the preparation of the truly self-powered sensor.

The obtained sensor worked in the following way. While the display with PB was connected to the CNP/beads anode it was changing the colour from blue to transparent. The

colour obtained after 100 s for different concentration was used to calibrate the sensor.

The device described here is the first truly self-powered sensor for AA reported so far. Moreover, its construction is very novel and make the sensor reusable. During work on our device Liu and Crooks [407] demonstrated a self-powered sensor based on a PB-display. However, our sensor is still the first example of a truly self-powered analytical tool giving quantitative information about the analyte concentration. This is because our sensor does not need any external power supply to work and to show a colour change related to the AA concentration. Our vision is that one day self-powered sensors with electrochromic displays will be used together with mobile phone apps [408]. The apps will analyse the colour change of the display and give quantitative information about the analyte. Thus expensive apparatus might be replaced with small, cheap and easy to operate sensors.

Chapter 7

Carbon nanotube growth

There are many ways of growing CNTs, as described in Section 1.1.2, but most of them require the use of big chambers heated to very high temperatures. The local heating method (see Sec. 1.1.2) is one of the CVD techniques which allow to grow CNTs by heating only a specific place on the sample. In this method Joule heating (resistive heating) is used to heat the substrate with the catalyst to the temperature suitable for CNT growth (typically more than 700 °C). The obtained tubes are of good quality and highly localised. Due to the fact that the substrate for the growth is heated only in the area designed for the CNTs the other parts of the substrate stay at relatively low temperature. Thus it is possible to grow CNTs on samples with microfabricated electronic circuits without damaging the metal leads. That makes the local heating a method compatible with on-chip microelectronics.

Vertically aligned CNTs having a good electric contact with a conductive substrate are very interesting as an electrode material. That is mainly due to exceptional electrochemical properties of CNTs and a large surface area of the obtained electrode. A direct growth of VACNTs on the conductive material seems to be the best way of obtaining a desired electrode. So far it was obtained e.g. on Ta, TiN, Pt and glassy carbon [409]. In fact it is very difficult to obtain mechanically stable electrodes with directly grown CNTs staying in electric contact with the substrate. Nevertheless a part of my thesis was devoted to coping with this issue and obtaining a miniature electrodes with directly grown CNTs.

In this chapter I will present an idea of obtaining a kind of a lab-on-chip device with CNTs directly grown by the local heating method. Then I will describe the problems which I faced during the very first steps of obtaining this device and will present the most interesting results of this project. Thus the biggest part of this chapter will be about growing the CNTs in the local heater, which was done in Edinburgh, with the cooperation with Eleanor Campbell Research Group.

7.1 Preparation

Samples for the CNT growth

The samples for the CNT growth were prepared by using microfabrication processes such as photolithography and electron beam lithography (done by Niklas Lindahl[1] in the Nanofabrication Laboratory at Chalmers University of Technology). A highly doped, n-type silicon wafer with a thin layer of grown silicon dioxide was used as a substrate. On the top of that wafer different patterns were fabricated - the larger patterns with the use of photolithography and the smaller patterns with the use of electron beam lithography. For the purpose of this work several types of samples were prepared. However, all of them can be assigned to two types of designs, from now on named as chip I and chip II design. The schemes of the designs are shown in the figures 7.1 and 7.2, respectively. Both kinds of chips have 3 side electrodes and a heater. The side electrodes have a rectangular shape of 200 µm × 450 µm and are fabricated to to be further used in post-growth electrochemical measurements. They are made of Pt (chip I where the heater was also made of Pt) or Au (chip II and chip I where the heater was made of Mo). The most important part of the chip is the heater located

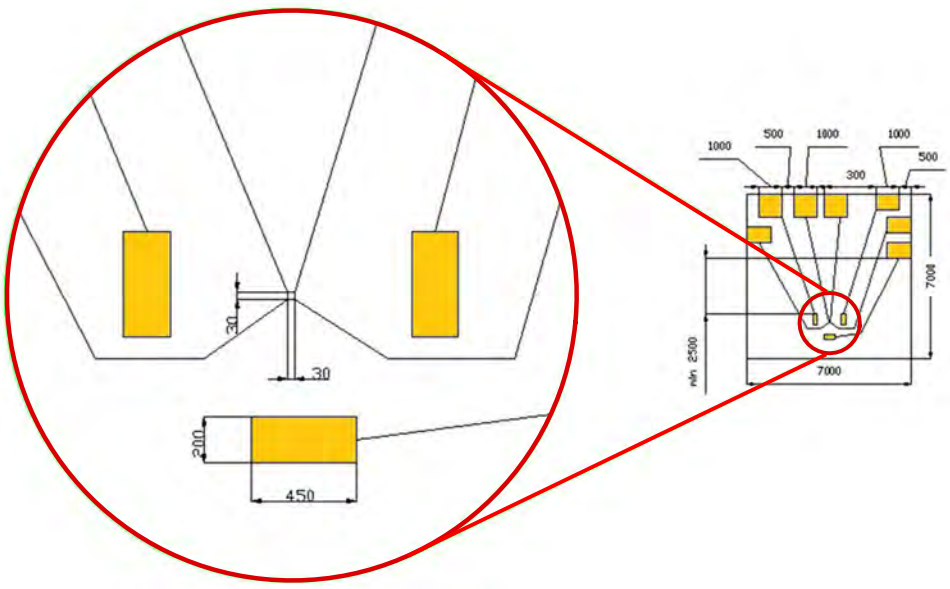

Figure 7.1: Scheme of the chip I design. The heater and 3 side electrodes are visible in the scaled up part of the figure. The scale is in µm

between the side electrodes. It has a shape of the square (ca. 30 µm × 30 µm) and it is made of either molybdenum or platinum (see Fig. 7.3, Materials), depending on the type of the sample. Both Mo and Pt layers are deposited on 10 nm layer of Ti on Si wafer and have a thickness of 100 nm (chip I) or 50 nm (design II). On the top of the square electrode a double layer of Al_2O_3 and iron that functions as catalyst for CNT growth is deposited by an electron

[1] Olofsson till 2011

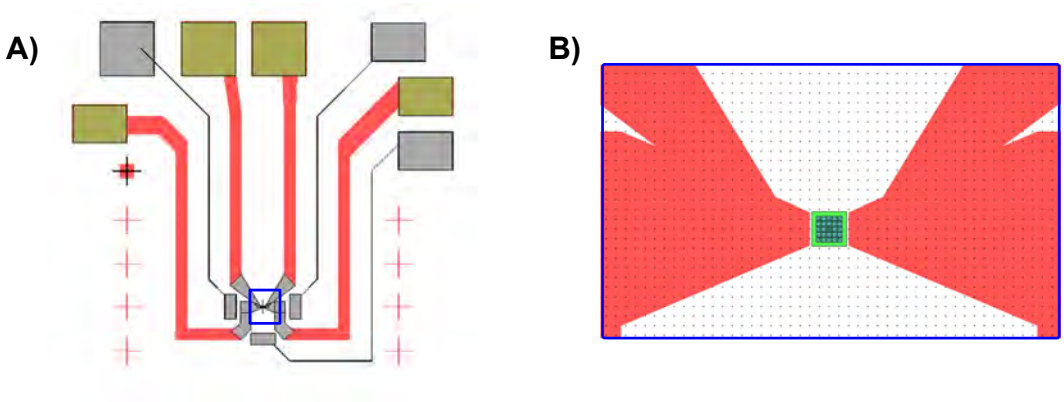

Figure 7.2: A) Scheme of the chip II design. B) Zoomed part of the chip II marked in A) by a blue frame. Different materials are depicted by the following colours: pink - Au covered by the insulating layer; dark khaki - Au, grey - Pt (from Niklas Lindahl).

beam evaporation. Three different patterns of Al_2O_3(5 nm)/Fe(1 nm) were fabricated (see Fig. 7.3, Catalyst pattern):

Full where the whole square was covered with Fe,
Stripes where 18 stripes of the Fe layers were fabricated (27 µm × 1 µm),
Boxes with 5 boxes of the Fe layers (5 µm × 5 µm).

Each square electrode was connected to four contact pads - to enable 4-probe measurements. Due to the fact that this electrode is heated during the growth process, it is named a heater.

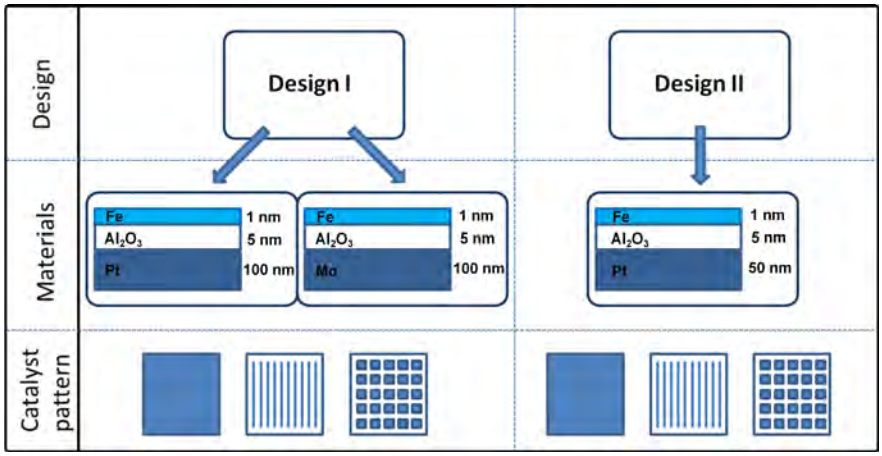

Figure 7.3: A comparison of materials and catalyst patterns fabricated on the heater of different designs.

The main differences between the chip I and the chip II are the thickness of the electric paths leading to the heater as well as the thickness of the heater. The heater was twice thinner on the chip II. The paths were made out of Pt in the chip I and Au in the chip II. Another significant difference between the two chips is depicted in Figure 7.3A - a grey area containing all 4 electrodes. This area was first made of Pt (50 nm) and then Au was deposited on it everywhere except the heater and a frame around the heater (5 µm in width).

During the microfabrication process an insulating layer of Si_3N_4 was deposited on the sample just before the evaporation of Al_2O_3 and Fe layers. Then the insulating layer was

plasma-etched at the defined places on the chip. As a result the following parts of the sample should be free from Si_3N_4: 3 side electrodes, the heater and the contact pads. Thus the different patterns of Al_2O_3 and Fe (see Fig. 7.2, Catalyst pattern) should have been deposited directly on the metal part of the heater (Pt or Mo). Moreover, there should have been an area in the shape of a frame left free from the insulating layer around the heater covered with the catalyst (a few micrometers wide).

Set-up for the CNT growth by the local heating method

The design of a growth chamber was previously developed in Eleanor Campbell Research Group (the University of Göteborg) by Staffan Dittmer [7]. The chamber is small enough (volume of ca. 200 cm^3) to fit into the Raman spectrophotometer (Renishaw In-Via Reflex micro-Raman system). It has an inlet and an outlet for the introduced gases, as shown in Figure 7.4A. Inside the chamber a table for the sample and metal needles (for making an electric contact to the contact pads) are placed (Fig. 7.4B). Four needles are connected to

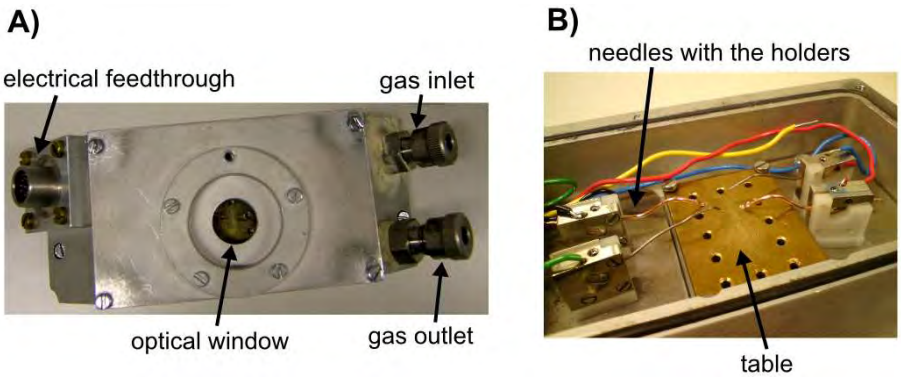

Figure 7.4: Photographs of the chamber used in the local heating method: A) closed chamber, B) inside the chamber.

two sourcemeters in a way that one of the sourcemeters is able to send the current and the other measures the voltage drop across the heater. A metal lid of the chamber has a quartz window. That design allows to look at the sample during the growth with an optical microscope or to perform *in situ* Raman measurements.

CNT growth

The CNT growth sample is placed on the table in the chamber. The local heater is connected through the needles to the sourcemeters. The chamber is closed, pumped out by the vacuum pumps and then twice filled with argon. Next the flow of Ar/H_2 (500/300 sccm) is introduced to the closed chamber. The gas output is opened when the pressure inside the chamber is just above the ambient. The heater is heated by increasing the current passing through it - up to the value when the CNT growth was expected. Then acetylene is introduced into

the chamber by flushing it with a gas mixture of $Ar/H_2/C_2H_2$ (500/300/6 sccm). The CNT growth can be observed by the digital camera and stopped by stopping the flow of C_2H_2.

7.2 Results and discussion

Visionary lab-on-chip device

The idea of obtaining the CNTs directly grown on the electrode surface was connected with obtaining a lab-on-chip device. Our vision was to get a chip with one CNT modified electrode and a few side electrodes. The CNTs would have an electric contact with the heater via carbon material deposited between the CNTs and the exposed metal part of the heater[2]. The side electrodes would be used e.g. (i) as a counter and a reference electrode - for making a 3-electrode-on-chip cell; (ii) for making a Zn anode for a biobattery (by analogy with the biobatteries with CNTs described in other chapters of this thesis) or (iii) for obtaining bioanodes. Moreover, the chip designs allow performing measurements in a drop or in a microfluidic channel. Thus the samples for growing CNTs by a local heating method presented here are very good basis for obtaining lab-on-chip devices such as miniaturised biobatteries, biofuel cells or biosensors with directly grown CNTs.

Facing reality

The chip designs used for the purpose of this thesis were never used before. They had been carefully planned to obtain the growth of CNTs. The samples used before in the same chamber had the heaters of the shape of a stripe (30 µm × 2 µm) [63] 15 times thinner than the square heater on the chips I and II. A part of our samples had the heaters made of Mo due to its high melting point (2607 °C) and compatibility with CNT growth, as was explained before [63]. The other part of the samples had platinum heaters because we expected that this material would work better as a substrate for CNTs used in electrochemical experiments.

The thickness of the layers deposited on the local heater (on Si) was optimised before. The 10 nm Ti layer acts as a good adhesion layer for Pt or Mo. The 5 nm of a porous Al_2O_3 layer is thick enough to prevent the catalyst sintering [410]. A slightly thicker insulating layer would not change the CNT growth but a too thick layer would prevent the growth. The thickness of a catalyst layer was 1 nm. Taking into account the results of the previous works the CNTs grown on the hater prepared as described are expected be multi-walled and relatively thin (up to 10 nm in diameter) [7, 63].

[2]The exposed metal part of the heater is synonymous with the frame-like area around the heater which was left without the catalyst and the insulating layer.

7.2.1 Temperature measurements

The heater is too small to properly measure its temperature by using contact probes. Any thermometer could easily change the temperature of the heated electrode due to the small thermal mass of the system. Moreover, it is not possible to determine the temperature by measuring the resistance of the heater because the resistance is also changed by chemical modification of the heater during heating. Thus a method based on the blackbody radiation was used to measure the temperature of the heater. The detailed description of this method can be found e.g. in the previous works [7,63]. It is based on the assumption that the heater is very similar to a black-body (a grey-body[3] assumption). In short, we used the spectrometer without the laser and Raman specific filters to measure the emission spectra of the heater. A tungsten lamp was used to calibrate the system used for the growth. The spectra obtained from the lamp were compared with the theoretical spectra of the black-body which are described by Planck's law. Thus a correlation function was obtained and further used for the determination of the temperature of the heater.

This way of temperature determination was used only for the few first attempts of CNT growth. We noticed that the longer we heat the sample the more likely it is damaged. Recording the spectrum is a relatively slow process, so it increases the probability of damaging the sample. Thus on the basis of a few temperature measurements we roughly estimated that the CNTs were grown at a temperature of ca. 800 °C. We correlated this temperature to the power dissipated across the heater, so that we knew in which power range satisfying CNTs were grown. For example the power more than 800 mW but less than 900 mW needed to be used for heating the heater with the full catalyst pattern. Other patterns required the use of different powers.

7.2.2 Optical and scanning electron microscopy

Due to the fact that the CNTs grown during local heating are relatively dense and long, they can be observed through the chamber window with an optical microscope (50× objective). The microscope is connected to the digital camera and further with the computer. Thus one can observe the growth process on a screen as a blackening of the heater and the formation of long curly black structures.

Chip I

All attempts at growing the CNTs with the use of the chip I with molybdenum were total failures. We were not able to heat the heater using the sourcemeters which were used pre-

[3] A grey body is a hypothetical source that would radiate as a black body but with an emissivity lower than 1 and constant with wavelength [411].

viously by Johan Ek Weis to grow the tubes on the striped heaters [63]. The use of a more powerful sourcemeter did not help as well. An unexpected observation was that the voltage measured by the same sourcemeter which was used for applying the current was from 1 to 2 orders of magnitude higher than the voltage measured by the second sourcemeter. We checked that it was not caused by a poor electrical connection between the contact pads and the wires. The problem with heating was probably caused by a bad microfabrication process or using too thin electric paths on the chip I.

Because of the unfeasibility of CNT growth on Mo by the local heating method we used a few samples to grow the tubes in a standard thermal CVD (TCVD). Three samples were heated in a tube furnace up to different temperatures: 800 °C, 750 °C and 700 °C under the same gas flow as used for the local heating, $Ar/H_2/C_2H_2$ (500/300/6 sccm). The carbon feedstock was introduced to the furnace for 10 min. As a result some carbon material was obtained on each sample. Further investigation by SEM showed that the biggest amount of material grown on the sample heated up to 800 °C - Fig. 7.5A. Closer view on the obtained carbon structures (not shown here) revealed very curly and thick nanotubes. Most likely these CNTs are covered with amorphous carbon.
Although some CNTs were grown on the chips I with Mo, they were never used for the electrochemical measurements. That was due to the fact that the golden electric paths leading to the square electrode were seriously damaged during heating the samples in the furnace.

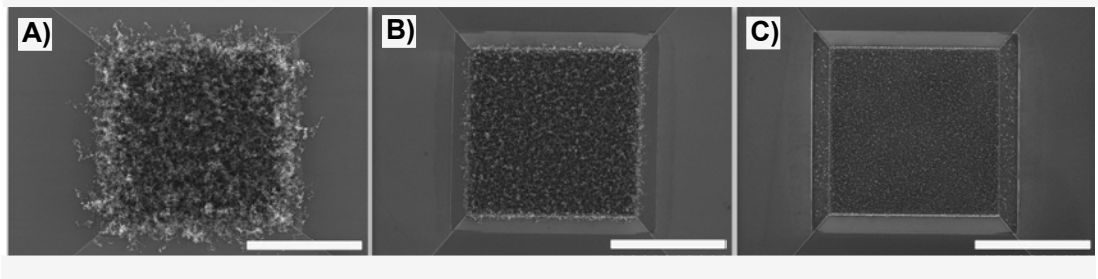

Figure 7.5: SEM images of the carbon material grown on chip I with Mo heaters by the standard TCVD technique at the temperature: A) 800 °C, B) 750 °C and C) 700 °C. Scale bars are 20 µm long

The use of the chips I with platinum heaters for CNT growth was more successful. Although it was not possible to grow the tubes in a very controlled and reproducible way, a few very nice results were obtained. We noticed that the best way to get a reasonable growth is to increase the temperature of the heater gradually in two steps. First the heater is heated by using a power of ca. 800 mW (for the full catalyst pattern). That corresponds to a temperature higher than 700 °C. Then the carbon feedstock is introduced into the chamber and the current is increased to increase the power just a little bit - up to ca. 850 mW. The stepwise increase of the temperature on the heater allowed us to avoid the problem of destroying the electric paths. We observed many examples of cracking or melting the metal paths in the close vicinity of the sides of the heater. These damages were caused by too much heat dissipated in an improper part of the chip. The longer a very high current was passed

trough the connections, the more likely they would be destroyed. Thus the stepwise heating reduced the chance of damaging the samples by reducing the temperature.

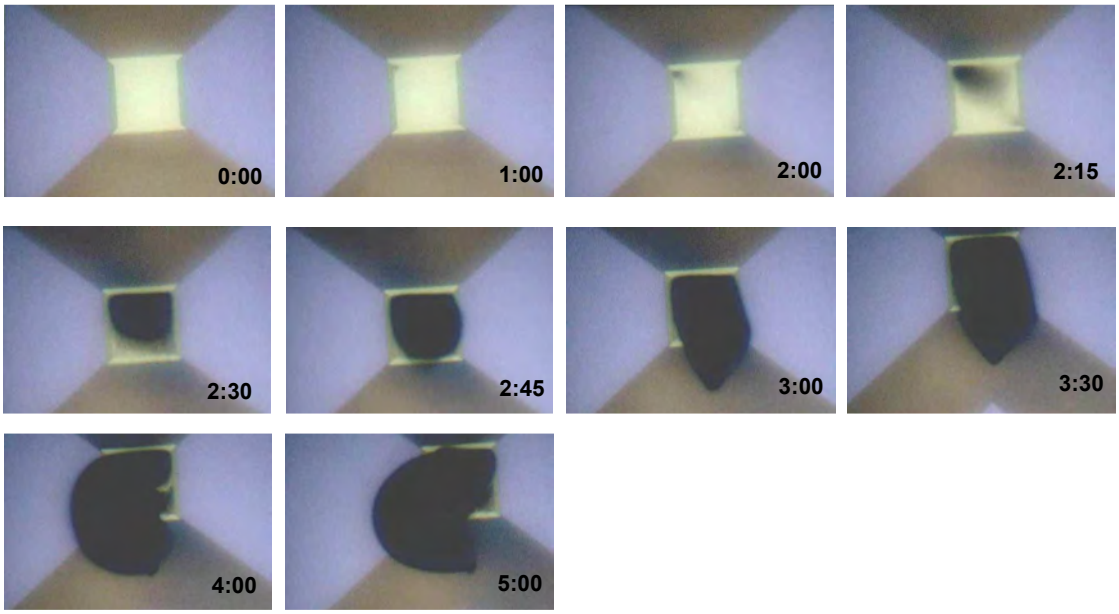

Figure 7.6: Snapshots taken during the growth of CNTs by the local heating method on the chip I with platinum heater (full heater covered with the catalyst layer). The numbers in each right corner indicate how many minutes and seconds have passed since the acetylene was introduced into the chamber.

The best results were obtained for the power related to a temperature of ca. 800 °C. Figure 7.6 represents an example of the CNTs growth observed with the use of the optical microscope. Each snapshot was taken after the specified time counted from the moment when C_2H_2 was introduced into the chamber. It is clearly visible that during the first 2 min almost no carbon material appeared on the heater. Relatively small amounts of the material started to appear in the corners of the heater (here the upper left and the lower right corners) which means that the temperature there is hight enough for the catalytic vapour deposition. In comparison with the results obtained on the striped heaters [63] 2 min is a very long time. In the other example the CNT growth was observed within a few seconds [63]. In case of our square heater just after the second minute the current passing through the heater was increased and an acceleration in a speed of growth was noticed. At first the CNTs were growing vertically to the electrode surface, thus only a blackening of the surface was observed (2 : 30 min). Then the tubes were too heavy and without any support from the sides they started to fold (after around 3 min). After the further growth (up to ca. 5 min) the CNTs turned on to their left side. Although the heater was still heated (till 10 min), no change in the shape of the grown structure was noticed.

SEM images in Figure 7.7 show the same sample as presented in Fig. 7.6. The CNTs were grown in a big bundle which fell on the substrate and curled. It is difficult to measure the length of the CNT bundle on the basis of the SEM images, but it is very likely that it is more than 100 μm (Fig. 7.7A). The single CNTs are entangled and very wavy (fig. 7.7D and

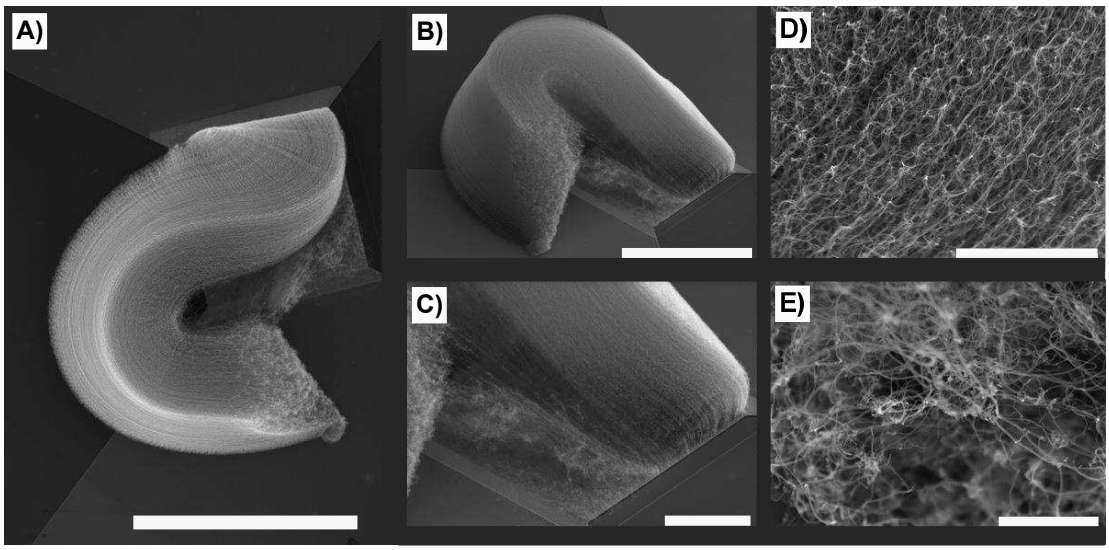

Figure 7.7: SEM images of the same CNTs as shown in the previous figure. The scale bares are A) 40, B) 30, C) 10, D) 2 and E) 1 µm long.

E). However, they are parallel to each other. Figure 7.7C (which is a closer view of Fig. 7.7B indicate that there is some carbon material deposited in the close vicinity of the edges of the heater. We expect that this material might help with obtaining the electrical connection between the CNTs and the metal part of the heater.

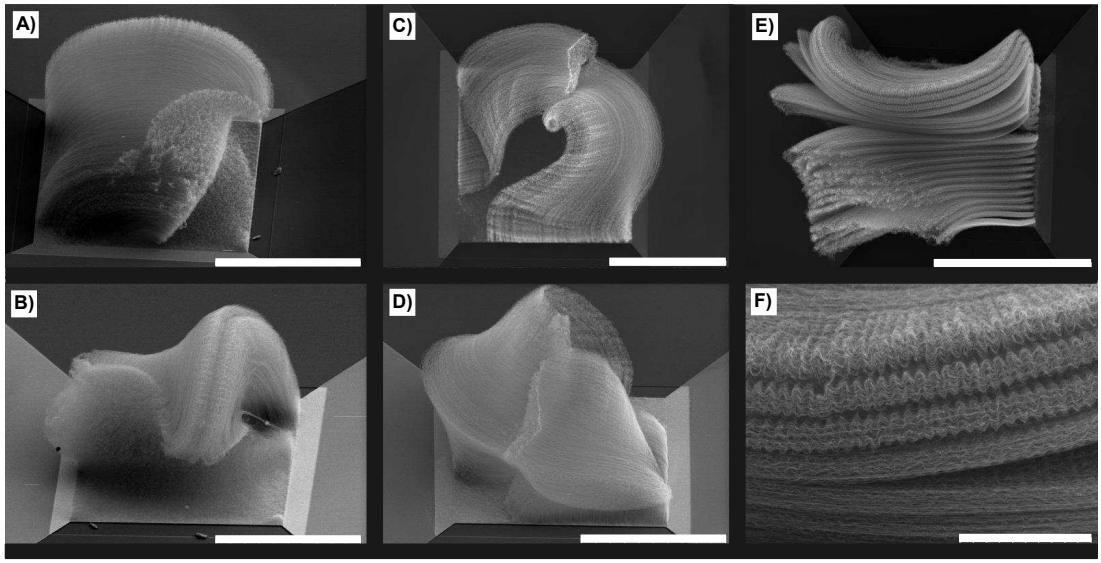

Figure 7.8: SEM images of CNTs grown on local heaters (chip I) made of Pt. The following images represent the same samples: A and B, C and D, E and F. Scale bars are A-D) 20 µm, E) 30 µm and F) 5 µm long.

In Figure 7.8 the SEM images of three different samples are presented - two images taken for each sample at various angles. One can clearly see (images A-D) that the CNTs do not cover the heaters in a homogeneous way. The CNTs were preferentially grown in three ways: (i) on one side of the heater (A and B), (ii) on two opposite corners (C and D) or (iii) along the diagonal of the heater (not shown). The diversity of the obtained ways of growth comes from the inhomogeneity of the heat dissipation along the heater. That in turn comes from the different ways of passing the current through platinum electrode as well as from the

overheating of some parts of the heater. The voltage across the heater could be applied by the electric paths localised along the same side of the electrode or in the opposite corners. Joule heating occurs where is an electron flow, thus different regions of the sample are heated in a different way. The CNTs are grown only in the areas where the temperature of the heater is suitable - not too low but also not too high. Overheating of the heater causes catalyst fouling and halted CNT growth. That is why the CNTs shown in Figure 7.8C and D are not grown along the diagonal of the heater.

An interesting observation is the fact that the CNTs form wavy structures on the outer part of the grown bundle. Figure 7.8F) is a nice example of this phenomenon. One can see that the closer to the centre of the heater the CNTs were grown, the more straight they are. Close to the edges of the heater very wavy structures are formed. This is a result of

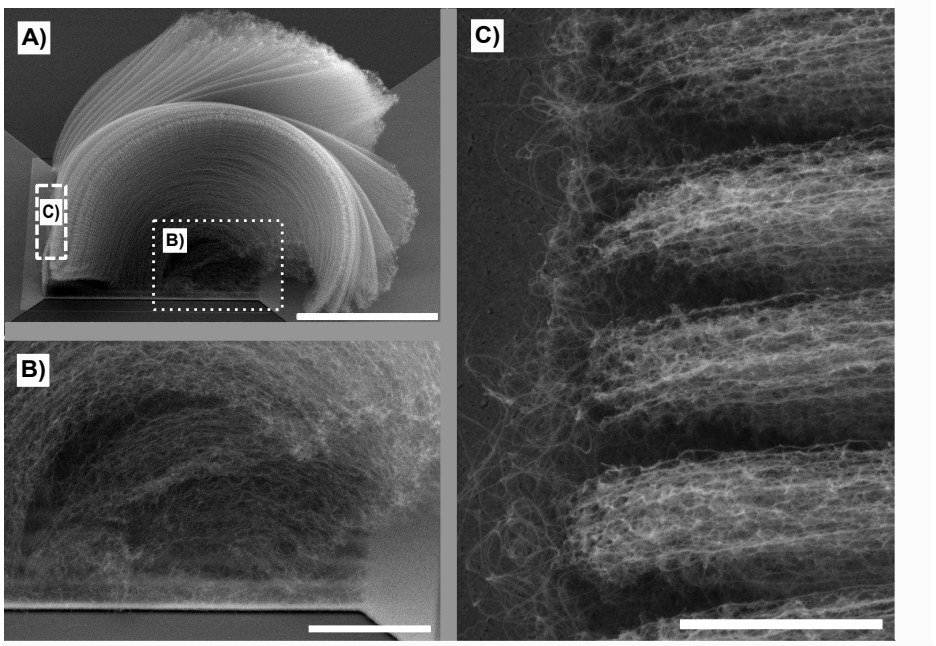

Figure 7.9: SEM images of CNTs grown on local heaters (chip I) made of Pt with the striped pattern of catalyst layer. Scale bars are A) 20 µm, B) 5 µm and C) 2 µm long.

non-homogenous CNT growth rate. The waves appeared because the CNTs on the edges are longer than in the middle part of the growth zone. The whole grown bundle has more or less the same length in the central and in the outer part. Thus the outer CNTs need to take a form of curly or wavy tubes whereas the central CNTs stay straight. A very similar observation concerning the local growth on the striped heater was described by Johan Ek Weiss [63]. In his example the CNTs formed the wavy structure in the inside part of the bundle.

Figure 7.9 represents the CNTs grown on the striped catalyst. The closer views (B and C) on the bottom part of the tubes indicate that they are touching the metal part of the heater. Thus an electric contact between the CNTs and the electrode is expected.

Chip II

Although some examples of successful CNT growth were achieved on the chip I, the obtained tubes were not homogeneously distributed on the heater. Moreover, most attempts of growing the CNTs resulted in damaging the sample, usually at the place where the heater was connected with the electric path. Chip II was designed to avoid the problem with the sample breaking during heating (thicker connections were connected to the square electrode). Moreover, a more homogeneous heat dissipation was expected due to the use of twice thinner heater than in case of the chip I.

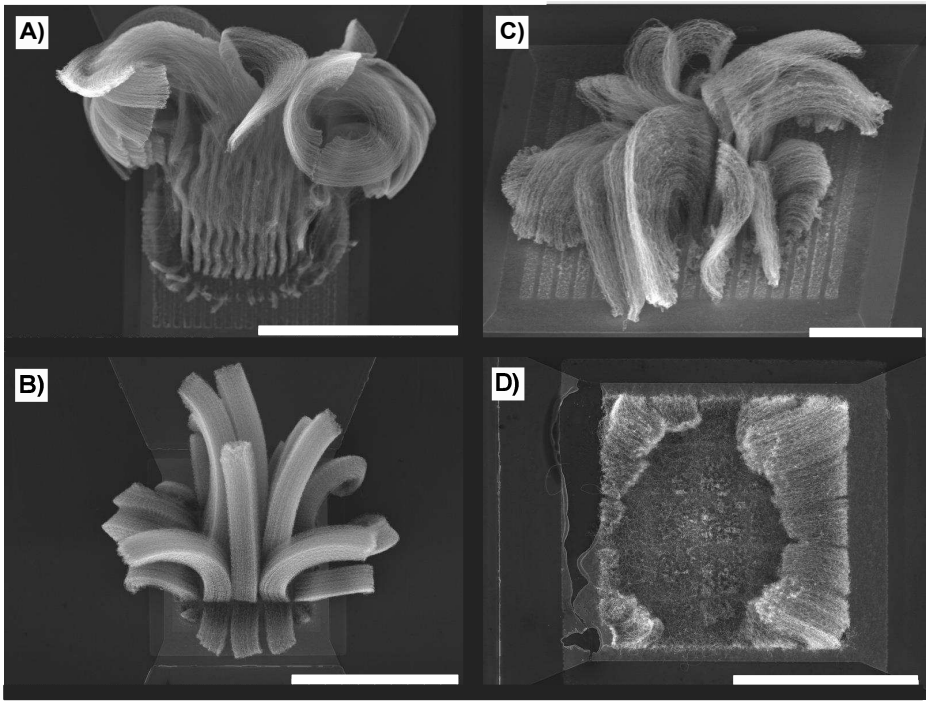

Figure 7.10: SEM images of CNTs grown on local heaters (chip II) made of Pt. Scale bars are A-B) 30 µm, C) 10 µm and D) 20 µm long.

The changes introduced to the sample design indeed changed the way of CNT growth. Figure 7.10 represents a few samples with different catalyst patterns obtained by heating the heater in the same way as it was done fo the chip I. Here it is clearly visible that the heat dissipation was different - the hottest zone was located in the central part of the heater. Thus the CNTs were nicely grown in the middle of the heater (Fig. 7.10A, B and C). In case of overheating the heater the CNTs were grown on the sides of this electrode (Fig. 7.10D).

Again we had the problem with damaging the substrate in the vicinity of the heater. An example of a broken part of a sample is shown in Figure 7.10D on the left to the heater. However, in case of the chip II the damages were not as frequent as in the case of the chip I. So again we were able to grow nice CNTs but not in a reproducible way.

7.2.3 Problems with conductivity

The CNTs directly grown on the chip I and the chip II were planned to be used for electrochemical purposes. Unexpectedly we had a problem with getting any signal from the CNT-electrode used as a working electrode in a 3-electrode cell. We started from checking the electrode response to a simple redox couple ($Fe(CN)_6^{3-}/Fe(CN)_6^{4-}$). No signal was obtained. We got only noise which indicated the lack of electric contact between the tubes and the heater.

We performed conductive AFM measurements to check the resistivity of the CNT-electrode. Different voltages were applied between the contact pad and the chosen places on the heater. The following places were checked: the exposed metal part; the part covered with the carbon material different that the tubes; the part with the CNTs; the part covered with the insulating layer. In case of having an electric contact we should have measured a current flow between the mentioned places. We expected to get a current response at least for the exposed metal or the exposed carbon material. But it was not possible to measure the current in any place on the heater and around it. Gentle touching the sample with the AFM tip did not give any signal. Only scratching the surface of the heater with the tip resulted in a current flow. However, these measurements were not reproducible and it was not possible to determine the resistance of the scratched sample.

The above mentioned problems with electrochemical and electric measurements are most likely the result of the presence of a thin residue of the insulating layer. We concluded that the Si_3N_4 was not etched properly before the deposition of the Al_2O_3/Fe bilayer. That is why the electric contact was not possible even with the "exposed" metal part of the heater. This part was etched from Si_3N_4 by plasma, but probably the exposure time to the plasma was not enough to remove all of the insulating layer. On one hand Si_3N_4 was successfully removed from the contact pads even though the etching was performed in the same conditions as for the heater. On the other hand one needs to take into account that the smaller areas are plasma-etched with a different speed than the bigger ones. Presumably this phenomenon was not properly taken into account during the microfabrication of the chips. As a result all the chips with the grown CNTs were useless from an electrochemical point of view. However, they are examples of beautiful CNT-structures obtained by the local heating method.

7.3 Conclusions

To the best of my knowledge the CNTs directly grown on the substrates of the designs described in this chapter have been never presented before. Most of the samples used in this thesis for the CNTs growth were damaged due to the thermal expansion of the materials located in the close vicinity of the heater. In most cases no tubes were grown because it

was impossible to sufficiently increase the temperature of the heater. However, we still got many samples with the CNTs grown by the local heater method. The SEM images of the chosen examples were presented in this chapter. Although the tubes were not distributed homogeneously on the electrode surface, they possibly could have been used as an electrode material. Unfortunately this possibility was not achieved because of the inappropriate sample preparation. The samples were designed in the way which should allow to get an electric contact between the grown CNTs and the local heater electrode. No electric contact was possible due to the presence of an insulating layer which was unintentionally left between the platinum part of the heater and a buffer layer.

The CNT growth on the chip I required a very high power. It was even noticed that the chamber became warm during the growth. That situation should not appear in the local heating method. However, during the growth on the chip II the sample was heated locally. The sample damages happened less often for the chip II design.

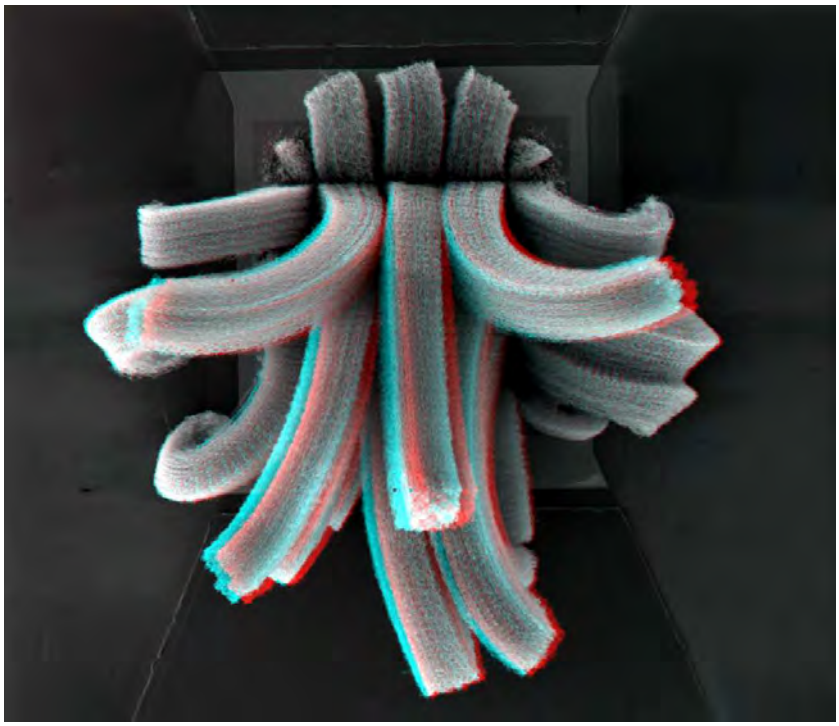

Figure 7.11: Anaglyph 3D of CNTs grown on local heater of the chip II design. Remark: Use 3D glasses to see a proper image.

Problems with growing CNTs in a repeatable was followed by another unexpected issue - the unfeasibility of obtaining the electric contact between the grown CNTs and the substrate. That made our CNTs not very interesting objects from the point of view of electrochemistry. Without having the above mentioned problems we should be able to obtain some lab-on-chip electrochemical systems. However, our CNTs are still attractive examples of the local heating growth what can be seen in Figure 7.11.

The idea of obtaining a kind of a lab-on-chip device with directly grown CNTs was not realised within my thesis. This project turned out to be more time consuming than

expected. Probably many more new chip designs should be tested to obtain the desired result. Moreover, some theoretical calculations concerning heat dissipation on the heaters should be done. I can only hope that in future someone will take into account our failures described here and use them to achieve the final goal - a multi-purpose lab-on-chip device with directly grown CNTs.

Chapter 8

Photoelectrochemical biofuel cell with titania nanotubes

Currently titania modified electrodes are very intensively studied as prospective photoanodes for photoelectrochemical cells (Section 1.6.3). Nanoparticulate TiO_2 has been considered as a very good material e.g. for dye-sensitizes solar cells (DSSCs). Recently nanotubular form of titania became interesting mainly due to the ability of formation of the electrodes with increased effective surface area - in comparison with the electrodes with TiO_2 nanoparticles (TNPs). Moreover, it was shown that the order and smoothness of titania nanotubes (TNTs) can be increased and as a result the electron diffusion length along the tubes can be increased. That in turn corresponds to an increase in conductivity and light to electricity conversion efficiencies [277]. Thus TNTs are expected to be better material for photoanodes than nanoparticulate titania.

Gust's group presented a hybrid photoelectrochemical BFC with the anode with porphyrin-sensitized nanoparticulate TiO_2 and $Hg|Hg_2SO_4$ cathode [326]. They used catalytic oxidation of glucose by glucose dehydrogenase (GDH) to generate the reduced form of NAD^+). NAD^+ was used by GDH and the obtained NADH was exploited for the regeneration of the dye. Since the porphyrin could be regenerated as long as glucose was present in the solution, the presented hybrid photoelectrochemical cell worked as a BFC. The anode described by Gust's group is hereafter called a Por/NADH/GDH/glucose system.

Very recently a simple way of improving the performance of a glucose/O_2 BFC was reported by Dong's group [334]. A biocathode with BOx was connected to a TNT-anode and illuminated with UV light. In the presence of 20 mM of glucose the photo-BFC generated maximum power of 47 $\mu W\,cm^{-2}$. The authors believe that their light-driven cell would generate electricity also under the outdoor solar irradiation.

In this chapter I will present the early stages of the work on obtaining photo-enhanced biofuel cells (photo-BFCs) and self-powered photo-sensor for glucose. The photo-enhancement

was done by the exchange of a typical bioanode into a photoanode which resulted in an increase of at least the cell voltage. The methods of the photo-BFC preparation were similar to the one presented by Gust's and Dong's groups, however our photoanodes were based only on TNTs.

A part of the work described in this chapter was done in the Robertson Research Group in Edinburgh. Dye-sensitized solar cells prepared in a standard way were used for making a comparison with our photo-BFCs.

8.1 Preparation

Growing titania nanotubes

The titania nanotubes (TNTs) were grown by the anodic etching of a titanium plate in 0.2 M HF solution. The solution (electrolyte) was prepared at least a few hours before the use and contained 1.6 or 10 % wt. H_2O in ethylene glycol.

The Ti plate had a shape of a square and an area of ca. 1 cm^2. It was first washed with EtOH and dried with a hair dryer. Then it was placed in a Teflon cell - as shown in Figure 8.1A. A rubber o-ring (0.9 cm in diameter) was used to prevent the electrolyte leakage

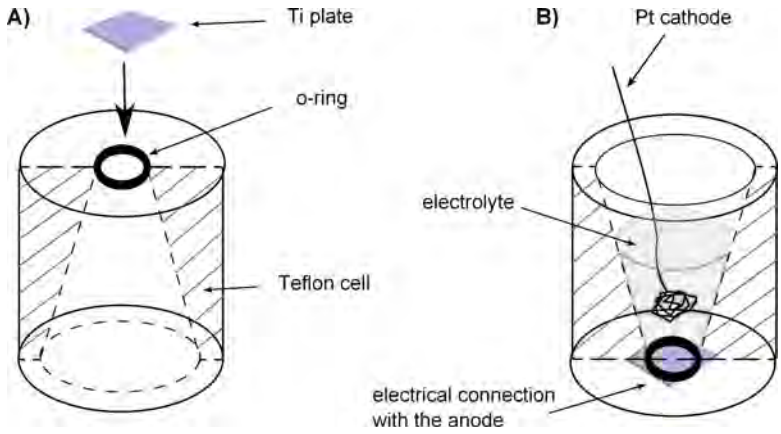

Figure 8.1: Scheme of the cell used for growing TiO_2 nanotubes: A) inserting Ti plate into the Teflon cell; B) a partial cross-section view on the cell used in the TNT growth.

between the plate and the cell. An electric contact with the titanium plate was achieved by the use of a flat round piece of metal in a shape of a lid. This metal part was placed on the top of the Ti plate (Fig. 8.1A) and pressed in the direction of the cell, so that the o-ring sealed the hole. Such a cell was gently turned up side down and filled with 10 ml of the electrolyte (Fig. 8.1B).

A platinum net was used as a cathode in a two-electrode cell. The cathode was cleaned by heating it in a Bunsen burner just before placing it into the cell (Fig. 8.1B). Inside the

cell the distance between the Ti anode and the Pt net was 1.5 cm. The growth of the TNTs was started by applying a voltage between the electrodes connected to the power supply device. The voltage was first increased up to 50 V (at once) and then it was monotonically increased up to 100 V with a speed of ca. 1 $mV\,s^{-1}$. The Ti plate was etched for 1, 2 or 4 h and during that time both the applied voltage and the current were controlled by two multimeters. After the desired time the cathode was taken out from the solution. Then the voltage on the power supply was decreased to 0 V.

After the TNT growth the electrolyte was removed from the cell and the anode was placed in EtOH for at least a few hours. Then it was dried in air and annealed in a tube furnace (in the air or argon) at 450 °C for 3 h. The as prepared samples were stored in ambient conditions when not in use.

For the TNT-electrode sensitization it was put into 0.1 mM solution (in chloroform) over night. Then the electrode was kept in chloroform for ca. 15 min to get rid of the dye molecules which were not properly adsorbed on the TNT surface. After drying the TNT electrode was masked by the insulating tape and immediately used for assembling a photo-BFC.

Synthesis of the porphyrin

5-(4-carboxyphenyl)-10,15,20-tris(4-methylphenyl)-porphyrin (Por) was synthesized according to the recipe found in [412]. 2.3 g 4-carboxybenzaldehyde was dissolved together with 5.44 ml tolylaldehyde in 150 ml propionic acid and stirred on a magnetic stirrer at reflux for 30 min. Then 4.5 ml pyrrole was added drop wise within a few minutes. The mixture was brought to the boil and then refluxed for another 90 min. After cooling down the crystallized product was filtered, washed with EtOH and purified by flash chromatography on silica. gel with $CHCl_3$ and MeOH (9:1). The synthesis was done in the cooperation with A. Listkowski.

Photo-biofuel cell assembly

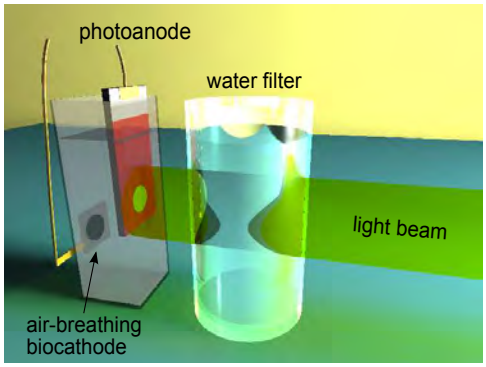

Figure 8.2: Scheme of the photo-biofuel cell illuminated by the beam of light passing through a water filter.

The cell was made of a plastic cuvette which let in the light of the wavelength between 300 and 900 nm. As a cathode the air-breathing biocathode was used (see Section 5.1). The Por-sensitized TNT-anode was immersed in the same solution as the biocathode, without any membrane separation (Fig. 8.2). The anode was placed close to the cell wall and exposed to the light beam. The light was generated by the Xe lamp and shone through a water filter (water in a quartz beaker). The distance between the lamp and the cell was adjusted to give a desired power of the incident light. The power of the light was measured with the use of a Power meter 815 (Newport Research) with the mask of the same area as the area of the photoanode.

Electrode modified with titania nanoparticles

Photoanodes with titania nanoparticles (TNP-electrode) were obtained by the modification of fluorine-doped tin oxide coated glass (FTO-electrode). The FTO-electrode (2.5 cm × 1.5 cm) was washed by sonication for 15 min in a detergent solution and rinsing in copious amount of water and EtOH. After drying in air the electrode was pre-treated in 40 mM aqueous solution of $TiCl_4$ at 70 °C. It was kept in the hot solution for 30 min and then washed with water, EtOH, and dried in ambient conditions.

Titania paste (Dyesol, with TNPs of 20 nm in diameter) was deposited on FTO-electrode by the doctor blading method. The paste was spread with a glass rod on FTO masked with the Scotch tape, so that a thin film (circular shape, 0.8 cm in diameter) was obtained. The obtained layer was levelled in EtOH vapour for ca. 5 min and dried in the air on a hot plate for 6 min at 125 °C. Then the paste was sintered in the furnace (without the air flow) in the following steps (i) 5 min at 325 °C, (ii) 20 min at 450 °C and (iii) 15 min at 500 °C. After cooling down to room temperature the electrode was again treated with $TiCl_4$ solution - in the same way was during the pre-treatment (30 min in the solution heated up to 70 °C). Washed and dried electrode was again sintered in the furnace for 15 min at 500 °C. After sintering the TNP-electrode was cool down to 80 °C and immersed into the ruthenium dye solution for around 20 h. 0.5 mM N719 Ru-dye in the mixture of acetonitrile and tert-butyl alcohol (1:1 by volume) was used. To remove loosely adsorbed dye molecules the electrode was immersed in the solvent mixture for at least 20 min. The sensitized TNP-electrode was dried by keeping it in the container filled with desiccant pellets. It is possible to store the sensitized TNP-electrode with desiccant pellets for at least a few days.

Electrodes with Pt nanoparticles

Platinum nanoparticle electrode (PtNP-electrode) was prepared by FTO-electrode (2.5 cm × 1.5 cm) modification. First a tiny hole was drilled through the electrode in its central

part. The electrode was washed by rinsing in water and 0.1 M HCl in EtOH, and sonication in acetone for 10 min. It was further heated in the furnace for 15 min at 400 °C to remove remained organic impurities. Then a drop (ca. 10 µl) of Platisol T was drop coated on FTO and heated for 15 min at 400 °C.

Electrolyte for DSSC

The iodine/iodide electrolyte used in DSSCs was prepared by dissolving the following chemicals:

- 0.7984 g 1-Butyl-3methylimidazolium iodide (0.6 M)
- 0.0381 g Iodine (0.03 M)
- 3.7 ml 4-tert-butylpiridine (0.5 M)
- 0.0059 g Guanidine thiocyanate (0.01 M)

in a mix of 4.25 ml acetonitrile and 0.75 ml valeronitrile. The obtained solution was stored in the fridge when not in use.

Dye-sensitized solar cell assembly

The dye-sensitized solar cell (DSSC) was assembled by sandwiching the TNP-electrode with the Pt-electrode. The cell was sealed with a square piece of Bynel foil with a hole (circle, 0.8 cm in diameter). The sealant was placed between the electrodes and melted on a hot plate at 220 °C. The electrodes were glued together by squeezing them on the hot plate with the sealant. Then the cell was sealed with a piece of Bynel foil placed on the top of the hole drilled in the PtNP-electrode. This time sealant was melted with the use of a soldering iron pressed through a thin Teflon foil.

The DSSC was filled with the iodine/iodide electrolyte in a following way. The Bynel layer which sealed the cell was pierced with a needle and the electrolyte was sucked into the cell by a vacuum back-filling. Namely the air inside the cell was replaced by the electrolyte with the use of a vacuum chamber. Then the cell was sealed with Bynel and a cover glass (0.13 mm thick) with the use of a soldering iron and Teflon foil. The sides of the electrodes were painted with a silver paint to obtain a better electric contact.

8.2 Results and discussion

Here I present the results of mainly electrochemical characterisation of TNT-photoanodes and photo-BFCs. Most of photoelectrochemical measurements done in Warsaw used Xe lamp

with a water filter as a light source. Thus one need to take into account that the spectrum of this light source is slightly different than the solar spectrum, with more higher-energy photons.

8.2.1 SEM images of titania nanotubes

SEM images of the TNTs grown for 2 h from two slightly different solutions are shown in Figure 8.3. Figure A presents the tubes grown from 0.2 M HF with 1.6 % wt. water. Although nicely vertically aligned tubes were obtained from this solution, they demonstrate the presence of so called nanograss [260]. The tube ends form structures similar to grass

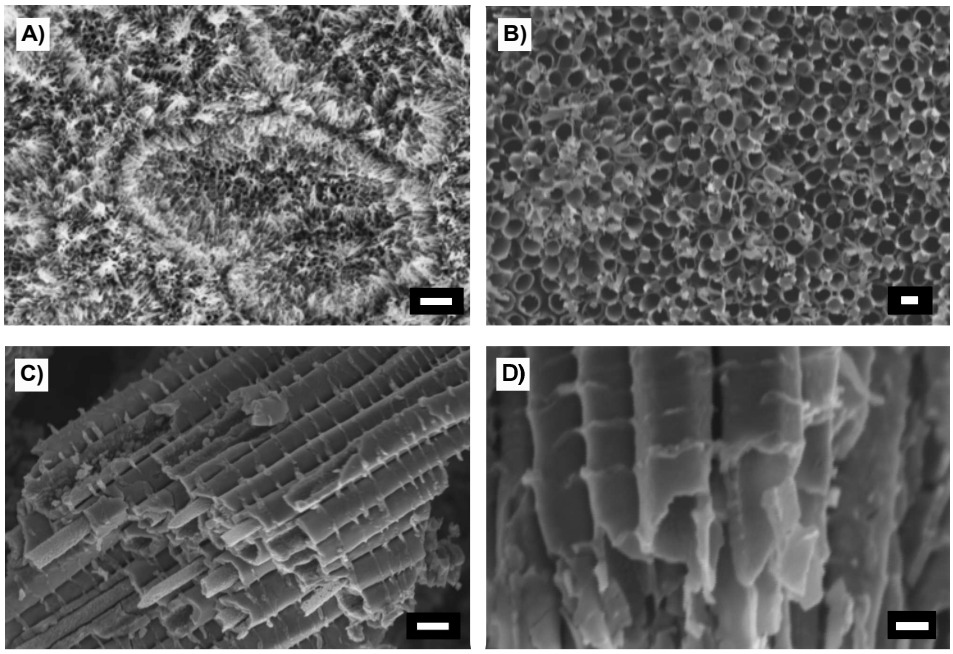

Figure 8.3: SEM images of TiO_2 nanotubes grown for 2 h in (A) 1.6% or in (B-D) the electrolyte with 10% wt. water. Scale bars are (A, C) 200 nm and (B, D) 100 nm long.

due to the inhomogeneous etching of the TNTs. To obtain TiO_2 TNTs without nanograss from the same electrolyte a few ways were tested. Neither the growth in lower temperature (by cooling the Teflon cell in ice) nor annealing Ti plates at 450 °C for 10 or 20 min before the etching eliminated the *grass effect*. Moreover, even sonication for 1 min of the grown tubes did not remove the nanograss as was expected. The TNTs with almost no nanograss (Fig. 8.3B - D were obtained during the growth from 0.2 M HF with 10 wt.% water (in ethylene glycol), thus the second electrolyte contained ca. 6 times more H_2O than the first one. Figure 8.3B shows the top view on the TNTs with the diameter of 93 nm and the wall thickness at the tube ends of 12 nm. Images C) and D) show the sidewalls of the bottom part of the same tubes. Closer to the bottom of the TNT layer the tube side walls are twice thicker than at the end, 24 nm thick.

An interesting observation is that the TNTs obtained from the second solution are double-walled. It is clearly visible in Fig. 8.3C that bottom part of the TNTs contain inner longitudinal structures. These structures are tubular (the open tubes were visible in images which are not shown here) and are not present at the tube ends. The same structures were observed in Schmuki's group and were described as carbon-rich shells [413]. These inner tubes are formed due to the presence of residual amount of the electrolyte which was trapped in the TNTs during etching. Depending on the speed of annealing of the etched sample the trapped electrolyte can be turned either into separated inner tubes or into an internal carbon-rich layer fused together with the TNT walls. However, the reported finding is contradictory to our observation. It was found [413] that the double-walled TNTs are formed when they are heated with the temperature increase rate of $1\,^{\circ}\mathrm{C\,s^{-1}}$. The heating rate of $50\,^{\circ}\mathrm{C\,s^{-1}}$ should lead to a complete fusion of the concentric tubes and the formation of single-walled structures. In our case the sample was annealed by putting it almost immediately from room temperature to the tube furnace heated up to 450 °C. Although the heating rate was not controlled very well in our case, it is easy to estimate that it was much larger than $50\,^{\circ}\mathrm{C\,s^{-1}}$. Thus our samples are expected to have single-walled morphology. The obtained double-walled TNTs indicate that not only the way of annealing affects the final morphology. Probably in our case much larger amount of the electrolyte was trapped inside the tubes, so that not all of it was burned-out.

Another important observation was that the TNT length was increased with the increased time growth. However, we were not able to measure the exact lengths because of the way of sample preparation for SEM. The obtained layer of TNTs was scratched before putting into the microscope, so that we could observe the tubes oriented under undefined angle to the electron beam.

8.2.2 Photoelectrochemical characterisation of the TNT-electrodes

Chronoamperometry was used to check the photocurrent response of the TNT-electrodes[1] annealed in air (TNT_{air}, solid line in Fig. 8.4A and in argon (TNT_{Ar}, dotted line) before (black) and after (blue) the sensitization with the porphyrin. A standard 3-electrode cell filled with McIlvaine's buffer was used where the WE was kept at a potential bias of 0.0 V vs. the RE. Each photoanode (WE) was first kept in darkness for 2 min and then it was illuminated with a desk lamp for 2 min. This intermittent anode irradiation was repeated several times and then the WE was left under the illumination for almost 1 h (except TNT_{Ar}). It is clearly visible that the photocurrent response is higher for the TNT_{air} than the TNT_{Ar}. That is the most likely due to the higher concentration of defects in the tubes annealed in the air. For both types of the tubes at the very beginning of the measurement the current density

[1]Experiments described in this section were done on the electrodes with the TiO_2 nanotubes grown from the electrolyte containing 1.6 wt.% H_2O.

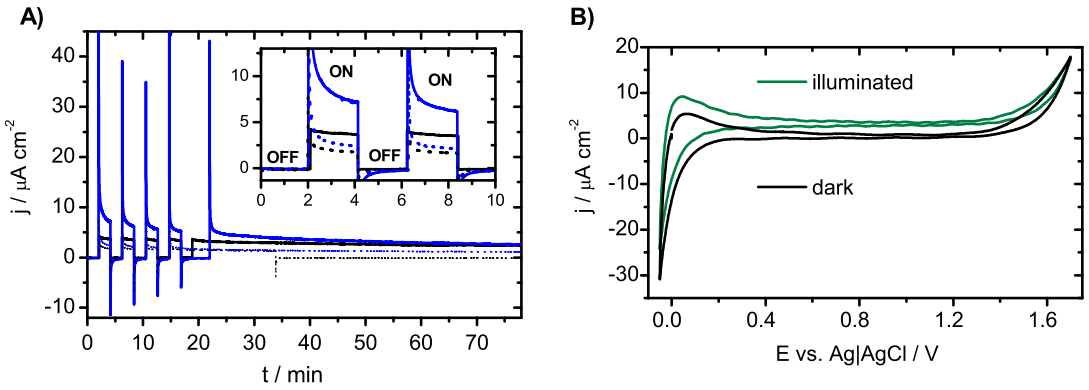

Figure 8.4: A) Photocurrent response of the TNTs grown for 2 h and annealed in the air (TNT_{air}, solid line) or in argon (TNT_{Ar}, dotted line). Black and blue lines correspond to the non-sensitized and the poprhyrin-sensitized TNT, respectively. Measurements taken in McIlvaine's buffer under the potential bias of 0 V vs. RE. B) CVs of the photoanode with TNTs grown for 4 h in Tris buffer (pH 4.8). In both cases (A and B) the TNT-electrode was illuminated with the desk lamp (ca. 125 mW cm^{-2})

is higher after the sensitization, with a more pronounced increase in case of the TNT_{air}. However, after ca. 1 h of constant illumination the photocurrent generated by the TNT_{air} was the same for the non-sensitized and the sensitized sample. Taking into account the presence of O_2 in aqueous electrolyte used in this experiment, the observed photocurrent decrease is explained by the photodegradation of the porphyrin. It is well known that TiO_2 exposed to light comprising UV part of the spectrum can generate highly reactive oxygen species (e.g. $OH^{\cdot}$, see Section 1.6) which are responsible for the oxidation of organic compounds. Thus we assume that the porphyrin was photooxidized or stripped off from the surface of the TNT-electrode during the long term exposure to the light.

Small anodic spikes visible in Fig. 8.4A (black lines) just at the beginning of the illumination of the non-sensitized electrodes are assigned to the photogeneration of the electron-hole pairs (e^--h^+) [414,415]. A further exponential decrease of the current is a result of a surface recombination of e^--h^+. The cathodic spikes appearing just after switching off the light are assigned to the back reaction of e^- from the conduction band with h^+ trapped at surface photogenerated species [414]. Much higher anodic spikes were observed for the sensitized TNTs as a result of the injection of the photoelectrons from the dye (from its excited state) to the conduction band of TiO_2. A very fast decrease of the current was probably caused by the lack of species which could regenerate the dye, thus the porphyrin was not able to inject more electrons to the TiO_2 conduction band.

Cyclic voltammetry of the TNT-electrode was performed in Tris buffer with and without the illumination (Fig. 8.4B) dark green and black line, respectively). The current photoresponse is visible as a shift of the voltammogram along the current density axis in the direction of more positive values. This shift comes from the photooxidation of water and other species present in the electrolyte, like Tris and chloride ions. A hysteretic structure which is visible on both CVs close to negative potentials (Fig. 8.4B) comes from the change in the sample capacitance under the applied potential. The change of the capacitance originates

from the exponential change of density of states [416] in titania, which related to electron accumulation and discharge in the TiO_2 nanostructures [417].

8.2.3 Dye-sensitized solar cells

The dye-sensitized solar cells with TNP-anodes were prepared and characterised in the Robertson Research Group in Edinburgh. The way of preparation was adopted from [418] because it describes a standardised way of obtaining efficient DSSC. Thus the DSSCs presented in this subsection should be treated as reference to our photo-BFCs comprising the TNT-anodes.

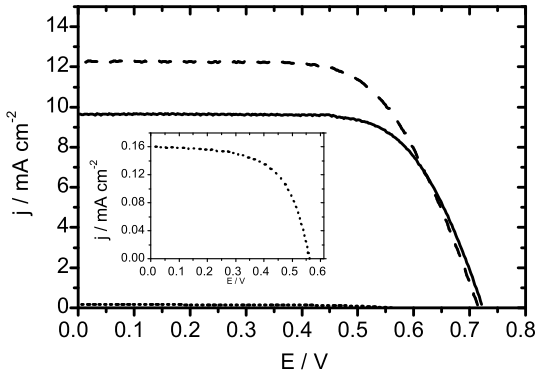

Figure 8.5: J-V curves of the cell with the non-sensitized photoanode ((i), dotted line) and of DSSCs illuminated with ((ii), dashed line) and without the mask ((iii), solid line). The measurements were taken under the illumination of 1 Sun with AM 1.5 G filter.

Figure 8.5 presents j-V curves for the solar cells with the TNP-anode which was (dotted line) not sensitized or (solid and dashed lines) sensitized with the Ru-dye. The measurements were performed under the illumination from a solar simulator (1 Sun equal to the light power of 100 mW cm^{-2}). The most important parameters of the cells obtained from Fig. 8.5 are listed in Table 8.1. Fill factors (FF) and the overall sunlight-to-electric-power conversion

Table 8.1: Solar cell parameters obtained from j-V curves plotted in Figure 8.5

Cell	j_{SC} / mA cm^{-2}	V_{OC} / V	FF	η
(i)	0.16	0.56	0.56	0.05%
(ii)	12.23	0.71	0.66	5.70%
(iii)	9.66	0.72	0.70	4.84%

j_{SC} - short circuit current, V_{OC} - open circuit voltage, FF - fill factor, η - energy conversion efficiency

efficiencies (η) were calculated according to equations 8.1 and 8.2 [418].

$$FF = \frac{I_{max}\ V_{max}}{I_{SC}\ V_{OC}} \tag{8.1}$$

$$\eta = \frac{P_{max}}{P_{in}} = \frac{I_{SC}\ V_{OC}\ FF}{P_{in}} \tag{8.2}$$

The values I_{max} and V_{max} stand for the current and the voltage of the cell corresponding to

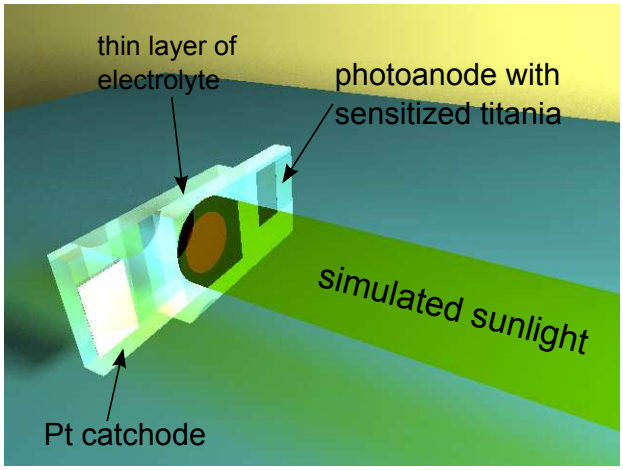

Figure 8.6: A schematic visualisation of illumination of a DSSC during the experiment.

its maximum power (P_{max}). P_{in} is the power of the incident light.

The graph (ii) (solid line) represents the situation when the whole cell was illuminated from the anode side (Fig. 8.6). In case of the graph (iii) (dashed line) the anode was covered with a mask and thus only the central part of the anode was illuminated. According to the guidelines given by the group leading in the study on DSSC [419] the use of a proper mask is required for a correct cell characterisation. However, the reported consequences of masking the cell were opposite to our results. Typically the short circuit current density (j_{SC}) is decreased when the mask is applied. Our DSSC gave higher j_{SC} after being masked. Most likely this effect was caused by the inhomogeneous titania layer. A multi-step procedure of the TNP-electrode preparation can easily result in obtaining a photoactive layer which is thicker in the middle of a circular electrode than on the edge. Since masking an anode is equal to illuminating its central part, this part of the TNP-electrode worked more efficiently in our DSSC than the part covered by the mask. The same observation was made for 5 different DSSCs. It was probably due to the adsorption of higher amount of the dye in the central part of the anode with more developed surface. More dye can absorb more light and thus can convert more solar energy into electrical energy. Our masked solar cell gave almost 18% increase of the energy conversion efficiency (η) in comparison with the same cell without the mask.

The j-V curve for the DSSC with the non-sensitized photoanode (Fig. 8.5 (i)) was registered to serve as a comparison to our photo-BFCs with bare TNTs (see Fig. 8.9). However, the comparison with the standard DSSC show more than hundredfold decrease in η for the DSSC with the bare TNP-electrode. This result highlights the importance of the presence of the dye on the photoactive titania. Without the dye TiO_2 is able to absorb the light mostly from the UV region which is a smaller fraction of the light getting to the anode surface. The dye absorbs the light of lower energies and gets first excited and then oxidised. The oxidation of the dye corresponds to the injection of the electrons to the conduction band of

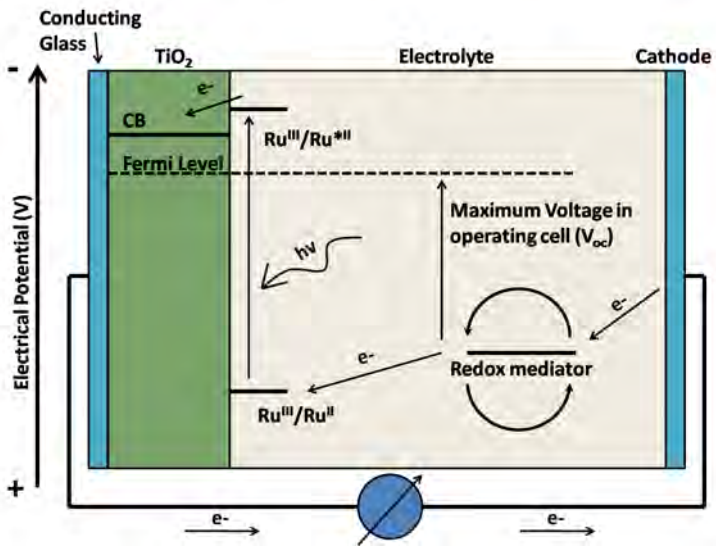

Figure 8.7: A scheme of a working DSSC [420].

nanoparticulate titania (see Fig. 8.7). All in all a huge decrease in the DSSC performance is expected when the anode is not sensitized with a proper dye.

8.2.4 Photoelectrochemical biofuel cell

Our first attempt to obtain a photo-BFC with TNT-electrode was similar to the idea presented by Gust's group [326] - the Por/NADH/GDH/glucose system (Fig. 1.31). We connected our efficient air-breathing biocathode with the photoanode with titania nanotubes sensitized with a chosen porphyrin (Por). The idea was that the porphyrin would sensitize the nanotubes, so that the photoanode would be able to harvest photons of energies not only corresponding to UV but also to the visible part of the solar spectrum. However, an important message here is that standard DSSCs contain non-aqueous electrolytes and they are sealed, so that they are not exposed to oxygen. The electrolytes in our photo-BFCs are based on water and are exposed to ambient conditions.

Most of our photo-BFCs were tested in the same way as the BFCs described in the previous chapters - by performing chronoamperometric measurements. We checked that V-j curves obtained in this way looked almost the same as the curves obtained by using cyclic voltammetry (data not shown). The latter method is typically used in DSSC characterisation as in Fig. 8.5 and will be used for the characterisation of a self-powered sensor for glucose.

The results obtained for the cells with the sensitized anode are presented in Figure 8.8 as graphs with black symbols. Triangles and diamonds correspond to the photoanodes with TNTs grown for 1 h (TNT_{1h}) and 2 h (TNT_{2h}), respectively. The cell parameters listed in Table 8.2 indicate that the photo-BFC with longer tubes gives ca. 1.5 times higher maximum power. As a consequence an energy conversion efficiency for the TNT_{2h} is 1.5 times higher.

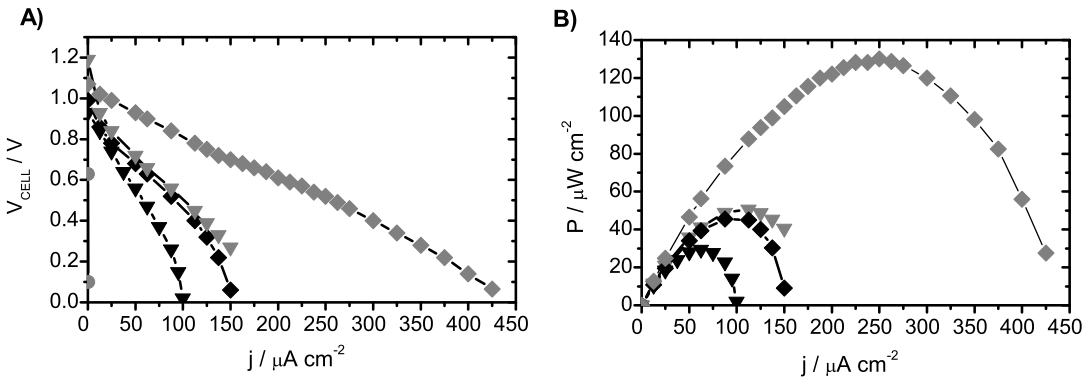

Figure 8.8: A) V-j curves and B) power outputs of the photo-BFCs under 1 Sun. Triangles and diamonds indicate that the photoanodes comprise the TNTs grown for 1 h and 2 h respectively. Circles state for the BFC kept in the darkness. Black symbols correspond to the situation when the BFCs comprise the photoanodes sensitized with Por and it is filled with 4 mM NADH, 15 Units GDH dm^{-3} and 1 M glucose in McIlvaine's buffer. Grey symbols represent the BFC with non-sensitized photoanode and catalase solution (in McIlvaine's buffer).

Table 8.2: Solar cell parameters obtained from j-V curves plotted in Figure 8.8 compared to the parameters of the cell described in [326].

Symbol	Type of anode	j_{SC}/ $\mu A\,cm^{-2}$	V_{OC}/ V	FF	P_{max}/ $\mu W\,cm^{-2}$	η/ %
black ▼	1 h, sensitized	100	0.93	0.31	29	0.029
black ♦	2 h, sensitized	150	0.99	0.31	45.5	0.046
grey ▼	1 h, non-sens.	165	1.19	0.25	50	0.050
grey ♦	2 h, non-sens.	440	1.07	0.28	130	0.130
not shown [326]	- , sensitized	55	1.10	0.61	37	3.7

P_{in} illuminating our cells = 1 Sun; P_{in} illuminating the cell described in [326] = 0.01 Sun with 520-nm irradiation

This enhancement is due to the increase of the current generated by the cell, since the OCV is negligibly different in both cases. A proper comparison with similar types of the cell obtained by Gust's group [326] is not possible because of different source of the light. Our source gave the light spectrum close to the solar spectrum, whereas their lamp illuminated the samples at 520 nm with the power of 1 $mW\,cm^{-2}$ (0.01 Sun). Although the parameters of their cell such as j_{SC} and P_{max} were lower than for our cell with TNT_{2h}, they obtained ca. 28 times higher energy conversion efficiency than our best cell presented in Fig. 8.8. Such a discrepancy in the obtained results might have been caused by harvesting more light by their cell or the use of different pH of Tris buffer in their and our cells (8.0 and 4.8, respectively). However, the most reasonable explanation is that in our case the dye was desorbed from the TNT-electrode surface. It was visible by a naked eye that our photoanode was gradually bleached during the measurements. Moreover, when it was exposed to light while being immersed in a small volume of electrolyte the electrolyte changed its colour. Not without reason it was underlined before that our photo-BFC was exposed to ambient conditions. That exposure caused that O_2 was present in the electrolyte. On the other hand having O_2 in the electrolyte was unavoidable in case of using the air-breathing biocathode. Consequently

oxygen was also present in the vicinity of the TNT-electrode and in our opinion it was a reason of the porphyrin degradation. It has been reported that oxygen found in the DSSCs is responsible for decreasing their performance by causing dye degradation. A few mechanisms of such degradation are possible: (i) oxygen is first turned into very reactive singlet oxygen by reacting with the dye and then it causes the dye degradation under irradiation [421]; (ii) photogenerated holes react with the dye molecules and oxidise them [422]; (iii) the degradation is caused by OH^- radicals [422] formed on TiO_2 surface; (iv) direct charge transfer between the TNTs and porphyrin molecules is involved [423]. However, it is possible that the dye is simply desorbed from the photoanode due to the presence of water which repels it.

Taking into account the above mentioned scenarios of the dye degradation and the fact that we observed the discolouration of the sensitized TNT-anode, we concluded that Por is not involved in the performance of our photo-BFC in the same way as in case of the solar cell described by Gust's group. Here Por does not stay on the TNT surface so it does not inject electrons to the conduction band of TiO_2 after being excited by the light. Thus NADH molecules are not necessary to regenerate the oxidised dye and generate NAD^+ species. Moreover, GDH and glucose are not used to replenish NAD^+. As a consequence our TNT-electrode is not a bioelectrode as in case of the BFC presented by Gust's group [326]. The TNT-electrode acts as a photoanode which oxidise water and other organic molecules present in the solution. Thus the scheme of the reactions occurring on the photoanode correspond to the situation presented in Fig. 1.29.

Our second type of photo-BFC comprises non-sensitized TNTs and McIlvaine's buffer with catalase ($33\,\mu g\,ml^{-1}$). This enzyme is responsible for a very fast decomposition of hydrogen peroxide, thus it was added to the electrolyte to avoid a negative influence of H_2O_2 on BOx. H_2O_2 is expected to be generated on the TNTs the same as $OH^{\cdot}$. Figure 8.8 (grey plots) as well as Table 8.2 show that a simple connection of our biocathode to the TNT-electrodes give much higher j_{SC}, V_{OC} and P_{max} than the complicated system used in the first type of our photo-BFC. Again the cell with the TNT_{2h} gives better parameters than the cell with the TNT_{1h}. The maximum power density for TNT_{2h} was $130\,\mu W\,cm^{-2}$ at 0.52 V. Fill factors for of the second type of BFCs have lower values than for the first type which means that more current generated by the cells is dissipated in internal losses. Worse (lower) fill factor values are related to the increased shunt[2] conductance (decreased shunt resistance). Thus more shunt current is present in the second type of our photo-BFC which is equal to more current short circuiting a some parts the cell by bypassing it without power generation [424].

To simply compare the cells comprising non-sensitized photoanodes we plotted j-V curves and power outputs of the cells from figures 8.5 and 8.8. Figure 8.9 shows that although j_{SC},

[2]Shunts are unwanted short circuits found in the cell.

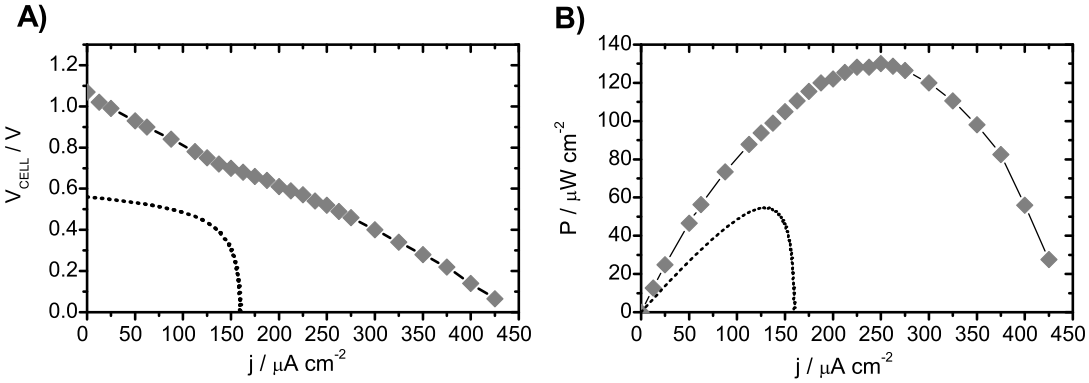

Figure 8.9: A) V-j curves and B) power outputs showing a comparison between the solar cells with non-sensitized photoanodes. Dotted line is taken from Fig. 8.5 and the graph with diamonds is taken from Fig. 8.8.

V_{OC} and P_{max} of our photo-BFC are better than the same parameters for the cell made in a standard way (with the TNP-anode), the shape of the V-i curve for the latter one (dotted line) better resembles the ideal shape. That observation is a result of the internal losses mentioned above for the second type of the photo-BFC. Moreover, the curves in Fig. 8.9A were obtained for the cells illuminated by Xe lamps with different filters. Thus lower currents generated by the standard type of the cell (dotted line) might be an effect of harvesting less high-energy photons which are filtered by the AM 1.5 G filter. The water filter used for the other cell (grey diamonds) might allow more high-energy photons to excite the TNTs. On the other hand the difference in the cell performances could be simply caused by the different type of TiO_2 nanostructures present on the photoanodes. The TNTs could give higher photocurrent than the TNPs.

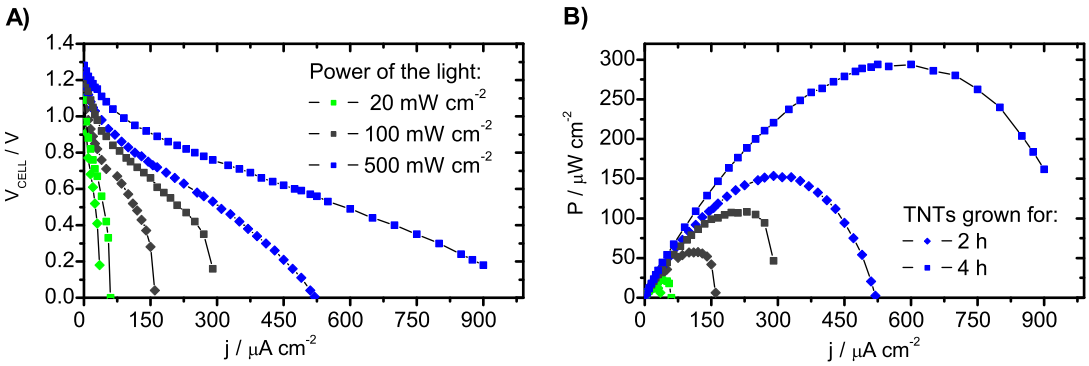

Figure 8.10: A) V-j curves and B) power outputs showing a comparison between the photo-BFCs with two types of TNT-anode (the TNTs were grown for 2 or 4 h - diamonds and squares, respectively) illuminated by the light beam of three different intensities (20, 100 and 500 mW cm^{-2} - green, dark grey and blue, respectively). McIlvaine's buffer (pH 4.8) was used as an electrolyte.

To check the influence of the photo-BFC performance irradiated with the light of different power we tested the cells with the TNT_{2h} and TNT_{4h} under 0.2, 1 and 5 Suns. The results are presented in Figure 8.10 and Table 8.3. It is clearly visible that V_{OC} changes very slightly for different illuminations. However, huge increase of the photocurrent is observed both with the increased length of the TNTs, as well as with the increased power of the incident light.

As a result the values of cell conversion efficiencies (η) are from 1.7 to 1.9 times higher for the tubes grown for 4 h than for the tubes grown 2 h. It is worth to stress that η values are decreasing with the increase of P_{in}, for both types of the TNTs. However, a big increase of P_{max} values was observed with increasing power of the incident light. For example ca. 13 times higher P_{max} was noted for the cell with the TNT_{4h} after changing P_{in} from 20 mW cm^{-2} (0.2 Sun) to 500 mW cm^{-2} (5 Suns).

Table 8.3: Solar cell parameters obtained from j-V curves plotted in Figure 8.10.

Symbol	TNTs grown for	P_{in} /mW cm^{-2}	V_{OC}/ V	P_{max} /μW cm^{-2}	V_{max}/ V	η/ %
green ◆	2 h	20	1.10	13.0	0.52	0.065
green ■	4 h	20	1.09	22.4	0.56	0.112
grey ◆	2 h	100	1.16	57.6	0.48	0.058
grey ■	4 h	100	1.23	108.1	0.47	0.108
blue ◆	2 h	500	1.22	153.7	0.53	0.031
blue ■	4 h	500	1.28	294.0	0.49	0.059

8.2.5 Self-powered photo-sensor for glucose based of a BFC

So far we mainly used McIlvaine's buffer (pH 4.8) as an electrolyte for our BFCs because our biocathode works slightly better in it than in e.g. phosphate buffer. However, McIlvaine's buffer contains citric acid which is oxidised on the TNT-anode. For the preparation of a sensor we wanted to avoid the oxidation of organic species other than the analyte. Thus we changed the electrolyte into phosphate buffer.

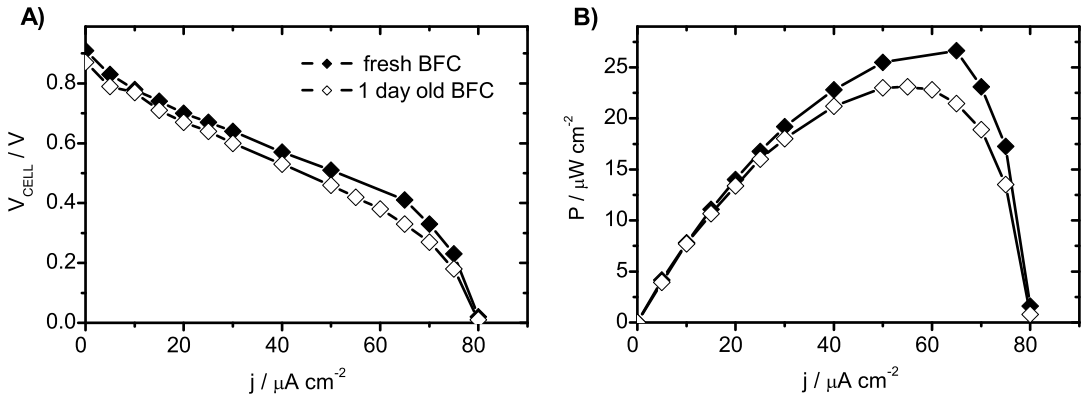

Figure 8.11: A) V-j curves and B) power outputs showing the performance of the same photo-BFC tested just after being assembled (full diamonds) and the day after (empty diamonds). The TNTs were grown for 2 h and the catalase solution in phosphate buffer (pH 4.8) was used as an electrolyte.

Figure 8.11 presents V-j curves and power outputs for the cell with the TNT_{2h} in phosphate buffer under the illumination of 1 Sun. A comparison with Fig. 8.8 (grey diamonds) indicates almost fivefold decrease in the power output when McIlvaine's buffer was replaced

with phosphate buffer. This is due to the presence of citric acid in McIlvaine's buffer. Organic molecules of the acid are oxidised on the photoanode so that the current generated by the cell increases. Besides, the cell with the non-syntetized TNTs show almost no change in the values of its parameters after one day (see Tab. 8.4). This small decrease is negligible in comparison with the change of parameter values of the Por/NADH/GDH/glucose cell (Fig. 8.11). The latter cell had ca. twice lower j_{SC} and V_{OC} after one day (data not shown).

Table 8.4: Solar cell parameters obtained from j-V curves plotted in Figure 8.11

Symbol	V_{OC}/ V	P_{max}/ μW cm^{-2}	V_{max}/ V	η/ %
◆	0.91	27	0.41	0.027
◇	0.87	23	0.42	0.023

Only 15 % decrease in maximum power generated by the cell with the TNT_{2h} in phosphate buffer after one day is a good result as for a BFC. The difference of the shapes of V-j curves representing the fresh cell and 1 day old cell indicates a decrease in the shunt resistance with time. Moreover, we noticed that BOx was leaking from the electrode.

The photo-BFC filled with phosphate buffer gives unchanged j_{SC} under the fixed P_{in}. Due to the fact that an increased concentration of glucose ($c_{glucose}$) causes an increase in j_{SC} we could use our photo-BFC as a self-powered sensor for glucose. J-V curves were obtained with the use of cyclic voltammetry (10 mV s^{-1}) and are shown in Figure 8.12A. The monotonic

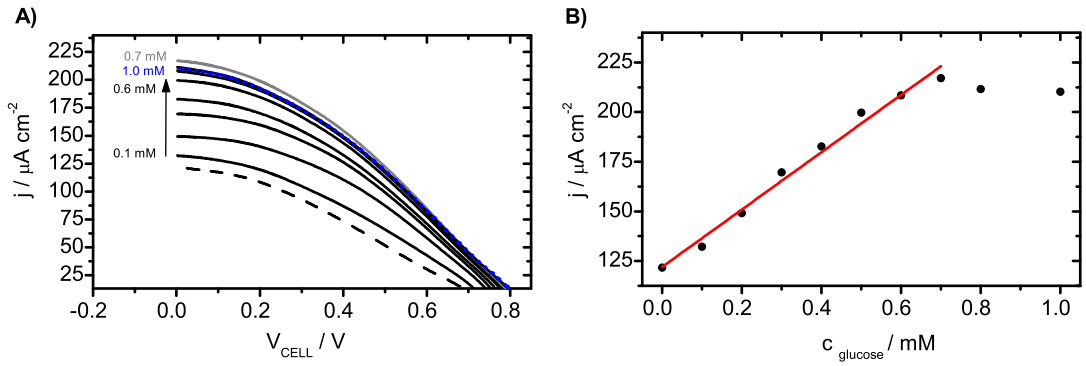

Figure 8.12: A) J-V curves for the photo-BFC with TNT_{4h} in (dashed line) phosphate buffer and the buffer with increasing concentration of glucose. B) The dependence between j_{SC} and glucose concentration and (red line) a linear fit to a part of this dependence.

increase of the photocurrent generated by the cell was observed up to glucose concentration of 0.7 mM. For $c_{glucose} > 0.7$ mM j_{SC} was saturated. Thus we got a calibration curve for our sensor by linear fitting to the data corresponding to glucose concentrations from 0.0 to 0.7 mM. The obtained relation $J_{SC} = (122 + 144.4\ c_{glucose})$ μA cm^{-2}(R^2=0.985) can be used to determine glucose concentration present in the photo-BFC on the basic of the measured short circuit current. Thus we showed the first example of a self-powered glucose photosensor based on a BFC. Moreover, this sensor is reusable because it gives the same j_{SC} in clear buffer after rinsing it copiously with water. Han *et al.* presented a photo-BFC with the

TNT-anode and BOx-cathode which is similar to our BFC [334]. Although their BFC uses glucose as a fuel, they did not show any dependence between the chosen cell parameter and glucose concentration.

8.3 Conclusions

We presented two types of photo-BFCs with air-breathing biocathodes and photoanodes based on titania nanotubes. The first type of our photo-BFC meant to exploit the Por/-NADH/GDH/glucose system for harvesting the visible light and the dye regeneration. In fact the dye was degraded on the anode surface in the presence of highly oxidative oxygen radicals. Thus the cell produced relatively low power output which was rapidly decreasing. The highest maximum power for the fresh BFC illuminated with 1 Sun was 45.5 $\mu W\,cm^{-2}$ at 0.52 V. From the point of view of DSSCs this is a very low value because it means that the cell converted 0.046 % of the power of the incident light into electricity. But as for a photo-BFC with the sensitized anode this result is better than e.g. the result presented by Gust's group - 37 $\mu W\,cm^{-2}$ at 0.82 V [326].

The second type of our photo-BFC comprised the non-sensitised TNTs and as a fuel it used water and organic species present in the electrolyte. The power outputs for this type of the cells were much higher than for the first type of the photo-BFC. Moreover, the maximum power increased with the increase of: the tube length and the power of the incident light. The best maximum power was obtained for the BFC with the TNT_{4h} filled with McIlvaine's buffer and illuminated by the solar simulator (with the water filter) with 5 Sun - 294 $\mu W\,cm^{-2}$ at 0.49 V. A similar photo-BFC was obtained by Dong's group [334] by connecting a titania nanotube photoanode and a biocathode comprising BOx. They used glucose as a fuel and illuminated the cell with UV light (0.5 Sun). The best maximum power generated by their cell was 47 $\mu W\,cm^{-2}$ at 0.79 V at glucose concentration of 20 mM [334]. Due to the differences in the source of light it is hard conclude which photo-BFC work better - our or the one presented by Dong's group. For sure our cell is a first example of the photoelectrochemical biofuel cell with TNT-anode and an air-breathing biocathode published so far.

The very first attempt to obtain a self-powered glucose sensor turned out to be successful. By the use of our photo-BFC with TNT_{4h} filled with phosphate buffer we obtained a sensor which shows a monotonic change of its short circuit current with the change of glucose concentration. The linear dependence was observed for the concentrations $0.0 - 0.7$ mM. We expect to be able to tune this concentration range by the TNT modification.

Chapter 9

Summary and conclusions

The study presented in this thesis concerns the modification of electrodes with carbon nanotubes CNTs and enzymes. Both non-functionalised and functionalised CNTs were used as a material increasing electroactive surface of the modified electrodes and enhancing efficiency of electron transfer between the electrode surface and the enzyme. Several biocatalysts were used - laccase, bilirubin oxidase), glucose oxidase and glucose dehydrogenase. They were immobilised within sol-gel silicate matrices. In this work I focused mostly on the preparation of the electrodes with the enzymes catalysing the reduction of oxygen, i.e. laccase and bilirubin oxidase.

At the beginning I presented a way of the preparation of electrodes with vertically aligned CNTs. The tubes were first grown by thermal chemical vapour deposition and then transferred to a conductive substrate - on an indium tin oxide electrode (ITO). Electric contact between the substrate and the tubes was achieved by the conductive adhesive. The obtained modified electrode showed a huge increase in the electroactive area in comparison with the bare ITO. It was further used as a platform for enzyme immobilisation. Examples of mediated glucose oxidation by glucose oxidase and glucose dehydrogenase were presented. Moreover mediated and non-mediated oxygen reduction on VACNT-electrode with laccase was studied in more detailed way. The prepared biocathodes formed biobatteries after the connection with a Zn wire as anode. Among all tested devices the best one had a biocathode with the VACNTs functionalised with pyrenesulfonic acid and laccase (non-mediated bioelectrocatalysis). The maximum power density for this device was 275 $\mu W\,cm^{-2}$, obtained at the cell potential of 1.50 V. This value is one of the very high power densities reported so far for the CNT/enzyme biofuel cells and biobatteries [259].

Further I described the preparation of non-mediated biocathodes with pyrene-tetrasulfonic acid-functionalised SWCNTs and bilirubin oxidase. I showed that the current density of O_2 reduction depends on the preparation procedure. For non-breathing electrodes (on ITO) the current depends not only on the diffusion of O_2 to the electrode surface but also on the

convective flow of the electrolyte. The latter has to be taken into account during electrochemical measurements if one wants to obtain reasonable results. Furthermore the performance of a breathing biocathode was studied. A breathing electrode is supported on a semipermeable membrane which is in contact with air on its one side and is in contact with an electrolyte on its other side. Our breathing biocathode turned out to be the best among all non-mediated systems with CNTs and bilirubin oxidase reported so far. It was used for the construction of the Zn/O_2 biobattery generating a maximum power density of 5.25 $mW\,cm^{-2}$ at ca 0.4 V in O_2. This battery was able to power a small watch and a stack of 4 batteries made a bike lamp with 2 LEDs shine. Thus it was proved that the constructed biobattery can be used for powering useful devices.

Our air-breathing biocathode was further used for the preparation of biofuel cells for ascorbic acid (AA). Together with the VACNT-electrode it gave a BFC with power outputs dependent on the AA concentration. Thus it can be treated as a self-powered sensor for AA. The connection of the breathing biocathode with an electrode modified with carbon nanoparticles (CNP) also gave a BFC for AA but with a little higher open circuit potential. The small difference in open circuit potential in comparison with the VACNT-BFC allowed the second type of BFC to be used as a truly self-powered AA sensor. This sensor was constructed by the connection of the CNP-BFC with Prussian blue electrochromic display. The display changes its colour with the speed dependent on the concentration of the analyte. We used the term truly self-powered sensor to underline that our sensor does not need any externally powered device to operate. Moreover we used it for the quantitative analysis of AA in orange juice.

The last two chapters of this thesis concern attempts to construct: a lab-on-chip device with directly grown CNTs and a photo-electrochemical biofuel cell with sensitized titania nanotubes. The first project was abandoned at its early stages due to problems with the sample preparation. Nevertheless the obtained results might be helpful for the future research. The first results of experiments concerning the photo-BFC show a steadily working BFC with photoactive but non-sensitized titania nanotubes. This kind of BFC gives a power density depending on the TNT length, the power of the light illuminating the cell and the concentration of organic species present in the electrolyte. Typically the power density is on the order of dozens to hundreds of $\mu W\,cm^{-2}$. Moreover the first example of a self-powered photo-sensor for glucose was presented here.

Bibliography

[1] Heller, A. *Phys. Chem. Chem. Phys.* **6**(2), 209 (2004). vi, 22, 27

[2] Zloczewska, A., Jönsson-Niedziolka, M., Rogalski, J., and Opallo, M. *Electrochim. Acta* **56**(11), 3947–3953 (2011). vii

[3] Urban, J., Zloczewska, A., Stryczniewicz, W., and Jönsson-Niedziolka, M. *Electrochem. Commun.* **34**, 94–97 (2013). vii

[4] Zloczewska, A. and Jönsson-Niedziolka, M. *J. Pow. Sources* **228**(0), 104–111 (2013). vii

[5] Zhao, X., Liu, Y., Inoue, S., Jones, R. O., and Ando, Y. *Phys. Rev. Lett.* **92**, 125502 (2004). 5

[6] Wang, X., Li, Q., Xie, J., Jin, Z., Wang, J., Li, Y., Jiang, K., and Fan, S. *Nano Lett.* **9**(9), 3137–3141 (2009). 5

[7] Dittmer, S., *Development of a method for highly localized growth of carbon nanotubes*, PhD thesis, Chalmers University of Technology (2008). 5, 12, 116, 117, 118

[8] Hodge, S. A., Bayazit, M. K., Coleman, S., and Hodge, S. A. *Chem. Soc. Rev.* **41**(12), 4409–4429 (2012). 6, 7

[9] Ando, Y. *J. Nanosci. Nanotechnol.* **10**(6), 3726–3738 (2010). 6, 9

[10] Iijima, S. *Nature* **318**, 56–58 (1991). 6, 12

[11] Endo, M., Koyama, T., and Hishiyama, Y. *Jpn. J. Appl. Phys.* **15**(11), 2073–2076 (1976). 6

[12] Oberlin, A., Endo, M., and Koyama, T. *Carbon* **14**(2), 133–135 (1976). 6

[13] Oberlin, A., Endo, M., and Koyama, T. *J. Cryst. Growth* **32**(3), 335 – 349 (1976). 6

[14] Radushkevich, L. V. and Lukyanovich, V. M. *Zhurnal Fizicheskoi Khimii* **26**, 88–95 (1952). 6

[15] Monthioux, M. and Kuznetsov, V. L. *Carbon* **44**, 1621–1623 (2006). 6

[16] White, C. T. and Todorov, T. N. *Nature* **393**, 240–242 (1998). 7

[17] Frank, S., Philippe Poncharal, P., Wang, Z. L., and de Heer, W. A. *Science* **280**(5370), 1744–1746 (1998). 7

[18] Dresselhaus, M. S., Dresselhaus, G., Charlier, J. C., and Hernández, E. *Phil. Trans. R. Soc. A* **362**(1823), 2065–98 (2004). 7

[19] Liang, W., Bockrath, M., Bozovic, D., Hafner, J. H., Tinkham, M., and Park, H. *Nature* **411**(6838), 665–9 (2001). 7

[20] Javey, A., Guo, J., Wang, Q., Lundstrom, M., and Dai, H. *Nature* **424**, 654–657 (2003). 7

[21] Park, S., Vosguerichian, M., and Bao, Z. *Nanosc.* **5**(5), 1727–52 (2013). 7

[22] Endo, M., Hayashi, T., Kim, Y. A., Terrones, M., and Dresselhaus, M. S. *Phil. Trans. R. Soc. A* **362**(1823), 2223–38 (2004).

[23] Brennan, L., Byrne, M. T., Bari, M., and Gun'ko, Y. K. *Adv. Energy Mater.* **1**(4), 472–485 (2011).

[24] Nanot, S., Hároz, E. H., Kim, J.-H., Hauge, R. H., and Kono, J. *Adv. Mater.* **24**(36), 4977–94 (2012).

[25] de Jonge, N. and Bonard, J.-M. *Phil. Trans. R. Soc. A* **362**(1823), 2239–66 (2004).

[26] Takahashi, T., Takei, K., Gillies, A. G., Fearing, R. S., and Javey, A. *Nano letters* **11**(12), 5408–13 (2011).

[27] Hwang, J.-Y., Shin, U. S., Jang, W.-C., Hyun, J. K., Wall, I. B., and Kim, H.-W. *Nanosc.* **5**(2), 487–97 (2013).

[28] Wang, C., Takei, K., Takahashi, T., and Javey, A. *Chem. Soc. Rev.* **42**(7), 2592–609 (2013).

[29] Pop, E., Mann, D., Wang, Q., Goodson, K., and Dai, H. *Nano Lett.* **6**(1), 96–100 (2006).

[30] Lu, J. P. *Phys. Rev. Lett.* **79**, 1297–1300 (1997).

[31] Hurt, R. H., Monthioux, M., and Kane, A. *Carbon* **44**(6), 1028–1033 (2006).

[32] Zhao, Y., Xing, G., and Chai, Z. *Nat. Nanotechnol.* **3**(4), 191–2 (2008).

[33] Zhao, X. and Liu, R. *Environ. Int.* **40**, 244–55 (2012).

[34] Poland, C. A., Duffin, R., Kinloch, I., Maynard, A., Wallace, W. A. H., Seaton, A., Stone, V., Brown, S., Macnee, W., and Donaldson, K. *Nat. Nanotechnol.* **3**(7), 423–8 (2008).

[35] Boczkowski, J. and Lanone, S. *Adv. Drug Delivery Rev.* **64**(15), 1694–9 (2012).

[36] Krätschmer, W., Lamb, L. D., Fostiropoulos, K., and Huffman, D. R. *Nature* **347**, 354 (1990).

[37] Kroto, H. W., Heath, J. R., O'Brien, S. C., Curl, R. F., and Smalley, R. E. *Nature* **318**, 162–163 (1985).

[38] Iijima, S. and Ichihashi, T. *Nature* **363**(6430), 603–605 (1993).

[39] Bethune, D. S., Kiang, C. H., de Vries, M. S., Gorman, G., Savoy, R., Vazquez, J., and Beyers, R. *Nature* **363**(6430), 605–607 (1993).

[40] Awasthi, K., Srivastava, A., and Srivastava, O. N. *J. Nanosci. Nanotechnol.* **5**(10), 1616–1636 (2005).

[41] Rodríguez-Manzo, J. a., Terrones, M., Terrones, H., Kroto, H. W., Sun, L., and Banhart, F. *Nat. Nanotechnol.* **2**(5), 307–11 (2007).

[42] Ohkohchi, M., Zhao, X., Wang, M., and Ando, Y. *Fullerene Sci. and Techn.* **4**(5), 977–988 (1996).

[43] Ando, Y., Zhao, X., Hirahara, K., Suenaga, K., Bandow, S., and Iijima, S. *Chem. Phys. Lett.* **323**, 580–585 (2000).

[44] Guo, T., Nikolaev, P., Thess, A., Colbert, D. T., and Smalley, R. E. *Chem. Phys. Lett.* **243**, 49–54 (1995).

[45] Thess, A., Lee, R., Nikolaev, P., Dai, H., Petit, P., Robert, J., Xu, C., Lee, Y. H., Kim, S. G., Rinzler, A. G., Colbert, D. T., Scuseria, G. E., Tománek, D., Fischer, J. E., and Smalley, R. E. *Science* **273**(5274), 483–487 (1996).

[46] Nessim, G. D. *Nanosc.* **2**(8), 1306–23 (2010).

[47] Rao, C. N. R., Sen, R., Satishkumar, B. C., and Govindaraj, A. *Chem. Commun.* , 1525–1526 (1998).

[48] Bonard, J.-M., Chauvin, P., and Klinke, C. *Nano Lett.* **2**, 665–667 (2002).

[49] Hofmann, S., Csányi, G., Ferrari, A. C., Payne, M. C., and Robertson, J. *Phys. Rev. Lett.* **95**, 036101 (2005).

[50] Jönsson, M., *Investigations of Plasma-Enhanced CVD Growth of Carbon Nanotubes and Potential Applications*, PhD thesis, Department of Physics, Göteborg University (2007).

[51] Lim, S. H., Luo, Z., Shen, Z., and Lin, J. *Nanosc. Res. Lett.* **5**(9), 1377–1386 (2010).

[52] Lee, S., Choi, S., Park, K. H., Chae, K. W., Cho, J. B., Ahn, Y., Park, J.-Y., and Koh, K. H. *Thin Solid Films* **516**(5), 700–705 (2008).

[53] Windle, A., "Introduction to poster session A: Synthesis," (2006). Slide for talk available at: http://nanotube.msu.edu/nt06/presentations/NT06S-Windle.pdf.

[54] Hata, K., Futaba, D. N., Mizuno, K., Namai, T., Yumura, M., and Iijima, S. *Science* **306**(5700), 1362–1364 (2004).

[55] Duesberg, G., Graham, A., Kreupl, F., Liebau, M., Seidel, R., Unger, E., and Hoenlein, W. *Diamond and Related Materials* **13**(2), 354–361 (2004).

[56] Chen, G. Y., Jensen, B., Stolojan, V., and Silva, S. R. P. *Carbon* **49**(1), 280–285 (2011).

[57] Ren, Z. F., Huang, Z. P., Xu, J. W., Wang, J. H., Bush, P., Siegal, M. P., and Provencio, P. N. *Science* **282**(5391), 1105–1107 (1998).

[58] Englander, O., Christensen, D., and Lin, L. *Appl. Phys. Lett.* **82**(26), 4797 (2003).

[59] Jungen, A., Stampfer, C., Tonteling, M., Schiesser, S., Sarangi, D., and Wierold, C., "Localised and cmos compatible growth of carbon nanotubes," in [*The 13th International Conference on Solid-State Sensors, Actuators and Microsystems*],

[60] Hart, A. J., van Laake, L., and Slocum, A. H. *Small* **3**(5), 772–7 (2007).

[61] Sunden, E. O., Wright, T. L., Lee, J., King, W. P., and Graham, S. *Appl. Phys. Lett.* **88**(3), 033107–1–033107–3 (2006).

[62] Sosnowchik, B. D., Lin, L., and Englander, O. *J. Appl. Phys.* **107**(5), 051101–051101–14 (2010).

[63] Weis, J. E., *Carbon nanotubes: in situ studies of growth and electromechanical properties*, PhD thesis University of Edinburgh (2011).

[64] Lubej, M. and Plazl, I. *Chem. Biochem. Eng. Q.* **26**(3), 277–284 (2012).

[65] Wagner, R. S. and Ellis, W. C. *Appl. Phys. Lett.* **4**(5), 89–90 (1964).

[66] Jiang, K., Feng, C., Liu, K., and Fan, S. *J. Nanosci, Nanotechnol.* **7**(4), 1494–1504 (2007).

[67] Yaropolov, A. I., Varfolomeev, S. D., and Berezin, I. V. *FEBS Lett.* **71**(2), 306–8 (1976).

[68] Hill, H. A. O. and Higgins, I. J. *Phil. Trans. R. Soc. Lond. A* **302**(1468), 267–273 (1981).

[69] Karyakin, A. A. *Bioelectrochem.* **88**, 70–5 (2012).

[70] Minteer, S. D. *Top. Catal.* **55**(16-18), 1157–1161 (2012).

[71] Aston, W. J. and Turner, A. P. F. *Genet. Eng. Rev.* **1**, 89–120 (1984).

[72] Moehlenbrock, M. J. and Minteer, S. D. *Chem. Soc. Rev.* **37**(6), 1188–1196 (2008).

[73] Kannan, A. M., Renugopalakrishnan, V., Filipek, S., Li, P., Audette, G. F., and Munukutla, L. *J. Nanosci. Nanotechnol.* **9**(3), 1665–1678 (2009).

[74] Brito, P. and Turner, A. P. F. *Electroanal.* **22**(7-8), 732–743 (2010).

[75] Freguia, S., Virdis, B., Harnisch, F., and Keller, J. *Electrochim. Acta* **82**, 165–174 (2012).

[76] Kano, K. and Ikeda, T. *Analytical Sciences* **16**(10), 1013–1021 (2000).

[77] Willner, I. and Katz, E. *Angew. Chem. Int. Ed.* **39**(7), 1180–1218 (2000).

[78] Habermüller, K., Mosbach, M., and Schuhmann, W. *Fresen. J Anal. Chem.* **366**(6-7), 560–568 (2000).

[79] Bilewicz, R. and Opallo, M., [*Fuel Cell Science: Theory, Fundamentals, and Biocatalysis*], ch. 5 Biocathodes for Dioxygen Reduction in Biofuel Cells, John Wiley & Sons, Ltd. (2011).

[80] Falk, M., Blum, Z., and Shleev, S. *Electrochim. Acta* **82**, 191–202 (2012).

[81] Cracknell, J. A., McNamara, T. P., Lowe, E. D., and Blanford, C. F. *Dalton Trans.* **40**(25), 6668–75 (2011).

[82] Solomon, E. I., Sundaram, U. M., and Machonkin, T. *Chem. Rev.* **96**(7), 2563–2606 (1996).

[83] Rodríguez Couto, S. and Toca Herrera, J. L. *Biotech. Adv.* **24**(5), 500–13 (2006).

[84] Soukharev, V., Mano, N., and Heller, A. *J. Am. Chem. Soc.* **126**(27), 8368–8369 (2004).

[85] Giardina, P., Faraco, V., Pezzella, C., Piscitelli, A., Vanhulle, S., and Sannia, G. *Cell. Mol. Life Sci.* **67**(3), 369–85 (2010).

[86] Guckert, J. A., Lowery, M. D., and Solomon, E. I. *J. Am. Chem. Soc.* **117**(10), 2817–2844 (1995).

[87] Solomon, E. I., Augustine, A. J., and Yoon, J. *Dalton Trans.* **0**, 3921–3932 (2008).

[88] Berezin, I. V., Bogdanovskaya, V. A., Varfolomeev, S. D., Tarasevich, M. R., and Yaropolov, A. I. *Dokl. Akad. Nauk SSSR* **240**, 615–618 (1978).

[89] Piontek, K., Antorini, M., and Choinowski, T. *J. Biol. Chem.* **277**(40), 37663–9 (2002).

[90] Christenson, A., Dimcheva, N., Ferapontova, E. E., Gorton, L., Ruzgas, T., Stoica, L., Shleev, S., Yaropolov, A. I., Haltrich, D., Thorneley, R. N. F., and Aust, S. D. *Electroanal.* **16**(1314), 1074–1092 (2004).

[91] Shleev, S., Christenson, A., Serezhenkov, V., Burbaev, D., Yaropolov, A., Gorton, L., and Ruzgas, T. *Biochem. J.* **385**, 745–54 (2005).

[92] Reinhammar, B. R. T. *Biochim. Biophys. Acta* **275**(2), 245 – 259 (1972).

[93] Shleev, S., Klis, M., Wang, Y., Rogalski, J., Bilewicz, R., and Gorton, L. *Electroanal.* **19**(10), 1039–1047 (2007).

[94] Schneider, P., Caspersen, M. B., Mondorf, K., Halkier, T., Skov, L. K., Østergaard, P. R., Brown, K. M., Brown, S. H., and Xu, F. *Enzyme Microb. Technol.* **25**(6), 502–508 (1999).

[95] Xu, F., Shin, W., Brown, S. H., Wahleithner, J. A., Sundaram, U. M., and Solomon, E. I. *Biochim. Biophys. Acta.* **1292**(2), 303–311 (1996).

[96] dos Santos, L., Climent, V., Blanford, C. F., and Armstrong, F. A. *Phys. Chem. Chem. Phys.* **12**(42), 13962–74 (2010).

[97] Christenson, A., Shleev, S., Mano, N., Heller, A., and Gorton, L. *Bioch. Biophys. Acta* **1757**(12), 1634–41 (2006).

[98] Page, C. C., Moser, C. C., Chen, X., and Dutton, P. L. *Nature* **402**(6757), 47–52 (1999).

[99] Ramírez, P., Mano, N., Andreu, R., Ruzgas, T., Heller, A., Gorton, L., and Shleev, S. *Biochim. Biophys. Acta* **1777**(10), 1364–9 (2008).

[100] Bankar, S. B., Bule, M. V., Singhal, R. S., and Ananthanarayan, L. *Biotechnol. Adv.* **27**(4), 489–501 (2009).

[101] Pluschkell, S., Hellmuth, K., and Rinas, U. *Biotechnol. Bioeng.* **51**(2), 215–220 (1996).

[102] Steiner, M.-S., Duerkop, A., and Wolfbeis, O. S. *Chem. Soc. Rev.* **40**(9), 4805–39 (2011).

[103] Heller, A. and Feldman, B. *Chem. Rev.* **108**(7), 2482–505 (2008).

[104] Boontim, N., Yoshimune, K., Lumyong, S., and Moriguchi, M. *Ann. Microbiol.* **54**(4), 481–492 (2004).

[105] John, J., Crennell, S. J., Hough, D. W., Danson, M. J., and Taylor, G. L. *Structure* **2**(5), 385 – 393 (1994).

[106] Matsushita, K., Ohno, Y., Shinagawa, E., Adachi, O., and Ameyam, M. *Agric. Biol. Chem.* **44**(7), 1505–1512 (1980).

[107] Pauly, H. E. and Pfleiderer, G. *Hoppe. Seylers Z Physiol. Chem.* **356**(10), 1613–1624 (1975).

[108] Sakurai, T. and Kataoka, K. *Chem Rec* **7**(4), 220–9 (2007).

[109] http://www.sony.net.

[110] http://en.wikipedia.org/wiki/Biobattery.

[111] Potter, M. C. *Proc. R. Soc. B, Biol. Sci.* (571).

[112] Yahiro, A. T., Lee, S. M., and Kimble, D. O. *Biochim. Biophys. Acta* **88**(2), 375 – 383 (1964).

[113] Schaetzle, O., Barrière, F., and Schröder, U. *Energy Environ. Sci.* **2**(1), 96 (2009).

[114] Fischback, M. B., Youn, J. K., Zhao, X., Wang, P., Park, H. G., Chang, H. N., Kim, J., and Ha, S. *Electroanal.* **18**(19-20), 2016–2022 (2006).

[115] Kim, J., Jia, H., and Wang, P. *Biotechnol. Adv.* **24**(3), 296–308 (2006).

[116] Gianfreda, L. and Scarfi, M. R. *Mol. Cell. Biochem.* (2), 97–128.

[117] Minteer, S. D., Atanassov, P., Luckarift, H. R., and Johnson, G. R. *Mater. Today* **15**(4), 166–173 (2012).

[118] Kim, J., Grate, J. W., and Wang, P. *Chem. Eng. Sci.* **61**(3), 1017–1026 (2006).

[119] Cinquin, P., Gondran, C., Giroud, F., Mazabrard, S., Pellissier, A., Boucher, F., Alcaraz, J.-P., Gorgy, K., Lenouvel, F., Mathé, S., Porcu, P., and Cosnier, S. *PLoS ONE* **5**, e10476 (2010).

[120] Ohm, O.-J. and Danilovic, D. *Pacing and Clin. Electrophysiol.* **20**(1), 2–9 (1997).

[121] Miyake, T., Haneda, K., Nagai, N., Yatagawa, Y., Onami, H., Yoshino, S., Abe, T., and Nishizawa, M. *Energy Environ. Sci.* **4**(12), 5008–5012 (2011).

[122] Halámková, L., Halámek, J., Bocharova, V., Szczupak, A., Alfonta, L., and Katz, E. *J. Am. Chem. Soc.* **134**(11), 5040–5043 (2012).

[123] Szczupak, A., Halamek, J., Halamkova, L., Bocharova, V., Alfonta, L., and Katz, E. *Energy Environ. Sci.* **5**, 8891–8895 (2012).

[124] MacVittie, K., Halamek, J., Halamkova, L., Southcott, M., Jemison, W. D., Lobel, R., and Katz, E. *Energy Environ. Sci.* **6**, 81–86 (2013).

[125] Rasmussen, M., Ritzmann, R. E., Lee, I., Pollack, A. J., and Scherson, D. *J. Am. Chem. Soc.* **134**(3), 1458–1460 (2012).

[126] Jia, W., Valdés-Ramírez, G., Bandodkar, A. J., Windmiller, J. R., and Wang, J. *Angew. Chem. Int. Ed.* **52**(28), 7233–7236 (2013).

[127] Sakai, H., Nakagawa, T., Tokita, Y., Hatazawa, T., Ikeda, T., Tsujimura, S., and Kano, K. *Energy Environ. Sci.* **2**, 133–138 (2009).

[128] Wingard, L. B., Shaw, C. H., and Castner, J. *Enzyme Microb. Technol.* **3**(4), 137–142 (1982).

[129] Palmore, G. T. R. and M., W. G., [*Enzymatic Conversion of Biomass for Fuels Production*], ch. 14 Microbial and Enzymatic Biofuel Cells, 271–290, American Chemical Society (1994).

[130] Bullen, R. A., Arnot, T. C., Lakeman, J. B., and Walsh, F. C. *Biosens. Bioelectron.* **21**(11), 2015–45 (2006).

[131] Thevenot, D. R., Tóth, K., Durst, R. A., and Wilson, G. S. *Pure Appl. Chem.* **71**(12), 2333–2348 (1999).

[132] Arechederra, R. L. and Minteer, S. D. *Anal. Bioanal. Chem* **400**(6), 1605–11 (2011).

[133] Katz, E., Bückmann, A. F., and Willner, I. *J. Am. Chem. Soc.* **123**(43), 10752–3 (2001).

[134] Willner, I. and Katz, E., "Self-powered biosensor ." Patent Application in Israel (2001).

[135] Willner, I. and Katz, E., "Self-powered biosensor ." Patent Application in U.S.A. (2002).

[136] Germain, M. N., Arechederra, R. L., and Minteer, S. D. *J. Am. Chem. Soc.* **130**(46), 15272–3 (2008).

[137] Hanashi, T., Yamazaki, T., Tsugawa, W., Ferri, S., Nakayama, D., Tomiyama, M., Ikebukuro, K., and Sode, K. *Biosens. Bioelectron.* **24**(7), 1837–1842 (2009).

[138] Miyake, T., Yoshino, S., Yamada, T., Hata, K., and Nishizawa, M. *J. Am. Chem. Soc.* **133**(13), 5129–34 (2011).

[139] Deng, L., Chen, C., Zhou, M., Guo, S., Wang, E., and Dong, S. *Anal. Chem.* **82**(10), 4283–7 (2010).

[140] Liu, Z., Cho, B., Ouyang, T., and Feldman, B. *Anal. Chem.* (7), 3403–9 (2012).

[141] Pardo-Yissar, V., Katz, E., Wasserman, J., and Willner, I. *J. Am. Chem. Soc.* **125**(3), 622–3 (2003).

[142] Wen, D., Deng, L., Guo, S., and Dong, S. *Anal. Chem.* **83**(10), 3968–72 (2011).

[143] Meredith, M. T. and Minteer, S. D. *Anal. Chem.* **83**(13), 5436–41 (2011).

[144] Zhang, L., Zhou, M., and Dong, S. *Anal. Chem.* **84**(23), 10345–9 (2012).

[145] Rasmussen, M. and Minteer, S. D. *Anal. Methods* **5**(5), 1140–44 (2013).

[146] Adams, R. *Anal. Chem.* **30**(9), 1576–1576 (1958).

[147] Hawley, M. D., Tatawawadi, S. V., Piekarski, S., and Adams, R. N. *J. Am. Chem. Soc.* **89**(2), 447–450 (1967).

[148] Dumitrescu, I., Unwin, P. R., and Macpherson, J. V. *Chem. Commun.* **7345**(45), 6886–901 (2009).

[149] McCreery, R. L. *Chem. Rev.* **108**(7), 2646–87 (2008).

[150] Britto, P. J., Santhanam, K. S. V., and Ajayan, P. M. *Bioelectrochem. Bioenerg.* **41**(1), 121–25 (1996).

[151] Musameh, M., Wang, J., Merkoci, A., and Lin, Y. *Electrochem. Commun.* **4**(10), 743–746 (2002).

[152] Gooding, J. J. *Electrochim. Acta* **50**(15), 3049–3060 (2005).

[153] Gong, K., Yan, Y., Zhang, M., Su, L., Xiong, S., and Mao, L. *Anal. Sci.: Inte. J. Jap. Soc. Anal. Chem.* **21**(12), 1383–93 (2005).

[154] Luo, H., Shi, Z., Li, N., Gu, Z., and Zhuang, Q. *Anal. Chem.* **73**(5), 915–920 (2001).

[155] Guiseppi-Elie, A., Lei, C., and Baughman, R. H. *Nanotechnology* **13**(5), 559 (2002).

[156] Wang, J., Li, M., Shi, Z., Li, N., and Gu, Z. *Electroanal.* **14**(3), 225–230 (2002).

[157] Wang, J., Musameh, M., and Lin, Y. *J. Am. Chem. Soc.* **125**(9), 2408–2409 (2003).

[158] Wu, K., Hu, S., Fei, J., and Bai, W. *Anal. Chim. Acta* **489**(2), 215–221 (2003).

[159] Wang, J. and Musameh, M. *Anal. Chem.* **75**(9), 2075–2079 (2003).

[160] Baughman, R. H., Cui, C., Zakhidov, A. A., Iqbal, Z., Barisci, J. N., Spinks, G. M., Wallace, G. G., Mazzoldi, A., De Rossi, D., Rinzler, A. G., Jaschinski, O., Roth, S., and Kertesz, M. *Science* **284**(5418), 1340–1344 (1999).

[161] Shaffer, M. S. P. and Windle, A. H. *Adv. Mater.* **11**(11), 937–941 (1999).

[162] Gavalas, V. G., Andrews, R., Bhattacharyya, D., and Bachas, L. G. *Nano Lett.* **1**(12), 719–721 (2001).

[163] Nakashima, N., Kobae, H., Sagara, T., and Murakami, H. *Chem. Phys. Chem.* **3**(5), 456–458 (2002).

[164] Luo, X.-L., Xu, J.-J., Wang, J.-L., and Chen, H.-Y. *Chem. Commun.* , 2169–2171 (2005).

[165] Girishkumar, G., Vinodgopal, K., and Kamat, P. V. *J. Phys. Chem. B* **108**(52), 19960–19966 (2004).

[166] Liu, Z., Shen, Z., Zhu, T., Hou, S., Ying, L., Shi, Z., and Gu, Z. *Langmuir* **16**(8), 3569–3573 (2000).

[167] Martin-Fernandez, I., Gabriel, G., Rius, G., Villa, R., Perez-Murano, F., Lora-Tamayo, E., and Godignon, P. *Microelectron. Eng.* **86**(4-6), 806–808 (2009).

[168] Zhu, Z. G., Garcia-Gancedo, L., Chen, C., Zhu, X. R., Xie, H. Q., Flewitt, A. J., and Milne, W. I. *Sensor. Actuat. B Chem.* **178**, 586–592 (2013).

[169] Khavrus, V. O., Weiser, M., Fritsch, M., Ummethala, R., Salvaggio, M. G., Schneider, M., Kusnezoff, M., and Leonhardt, A. *Chem. Vap. Dep.* **18**(1-3), 53–60 (2012).

[170] Lawrence, N. S., Deo, R. P., and Wang, J. *Anal. Chim. Acta* **517**(1-2), 131–137 (2004).

[171] Salimi, A., Hallaj, R., and Khayatian, G.-R. *Electroanal.* **17**(10), 873–879 (2005).

[172] Deo, R. P. and Wang, J. *Electrochem. Commun.* **6**(3), 284–287 (2004).

[173] Wu, F.-H., Zhao, G.-C., and Wei, X.-W. *Electrochem. Commun.* **4**(9), 690–694 (2002).

[174] Wang, J. and Musameh, M. *Anal. Chim. Acta* **511**(1), 33–36 (2004).

[175] Ye, J.-S., Wen, Y., De Zhang, W., Gan, L., Xu, G., and Sheu, F.-S. *Electroanal.* **15**(21), 1693–1698 (2003).

[176] Kachoosangi, R. T., Wildgoose, G. G., and Compton, R. G. *Analyst* **133**(7), 888–95 (2008).

[177] Bertoncello, P., Edgeworth, J. P., Macpherson, J. V., and Unwin, P. R. *J. Am. Chem. Soc.* **129**(36), 10982–3 (2007).

[178] Sansuk, S., Bitziou, E., Joseph, M. B., Covington, J. A., Boutelle, M. G., Unwin, P. R., and Macpherson, J. V. *Anal. Chem.* **85**(1), 163–9 (2013).

[179] Wang, J. *Electroanal.* **17**(1), 7–14 (2005).

[180] Banks, C. E. and Compton, R. G. *Analyst* **131**(1), 15–21 (2006).

[181] Banks, C. E., Crossley, A., Salter, C., Wilkins, S. J., and Compton, R. G. *Angew. Chem. Int. Ed.* **45**(16), 2533–2537 (2006).

[182] Šljukić, B., Banks, C. E., and Compton, R. G. *Nano Lett.* **6**(7), 1556–1558 (2006).

[183] Dai, X., Wildgoose, G. G., and Compton, R. G. *Analyst* **131**, 901–906 (2006).

[184] Pumera, M. *Langmuir* **23**(11), 6453–6458 (2007).

[185] Pumera, M. and Iwai, H. *J. Phys. Chem. C* **113**(11), 4401–4405 (2009).

[186] Dumitrescu, I., Wilson, N. R., and Macpherson, J. V. *J. Phys. Chem. C* **111**(35), 12944–12953 (2007).

[187] Pumera, M., Sasaki, T., and Iwai, H. *Chem. Asian J.* **3**(12), 2046–55 (2008).

[188] Moore, R. R., Banks, C. E., and Compton, R. G. *Anal. Chem.* **76**(10), 2677–2682 (2004).

[189] Banks, C. E., Moore, R. R., Davies, T. J., and Compton, R. G. *Chem. Commun.* , 1804–1805 (2004).

[190] Banks, C. E., Davies, T. J., Wildgoose, G. G., and Compton, R. G. *Chem. Commun.* (7), 829–41 (2005).

[191] Banks, C. E. and Compton, R. G. *Analyst* **130**, 1232–1239 (2005).

[192] Gong, K., Chakrabarti, S., and Dai, L. *Angew. Chem. Int. Ed.* **47**(29), 5446–5450 (2008).

[193] Heller, I., Kong, J., Heering, H. A., Williams, K. A., Lemay, S. G., and Dekker, C. *Nano Lett.* **5**(1), 137–142 (2005).

[194] Holloway, A. F., Toghill, K., Wildgoose, G. G., Compton, R. G., Ward, M. A. H., Tobias, G., Llewellyn, S. A., Ballesteros, B., Green, M. L. H., and Crossley, A. *J. Phys. Chem. C* **112**(28), 10389–10397 (2008).

[195] Chou, A., Bocking, T., Singh, N. K., and Gooding, J. J. *Chem. Commun.* , 842–844 (2005).

[196] Ebejer, N., Schnippering, M., Colburn, A. W., Edwards, M. A., and Unwin, P. R. *Anal. Chem.* **82**(22), 9141–9145 (2010).

[197] Lai, S. C. S., Dudin, P. V., Macpherson, J. V., and Unwin, P. R. *J. Am. Chem. Soc.* **133**(28), 10744–10747 (2011).

[198] Lai, S. C. S., Patel, A. N., McKelvey, K., and Unwin, P. R. *Angew. Chem. Int. Ed.* **51**(22), 5405–8 (2012).

[199] Miller, T. S., Ebejer, N., Güell, A. G., Macpherson, J. V., and Unwin, P. R. *Chem. Commun.* **48**(60), 7435–7 (2012).

[200] Ji, X., Kadara, R. O., Krussma, J., Chen, Q., and Banks, C. E. *Electroanal.* **22**(1), 7–19 (2010).

[201] Streeter, I., Wildgoose, G. G., Shao, L., and Compton, R. G. *Sens. Actuators, B* **133**(2), 462–466 (2008).

[202] Gao, C., Guo, Z., Liu, J.-H., and Huang, X.-J. *Nanosc.* **4**(6), 1948–63 (2012).

[203] Guo, L., Yin, N., Nie, D., Fu, F., and Chen, G. *Chem. Commun.* **47**, 10665–10667 (2011).

[204] Miyake, Y., Togashi, H., Tashiro, M., Yamaguchi, H., Oda, S., Kudo, M., Tanaka, Y., Kondo, Y., Sawa, R., Fujimoto, T., Machinami, T., and Ono, A. **128**(7), 2172–2173 (2006).

[205] Katz, E. and Willner, I. *Chem. Phys. Chem.* **5**(8), 1085–1104 (2004).

[206] Moulton, S. E., M. A. I. W. G. G. *Sens. Lett.* **3**(3), 183–193 (2005).

[207] Hu, X. and Dong, S. *J. Mater. Chem.* **18**, 1279–1295 (2008).

[208] Ali, S. R., Parajuli, R. R., Balogun, Y., Ma, Y., and He, H. *Sens.* **8**(12), 8423–8452 (2008).

[209] Koh, J., Kim, B., Hong, S., Lim, H., and Choi, H. C. *J. Mater. Sci. Technol.* **24**(4), 578–588 (2008).

[210] Wang, J. and Lin, Y. *TrAC Trends Anal. Chem.* **27**(7), 619–626 (2008).

[211] Guo, G., Wu, L., Wang, C., and Fang, J. *Prog. Chem.* **21**(10), 2084–2092 (2009).

[212] Meng, L., Fu, C., and Lu, Q. *Prog. Nat. Sci.* **19**(7), 801–810 (2009).

[213] Santiago-Rodriguez, L., Sanchez-Pomales, G., and Cabrera, C. R. *Israel J. Chem.* **50**(3), 277–290 (2010).

[214] Zhang, W.-D., Xu, B., and Jiang, L.-C. *J. Mater. Chem.* **20**, 6383–6391 (2010).

[215] Gavalas, V. G., Andrews, R., Bhattacharyya, D., and Bachas, L. G. *Nano Lett.* **1**(12), 719–721 (2001).

[216] Walcarius, A., Mandler, D., Cox, J. A., Collinson, M., and Lev, O. *J. Mater. Chem.* **15**(35-36), 3663–3689 (2005).

[217] Gooding, J. J., Wibowo, R., Liu, J., Yang, W., Losic, D., Orbons, S., Mearns, F. J., Shapter, J. G., and Hibbert, D. B. *J. Am. Chem. Soc.* **125**(30), 9006–9007 (2003).

[218] Yu, X., Chattopadhyay, D., Galeska, I., Papadimitrakopoulos, F., and Rusling, J. F. *Electrochem. Commun.* **5**(5), 408–411 (2003).

[219] Patolsky, F., Weizmann, Y., and Willner, I. *Angew. Chem. Int. Ed.* **43**(16), 2113–2117 (2004).

[220] Wang, J., Kawde, A.-N., and Musameh, M. *Analyst* **128**, 912–916 (2003).

[221] Vashist, S. K., Zheng, D., Al-Rubeaan, K., Luong, J. H. T., and Sheu, F.-S. *Biotechnology Advances* **29**(2), 169–188 (2011).

[222] Kim, J. H., Jin, J.-H., Lee, J.-Y., Park, E. J., and Min, N. K. *Bioconj. Chem.* **23**(10), 2078–2086 (2012).

[223] Tasca, F., Harreither, W., Ludwig, R., Gooding, J. J., and Gorton, L. *Anal. Chem.* **83**(8), 3042–9 (2011).

[224] Bahr, J. L. and Tour, J. M. *Chem. Mater.* **13**(11), 3823–3824 (2001).

[225] Avnir, D., Braun, S., Lev, O., and Ottolenghi, M. *Chem. Mater.* **6**(10), 1605–1614 (1994).

[226] Frenkel-Mullerad, H. and Avnir, D. *J. Am. Chem. Soc.* **127**(22), 8077–8081 (2005).

[227] Dickey, F. H. *J. Phys. Chem.* **59**(8), 695–707 (1955).

[228] Johnson, P. and Whateley, T. L. *J. Colloid Interface Sci.* **37**(3), 557–563 (1971).

[229] Gill, I. *Chem. Mater.* **13**(10), 3404–3421 (2001).

[230] Glad, M., Norrlöw, O., Sellergren, B., Siegbahn, N., and Mosbach, K. *J. Chromatography A* **347**(0), 11–23 (1985).

[231] Gavalas, V. G., Law, S. A., Ball, J. Ch. andAndrews, R., and Bachas, L. G. *Analytical Biochemistry* **329**(2), 247 – 252 (2004).

[232] Salimi, A., Compton, R. G., and Hallaj, R. *Anal. Biochem.* **333**(1), 49–56 (2004).

[233] Jonsson, M., Szot, K., Niedziolka, J., Rogalski, J., Karnicka, K., Kulesza, P., and Opallo, M. *J. Nanosci. Nanotechnol.* **9**(4), 2346–2352 (2009).

[234] Lim, J., Cirigliano, N., Wang, J., and Dunn, B. *Phys. Chem. Chem. Phys.* **9**, 1809–1814 (2007).

[235] Wang, Z., Etienne, M., Pöller, S., Schuhmann, W., Kohring, G.-W., Mamane, V., and Walcarius, A. *Electroanal.* **24**(2), 376–385 (2012).

[236] Urbanová, V., Etienne, M., and Walcarius, A. *Electroanal.* **25**(1), 85–93 (2013).

[237] Mazurenko, I., Etienne, M., Tananaiko, O., Zaitsev, V., and Walcarius, A. *Electrochim. Acta* **83**, 359–366 (2012).

[238] Hou, S., Ou, Z., Chen, Q., and Wu, B. *Biosens. Bioelectron.* **33**(1), 44–49 (2012).

[239] Palmore, G. T. R. and Kim, H.-H. *J. Electroanal. Chem.* **464**(1), 110–117 (1999).

[240] Karnicka, K., Miecznikowski, K., Kowalewska, B., Skunik, M., Opallo, M., Rogalski, J., Schuhmann, W., and Kulesza, P. J. *Anal. Chem.* **80**(19), 7643–7648 (2008).

[241] Tan, Y., Xie, Q., Huang, J., Duan, W., Ma, M., and Yao, S. *Electroanal.* **20**(14), 1599–1606 (2008).

[242] Ivnitski, D., Artyushkova, K., Rincón, R. A., Atanassov, P., Luckarift, H. R., and Johnson, G. R. *Small* **4**(3), 357–64 (2008).

[243] Rowiński, P., Bilewicz, R., Stébé, M.-J., and Rogalska, E. *Anal. Chem.* **76**(2), 283–291 (2004).

[244] Nazaruk, E. and Bilewicz, R. *Bioelectrochem.* **71**(1), 8 – 14 (2007).

[245] Nazaruk, E., Smoliński, S., Swatko-Ossor, M., Ginalska, G., Fiedurek, J., Rogalski, J., and Bilewicz, R. *J. Power Sources* **183**(2), 533–538 (2008).

[246] K., S., Nazaruk, E., Rogalski, J., and Bilewicz, R. *Electrochimica Acta* **53**(11), 3983–3990 (2008).

[247] Nazaruk, E., Sadowska, K., Madrak, K., Biernat, J., Rogalski, J., and Bilewicz, R. *Electroanal.* **21**(3-5), 507–511.

[248] Nazaruk, E., Sadowska, K., Biernat, J. F., Rogalski, J., Ginalska, G., and Bilewicz, R. *Anal. Bioanal. Chem.* **398**(4), 1651–60 (2010).

[249] Liu, G. and Lin, Y. *Anal. Chem.* **78**(3), 835–843 (2006).

[250] Liu, G. D. and Lin, Y. H. *J. Nanosci. Nanotechnol.* **6**(4), 848–953 (2006).

[251] Wang, J., Liu, G., and Lin, Y. *Analyst* **131**, 477–483 (2006).

[252] Gao, F., Viry, L., Maugey, M., Poulin, P., and Mano, N. *Nature Commun.* **1**, 2 (2010).

[253] Zhao, H., Zhou, H. M., Zhang, J. X., Zheng, W., and Zheng, Y. F. *Biosens. Bioelectron.* **25**(2), 463–468 (2009).

[254] Zhang, M., Smith, A., and Gorski, W. *Anal. Chem.* **76**(17), 5045–5050 (2004).

[255] Hussein, L., Urban, G., and Krüger, M. *Phys. Chem. Chem. Phys.* **13**(13), 5831–9 (2011).

[256] Zebda, A., Gondran, C., Le Goff, A., Holzinger, M., Cinquin, P., and Cosnier, S. *Nature Commun.* **2**, 370 (2011).

[257] Jönsson-Niedziolka, M., Szot, K., Rogalski, J., and Opallo, M. *Electrochem. Commun.* **11**(5), 1042–1044 (2009).

[258] Jönsson-Niedziolka, M., Kaminska, A., and Opallo, M. *Electrochim. Acta* **55**(28), 8744–8750 (2010).

[259] Holzinger, M., Le Goff, A., and Cosnier, S. *Electrochim. Acta* **82**, 179–190 (2012).

[260] Roy, P., Berger, S., and Schmuki, P. *Angew. Chem. Int. Ed.* **50**(13), 2904–39 (2011).

[261] Fujishima, A. and Honda, K. *Nature* **238**(5358), 37–38 (1972).

[262] Kavan, L. *Chem. Rec.* .

[263] Kavan, L., Grätzel, M., Gilbert, S. E., Klemenz, C., and Scheel, H. J. *J. Am. Soc. Chem.* **118**(28), 6716–6723 (1996).

[264] Reyes-Coronado, D., Rodríguez-Gattorno, G., Espinosa-Pesqueira, M. E., Cab, C., de Coss, R., and Oskam, G. *Nanotechnol.* **19**(14), 145605–10 (2008).

[265] Wu, Z. Y., Ouvrard, G., Gressier, P., and Natoli, C. R. *Phys. Rev. B* **55**, 10382–10391 (1997).

[266] Asahi, R., Taga, Y., Mannstadt, W., and Freeman, A. J. *Phys. Rev. B* **61**, 7459–7465 (2000).

[267] Nowotny, J., [*Oxide Semiconductors for Solar Energy Conversion. Titanium dioxide*], CRC Press, Taylor & Francis Group (2012).

[268] Tang, H., Prasad, K., Sanjinès, R., Schmid, P. E., and Lévy, F. *J. Appl. Phys.* **75**(4), 2042 (1994).

[269] Forro, L., Chauvet, O., Emin, D., Zuppiroli, L., Berger, H., and Lévy, F. *J. Appl. Phys.* **75**(1), 633 (1994).

[270] Carp, O. *Prog. Solid State Ch.* **32**(1-2), 33–177 (2004).

[271] Nakata, K. and Fujishima, A. *J. Photochem. Photobiol. C: Photochem. Rev.* **13**(3), 169–189 (2012).

[272] Song, Y.-Y., Roy, P., Paramasivam, I., and Schmuki, P. *Angew. Chem. Int. Ed.* **49**(2), 351–4 (2010).

[273] Park, J., Bauer, S., von der Mark, K., and Schmuki, P. *Nano Lett.* **7**(6), 1686–1691 (2007).

[274] Lan, M.-Y., Liu, C.-P., Huang, H.-H., Chang, J.-K., and Lee, S.-W. *Nanosc. Res. Lett.* (1), 150 (2013).

[275] Macak, J. M., Tsuchiya, H., Ghicov, A., Yasuda, K., Hahn, R., Bauer, S., and Schmuki, P. *Curr. Opin. Solid State Mater. Sci.* **11**(1-2), 3–18 (2007).

[276] Xiao, P., Zhang, Y., Garcia, B. B., Sepehri, S., Liu, D., and Cao, G. *J. Nanosci. Nanotechnol.* **9**(4), 2426–2436 (2009).

[277] Lynch, R. P., Ghicov, A., and Schmuki, P. *J. Electrochem. Soc.* **157**(3), G76 (2010).

[278] Adachi, M., Murata, Y., Harada, M., and Yoshikawa, S. *Chem. Lett.* (8), 942–943 (2000).

[279] Chu, S.-Z., Inoue, S., Wada, K., Li, D., Haneda, H., and Awatsu, S. *J. Phys. Chem. B* **107**(27), 6586–6589 (2003).

[280] Varghese, O., Gong, D., Paulose, M., Ong, K. G., Dickey, E. C., and Grimes, C. A. *Adv. Mater.* **15**(7-8), 624–627 (2003).

[281] Mor, G. K., Carvalho, M. A., Varghese, O. K., Pishko, M. V., and Grimes, C. A. *J. Mater. Res.* **19**(2), 628–634 (2004).

[282] Paulose, M., Varghese, O. K., Mor, G. K., Grimes, C. A., and Ong, K. G. *Nanotechnol.* **17**(2), 398–402 (2006).

[283] Mor, G. K., Shankar, K., Paulose, M., Varghese, O. K., and Grimes, C. A. *Nano Lett.* **5**(1), 191–195 (2005).

[284] Varghese, O. K., Paulose, M., Shankar, K., Mor, G. K., and Grimes, C. A. *J. Nanosci. Nanotechnol.* **5**(7), 1158–1165 (2005).

[285] Uchida, S., Chiba, R., Tomiha, M., Masaki, N., and Shirai, M. *Electrochem.* **70**(6), 418–420 (2002).

[286] Adachi, M., Murata, Y., Okada, I., and Yoshikawa, S. *J. Electrochem. Soc.* **150**(8), G488–G493 (2003).

[287] Mor, G. K., Varghese, O. K., Paulose, M., Shankar, K., and Grimes, C. A. *Sol. Energ. Mat. Sol. C.* **90**(14), 2011–2075 (2006).

[288] Song, Y.-Y., Schmidt-Stein, F., Bauer, S., and Schmuki, P. *J. Am. Chem. Soc.* **131**(12), 4230–2 (2009).

[289] Quan, X., Yang, S., Ruan, X., and Zhao, H. *Environ. Sci. Technol.* **39**(10), 3770–5 (2005).

[290] Su, Z. and Zhou, W. *J. Mat. Chem.* (25), 8955.

[291] Hoyer, P. *Langmuir* **12**(6), 1411–1413 (1996).

[292] Lakshmi, B. B., Dorhout, P. K., and Martin, C. R. *Chem. Mater.* **9**(3), 857–862 (1997).

[293] Xia, Y., Yang, P., Sun, Y., Wu, Y., Mayers, B., Gates, B., Yin, Y., Kim, F., and Yan, H. *Adv. Mater.* **15**(5), 353–389 (2003).

[294] Zwilling, V., Darque-Ceretti, E., Boutry-Forveille, A., David, D., Perrin, M. Y., and Aucouturier, M. *Surf. Interface Anal.* **27**(7), 629–637 (1999).

[295] Gong, D., Grimes, C. A., Varghese, O. K., Hu, W., Singh, R. S., Chen, Z., and Dickey, E. C. *J. Mater. Res.* **16**(12), 3331–3334 (2001).

[296] Macak, J. M., Tsuchiya, H., Taveira, L., Aldabergerova, S., and Schmuki, P. *Angew. Chem. Int. Ed.* **44**(45), 7463–7465 (2005).

[297] Macak, J. M., Sirotna, K., and Schmuki, P. *Electrochim. Acta* **50**(18), 3679–3684 (2005).

[298] Macak, J. M., Tsuchiya, H., and Schmuki, P. *Angew. Chem. Int. Ed.* **44**(14), 2100–2102 (2005).

[299] Beranek, R., Hildebrand, H., and Schmuki, P. *Electrochem. Solid-State Lett.* **6**, B12–B14 (2003).

[300] Li, Y., Yu, X., and Yang, Q. *J. Sensors* , 1–19 (2009).

[301] Allam, N. K. and Grimes, C. A. *J. Phys. Chem. C* **111**(35), 13028–13032 (2007).

[302] Allam, N. K., Shankar, K., and Grimes, C. A. *J. Mater. Chem.* **18**(20), 2341–2348 (2008).

[303] Fujishima, A., Kikuchi, S., and Honda, K. *J. Chem. Soc. Jpn. Ind. Chem. Sect.* **72**, 108–113 (1969).

[304] Fujishima, A., Sakamoto, A., and Honda, K. *Seisan Kenkyu* **21**, 450–452 (1969).

[305] Fujishima, A. and Honda, K. *Bull. Chem. Soc. Jpn.* **44**, 1148–1150 (1971).

[306] Fujishima, A., Kohayakawa, K., and Honda, K. *J. Electrochem. Soc.* **122**(11), 1487 (1975).

[307] O'Regan, B. and Grätzel, M. *Nature* **353**(6346), 737–740 (1991).

[308] Kuchibhatla, V. N. T. S., Karakoti, A. S., Bera, D., and Seal, S. *Prog. Mater. Sci.* **52**(5), 699–913 (2007).

[309] van der Zanden, B. and Goossens, A. *J. Phys. Chem. B* **104**(30), 7171–7178 (2000).

[310] Li, Y., Hagen, J., Schaffrath, W., Otschik, P., and Haarer, D. *Sol. Energ. Mater. Solar Cells* **56**(2), 167–174 (1999).

[311] Berger, T., Monllor-Satoca, D., Jankulovska, M., Lana-Villarreal, T., and Gómez, R. *Chem Phys. Chem.* **13**(12), 2824–75 (2012).

[312] Kay, A. and Grätzel, M. *Sol. Energ. Mater. Solar Cells* **44**, 99–117 (1996).

[313] Tsoukleris, D. S., Arabatzis, I. M., Chatzivasiloglou, E., Kontos, A. I., Belessi, V., Bernard, M. C., and Falaras, P. *Sol. Energ.* **79**(4), 422–430 (2005).

[314] Mechiakh, R., Sedrine, N. B., Chtourou, R., and Bensaha, R. *Appl. Surf. Sci.* **257**(3), 670–676 (2010).

[315] Cui, H., Shen, H.-S., Gao, Y.-M., Dwight, K., and Wold, A. *Mater. Res. Bull.* **28**(3), 195–201 (1993).

[316] Matthews, D. Kay, A. and Grätzel, M. *Aust. J. Chem.* **47**, 1869–1877 (1994).

[317] Yang, Y., Qu, L., Dai, L., Kang, T.-S., and Durstock, M. *Adv. Mater.* **19**(9), 1239–1243 (2007).

[318] Jarernboon, W., Pimanpang, S., Maensiri, S., Swatsitang, E., and Amornkitbamrung, V. *Thin Solid Films* **517**(16), 4663–4667 (2009).

[319] Karuppuchamy, S., Nonomura, K., Yoshida, T., Sugiura, T., and Minoura, H. *Solid State Ionics* **151**(1-4), 19–27 (2002).

[320] Halary, E., Benvenuti, G., Wagner, F., and Hoffmann, P. *Appl. Surf. Sci.* **154**, 146–151 (2000).

[321] Nakaso, K., Okuyama, K., Shimada, M., and Pratsinis, S. E. *Chem. Eng. Sci.* **58**(15), 3327–3335 (2003).

[322] Yamabi, S. and Imai, H. *Chem. Mater.* **14**(2), 609–614 (2002).

[323] Berger, T., Lana-Villarreal, T., Monllor-Satoca, D., and Gómez, R. *Chem. Phys. Lett.* **447**(1-3), 91–95 (2007).

[324] Gerischer, H. *Electrochim. Acta* **35**(11-12), 1677–1699 (1990).

[325] de la Garza, L., Jeong, G., Liddell, P. A., Sotomura, T., Moore, T. A., Moore, A. L., and Gust, D. *J. Phys. Chem. B* **107**(37), 10252–10260 (2003).

[326] Brune, A., Jeong, G., Liddell, P. A., Sotomura, T., Moore, T. A., Moore, A. L., and Gust, D. **20**(19), 8366–71 (2004).

[327] Yang, J., Wang, K., Liang, L., Feng, L., Zhang, Y., Sun, B., and Xing, W. *Catal. Commun.* **20**(0), 76–79 (2012).

[328] Wang, K. Q. and Tang, J. *Adv. Mater. Res.* **496**, 399–402 (2012).

[329] Wang, K. and Gao, Y. *Adv. Mater. Res.* **417**, 2036–2039 (2012).

[330] Yang, J., Feng, L., Si, F., Zhang, Y., Liu, C., Xing, W., and Wang, K. *J. Pow. Sourc.* **222**, 344–350 (2013).

[331] Hambourger, M., Gervaldo, M., Svedruzic, D., King, P. W., Gust, D., Ghirardi, M., Moore, A. L., and Moore, T. A. *J. Am. Chem. Soc.* **130**(6), 2015–2022 (2008).

[332] Yehezkeli, O., Tel-Vered, R., Wasserman, J., Trifonov, A., Michaeli, D., Nechushtai, R., and Willner, I. *Nat. Commun.* **3**, 742 (2012).

[333] Tsujimura, S., Tatsumi, H., Ogawa, O., Shimizu, S., Kano, K., and Ikeda, T. *J. Electroanal. Chem.* **496**(1-2), 69–75 (2001).

[334] Han, L., Bai, L., Zhu, C., Wang, Y., and Dong, S. *Chem. Commun.* **48**, 6103–6105 (2012).

[335] Rogalski, J., Dawidowicz, A., Jóźwik, E., and Leonowicz, A. *J. Mol. Catal. B-Enzym.* **6**(1-2), 29–39 (1999).

[336] Watkins, J. D., Lawrence, R., Taylor, J. E., Bull, S. D., Nelson, G. W., Foord, J. S., Wolverson, D., Rassaei, L., Evans, N. D. M., Gascon, S. A., and Marken, F. *Phys. Chem. Chem. Phys.* **12**(18), 4872–8 (2010).

[337] Bard, A. and Faulkner, L., [*Electrochemical Methods: Fundamentals and Applications*], Wiley (2001).

[338] Compton, R. and Banks, C., [*Understanding voltammetry*], World Scientific Publishing Company, Incorporated (2007).

[339] [*Electrochemial Dictionary*], Springer (2008).

[340] http://departments.colgate.edu.

[341] http://en.wikipedia.org/wiki/File:Atomic force microscope block diagram.svg.

[342] Lu, J., Tang, H., Xu, C., and Jiang, S. P. *J. Mater. Chem.* **22**(12), 5810 (2012).

[343] Janusz, G., *Comparative analysis of fungi laccases*, PhD thesis, Maria Curie-Sklodowska University (2005).

[344] Tsionsky, M., Gun, G., Glezer, V., and Lev, O. *Anal. Chem.* **66**(10), 1747–1753 (1994).

[345] Szot, K., *Electrodes modified with carbon nanoparticles and enzymes*, PhD thesis, Institute of Physical Chemistry, Polish Acadamy of Sciences (2012).

[346] Ebbesen, T. W. and Ajayan, P. M. *Nature* **358**, 220–222 (1992).

[347] Planeix, J. M., Coustel, N., Coq, B., Brotons, V., Kumbhar, P. S., Dutartre, R., Geneste, P., Bernier, P., and Ajayan, P. M. *J. Am. Chem. Soc.* **116**(17), 7935–7936 (1994).

[348] Liu, J., Chou, A., Rahmat, W., P.-R., M. N., and Gooding, J. J. *Electroanal.* **17**(1), 38–46 (2005).

[349] Li, W. Z., Xie, S. S., Qian, L. X., Chang, B. H., Zou, B. S., Zhou, W. Y., Zhao, R. A., and Wang, G. *Science* **274**(5293), 1701–1703 (1996).

[350] Sotiropoulou, S. and Chaniotakis, N. A. *Anal. Bioanal. Chem.* **375**(1), 103–105 (2003).

[351] Roy, S., Vedala, H., and Choi, W. *Nanotechnol.* **17**(4), S14 (2006).

[352] Liu, X., Baronian, K. H. R., and Downard, A. J. *Carbon* **47**(2), 500–506 (2009).

[353] Tsierkezos, N. G. and Ritter, U. *J. Solid State Electrochem.* **14**(6), 1101–1107 (2010).

[354] *J. Mater. Sci.: Mater. Electron.* **15**(8) (2004).

[355] Gooding, J. J., Chou, A., Liu, J., Losic, D., Shapter, J. G., and Hibbert, D. B. *Electrochem. Commun.* **9**(7), 1677–1683 (2007).

[356] Yang, Q., Qu, Y., Bo, Y., Wen, Y., and Huang, S. *Microchim. Acta* **168**(3-4), 197–203 (2010).

[357] Jeong, G.-H., Olofsson, N., Falk, L. K. L., and Campbell, E. E. B. *Carbon* **47**(3), 696–704 (2009).

[358] [*Carbon Nanotube Synthesis and Growth Mechanism, Carbon Nanotubes - Synthesis, Characterization, Applications*], InTech (2011). Available from: http://www.intechopen.com/books/carbon-nanotubes-synthesis-characterization-applications/carbonnanotube-synthesis-and-growth-mechanism.

[359] Szamocki, R., Reculusa, S., Ravaine, S., Bartlett, P. N., Kuhn, A., and Hempelmann, R. *Angew. Chem. Int. Ed.* **45**(8), 1317–1321 (2006).

[360] Macdonald, S. M., Szot, K., Niedziolka, J., Marken, F., and Opallo, M. *J. Solid State Electrochem.* **12**(3), 287–293 (2008).

[361] Wadhawan, J. D., Evans, R. G., and Compton, R. G. *J. Electroanal. Chem.* **533**(1-2), 71–84 (2002).

[362] Niedziolka, J., Szot, K., Marken, F., and Opallo, M. *Electroanal.* **19**(2-3), 155–160 (2007).

[363] Arias-Carrión, O. and Pöppel, E. *Acta Neurobiol. Exp.* **67**(4), 481–488 (2007).

[364] Celebanska, A., Tomaszewska, D., Lesniewski, A., and Opallo, M. *Biosens. Bioelectron.* **26**(11), 4417–4422 (2011).

[365] Nogala, W., Rozniecka, E., Zawisza, I., Rogalski, J., and Opallo, M. *Electrochem. Commun.* **8**(12), 1850–1854 (2006).

[366] Zawisza, I., Rogalski, J., and Opallo, M. *J. Electroanal. Chem.* **588**(2), 244–252 (2006).

[367] Nogala, W., Rozniecka, E., Rogalski, J., and Opallo, M. *J. Electroanal. Chem.* **608**(1), 31–36 (2007).

[368] Szot, K., Nogala, W., Niedziolka-Jönsson, J., Jönsson-Niedziolka, M., Marken, F., Rogalski, J., Kirchner, C. N., Wittstock, G., and Opallo, M. *Electrochim. Acta* **54**(20), 4620–4625 (2009).

[369] Farneth, W. E. and D'Amore, M. B. *J. Electroanal. Chem.* **581**(2), 197–205 (2005).

[370] Shin, W., Lee, J., Kim, Y., Steinfink, H., and Heller, A. *Journal of the American Chemical Society* **127**(42), 14590–14591 (2005).

[371] Léger, C. and Bertrand, P. *Chem. Rev.* **108**(7), 2379–438 (2008).

[372] Deng, L., Shang, L., Wang, Y., Wang, T., Chen, H., and Dong, S. *Electrochem. Commun.* **10**(7), 1012–1015 (2008).

[373] Jönsson-Niedziolka, M., Kaminska, A., and Opallo, M. *Electrochim. Acta* **55**(28), 8744–8750 (2010).

[374] Salaj-Kosla, U., Pöller, S., Beyl, Y., Scanlon, M. D., Beloshapkin, S., Shleev, S., Schuhmann, W., and Magner, E. *Electrochem. Commun.* **16**(1), 92–95 (2012).

[375] Amatore, C., Pebay, C., Thouin, L., and Wang, A. *Electrochem. Commun.* **11**(6), 1269–1272 (2009).

[376] Amatore, C., Pebay, C., Thouin, L., Wang, A., and Warkocz, J.-S. *Anal. Chem.* **82**(16), 6933–6939 (2010).

[377] Limoges, B. and Savéant, J.-M. *J. Electroanal. Chem.* **562**(1), 43–52 (2004).

[378] Jönsson-Niedziolka, M., Szot, K., Rogalski, J., and Opallo, M. *Electrochem. Commun.* **11**(5), 1042–1044 (2009).

[379] Shen, Y., Trauble, M., and Wittstock, G. *Anal. Chem.* **80**(3), 750–759 (2008).

[380] Barton, S. C. *Electrochim. Acta* **50**(10), 2145–2153 (2005).

[381] [*Biofuel's Engineering Process Technology*], ch. Enzyme-Based Microfluidic Biofuel Cell To Generate Micropower, InTech (2011).

[382] Tsujimura, S., Kano, K., and Ikeda, T. *J. Electroanal. Chem.* **576**(1), 113–120 (2005).

[383] Tarasevich, M. R., Bogdanovskaya, V. A., and Kapustin, A. V. *Electrochem. Commun.* **5**(6), 491–496 (2003).

[384] Kontani, R., Tsujimura, S., and Kano, K. *Bioelectrochem.* **76**(1-2), 10–13 (2009).

[385] Nogala, W., Celebanska, A., Wittstock, G., and Opallo, M. *Fuel Cells* **10**(6), 1157–1163 (2010).

[386] Gellett, W., Schumacher, J., Kesmez, M., Le, D., and Minteer, S. D. *J. Electrochem. Soc.* **157**(4), B557–B562 (2010).

[387] Rincón, R. A., Lau, C., Luckarift, H. R., Garcia, K. E., Adkins, E., Johnson, G. R., and Atanassov, P. *Biosens. Bioelectron.* **27**(1), 132–136 (2011).

[388] Sakai, H., Nakagawa, T., Tokita, Y., Hatazawa, T., Ikeda, T., Tsujimura, S., and Kano, K. *Energy Environ. Sci.* **2**, 133–138 (2009).

[389] Gupta, G., Lau, C., Branch, B., Rajendran, V., Ivnitski, D., and Atanassov, P. *Electrochim. Acta* **56**(28), 10767–10771 (2011).

[390] Lau, C., Adkins, E. R., Ramasamy, R. P., Luckarift, H. R., Johnson, G. R., and Atanassov, P. *Adv. Energy Mater.* **2**(1), 162–168 (2012).

[391] Coman, V., Ludwig, R., Harreither, W., Haltrich, D., Gorton, L., Ruzgas, T., and Shleev, S. *Fuel Cells* **10**(1), 9–16 (2010).

[392] Jensen, U. B., Lörcher, S., Vagin, M., Chevallier, J., Shipovskov, S., Koroleva, O., Besenbacher, F., and Ferapontova, E. E. *Electrochim. Acta* **62**, 218–226 (2012).

[393] Shleev, S., Shumakovich, G., Morozova, O., and Yaropolov, A. *Fuel Cells* **10**(4), 726–733 (2010).

[394] Lesniewski, A., Niedziolka-Jonsson, J., Sirieix-Plenet, J., Gaillon, L., and Opallo, M. *Electrochem. Commun.* **11**(6), 1305–1307 (2009).

[395] Stöber, W., Fink, A., and Bohn, E. *J. Colloid Interface Sci.* **26**(1), 62–69 (1968).

[396] García-Jareño, J. J., Benito, D., Navarro-Laboulais, J., and Vicente, F. *J. Chem. Edu.* **75**(7), 881 (1998).

[397] Ping, J., Mao, X., Fan, K., Li, D., Ru, S., Wu, J., and Ying, Y. *Ionics* **16**(6), 523–527 (2010).

[398] Procházková, A., Krivánková, L., and Boček, P. *Electrophoresis* **19**(2), 300–4 (1998).

[399] Vermeir, S., Nicolaï, B. M., Verboven, P., Van Gerwen, P., Baeten, B., Hoflack, L., Vulsteke, V., and Lammertyn, J. *Anal. Chem.* **79**(16), 6119–27 (2007).

[400] Li, X., Zhang, L., Su, L., Ohsaka, T., and Mao, L. *Fuel Cells* **9**(1), 85–91 (2009).

[401] Qian, Q., Su, L., Yu, P., Cheng, H., Lin, Y., Jin, X., and Mao, L. *J. Phys. Chem. B* **116**(17), 5185–91 (2012).

[402] Itaya, K., Ataka, T., and Toshima, S. *J. Am. Chem. Soc.* **104**(18), 4767–4772 (1982).

[403] Koncki, R., Lenarczuk, T., and Głąb, S. *Anal. Chim. Acta* **424**(1), 27–35 (2000).

[404] Pierre, J. L. and Gautier-Luneau, I. *Biometals* **13**(1), 91–96 (2000).

[405] Möller, M., Leyland, N., Copeland, G., and Cassidy, M. *Eur. Phys. J. Appl. Phys.* **51**(3), 33205 (2010).

[406] Szot, K., Watkins, J. D., Bull, S. D., Marken, F., and Opallo, M. *Electrochem. Commun.* **12**(6), 737–739 (2010).

[407] Liu, H. and Crooks, R. M. *Anal. Chem.* **84**(5), 2528–32 (2012).

[408] Delaney, J. L., Hogan, C. F., Tian, J., and Shen, W. *Anal. Chem.* **83**(4), 1300–1306 (2011).

[409] Park, S., Dong-Won, P., Yang, C.-S., Kim, K.-R., Kwak, J.-H., So, H.-M., Ahn, C. W., Kim, B. S., Chang, H., and Lee, J.-O. *ACS Nano* **5**(9), 7061–7068 (2011).

[410] Wang, Y., Luo, Z., Li, B., Ho, P. S., Yao, Z., Shi, L., Bryan, E. N., and Nemanich, R. J. *J. Appl. Phys.* **101**(12), 124310 (2007).

[411] http://www.springerreference.com.

[412] Bakleh, M. E., Sol, V., Estieu-Gionnet, K., Granet, R., Déléris, G., and Krausz, P. *Tetrahedron* **65**(36), 7385–7392 (2009).

[413] Albu, S. P., Ghicov, A., Aldabergenova, S., Drechsel, P., LeClere, D., Thompson, G. E., Macak, J. M., and Schmuki, P. *Adv. Mater.* **20**(21), 4135–4139 (2008).

[414] Tafalla, D. *J. Electrochem. Soc.* **137**(6), 1810 (1990).

[415] Spadavecchia, F., Ardizzone, S., Cappelletti, G., Falciola, L., Ceotto, M., and Lotti, D. *J. Appl. Electrochem.* **43**(2), 217–225 (2012).

[416] Bisquert, J., Fabregat-Santiago, F., Mora-Seró, I., Garcia-Belmonte, G., Barea, E. M., and Palomares, E. *Inorg. Chim. Acta* **361**(3), 684–698 (2008).

[417] Willis, R. L., Olson, C., O'Regan, B., Lutz, T.and Nelson, J., and Durrant, J. R. *J. Phys. Chem. B* **106**(31), 7605–7613 (2002).

[418] Kalyanasundaram, K., ed., [*Dye-sensitized solar cells*], EPFL Press (2010).

[419] Ito, S., Nazeeruddin, M. K., Liska, P., Comte, P., Charvet, R., Péchy, P., Jirousek, M., Kay, A., Zakeeruddin, S. M., and Grätzel, M. *Prog. Photovolt: Res. Appl.* **14**(7), 589–601 (2006).

[420] http://www.jhu.edu/chem/meyer/Research/Research.html.

[421] Gorman, A. A. and Rodgers, M. A. J. *Chem. Soc. Rev.* **10**, 205–231 (1981).

[422] Fujishima, A., Zhang, X., and Tryk, D. A. *Surf. Sci. Rep.* **63**(12), 515–582 (2008).

[423] Guo, M. Y., Ng, A. M. C., Liu, F., Djurišić, A. B., and Chan, W. K. *Appl. Catal. B* **107**(1-2), 150–157 (2011).

[424] Solometric, http://www.solmetric.com, *Guide To Interpreting I-V Curve Measurements of PV Arrays* (March 2011).

List of Papers

1. A. Zloczewska, M. Jönsson-Niedziolka, J. Rogalski and M. Opallo, Vertically aligned carbon nanotube film electrodes for bioelectrocatalytic dioxygen reduction, *Electrochimica Acta* (2011), vol. 55, pp 3947-3953.

2. A. Zloczewska and M. Jönsson-Niedziolka, Efficient air-breathing biocathodes for zinc/oxygen batteries, *Journal of Power Sources* (2013), vol. 28, pp 104-111,

3. J. Urban, A. Zloczewska, W. Stryczniewicz and M. Jönsson-Niedziolka, Enzymatic oxygen reduction under quiescent conditions - the importance of convection, *Electrochimistry Communications* (2013), vol. 34, pp 94-97,

4. A. Zloczewska, A. Celebanska, K. Szot, D. Tomaszewska, M. Opallo, M. Jönsson-Niedziolka, Self-Powered Biosensor for Ascorbic Acid with a Prussian Blue Electrochromic Display, *Biosensors and Bioelectronics, submitted manuscript, under revision.*